Modeling the Experimental Uncertainty of Identifying Dynamic Coefficients for Tilting-Pad Journal Bearings

---

A

Dissertation

Presented to

the faculty of the School of Engineering and Applied Science

University of Virginia

---

in partial fulfillment

of the requirements for the degree

Doctor of Philosophy

by

Benstone I Schwartz

August 2020

APPROVAL SHEET

This

Dissertation

is submitted in partial fulfillment of the requirements
for the degree of

Doctor of Philosophy

Author: Benstone I Schwartz

This Dissertation has been read and approved by the examing committee:

Advisor: Dr. Roger Fittro

Advisor: Dr. Carl Knospe

Committee Member: Dr. Houston Wood

Committee Member: Dr. Christopher Goyne

Committee Member: Dr. Zongli Lin

Committee Member:

Committee Member:

Committee Member:

Accepted for the School of Engineering and Applied Science:

Craig H. Benson, School of Engineering and Applied Science

August 2020

ACKNOWLEDGMENTS

A patient support network enabled the successful completion of this dissertation and the research presented within. While the full extent of the support I received cannot be condensed into a short section, I wanted to make sure that I highlighted what I could.

I am grateful for the Rotating Machinery and Controls (ROMAC) Laboratory at the University of Virginia (UVA) for their long-term support of my research and education. My co-advisors, Dr. Roger Fittro and Dr. Carl Knospe, were invaluable in providing insight and also keeping me on track. I'm sure they remember many meetings where I'd gotten distracted by an idea that was as interesting as it was unrelated to the primary thrust of my research.

More generally, the ROMAC family was always around to offer an ear when I needed to vent some stress or offer some thoughts when I was stuck. The adventures we had (like completely redesigning our office space) will always be with me. Lori Pedersen always had just the right snacks available when I needed to stress-eat some sugary calories. I also need to thank Brenda Perkins who patiently answered every question I had about administrative details.

Another big thanks goes to the industrial members of ROMAC. It is necessary to highlight the engineers at BRG Machinery Consulting, especially Hunter Cloud, Minhui He, Eric Maslen, and Jim Byrne. They provided practical insight into the applications of my research and the mechanical design of the test rig.

Lastly and perhaps most importantly, a huge thank you to my wife, Carolyn, who was by my side this whole time and kept encouraging me even when I was running out of steam. Carolyn - Through the good times and the stressful times, you provided a solid foundation for me to stand on. I couldn't have done it without you.

ABSTRACT

Tilting-pad journal bearings (TPJBs) support the rotors of systems in many industries such as power generation, HVAC, and oil & gas. Reliable operation with little to no unplanned downtime is paramount. Stability predictions using rotordynamic analysis tools ensure safe and reliable operation. As demands on rotating machinery push operating conditions towards higher speeds and more demanding loads, the accuracy of rotordynamic analysis becomes critical. Accurate rotordynamic analysis relies on having accurate component level models, especially for the bearings, such as TPJBs. The dynamic behavior of the TPJBs, expressed as stiffness and damping coefficients, are used in system-level analyses. The coefficients are predicted with a variety of TPJB models used in different bearing codes. Bearing codes must be validated by comparing predictions with experimental data. Validation experiments for TPJB bearing codes are often performed on dedicated test rigs.

Reliable validation for TPJB models requires data from test rig to have the lowest uncertainty possible. The state-of-the-art for performing and presenting uncertainty analysis is inadequate for confidently validating TPJB dynamic coefficients. Therefore, a framework for analyzing the uncertainty of TPJB coefficient identification that is more suitable to the problem is proposed in this dissertation.

First, the framework is described and applied to single-axis models. The framework is a simulation-based method that (1) defines a truth model to represent the physics of the test rig and expected measurement errors, (2) establishes an identification model that will process simulated measurements into dynamic coefficients, and (3) compares the coefficients identified in the simulation using the identification model with the true values defined in the truth model. Through the single-axis applications, important trends that affect the uncertainty of TPJB coefficient identification are identified. These trends are applicable for TPJBs and other components (such as seals) on rotating machines with behavior described by stiffness and damping coefficients. Furthermore, some common assumptions used in TPJB identification experiments are shown to be problematic, especially when identifying dynamic

coefficients in high performance conditions (e.g. - high rotation speeds or high-frequency excitations).

The models are extended to higher-fidelity models in two-axes. First, uncertainty analysis is performed using models based on existing test rigs and compared with the single-axis models. The results in the higher-fidelity models support the results from the single-axis models and add further details into TPJB identification uncertainties. For example, identifying the cross-coupled coefficients of TPJBs is incredibly challenging due to the small magnitude of the cross-coupling. While at a system level these uncertainties may not change the dynamics significantly, they add challenges to bearing model validation. Second, the utility of the uncertainty analysis is demonstrated by updating the design of a new test rig for TPJB dynamic coefficient identification. The uncertainty analysis serves as a design tool to make changes that would reduce uncertainty.

Improving the analysis of uncertainty for TPJB coefficient identification will lead to test rig designs and experimental methods that reduce the identification uncertainty and allow more accurate model validation. This will ultimately improve TPJB modeling for rotordynamic analysis and increase rotating machine performance and reliability.

Contents

List of Figures

List of Tables

Nomenclature

δ Complex value representing error in magnitude and phase, used in measurement error models

$\frac{\delta f}{\delta x_i}, \frac{\partial f}{\partial x_i}$ Influence of parameter x_i on uncertainty of functional relationship between measurements and computed parameter

$\hat{\mathbf{H}}, \hat{\mathbf{H}}(\omega)$ Identified/measured frequency response matrix

$\hat{A}$ Measured acceleration (including error model), frequency domain

$\hat{c}$ Identified damping

$\hat{F}$ Measured force (including error model), frequency domain

$\hat{k}$ Identified stiffness

$\hat{X}$ Measured displacement (including error model), frequency domain

$\Im()$ Imaginary component of complex number

$\mathbf{F}$ Applied force matrix

$\mathbf{H}, \mathbf{H}(\omega)$ Frequency response matrix

$\mathbf{U}$ System response matrix

ω test frequency, rad/s

$\Re()$ Real component of complex number

A Acceleration of excited component, frequency domain

c Damping of bearing approximation in SDoF Model

F Applied force on excited component, frequency domain

f Applied force on excited component in SDoF Model

j Unit imaginary number, $\sqrt{-1}$

k Stiffness of bearing approximation in SDoF Model

m Mass of excited component in SDoF Model

s complex frequency

$u(x_i)$ Uncertainty of component x_i of functional relationship between measurements and computed parameter

$u_c(y)$ Total uncertainty as defined by the GUM for a functional relationship between measurements and computed parameter y

X Response of excited component, frequency domain

x Response of excited comopnent in SDoF Model, frequency domain

2DoF Two Degrees-of-Freedom

AMB Active Magnetic Bearing

C.I. Confidence Interval

SDoF Single Degree of Freedom

TPJB Tilting-Pad Journal Bearing

Chapter 1

Introduction

Rotating machines convert and transmit energy in industries such as power generation, aviation, HVAC, and oil & gas. The reliability of rotating machines is of utmost importance to minimize unplanned costs. In examples such as jet engines, reliability is tied directly to human safety. Accurate modeling ensures safe, reliable operation and this requires modeling the supporting bearings. Bearings enable relative motion between stationary components and rotating components while providing support for the weight of the rotor and dynamic forces experienced during operation. A strong argument can be made for bearings being the most important components in a rotating machine. Therefore, contributions to bearing modeling and model validation are always worthwhile.

(a) Jet Engine

(b) Steam Turbine

(c) Turbocharger

Figure 1.1: Examples of Rotating Machines

1.1 Bearings Overview

Most bearings for rotating machinery can be classified as rolling element bearings, hydrodynamic bearings, or magnetic bearings. A high-level summary is provided to illustrate some of the trade-offs to be considered during bearing selection. The trade-offs make it important to have accurate models so an appropriate bearing design can be selected based on the system requirements. Some references are provided as a starting point if more information is required regarding the different bearing types. A comprehensive description of each bearing type is not the scope of this section.

This dissertation focuses on radial, oil-lubricated hydrodynamic tilting-pad journal bearings (TPJBs) . Section 1.2 covers TPJBs in more detail. The objectives of this dissertation (stated in 1.4) focus on TPJBs, but the developments of the research in this dissertation are relevant for all types of bearings.

Rolling element bearings [1] have elements of circular cross section -

balls or rollers (cylinders or conical frustums) - sandwiched between the rotor and stator in machined elements called races. The rotor is supported on the elements and races of the bearing. Friction is reduced by allowing rotation through the rolling of the elements instead of sliding between the rotor and stator. For high-performance applications some form of lubrication is required and this can make modeling more challenging. Rolling element bearings are practical for many applications due to their high load capacity and relatively small required volume. However, rolling element bearings have little damping. If an application calls for damping, this must be added externally through means such as a squeeze-film damper around the bearing.

Hydrodynamic bearings [2] support the rotor using pressure built up in a fluid film. The fluid-film pressure eliminates contact between the rotor and the stator during standard operation, minimizing friction and wear. The fluid-film also provides damping. The reduction of wear and addition of damping compare favorably with rolling element bearings. However, hydrodynamic bearings face challenges in wear during startup when the hydrodynamic pressure has not been generated yet. This can be alleviated by externally pressurizing the fluid but the required pumping mechanism adds cost and complexity. Hydrodynamic bearings can have a load capacity comparable to the load capacity of rolling element bearings. This depends significantly on the lubricating fluid used and operating conditions such as rotation speed. When a fluid like oil is used, hydrodynamic bearings could have a much higher load capacity than rolling element bearings. When the fluid is air, the load capacity would be significantly lower unless the rotating speed of the system is high enough (which is unlikely due to the challenges in achieving the speeds required for equivalent load capacity). Still, growing interest in oil-free systems drives research into gas bearings and foil bearings.

Magnetic bearings [3] levitate rotors using electromagnetic forces. Magnetic bearings share the non-contact benefits of hydrodynamic bearings without the added wear at low speeds during startup and shutdown. Magnetic bearings are typically active magnetic bearings (AMBs) - designed to be active systems using electromagnets in opposing pairs with a controller determining the current in each electromagnet coil. Passive magnetic bearings exist, often using permanent magnets pushing against permanent magnets or reactive eddy currents to generate forces. Unit load capacity, stiffness, and damping are generally lower in passive magnetic bearings than in comparable AMBs. The maximum unit load capacity of AMBs is significantly lower compared with oil-lubricated hydrodynamic bearings and rolling element bearings. AMBs also require power amplifiers and a controller to function, often leading to higher initial costs. The active control of AMBs offers a compelling alternative to passive bearings including hydrodynamic bearings and rolling element bearings when the other design trade-offs can be tolerated. For example, actively controlled AMBs can incorporate on-line methods for vibration control. [4]

1.2 TPJBs in Rotating Machinery

Developments Leading to TPJBs

The foundation of hydrodynamic lubrication began in the 1880s with Beauchamp Tower's experimental discoveries [5] and Osborne Reynolds' mathematical modeling [6]. At the time, the basic requirements for hydrodynamic lubrication (a rotating shaft with oil as a lubricant) were actively used. However, hydrodynamic force was an unknown side effect rather than a deliberately harnessed phenomenon.

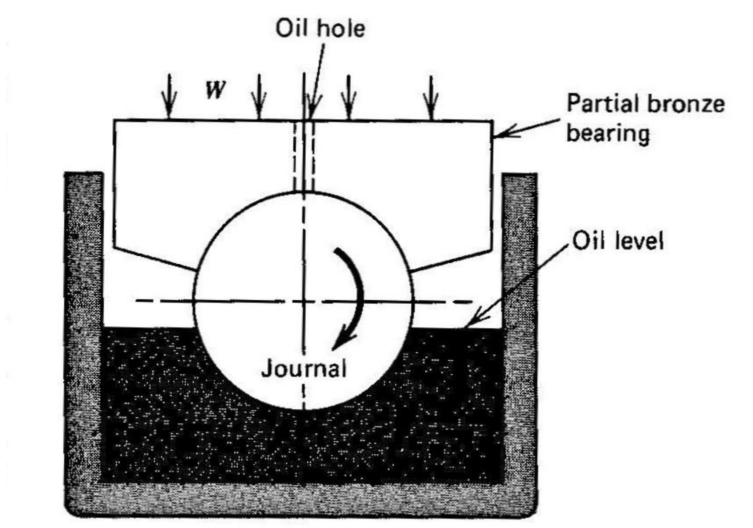

Figure 1.2: Diagram of Beauchamp Tower's Experimental Setup

Tower began by collecting a variety of data and experience from his peers and conducting his own experiments. Figure 1.2 shows a test rig Tower used for his own studies. Tower noticed that as the journal was rotating, a plug used to close the oil hole kept being pushed out. He could not fully explain this phenomenon. Reynolds' was able to take the experience and data from

Tower's experiments and corroborate it with a mathematical model. Tower's and Reynolds' work shed light on the pressures generated by oil films in rotating machinery. With this new understanding, the working principle of plain journal bearings could be harnessed.

As demands on systems supported by fluid-film bearings increased, cases began to be reported of large forces transmitted to other parts of the system under certain conditions. The first documented case came from Newkirk in 1924 [7]. This led to further investigation of hydrodynamic lubrication and instability mechanisms by many researchers including Lund [8], Crandall [9], and Leonard & Rowe [10]. Wachel observed through case studies that changes to bearings supporting a rotating system can significantly affect stability. [11]

Studying instability demonstrated the importance of bearings in ensuring stable operation. As a result, plain journal bearings evolved into more sophisticated variations (shown in Figure 1.3) such as elliptical bearings, offset-halves bearings, and lobed bearings. All these designs are classified as fixed-geometry journal bearings. The modifications in these designs aimed to reduce the effects of cross-coupled forces that can lead to instability. [12]

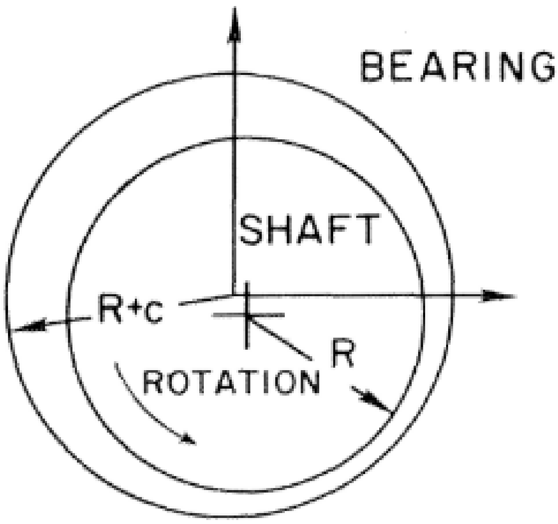

(a) Plain Journal Bearing

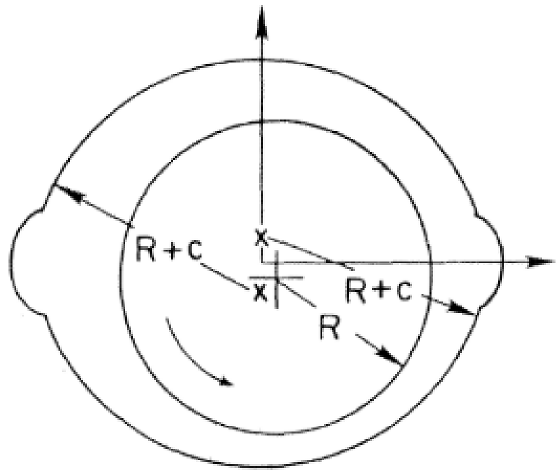

(b) Elliptical Bearing

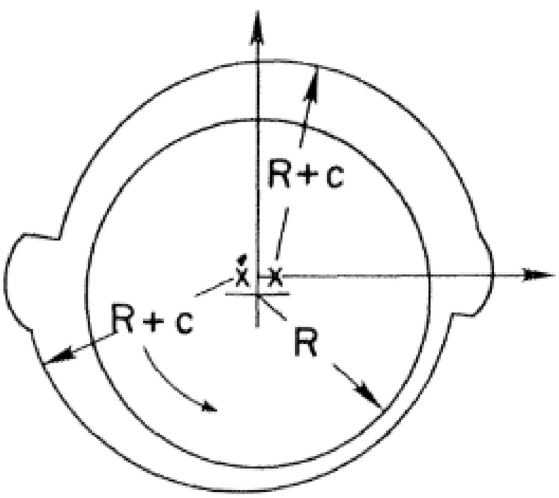

(c) Offset-Halves Bearing

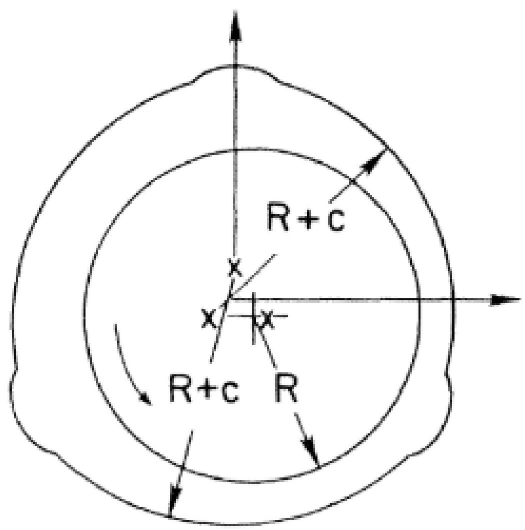

(d) 3-Lobed Bearing

Figure 1.3: Fixed geometry bearing designs reproduced from Allaire & Flack [13]

Cross-coupling means that a displacement or velocity along an axis leads to a force along a perpendicular axis. When static loads such as the weight of the rotor are applied, the rotor displaces in the direction of the load as well as a perpendicular direction. Figure 1.4a shows a plot of rotor eccentricity as static load is increased.

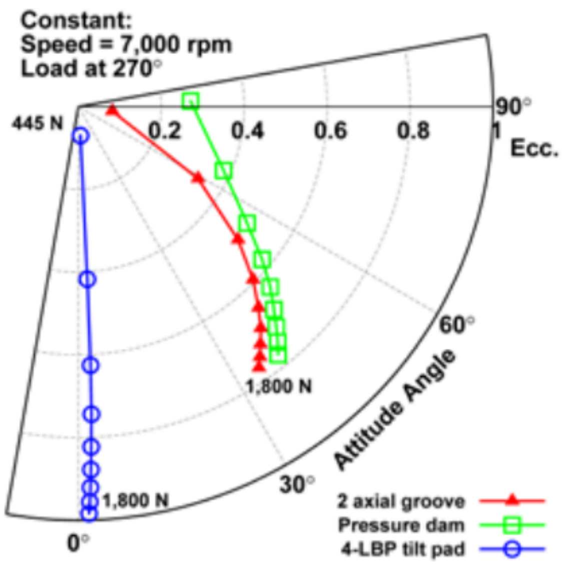

(a) Operating eccentricity as applied load varies

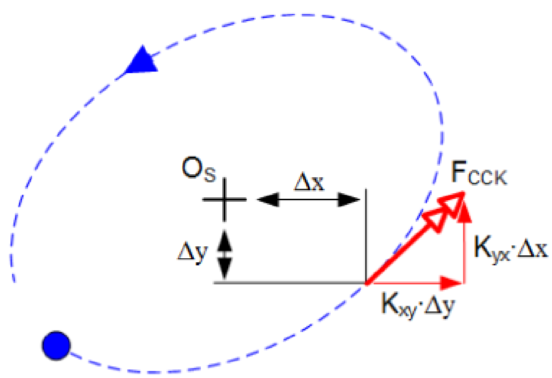

(b) Forces on the rotor during whirling motion

Figure 1.4: Effects of cross-coupling reproduced from He et al. [2]

The movement in the direction perpendicular to the load direction is an effect of cross-coupling. Another effect of the cross-coupling happens when the rotor is whirling about its operating point. Since systems cannot be balanced perfectly, every rotating machine will have some whirl. The rotor displaces along the direction of the rotating unbalance vector and this results in cross-coupled forces applied perpendicular to the unbalance vector's direction. The resulting cross-coupled forces could point in the same direction as the whirling motion, injecting more energy into vibrations and potentially driving the system unstable. Figure 1.4b shows a diagram of cross-coupled forces during whirl.

As long as enough damping is present the vibration will not grow in magnitude over time. Ensuring cross-coupled forces don't overwhelm the available damping is a critical design step that becomes increasingly challenging with fixed geometry bearings as high-performance rotating machines trend higher in rotating speeds.

Benefits of TPJBs

The typical TPJB design significantly reduces cross-coupling in hydrodynamic bearings. In a TPJB, there are pads (or shoes as they are sometimes called) that can pivot. Four pads and five pads are common in radial bearings. In response to rotor displacements from static loads or dynamic forces around the operating point, the pads can rotate about an axis parallel to the rotor's axis. Some pivot designs can even allow the pads to tilt along with any static or dynamic shaft slope. As a result, the cross-coupling can be negligible compared with fixed geometry bearings. Figure 1.4(a) includes the operating point changes in a TPJB as applied load increases. The operating point shifts almost completely in the direction of the applied load, indicating negligible cross-coupling. Nicholas [14] provided a survey of several cases of axial compressors where TPJBs demonstrated increased stability relative to fixed-geometry bearings. Some examples of TPJB designs are shown in Figure 1.5.

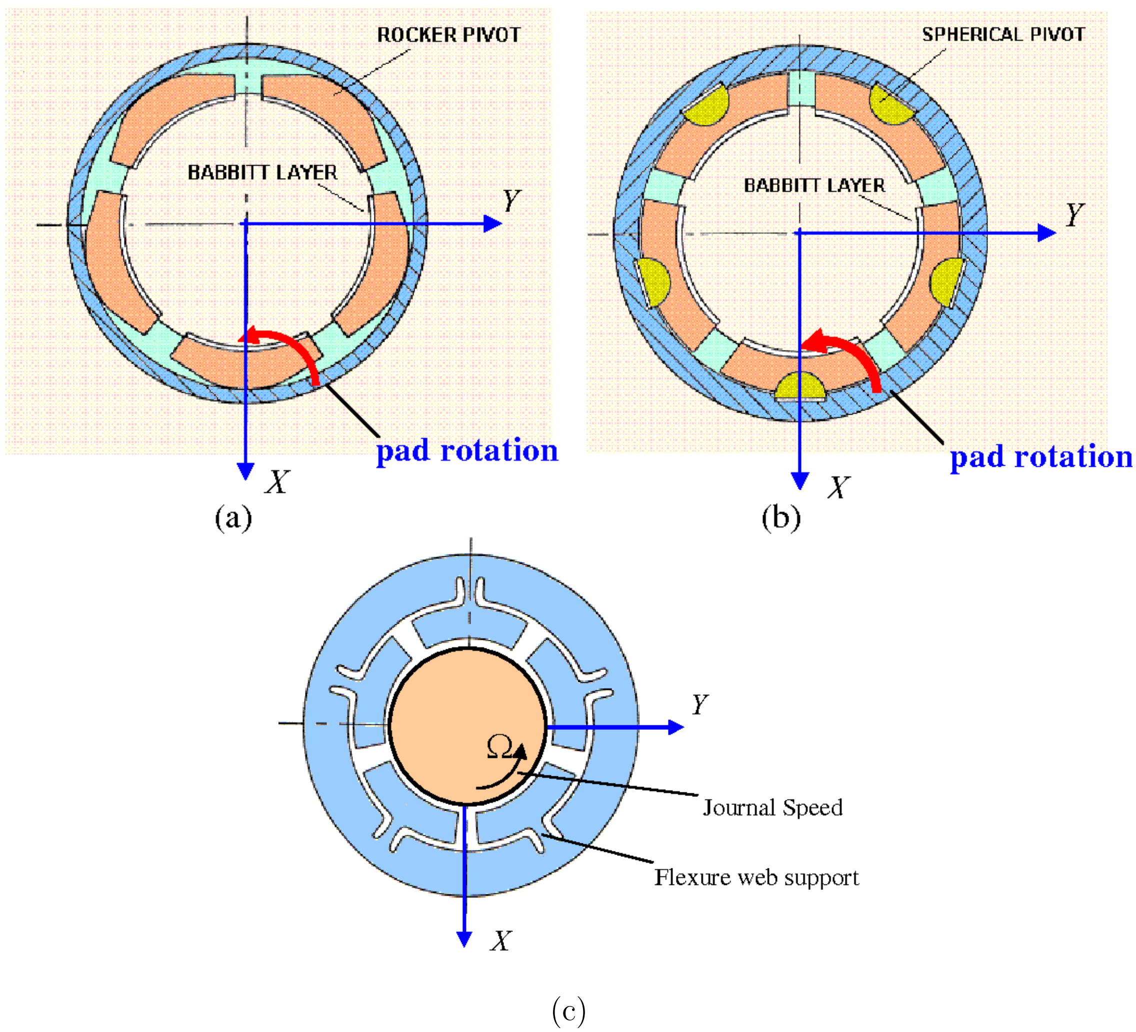

Figure 1.5: Examples of Tilting-Pad Journal Bearings reproduced from San Andres [15]. (a) Rocker Pivot TPJB, (b) Spherical Pivot TPJB, and (c) Flexure Pivot TPJB

TPJBs are becoming increasingly important as rotating machines increase in operating speed and loads. The growing demands on systems place greater burdens of accuracy on models used to predict the system behavior.

1.3 Motivations

If modeling can't predict a rotating system's behavior accurately, the consequences range from lost time and production to lost lives [16]. Rieger [17] described the costs of five types of rotating equipment failures seen in turbines. One example saw approximately 1.1 billion USD (in 1983) lost over the span of 11 years due to blade failures. Three of the five types of failures Rieger discussed (blade cracking/failure, disk cracking/rupture, and rotor burst) are associated with undesirable dynamic behaviors of the rotor such as resonance and "whirl unbalance." Though Rieger's discussion focused on gas turbines in power generation, the high cost of rotating machinery exhibiting undesirable behavior has been documented more broadly.

Gunter & Weaver [18] reviewed the redesign of the Kaybob compressor, a notable case of high costs of addressing excessive vibrations. The case study highlighted the need for accurate component models (e.g. - bearings) for rotordynamic analysis. The Kaybob compressor suffered from self-excited, subsynchronous whirl leading to vibration beyond acceptable limits. This instability led to expensive troubleshooting including bearing design modifications, the addition of squeeze film dampers, and ultimately a complete redesign of the rotor which was made to be shorter and stiffer. These efforts took more than five months and cost more than 100 million USD. The engineers working on the Kaybob compressors did not have access to many state-of-the-art models and rotordynamic analysis software available today. Gunter & Weaver developed new models of the Kaybob compressor bearings and incorporated these into stability analyses with modern rotordynamic analysis software. The tools available to Gunter & Weaver in 2016 predicted the results experienced by the engineers originally working with the Kaybob compressors. Additional bearing configurations were modeled and showed that if modern tools and understanding were available, the Kaybob engineers could have resolved the instability issues in less time and with lower costs. The results showed that computerized analysis, provided the models in the analysis are sufficiently accurate, can predict system behavior with enough fidelity to consider replacing experimentation which requires significantly more time and money.

In a similar review, Childs [19] revisited the analysis of a machine suffering from “large and damaging subsynchronous whirling motion”: The Space Shuttle Main Engine (SSME) High-Pressure Fuel Turbopump (HPFTP). Engineers analyzed the system’s stability before testing. At the time, stability analysis was typically performed only if testing revealed problems that needed to be diagnosed. However, even with preliminary analysis, early tests still showed some issues and changes were made to the design to try and reduce the vibration issues. Two attempted changes included additional dampers and asymmetrically stiffened bearing housings. The drawback to these two options was an increase in synchronous vibration levels. The final solution involved further modifying the bearing housings, stiffening the rotor, and modifying the seals. Each design iteration was reviewed with modern tools and the results are generally in line with the experimental results, just like in Gunter & Weaver's review of the Kaybob compressor redesign. In a concluding comment Childs stated, "there is a serious deficiency in test data for the component elements which must be modeled and incorporated into an overall rotordynamic model." In this dissertation it is shown that there is an additional requirement: The test data must come with comprehensive uncertainty analysis to ensure that the experimental results are adequately validating models of the component elements.

The deficiency of experimental data for component model validation is echoed by an API study conducted by Kocur et al. [20] This study found that there is large variation in dynamic coefficient predictions for bearings (and seals) leading to large variations in stability predictions. In this study, engineers and researchers with rotordynamic modeling capabilities were presented with identical bearing, seal, and rotor designs to analyze from a compressor system with available experimental data. The data was not provided to the engineers and researchers. First, bearing and seal coefficients were requested. Figure 1.6 shows the bearing coefficients collected in the study. The bearing coefficient predictions varied by almost an order of magnitude.

The surveyors analyzed the stability of the system using the various predictions of bearing coefficients. To isolate the coefficient variation as the

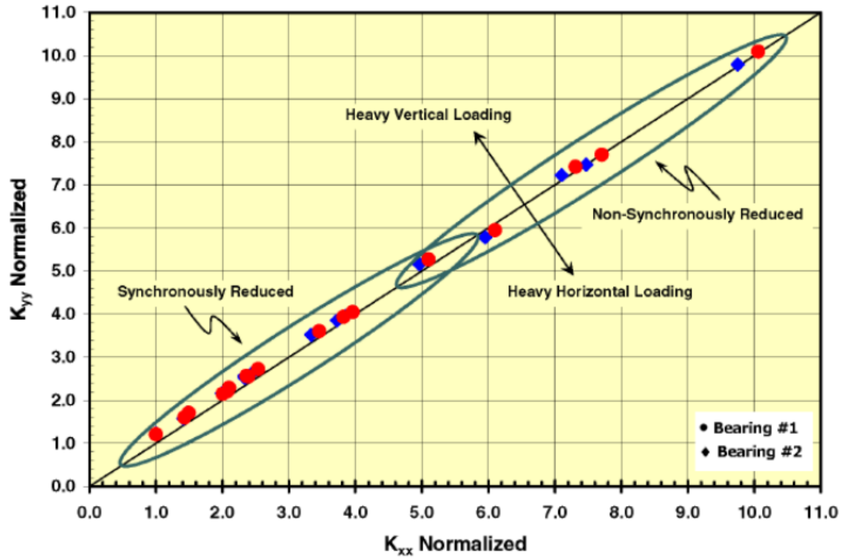

(a) Principal Stiffness Coefficients

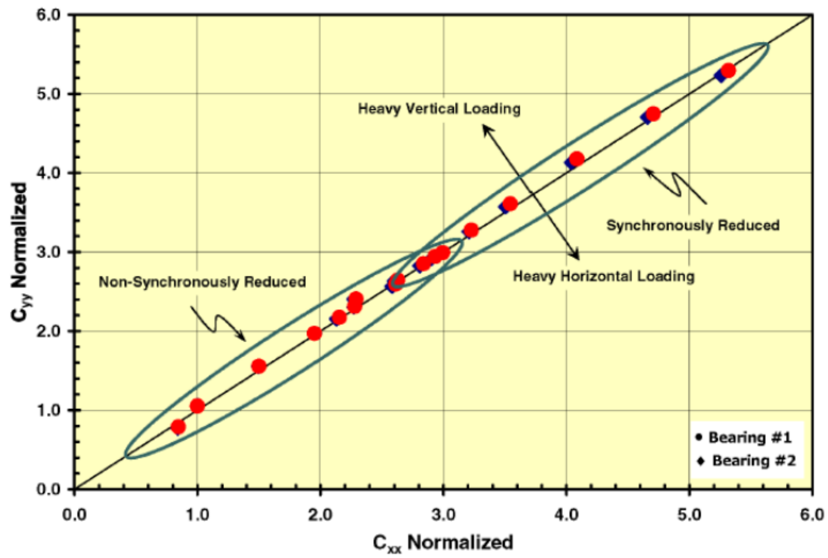

(b) Principal Damping Coefficients

Figure 1.6: Collected Coefficient Predictions (Reproduced from Kocur et al. [20])

source of predicted stability variation, a common eigenvalue solver and identical rotor model were used in all stability calculations. This resulted in significant variation in predictions of stability and critical speeds as seen in Figure 1.7. The stability analyses often predicted more stability than experimentally measured for the system analyzed.

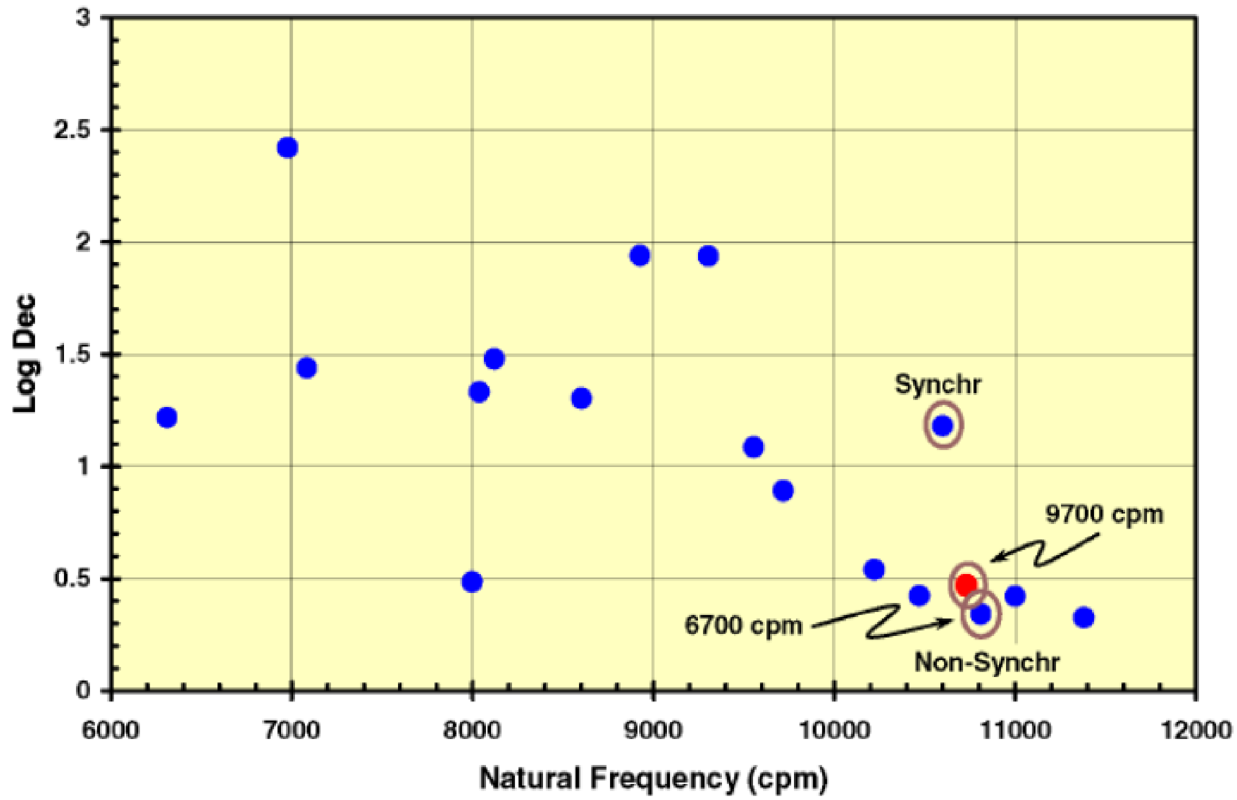

Figure 1.7: Predicted Stability Values with Bearing Coefficients Only (Reproduced from Kocur et al. [20])

Kocur et al. [20] then compared several different bearing models with the goal of understanding the main source of variation. Ultimately, one of the major conclusions from this survey was that “a gold standard of experimental data is needed for both tilting pad journal bearings and gas labyrinth seal dynamic coefficients.” This data would be used in validating bearing models and minimize the variation of predicted bearing dynamic coefficients.

Two studies separated by almost 30 years - Childs et al. [19] and Kocur et al. [20] - highlighted a need for accurate experimental data. Gunter &

Weaver [18] added additional support for this by showing how challenges faced by engineers in the past can be mitigated with more accurate models. The bearings supporting rotating machinery in particular need to be modeled with increasing accuracy. In short, to mitigate challenges facing rotating machinery now and in the future, improved prediction tools relying on more accurate models need to be developed. Therefore, the uncertainty in experimental validation of models must be understood.

The Need for Understanding Uncertainty

In this dissertation, a framework will be developed for modeling the uncertainty of experimentally identifying TPJB dynamic coefficients (i.e. - stiffness and damping). While this dissertation focuses on TPJBs, the same uncertainty analysis framework is applicable to the identification of dynamic coefficients for other components such as other bearing types (e.g. - foil bearings) and seals.

Understanding the identification uncertainty is crucial to ensure confidence in model validation. If a bearing design is being tested but the experimental uncertainty is large, the model's ability to predict the physical behavior cannot be confidently validated. In addition to evaluating a model's ability to predict behavior, two models can be compared. Large uncertainties would not allow for determining if one model is better than the other as they may both - within uncertainty bounds - capture the experimentally measured behavior. This dissertation seeks to advance the state-of-the-art of uncertainty analysis for dynamic coefficient identification of TPJBs. By providing a path to understanding and managing experimental uncertainty for dynamic coefficient identification, predictive models can be validated with greater confidence for rotating machines.

1.4 Dissertation Objective

This dissertation has three main objectives.

The first objective of this dissertation is to establish a formal framework for modeling the experimental uncertainties of dynamic coefficient identification under specific operating conditions. The framework should be used by engineers and researchers to have a consistent method of analyzing uncertainty for TPJB coefficient identification experiments.

The second objective of this dissertation is to investigate the influence of various aspects of the bearing and test rig design on the uncertainty of identified dynamic coefficients. Considerations will include test rig design choices (such as force measurement scheme), parameters of the bearing being tested, and differences in dynamics between the physical system and models used for identification. Some important factors will be identified for engineers and researchers to consider for coefficient identification experiments and the design of test rigs for those experiments.

The third objective of this dissertation is to complete the design of a test rig to identify TPJB dynamic coefficients with acceptable accuracy over a range of excitation frequencies from 10 Hz to 500 Hz and rotor speeds up to 22,000 RPM. Bearings tested will have a journal diameter of 5 inches and an axial length between 2.5 inches (L/D=0.5) and 3.75 inches (L/D=0.75). Feedback from industrial members of the Rotating Machinery and Controls Laboratory (ROMAC Lab) at the University of Virginia (UVA) established the standard for acceptable accuracy. Identification accuracy will be modeled and evaluated with uncertainty analysis using the framework developed in this dissertation.

1.5 Dissertation Outline

This dissertation is divided into 6 chapters:

Chapter 1 introduced the motivation, context, and scope of the dissertation.

Chapter 2 describes the state-of-the-art of uncertainty analysis pertaining to rotordynamic coefficient identification and reviews the uncertainty analysis of dynamic coefficient identification in TPJB experiments. The publications reviewed are grouped according to whether they contain uncertainty analysis or not. The publications with uncertainty analysis are further grouped according to whether the analysis includes uncertainty from systematic sources of error or not.

Chapter 3 develops the uncertainty analysis framework. Because TPJBs have minimal cross-coupled stiffness and damping, single-axis models are used as representative approximations of systems with TPJBs (which includes test rigs identifying TPJB coefficients). The single-axis models are used to simultaneously describe the uncertainty analysis framework and gain insight into significant factors affecting the uncertainties of dynamic coefficient identification.

Chapter 4 will extend the uncertainty analysis framework in two ways. First, the uncertainty analysis is extended with a second axis to increase fidelity. Second, a model based on a test rig is developed to compare with analysis of uncertainty in the literature. Ultimately, the uncertainty analysis with increased fidelity supports the results in Chapter 3.

Chapter 5 demonstrates a novel application of uncertainty analysis to test rig design using the framework developed in this dissertation. The design of a test rig is modified to reduce the modeled uncertainty of TPJB dynamic coefficient identification.

Chapter 6 summarizes the contributions and recommendations based on the research presented in this dissertation.

Chapter 2

Reviewing Uncertainty Analysis of TPJB Coefficient Identification Experiments

The state-of-the-art of uncertainty analysis in TPJB dynamic coefficient identification experiments will be established by reviewing published literature presenting experimentally identified dynamic coefficients for TPJBs. While there are many experimental results presented for other bearing types as well as theoretical or analytical works for TPJBs, the scope of the included literature will be limited to experimental results and to TPJBs (excluding active TPJBs). The uncertainty analysis performed for the experimental TPJB coefficient identification will be reviewed.

Literature will be classified into three categories based on the type of uncertainty analysis performed: 1) No uncertainty analysis, 2) uncertainty analysis including uncertainty only from random error sources, and 3) uncertainty analysis including uncertainty from systematic error sources. Literature in the first two categories will only be addressed briefly because the goal of this chapter is to review the completeness of uncertainty analysis when including systematic sources. In the third category, where systematic error sources are considered, each publication will be summarized in greater detail and the methods of computing the uncertainty will be reviewed.

For a broader look at identification experiments, reviews by Tiwari et al. [21] and Dimond et al. [22] are recommended as starting points. Tiwari et al. [21] covered literature from 1956 to 2003 and provided an overview of identification for components including hydrodynamic bearings, hydrostatic bearings, ball bearings, seals, and more. The details provided include descriptions of experimental measurement techniques, mathematical modeling, parameter extraction algorithms, and uncertainty in the estimates. Dimond et al. [22] reviewed identification experiments of hydrodynamic bearings specifically, focusing on providing some comparison of different methods of exciting the system for testing. This review indicated that "methods of evaluating the effects of measurement uncertainty on overall bearing coefficient confidence levels are reviewed." However, the details of uncertainty analysis performed - when the literature contains it - are not provided and analyzed.

The two broader reviews provided data suggesting two challenges related to uncertainty analysis. First, many experiments covered did not perform uncertainty analysis. Second, when uncertainty analysis was performed, the method of performing the analysis was not consistent. Taken together, this means that meaningful comparison of uncertainty (and thus accuracy) of experimental results is difficult, if not impossible.

This dissertation's first objective of establishing a framework for uncertainty analysis will begin to address these issues. With the framework established, engineers and researchers will have a lower barrier of entry to including truly comprehensive uncertainty analysis with a consistency that allows comparisons between efforts by different groups.

2.1 Tests Rigs for Bearing Model Validation

Comprehensive uncertainty analysis for TPJB dynamic coefficient identification requires models of test rigs used for these experiments. In this section, one of the most significant design choices for test rig design is highlighted and several other important modeling considerations are noted. Test rigs for TPJB coefficient identification can broadly be classified into two types based on where in the system dynamic excitation is applied.

The first type of test rig has dynamic excitation applied to the bearing stator, typically through the housing, while the rotor is held as rigidly as possible, such as with rolling element bearings. This configuration is common because it is easier to apply forces and place sensors on a stationary component than a rotating component.

The second type of test rig has dynamic excitation applied to the rotor while the housing is fixed to the substructure. Historically, there were few ways of implementing this type of excitation. One example is using known unbalance weights as a source of excitation. A drawback to this is the excitation can only be applied synchronous to the rotor speed. Recently, magnetic bearings have become more available and are able to provide asynchronous excitation forces directly to the rotor.

A system in the field will have bearing housings that are fixed to the foundation and the usual forces of concern (such as unbalance) act on the rotor. The second type of test rig, though less common for bearing identification experiments, nominally represents the physics of a system in the field more accurately. Typically, it is assumed that the difference between the two test rig configurations is negligible. Under some conditions such as low-speed operation this may be a suitable assumption. However, with high-speed machinery experiencing high-frequency forces, the difference may be more noticeable. Wilkes & Childs [23] explored this topic and found that depending on bearing's dynamic properties, applying excitation forces on the bearing housing versus applying excitation forces on the shaft may lead to significant differences.

Figure 2.1 and 2.2 show dynamic coefficients of two different bearing models identified in a simulation. The simulations were performed twice, once modeling the application of dynamic forces on the stator and a second time modeling the application of dynamic forces on the rotor. Figure 2.1 highlights a case where the difference in dynamic force application did not lead to significant differences. Figure 2.2 shows a case where significant differences are observed between the two methods of applying dynamic forces.

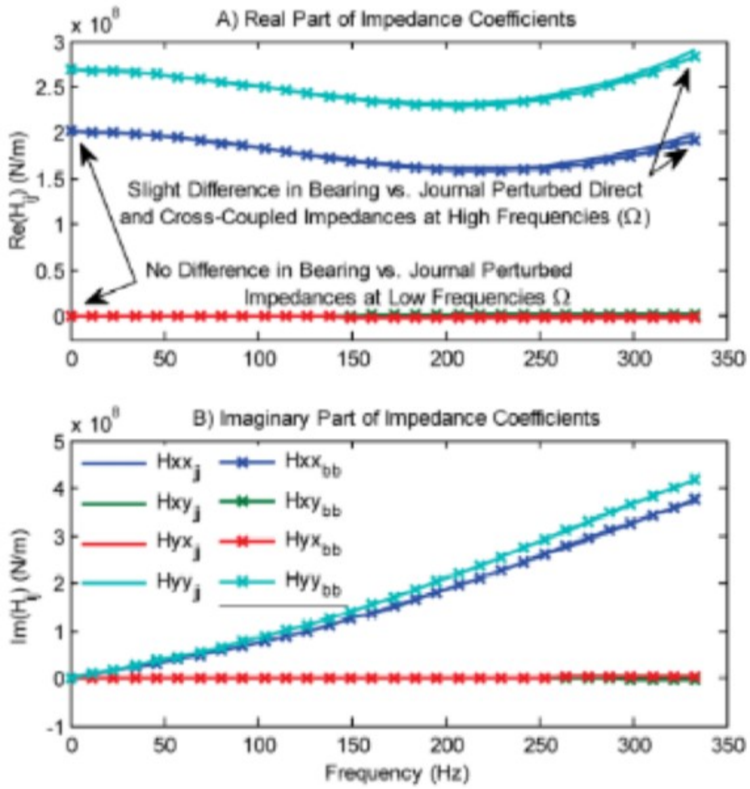

Figure 2.1: Comparing Test Rigs with Excited Housing vs. Excited Rotor with Bearing Design Showing Slight Difference - Reproduced from Wilkes & Childs [23]

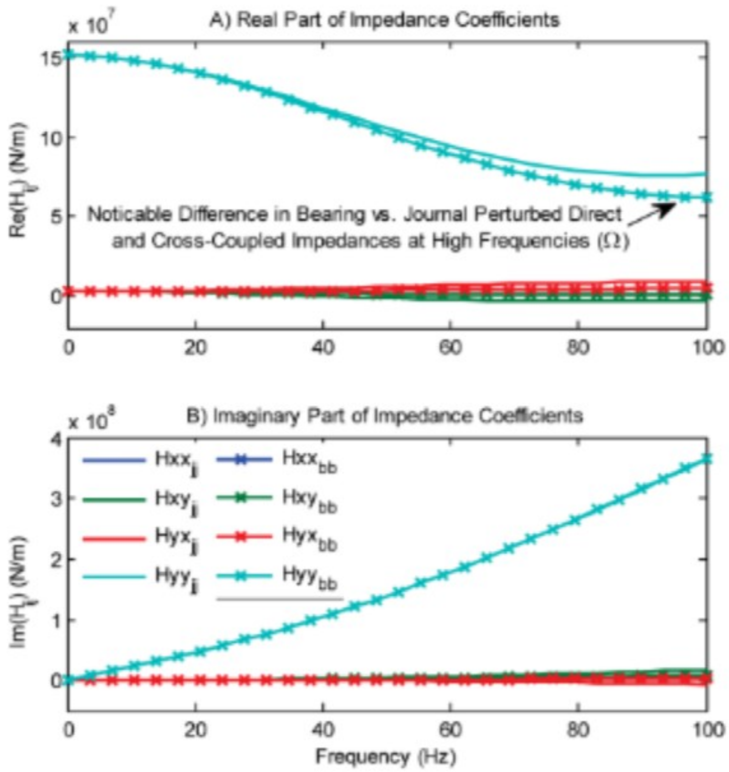

Figure 2.2: Comparing Test Rigs with Excited Housing vs. Excited Rotor with Bearing Design Showing Significant Difference - Reproduced from Wilkes & Childs [23]

While this topic is not a focus of this dissertation, the effect of designing a test rig of the first type rather than the second type can be evaluated with the uncertainty analysis framework presented in this dissertation using the models developed by Wilkes & Childs [23]. Other design factors that can be similarly evaluated with the framework in this dissertation include:

- including two test bearings and not needing additional support bearings vs. identifying a single bearing and needing at least one other bearing to support the rotor
- choice of displacement sensor system (e.g. - eddy current displacement

sensor vs. capacitive displacement sensor)

- choice of force sensor system (e.g. - strain gage load cell vs. piezoelectric load cell)

In this dissertation, it is proposed that understanding the effect on uncertainty of various design choices is important to design the best possible test rig for the operating conditions with which TPJB dynamic coefficients will be identified.

2.2 Uncertainty of Dynamic Coefficient Identification

The identification experiment applies a force on the target component and measures the response of the rotor. Typically, a prescribed force applied on the excited component is measured as an input and the relative displacement between the rotor and stator is measured as an output. With these measurements, it is possible to compute dynamic coefficients for a test bearing. The identification can be performed in the time domain or in the frequency domain. In principle it does not matter which domain is chosen but the effect of noise or errors may affect one more than the other. [24] [25] The reviews cited earlier by Tiwari et al. [21] and Dimond et al. [22] provide more details on identification methods for components of rotating machinery.

Measurements of force and displacement for coefficient identification can come directly from a sensor or be constructed from the data of several sensors. A measurement will differ from the truth with some errors. Errors can be random or systematic. If only random errors are present, then multiple measurements will show scatter about the truth. As the number of samples increases, the mean of the measurements will approach the truth. If only systematic errors are present, multiple measurements will have a consistent deviation from the truth. Figure 2.3 is a popular representation of systematic and random errors and how they affect measurements. The bullseye (center) of the target represents the truth the sensor attempts to measure. Each dot represents a separate measurement.

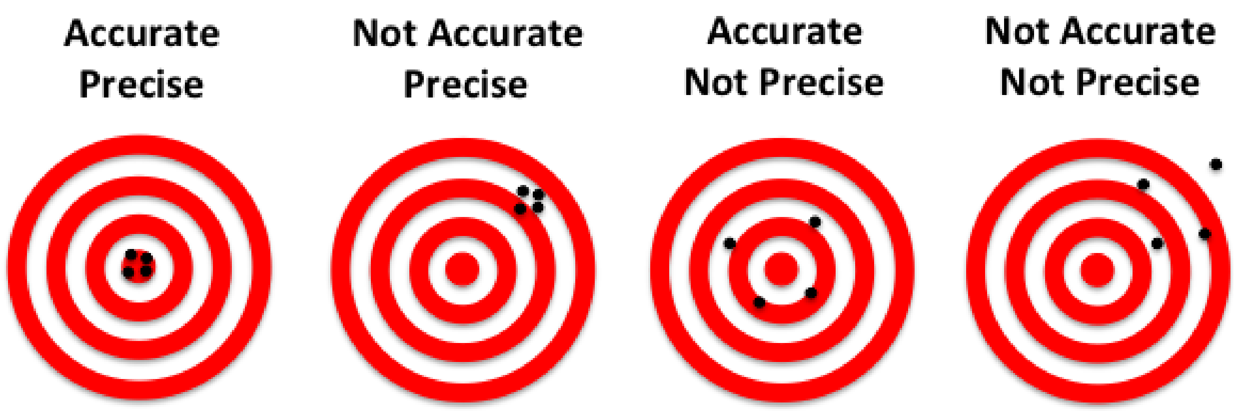

Figure 2.3: Typical Representation of Accuracy vs. Precision

If the truth is known, the errors can be directly quantified. This principle is used for calibrating sensors and developing estimates of the uncertainty in sensor measurements. Usually there is some standard for calibrating sensors, such as using "proof loads" to calibrate force sensor systems. Sensor vendors typically provide calibration information in traceable certificates. When the truth is not known, if the errors are known exactly the measurements can be compensated to obtain the truth. In bearing dynamic coefficient identification, the truth as well as the errors are unknown. After all, there is no “standard bearing” with accurately known coefficients to calibrate a test rig!

Uncertainty is a characterization of the range of values that the truth will most likely lie within. To adequately understand the uncertainty of a measurement, the effects of both systematic errors and random errors must be considered. If an analysis is performed with only the effect of random errors, it is possible to estimate how precise the measurements are but not how accurate. In a case such as dynamic coefficient identification where the truth and errors are unknown, estimates of uncertainty (and thus accuracy) can be developed from models including a bearing model, rotor model, etc. This process is referred to as uncertainty analysis.

In essence, the test rig and its dynamics are treated as a “dynamic coefficient sensor” for a bearing being tested. The errors that lead to identification uncertainty are the result of errors related to the subcomponents of the “dynamic coefficient sensor” such as dynamic models used to describe the physics and the measurement sensors. Each subcomponent can have their own uncertainties. Sensor uncertainty provides helpful parallels to understand uncertainty for TPJB dynamic coefficient identification.

2.2.1 Examples of Uncertainty in Sensors

Since a typical experiment to identify TPJB coefficients measures the displacement response of the excited component, the uncertainty associated with displacement measurements is a good example of how sensor vendors can describe the uncertainty of measurement. One sensor vendor, Lion Precision, highlights three types of measurement error due to deviations from the ideal voltage curve. Figure 2.4 shows an ideal voltage curve compared with three highlighted types of deviation from the ideal.

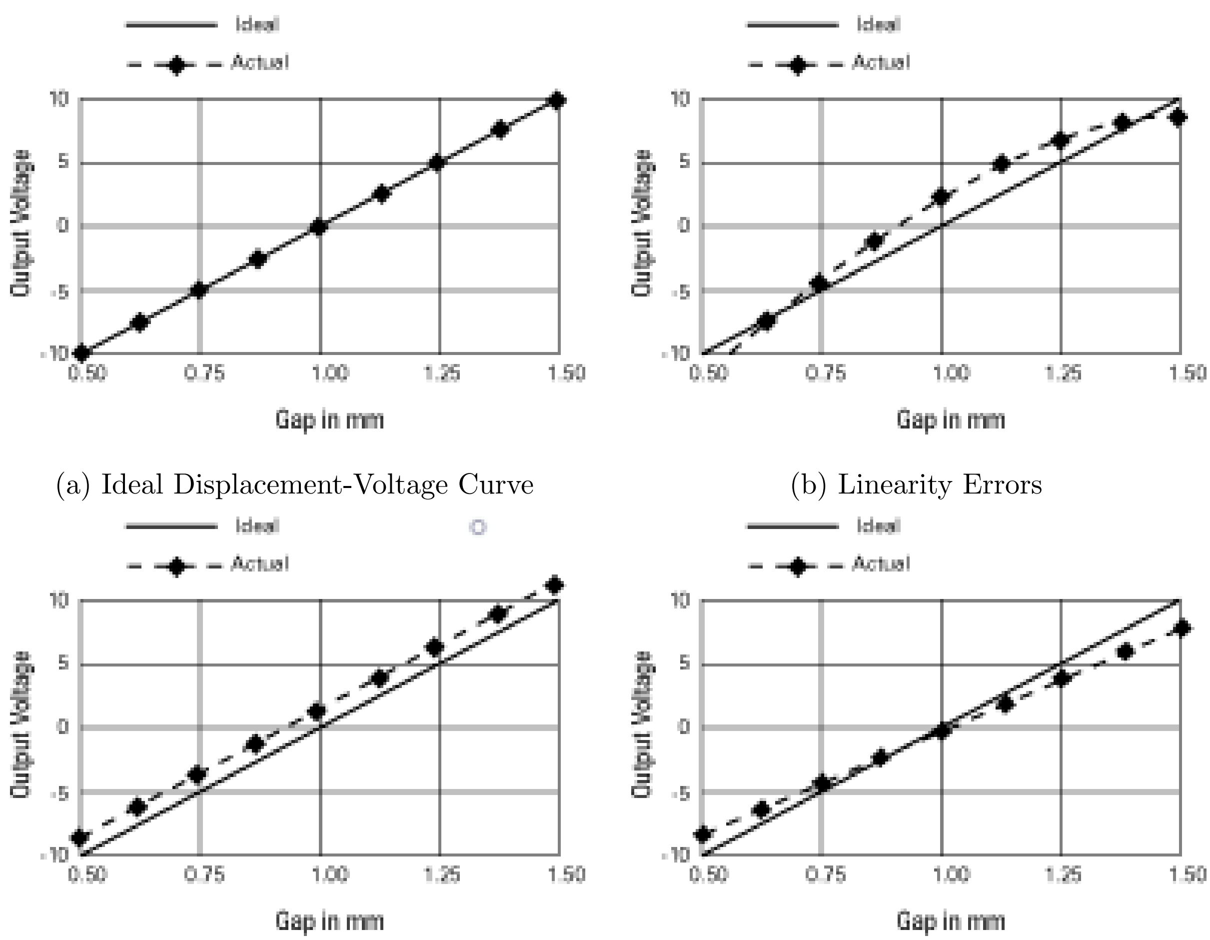

(a) Ideal Displacement-Voltage Curve

(b) Linearity Errors

(c) Offset Errors

(d) Sensitivity Error

Figure 2.4: Displacement-Voltage Curves reproduced from Lion Precision TechNote [26]

Another specification related to uncertainty in sensors is resolution. Resolution is a function primarily of electrical noise that cannot be eliminated completely. While filtering can help with resolution, there is a trade-off between resolution and bandwidth. Heavy filtering to remove noise will reduce the bandwidth of the sensor. Figure 2.5 shows two examples of noise levels for a sensor.

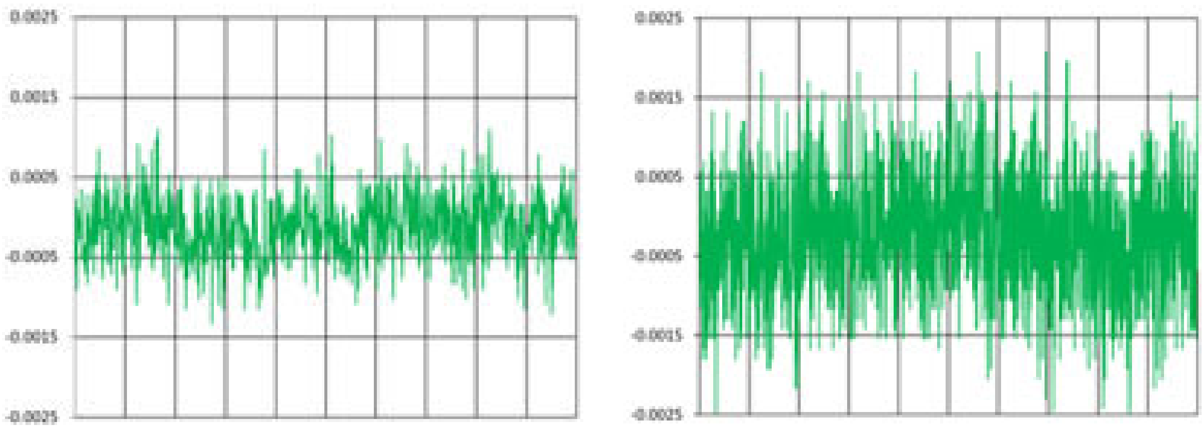

(a) Noise for 100 Hz sensor bandwidth

(b) Noise for 10 kHz sensor bandwidth

Figure 2.5: Sensor Noise Measurements reproduced from Lion Precision TechNote [26]

Measurement uncertainties are typically summarized in specifications such as the specifications for Lion Precision's CPL190/CPL290 capacitive displacement sensor product shown in Figure 2.6.

Uncertainties in displacement measurement as well as other measurement uncertainties will contribute to the uncertainty of identified coefficients. It is important to note that the measurement uncertainty is not summarized by a single parameter but described with several different descriptors (e.g. - linearity errors, sensitivity errors, resolution). In this dissertation it is shown

Specifications

Resolution[1]:	0.0005% @100 Hz 0.003% @ 15 kHz
Selectable Bandwidth:	100 Hz, 1, 10, 15 kHz
Linearity[2]:	<0.2% F.S. typical
Max Drift:	0.04% F.S./°C
Operating Temp:	4-50 °C
Front-Panel BNC:	±10V, 0 Ω, 10mA max
Rear-Panel National Inst.:	±10V, 0 Ω, Differential

1 Dependent on probe, range, and bandwidth. See next page for details.
2 Dependent on probe and range. See next page for details.

Listed specifications assume a two meter probe cable; Flat measurement area diameter at least 1.3 times larger than the Sensing Area diameter with no customizations.

Different probe body styles/sizes are available for each Sensing Area.

Figure 2.6: Specification for Lion Precision CPL190/CPL290 capacitive displacement sensor system obtained from Lion Precision website [27]

that the uncertainty of identified dynamic coefficients is the same way and the experimental uncertainty must be carefully described to ensure a complete understanding of the confidence level in the results.

Much like specifications of sensors for displacement, force, pressure, etc., a test rig for identifying dynamic coefficients can be conceptualized as a sensor for stiffness and damping parameters. Thus it would be convenient to have a unified system of conveying uncertainty for use with various "dynamic coefficient sensors." The framework in this dissertation establishes a foundation for such a system.

2.2.2 Existing Frameworks for Uncertainty

Uncertainty analysis is addressed in standards such as, "Evaluation of measurement data - Guide to the expression of uncertainty in measurement" (hereafter referred to as the GUM) [28] and ISO 5724-1:1994 [29]. The American Society of Mechanical Engineers holds a Verification and Validation Symposium dedicated to addressing topics including uncertainty analysis. The international standards are useful to establish a basic understanding of uncertainty analysis that applies to many applications, but the trade-off for being general is that specific cases such as bearing coefficient identification are not completely addressed by following these specifications.

In a comparison between the ISO specification and the GUM, Deldossi & Zappa [30] provided a summary that indicates the ISO specification is not suitable for analyzing the uncertainty of identified bearing coefficients. One of the key assumptions of the ISO specification is that the measurand is directly measurable. The specification establishes the idea of "trueness" and "precision." A measure of trueness requires a reference value which is not available for TPJB dynamic coefficients.

The GUM on the other hand looks at the measurand being a result of some function of other variables. This function is analyzed in two ways: Type A analysis for uncertainty and Type B analysis for uncertainty. Type A analysis is defined as a "method of evaluation of uncertainty by the statistical analysis of a series of observations." In other words, it looks at the repeatability of measurements (and other statistical measures) without considering how far away from the true quantity the measurements may be. Type B analysis is a broad category for anything else (a "method of evaluation of uncertainty by means other than the statistical analysis of series of observations"). While the GUM offers a great foundation to build on, the specification itself indicates that care must be taken to ensure the final analysis is applicable to the evaluated experiment.

One of the challenges for the methods described in the GUM is that dynamic coefficients are not calculated with a functional relationship in the form the GUM framework assumes for uncertainty analysis. The GUM computes uncertainty as:

$$u_c(y) = \sqrt{\sum_{i=1}^{N} (\frac{\delta f}{\delta x_i})^2 u^2(x_i)} \tag{2.1}$$

The total uncertainty, u_c, is found by taking the square root of the sum of the squares of the product of the elemental uncertainty, $u(x_i)$, and the influence of that uncertainty on the functional relationship determining the computed parameter, $\frac{\partial f}{\partial x_i}$.

The functional relationship between the measured quantities $(x_1, x_2, ...)$ and the computed parameter (Y) is defined by f:

$$Y = f(x_1, x_2, ...) \tag{2.2}$$

Modern dynamic coefficient identification is typically not computed by a direct functional relationship between measured quantities such as force and displacement. The computation is an optimization process of some sort such as least-squares-regression analysis. The GUM addresses some of these issues in a supplement [31] where some of the requirements (such as defining partial derivatives) are relaxed by using a Monte Carlo method. However, even in this supplement, the applications of the GUM framework are not fully applicable to dynamic coefficient identification. The principle requirement for the GUM is the determination of a measurement model and there is no formally established method to evaluate the selection of the measurement model itself.

For dynamic coefficient identification, the measurement model will not capture all the physics affecting a test rig. The GUM Monte Carlo method suggested by the GUM supplement will determine the uncertainty if the measurement model matches the truth but cannot determine which models of the physics of a test rig are significant. For example, if a rotor on a test rig to identify bearing coefficients is considered "rigid enough", it is assumed to be rigid in the measurement model (i.e. - the measurement model does not include any representation of rotor flexibility). The GUM does not provide details on how the impact of the assumption may be evaluated.

In reaching the three main objectives of this dissertation, a method of determining the models of physics to include in the measurement model will be presented. By establishing this process as a part of a framework that engineers and researchers can use for rotordynamic component dynamic coefficient identification, experimental results can be meaningfully compared with each other and test rig designs can be improved through the use of simulations.

2.2.3 Other Frameworks for Uncertainty

Another field where uncertainty has been extensively explored is controls. The concept of robustness develops criteria for making sure a system can meet desired specifications even with modeling uncertainties. One framework for handling uncertainty in this field is the linear fractional transformation (LFT) framework shown in Figure 2.7.

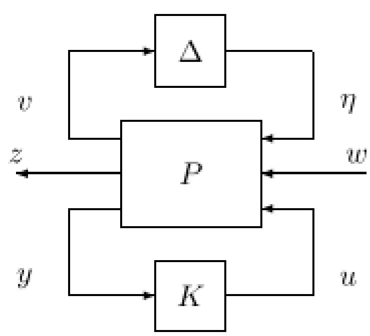

Figure 2.7: General LFT Framework Reproduced from Zhou [32]

The LFT framework in particular was considered carefully for its applicability to the problem of identifying dynamic coefficients. In Kemin Zhou's book [32] one of the illustrative examples is actually a mass-spring-damper system with uncertain parameters. The system dynamics including the uncertainties can be expressed with the ideas of the LFT and a diagram of this is shown in Figure 2.8.

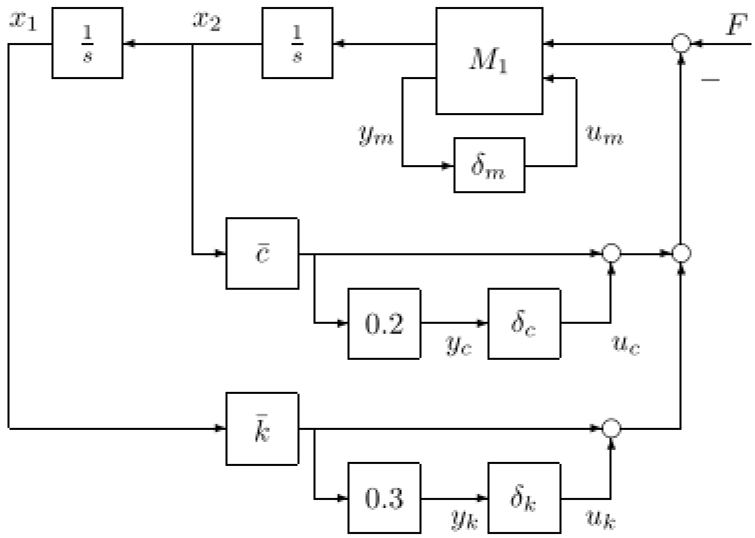

Figure 2.8: Mass Spring Damper with Uncertain Parameters from Zhou [32]

It was determined that as modeling complexity increased for dynamic coefficient identification test rigs, the problem would quickly become intractable. Rather than looking at the responses to inputs based on parameter uncertainties, the uncertainty analysis for dynamic coefficient identification is actually trying to identify the uncertainties of these parameters (represented by δ_m, δ_c, and δ_k in Figure 2.8). Because of the difference in the end-goal, the LFT framework requires significant modification to be applied in the context of bearing dynamic coefficient identification. For practical purposes a different approach was developed in this dissertation suitable for academic researchers as well as engineers in industry. More details are presented in Chapter 3.

2.3 Review of Uncertainty Analysis for TPJB Coefficient Identification

Published literature presenting experimentally measured TPJB dynamic coefficients have the associated uncertainty analysis reviewed. The review's scope excludes purely theoretical investigations of TPJB dynamic coefficients though they may be referenced. The collected works are classified into three categories: 1) experiments with no uncertainty analysis, 2) experiments that only analyze repeatability, and 3) experiments that perform comprehensive uncertainty analysis including the influence of systematic errors. Tables 2.3.1, 2.3.2, and 2.3.3 summarize the publications in each category. The first two categories are treated more briefly than the third group. For the purpose of this dissertation, the focus is on publications with uncertainty analysis that at least superficially includes the effect of systematic errors on the uncertainty of identified dynamic coefficients.

2.3.1 Experiments with No Uncertainty Analysis

The publications listed in 2.3.1 experimentally identify TPJB dynamic coefficients but do not analyze uncertainty. The test rigs used for the identification varied significantly between the groups that published these papers and without any uncertainty analysis, direct comparison of the accuracy of identification is not possible. A comprehensive uncertainty analysis - including both the effect of random errors and systematic errors -

would allow the comparison of the accuracy and precision of identified coefficients between experiments.

Table 2.3.1: Experimentally Identified TPJB Coefficients Without Uncertainty Analysis

	Year	Authors	Title
[33]	1956	Hagg, AC; Sankey, GO	Some dynamic properties of oil-film journal bearings with reference to the unbalance vibration of rotors
[34]	1972	Glienicke, J.; Han, D. C.; Leonhard, M.	Practical determination and use of bearing dynamic coefficients
[35]	1980	Hisa, S; Matsuura, T; Someya, T	Experiments on the dynamic characteristics of large scale journal bearings
[36]	1997	Reddy, D Sudheer Kumar; Swarnamami, S; Prabhu, BS	Experimental investigation on the performance characteristics of tilting pad journal bearings for small LD ratios
[37]	1999	Ha, Hyun Cheon; Yang, Seong Heon	Excitation frequency effects on the stiffness and damping coefficients of a five-pad tilting pad journal bearing
[38]	2013	Kukla, Sebastian; Hagemann, Thomas; Schwarze, Hubert	Measurement and Prediction of the Dynamic Characteristics of a Large Turbine Tilting-Pad Bearing Under High Circumferential Speeds
[39]	2015	Chatterton, Steven; Pennacchi, Paolo; Dang, Phuoc Vinh; Vania, Andrea	Identification dynamic force coefficients of a five-pad tilting-pad journal bearing
[40]	2015	Dang, Phuoc Vinh; Chatterton, Steven; Pennacchi, Paolo; Vania, Andrea; Cangioli, Filippo	Behavior of a tilting-pad journal bearing with different load directions
[41]	2016	Dang, Phuoc V.; Chatterton, Steven; Pennacchi, Paolo; Vania, Andrea	Effect of the load direction on non-nominal five-pad tilting-pad journal bearings

Hagg and Sankey [33] identified dynamic coefficients of a 150-degree partial arc bearing and a 4-pad tilting-pad journal bearing. The experiments were performed on the test rig shown in Figure 2.9. Forces were applied on the rotor using a known unbalance. The vertical orientation of the system is atypical. A comprehensive uncertainty analysis would be able to estimate the impact of dynamics such as the effect of the motor unbalance on the identified dynamic coefficients' accuracy.

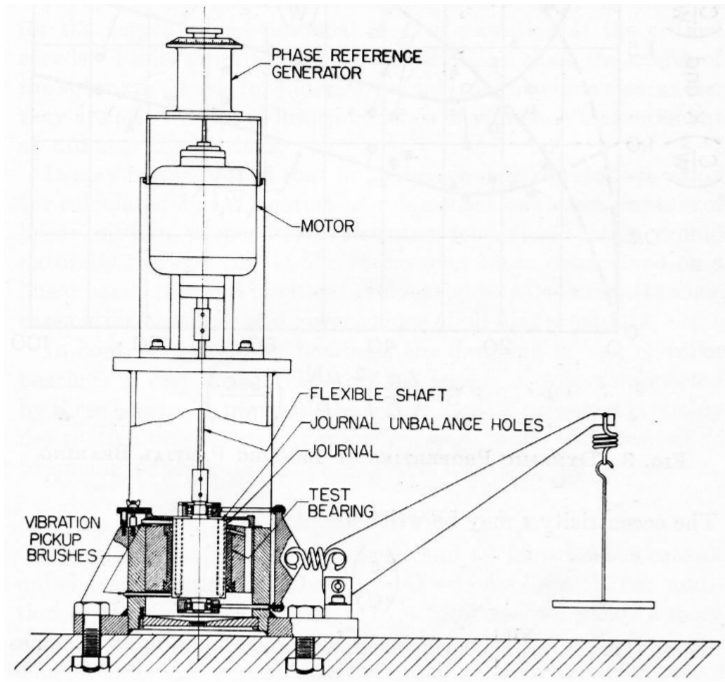

Figure 2.9: Diagram of Hagg and Sankey test rig reproduced from [33]

Reddy et al. [36] identified performance characteristics and dynamic coefficients of a TPJB. The test rig resembled a Jeffcott rotor with a ball-bearing on one side and the test bearing on the other end as seen in Figure 2.10. A non-contact electromagnetic actuator applied test forces to

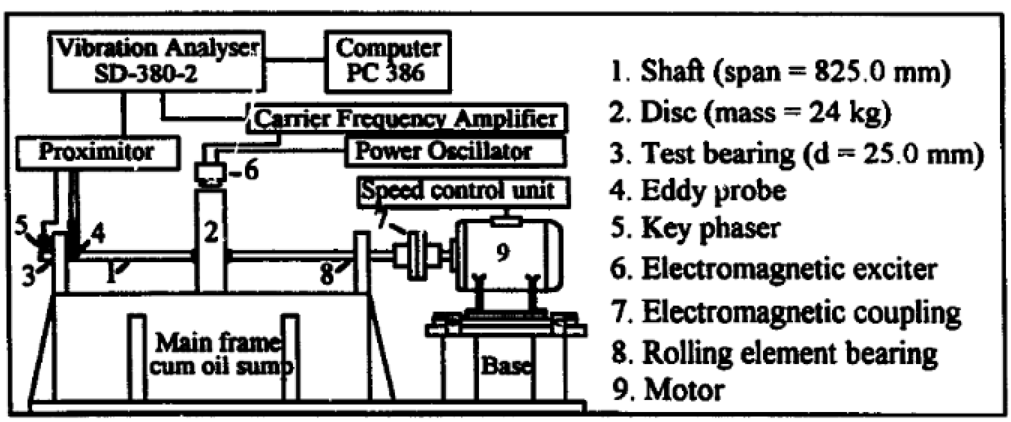

Figure 2.10: Diagram of Reddy et al. test rig reproduced from [36]

the mass at the center of the rotor. In this configuration, the measurements would be affected by the dynamics of the ball bearing and the rotor in addition to the TPJB. Following the process set up in Arumugam et al. [42], the non-TPJB dynamics of the system were accounted for by using a finite element model which included models of the test setup's ball bearing and rotor. The finite element models will have some errors relative to the true physical system. The errors may contribute significantly to coefficient identification uncertainty and a comprehensive uncertainty analysis would provide data to help make evaluate the impact.

Glienicke et al. [34] investigated the dynamic coefficients of 4 types of bearings including a 4-pad TPJB. Only damping results are presented however. In addition to the experimental results, theoretical investigations of factors affecting important bearing properties are presented. With respect to the dynamic coefficients, no uncertainty analysis is presented.

Hisa et al. [35], Ha & Yang [37], and Kukla et al. [38] used similar test rigs to identify TPJB dynamic coefficients. Depictions of the test rigs can be seen in Figure 2.11.

In these experiments, pneumatic bellows provided static loading. Each experiment applied the dynamic excitation differently to the bearing housing. Hisa et al. used pneumatic bellows, Ha & Yang used hydraulic actuators, and Kukla et al. used a set of vibration generators comprised of two pairs of imbalanced shafts supported in a massive housing. In each rig the two actuators were connected to the bearing housing in two orthogonal directions.

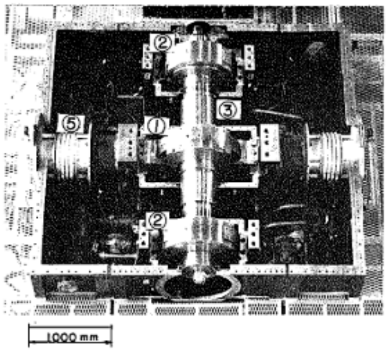

(a) Hisa et al. [35]

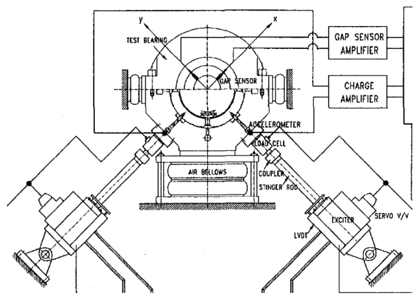

(b) Ha & Yang [37]

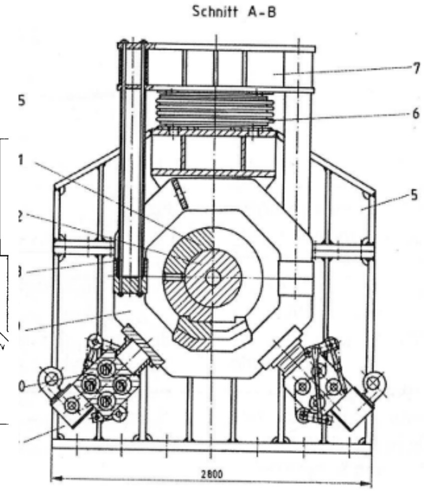

(c) Kukla et al. [38]

(c)

Figure 2.11: Similarly Designed Test Rigs

Dang et al. [40] [41] present two studies for TPJBs investigating the effect of load direction on bearing performance and dynamic coefficients. The test rig used by Dang et al. differs from the others discussed so far by having two TPJBs used in the experiment as seen in Figure 2.12. Furthermore, rather than measuring the applied force, the force measured by the load cells attached to the bearing housings were used as an estimate of the hydrodynamic force generated within the bearing. Section 3.1.5 shows that under some conditions, measurements of hydrodynamic force can reduce identification uncertainty. However, the extent to which it might reduce uncertainty must be carefully analyzed with a comprehensive uncertainty analysis. Furthermore, the effect of having another fluid-film bearing in the system and any methods of compensating for additional dynamics would also have to be evaluated.

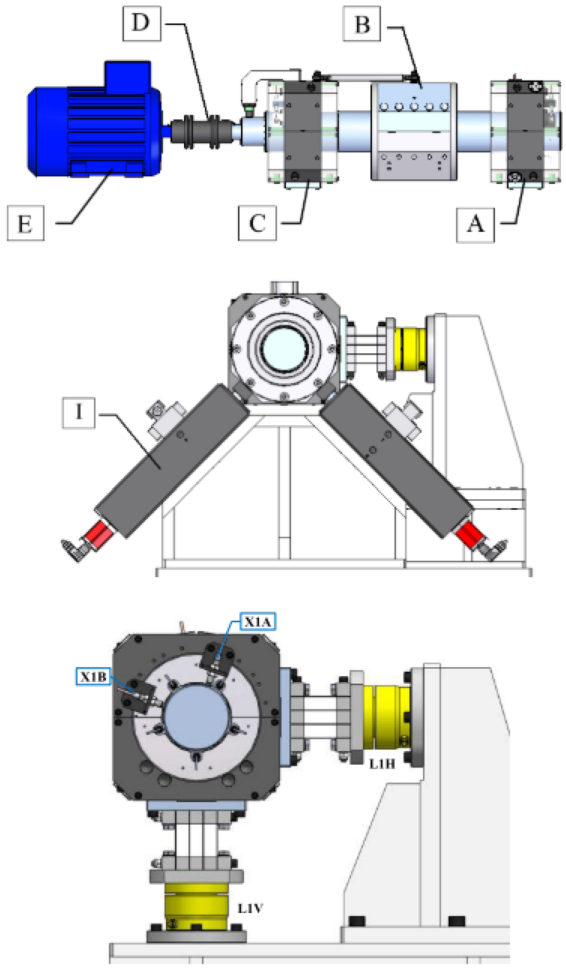

Figure 2.12: Diagram of Dang et al. test rig reproduced from [40]

Summary of Publications with No Uncertainty Analysis

The published literature in this section cover several distinct types of test rigs. Without uncertainty analysis, the confidence in the results cannot be estimated. Furthermore, consistent uncertainty analysis would allow comparisons between the capabilities of the test rigs. Due to the differences in mechanical design and component selection, even similar concepts such as Hisa et al., Ha & Yang, and Kukla et al. will have different uncertainties in the identified coefficients operating at the same conditions. This means each test rig could have operating conditions in which they are more accurate than the other test rigs and operating conditions in which they are less accurate than other test rigs. A comprehensive uncertainty analysis is required to properly understand the relative capabilities of the test rigs with respect to identified dynamic coefficient uncertainty.

2.3.2 Experimental Uncertainty Analysis Only Including Random Errors

The publications listed in Table 2.3.2 analyze one component of the total uncertainty when identifying dynamic coefficients of TPJBs: uncertainty from random errors. Analyzing the uncertainty from random errors will estimate the repeatability of the results presented. Without an analysis of the uncertainty from systematic errors, there is no estimate of how the identified coefficients may compare to the true values especially as a result of unmodeled dynamics. The results may capture the TPJB dynamic coefficients well or the identified coefficients may be inaccurate. This cannot be differentiated by only analyzing the repeatability or other similar statistical measure associated only with random errors.

Table 2.3.2: Experimentally Identified TPJB Dynamic Coefficients With Uncertainty Only Including Random Errors

	Year	Authors	Title
[42]	1994	Arumugam, P; Swarnamami, S; Prabhu, BS	Experimental identification of linearized oil film coefficients of cylindrical and tilting pad bearings
[43]	2006	Rodriguez, Luis E; Childs, Dara W	Frequency Dependency of Measured and Predicted Rotordynamic Coefficients for a Load-on-Pad Flexible-Pivot Tilting-Pad Bearing
[44]	2006	Al-Ghasem, Adnan M; Childs, Dara W	Rotordynamic Coefficients Measurements Versus Predictions for a High-Speed Flexure-Pivot Tilting-Pad Bearing (Load-Between-Pad Configuration)
[45]	2006	Hensley, Eric	Rotordynamic Coefficients for a Load-Between-Pad , Flexible-Pivot Tilting Pad Bearing At High Loads
[46] ([47])	2009	Childs, Dara W; Harris, Joel	Static Performance Characteristics and Rotordynamic Coefficients for a Four-Pad Ball-in-Socket Tilting Pad Journal Bearing
[48]	2011	Delgado, Adolfo; Vannini, Giuseppe; Ertas, Bugra; Drexel, Michael; Naldi, Lorenzo	Identification and Prediction of Force Coefficients in a Five-Pad and Four-Pad Tilting Pad Bearing for Load-on-Pad and Load-Between-Pad Configurations
[49]	2012	Kulhanek, Chris D; Childs, Dara W	Measured Static and Rotordynamic Coefficient Results for a Rocker-Pivot, Tilting-Pad Bearing With 50 and 60% Offsets
[50]	2011	Childs, Dara W.;	Tilting-pad bearings: measured frequency characteristics of their rotordynamic coefficients
[51]	2011	Childs, Dara W.; Carter, C.	Rotordynamic Characteristics of a Five Pad, Rocker-Pivot, Tilting Pad Bearing in a Load-on-Pad Configuration; Comparisons to Predictions and Load-Between-Pad Results
[52]	2012	Kulhanek, Chris. D.	Dynamic and Static Characteristics of a Rocker- Pivot , Tilting-Pad Bearing With 50 % and 60 % Offsets Dynamic and Static Characteristics of a Rocker- Pivot , Tilting-Pad Bearing With 50 % and 60 % Offsets
[53]	2012	Delgado, Adolfo; Libraschi, Mirko; Vannini, Giuseppe	Dynamic characterization of tilting pad journal bearings from component and system level testing
[54]	2013	Wilkes, Jason C. & Childs, Dara W.	Improving Tilting-Pad Journal Bearing Predictions-Part II: Comparison of Measured and Predicted Rotor-Pad Transfer Functions for a Rocker-Pivot Tilting-Pad Journal Bearing
[55]	2014	Coghlan, David M.	Static, Rotordynamic, and Thermal Characteristics of a Four Pad Spherical-Seat Tilting Pad Journal Bearing with Four Methods of Directed Lubrication
[56]	2014	Tschoepe, David Patrick	Measurements versus predictions for the static and dynamic characteristics of a four-pad, rocker-pivot, tilting-pad journal bearing
[57]	2016	Gaines, Jennifer E & Childs, Dara W	The Impact of Pad Flexibility on the Rotordynamic Coefficients of Tilting-Pad Journal Bearings
[58]	2017	Coghlan, David M; Childs, Dara W	Characteristics of a Spherical Seat TPJB With Four Methods of Directed Lubrication—Part II: Rotordynamic Performance

Arumugam et al. [42] state that "the identification algorithm presented here [in the paper] can identify the bearing coefficients exactly, if the FRFs [frequency response functions] are free from noise." To evaluate this, a simulation study is performed with random noise added. One of the implications of this simulation study's results is that smaller parameters being identified (i.e. - smaller stiffness or damping values) may have larger errors. There is an investigation of the effect of fluid inertia on the identification but a variational study is not performed. Only a single case of inertia is simulated. On the experimental side, one of the results presented (shown in Figure 2.13) compares frequency response functions (FRFs) including the identified bearing model in finite element analysis of the rotor-bearing system. The authors indicate that the comparison with measured response is "satisfactory" but there is no explanation for the discrepancy in the prediction versus the experimentally measured FRF at 750 rpm and 1250 rpm. It is possible the system is affected by the dynamics of some part of the test rig which could be increasing the uncertainty. In that case, the comparison may fall within the expected uncertainty bounds. On the other hand, the expected uncertainty may be small compared with the discrepancy between the prediction and measured FRF at 750 rpm and 1250 rpm. This would indicate some effect that is not captured in the model of the experiment. Either possibility is difficult to support without a comprehensive uncertainty analysis that includes the contributions of systematic errors and dynamics of the system.

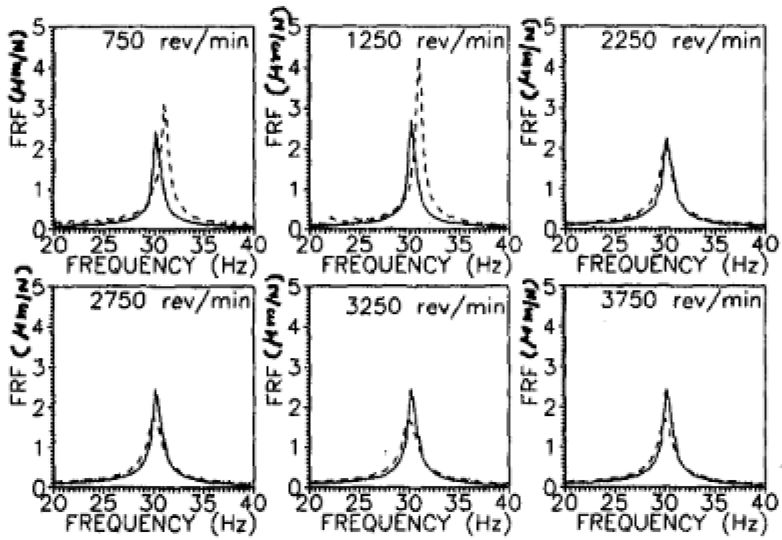

Figure 2.13: FRF results from Arumugam et al.[42]

Delgado et al. [48] identify TPJB coefficients and present results with uncertainty values. One major drawback to the results is that the method of computing the uncertainty is not presented. Due to the similarity of the identification method and the contents of the results (e.g. - including mass matrix), it is assumed that the uncertainty computation is similar to the uncertainty computations in the remaining publications.

Besides Arumugam et al. [42] and Delgado et al. [48], the remaining publications all contain experimental results on TPJBs performed at the same research facility. The test rig used for these studies is shown in Figure 2.14.

The analysis of uncertainty in these publications is consistently defined as the 95% confidence internal of the curve fit of the frequency response. This is used to place error bars on the identified results. In Rodriguez and Childs [43], the error bars from this method are explicitly stated to be "not uncertainties but are a measure of the reproducibility of the results." Therefore it is evident

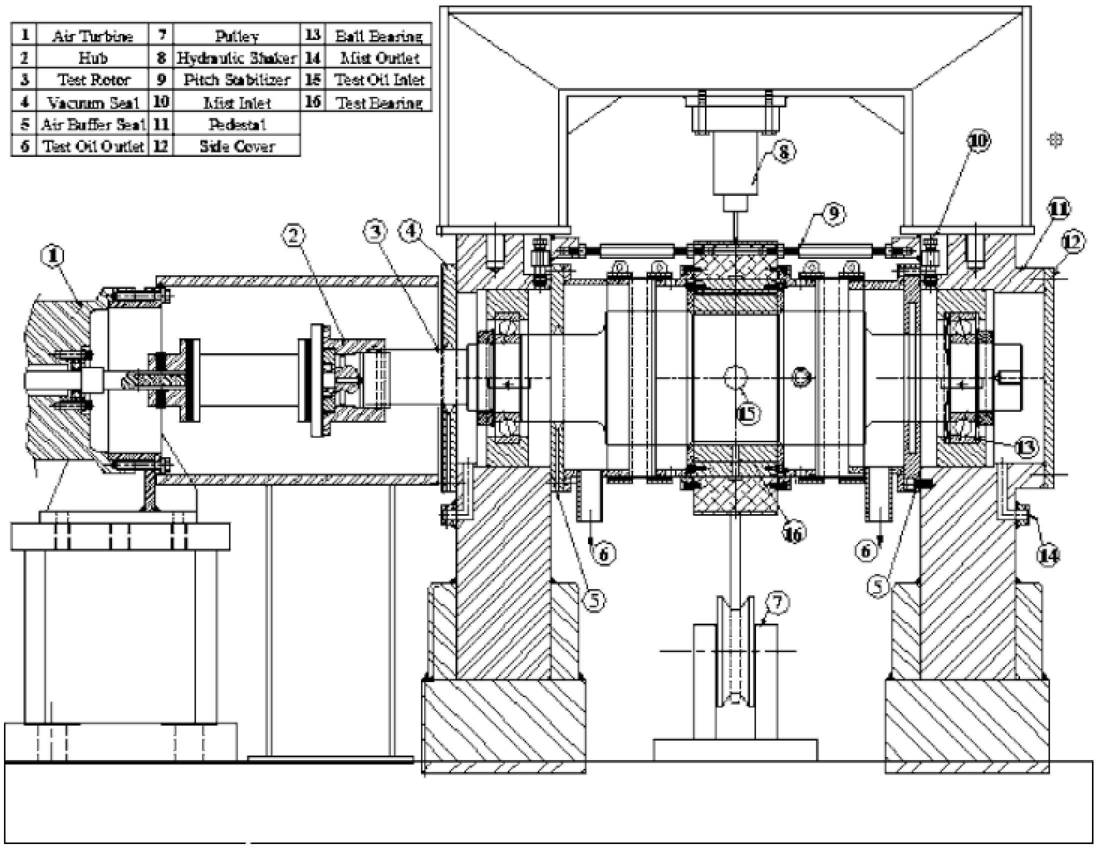

Figure 2.14: Diagram of test rig for remaining publications reproduced from [44]

that uncertainty from systematic error sources are not analyzed. The system's dynamics are considered, however, and it is clear that careful thought was put into the identification process. For example, "dry shakes" are performed to determine if pad dynamics are a significant influence [46]. This dissertation provides a guide for researchers and engineers to harmonize the quantification of uncertainty as a result of dynamics in the system - including when the dynamics are not a significant contributor to the uncertainty. Childs and Harris [46] state that they "see no evidence in our tests that the relative pad motion has any perceptible influence on housing acceleration measurements" but without a quantified estimate of the effect on uncertainty, the reader cannot evaluate the significance of the impact on identification uncertainty from a small effect on the acceleration measurement.

Summary of Publications With Experimental Uncertainty Analysis Only Including Random Errors

While it is good that uncertainty analysis is included, there are unaddressed challenges with the uncertainty analysis when only random errors are included. For example, in the Arumugam et al. work, the results may repeatably identify dynamic coefficients that are different from the theoretical models and/or actual bearing coefficients. There was no method used for estimating if the differences may fall within expected bounds or if the differences indicate an issue that should be addressed. The “dry shakes” discussed are another example of effects that are not captured well with repeatability. A comprehensive uncertainty analysis should 1) quantify the effect to determine if it is expected to be large or small and 2) allow for understanding how the effect is affected by operating conditions.

Another challenge is the lack of consistency in uncertainty analysis method. The uncertainty presented in one publication may not be compared directly with another if the analysis is performed differently.

The uncertainty analysis framework developed in this dissertation in Chapters 3 and 4 will address both of these challenges.

2.3.3 Experimental Uncertainty Analysis Including Random and Systematic Errors

Literature is considered to include systematic errors if they explicitly reference elemental uncertainties and state that uncertainty was computed with the referenced values. For example, computing coefficient uncertainty using uncertainties of sensors that are associated with systematic errors would place the publication in this category. However, the method of calculating the uncertainty may not completely incorporate the effect of systematic errors on the uncertainty. The literature in this section will have the uncertainty analysis method carefully evaluated to determine how the final uncertainty values presented include uncertainty from systematic error. One such check will be to determine if differences in system dynamics between would have an effect on the uncertainty. If this would not have an effect, then the uncertainty analysis is deemed to not properly account for systematic errors. An example of dynamics to consider is the rotor's flexibility. Variations in rotor model would lead to variations in system critical frequencies, which would affect how sensitive the test rig is to bearing dynamics around those frequencies. Though an experiment may not be investigating the affected frequencies, the uncertainty analysis method must be able to account for those effects in theory.

Table 2.3.3 presents all the publications considered in this section together in one chart. The review of the publications is grouped by test rig.

Table 2.3.3: Publications That May Analyze Uncertainty Comprehensively

	Year	Authors	Title
[59]	1999	Pettinato, Brian; De Choudhury, Pranabesh	Test results of key and spherical pivot five-shoe tilt pad journal bearings—part II: dynamic measurements
[60]	1999	Wygant, Karl D; Barrett, Lloyd E; Flack, Ronald D	Influence of Pad Pivot Friction on Tilting-Pad Journal Bearing Measurements - Part II: Dynamic Coefficients
[61]	2004	Wygant, Karl D; Flack, Ronald D; Barrett, Lloyd, E	Measured Performance of Tilting-Pad Journal Bearings over a Range of Preloads-Part II: Dynamic Operating Conditions
[62]	2006	Dmochowski, W. M.; Blair, B.	Effect of oil evacuation on the static and dynamic properties of tilting pad journal bearings
[63]	2006	Flack, Ronald D; Wygant, Karl D; Barrett, Lloyd, E	Measured Dynamic Performance of a Tilting Pad Journal Bearing over a Range of Forcing Frequencies
[64]	2007	Dmochowski, Waldemar	Dynamic Properties of Tilting-Pad Journal Bearings: Experimental and Theoretical Investigation of Frequency Effects due to Pivot Flexibility
[65]	2014	Simmons, Gregory F; Varela, Alejandro Cerda; Santos, Ilmar Ferriera; Glavatskih, Sergei	Dynamic characteristics of polymer faced tilting pad journal bearings
[66]	2018	Ciulli, Enrico; Forte, Paola; Libraschi, Mirko; Naldi, Lorenzo, Nuti, Matteo	Characterization of High-Power Turbomachinery Tilting Pad Journal Bearings: First Results Obtained on a Novel Test Bench

Pettinato et al. [59]

Pettinato et al. [59] compared the performance of five-pad TPJBs with key seat pivots and five-pad TPJBs with spherical seat pivots. The test rig (shown in Figure 2.15) is described in detail in a previous paper by Pettinato et al. [67]. A rotor supported by a main bearing and a test bearing is connected to a motor. A third partial arc hydrostatic bearing transmits forces from a loading system to the rotor. The test bearing is at the opposite end of the coupling to the motor and has an unbalance plane outboard of the bearing to apply unbalance forces.

Stiffness coefficients were identified first and then used to identify

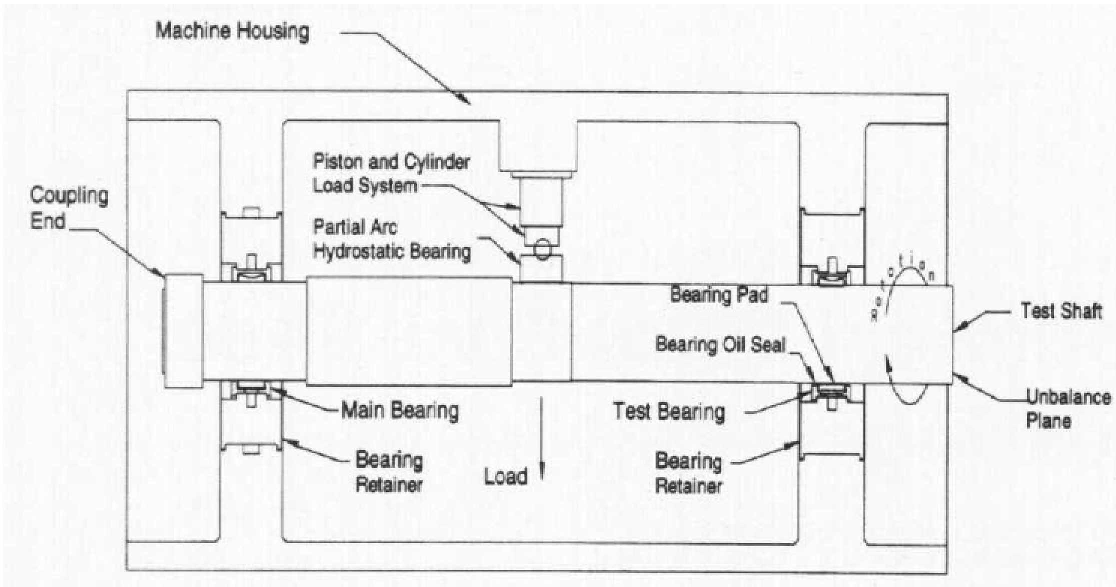

Figure 2.15: Diagram of Pettinato et al. test rig reproduced from [67]

damping. The vertical stiffness coefficient was derived using the eccentricity ratio and Sommerfeld number. The horizontal stiffness coefficient was measured by applying a horizontal force and measuring the resulting displacement. Damping was determined by iterating damping values until predicted values matched the measured vibration data. The previously identified stiffness values were used for these iterations. An additional parameter, radial pivot stiffness, was also measured by loading the shaft in a newly installed bearing without oil present.

Uncertainty was "calculated for a 95 percent confidence by either a least squares method or statistically." Some of the measurement uncertainties are presented in Figure 2.16. The stated uncertainties in vertical stiffness are "typically ±10%" and horizontal stiffness are "typically ±25%". For damping, uncertainties were "typically on the order of ±35%, but sometimes ranged as high as ±100%".

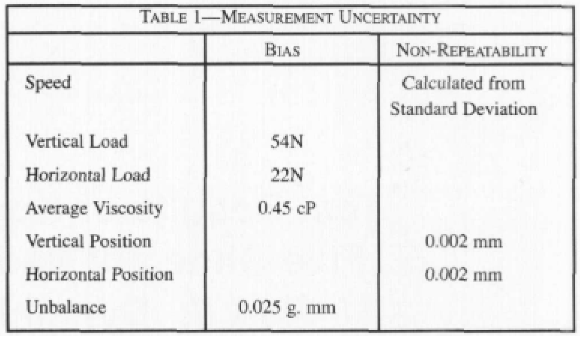

TABLE 1—MEASUREMENT UNCERTAINTY		
	BIAS	NON-REPEATABILITY
Speed		Calculated from Standard Deviation
Vertical Load	54N	
Horizontal Load	22N	
Average Viscosity	0.45 cP	
Vertical Position		0.002 mm
Horizontal Position		0.002 mm
Unbalance	0.025 g. mm	

Figure 2.16: Table of factors used to compute uncertainty reproduced from [59]

For the vertical stiffness, after the data points are gathered, the variance in curve fit coefficients of many fits sorted by F-statistic are used to estimate uncertainty. This is ultimately a measure of repeatability and cannot estimate the effect of systematic errors. Presumably this is the method that computed uncertainty "statistically." The other method using a least squares method is not explicitly defined. A content review of one of the sources [68] suggests that References (8) (9) in Pettinato et al. focus on statistical analyses. Reference (8) in Pettinato et al. is an older version of a book by Ernest Doebelin [69]. In this particular book there is a section on uncertainty that includes detailed discussion of computing total uncertainty. There are two formulations for estimating the final accuracy based on the available information. If the elemental uncertainties (such as measurement error) is given as absolute limits of error, then the total uncertainty in absolute terms can be estimated as given in Equation (3.32) in Doebelin

[69]:

$$|\Delta u_1 \frac{\partial f}{\partial u_1}| + |\Delta u_2 \frac{\partial f}{\partial u_2}| + ... + |\Delta u_n \frac{\partial f}{\partial u_n}| \tag{2.3}$$

In the case that the elemental uncertainties are not limits of error but rather statistical bounds, the total uncertainty formulation changes to:

$$\sqrt{\left(\Delta u_1 \frac{\partial f}{\partial u_1}\right)^2 + \left(\Delta u_2 \frac{\partial f}{\partial u_2}\right)^2 + ... + \left(\Delta u_n \frac{\partial f}{\partial u_n}\right)^2} \tag{2.4}$$

The referenced resources and Figure 2.16 strongly suggest that sources of uncertainty from systematic errors are considered. However, the method of combining the uncertainties cannot include all possible systematic sources of uncertainty. For example, though the rotor may be relatively stiff compared to the bearing, it is not fully rigid. As shown in Section 3.3, when the measurement model does not include the rotor flexibility, the coefficients can still be affected even if the rotor is extremely rigid. This is especially true for damping. The effect is typically a bias or offset. If some quantification of rotor flexibility effect was included in Equations 2.3 or 2.4 directly, the result would suggest a range of uncertainty rather than a bias. Some other considerations that are not captured in the analysis would be the effects of other components attached to the shaft such as the main bearing, the partial arc bearing where static loading was applied, and the coupling to the motor.

The uncertainty analysis presented in this paper used a method of computing uncertainty that would not be suitable for including the effect of various dynamics that may affect the coefficient identification, especially for a high performance bearing (e.g. - high loads and/or high speed).

Wygant et al. [60] [61] and Flack et al. [63]

Wygant, Flack, & Barrett performed three experiments identifying TPJB dynamic coefficients focusing on the effect of two different factors. The first experiment [60] investigated the differences in TPJB dynamic coefficients between two types of pivots (spherical seated ball with socket pad pivots and line contact rocker-back pad pivots). The second experiment [61] investigated the effect of pad preload on TPJB dynamic coefficients. The third experiment [63] measured dynamic coefficients over a range of forcing frequencies including frequencies not equal to the rotating speed. These three experiments were performed on the test rig shown in Figure 2.17.

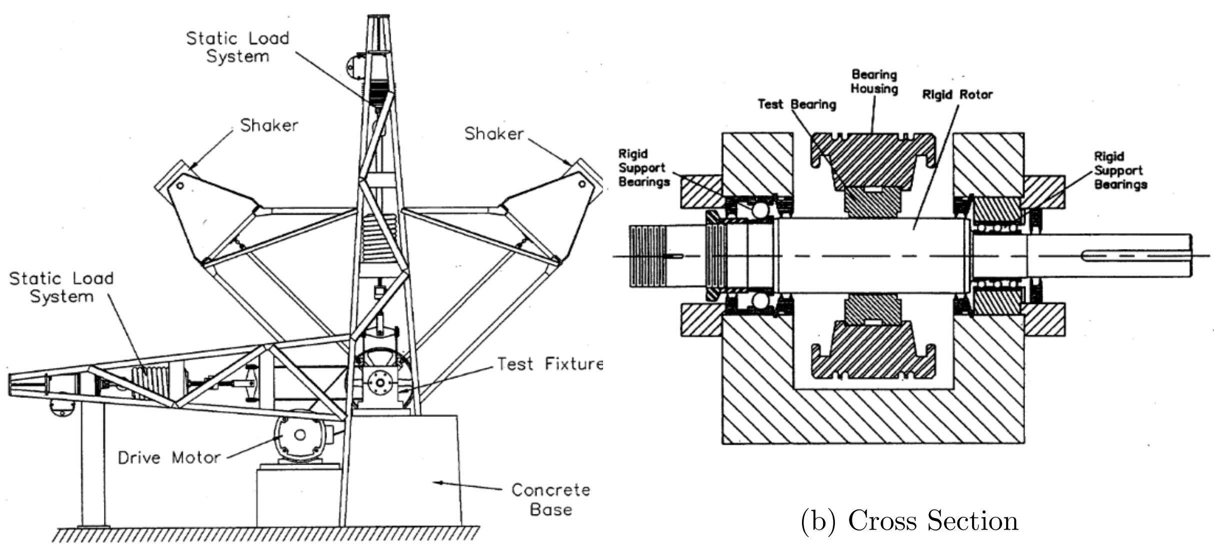

(b) Cross Section

y

(a) Test Rig Overview

Figure 2.17: Test Rig used by Wygant et al. reproduced from [70]

The test rig is comprised of a test bearing housed in a floating stator that has shakers connected to it for dynamic loading. A static loading mechanism is also connected via a soft spring to minimize the impact on dynamics while loading the bearing to the testing point. The rotor is designed to be rigid relative to the test bearing and is held by rolling element bearings on either side of the test bearing. The test rotor is driven by a motor connected via belt-and-pulley system.

The method for computing the uncertainty presented for dynamic coefficients identified in these experiments is described in Kostrzewsky & Flack [71]. This method is simulation-based and begins by selecting a set of coefficients for the truth model. This would typically be based on bearing operating conditions such as shaft speed, static load, clearance, etc. Once the bearing's truth model stiffness and damping are determined, the response to dynamic excitation is computed. The dynamic excitation can be selected to generate a specific response so long as there are two sets of linearly independent excitations defined. At this point if the force data and response data are used to identify the bearing coefficients, the truth model is obtained again. The elemental uncertainties affecting the identification are identified and these can be applied to the force and displacement data generated with the truth model. The perturbed data is used to identify coefficients that are different from truth. By varying each uncertainty individually, the coefficient uncertainty from each elemental uncertainty can be computed. The total uncertainty is a root-mean-square summation of the individual contributions.

The root-mean-square combination of the individual contributions of each uncertainty is similar to the method described in Doebelin [69]. The main difference is that Kostrzewsky & Flack are simulating the identification with each individual uncertainty varied to determine the contribution to the total uncertainty. The simulation is key, as the truth values for a virtual bearing can be placed within models of the rotor, housing, foundation, and other interacting systems of the test rig. Furthermore, since the simulation includes a model of the identification scheme, that aspect can also be evaluated to see if it contributes to uncertainty. Kostrzewsky & Flack were able to use this technique to determine the best points in each orbit for data measurement.

One notable drawback is the root-mean-square combination of uncertainty. This combination of elemental uncertainty is not suitable for including any biases or offsets from systematic effects such as rotor flexibility. While the simulation method of analyzing uncertainty can, in principle, account for dynamics such as rotor flexibility, the combination of contributions to uncertainty needs to be adjusted to properly account for biases in identified coefficients.

This method of uncertainty analysis used by Wygant et al. [60] [61] and Flack et al. [63] is well-suited for comprehensive uncertainty analysis if a different method of pulling together the contributions to uncertainty can be used and the results presented properly. The framework developed in this dissertation will address this.

Dmochowski & Blair [62] and Dmochowski [64]

Dmochowski & Blair [62] investigated how stiffness and damping properties of TPJBs are affected by oil evacuation. Dmochowski [64] investigated how pivot stiffness affects the dynamic coefficients of TPJBs. These studies were performed on the test rig shown in Figure 2.18. A rotating shaft (1) supported by high-precision, angular contact ball bearings. The test-bearing stator is excited with two orthogonal electromagnetic shakers (3 & 4) attached with a steel rod and flexible element assembly (5) to minimize the impact on the lateral motion of the bearing stator. A static load is applied through a tensioned cable (6) connected via soft springs (7) to minimize the variation of static loading due to the bearing vibration.

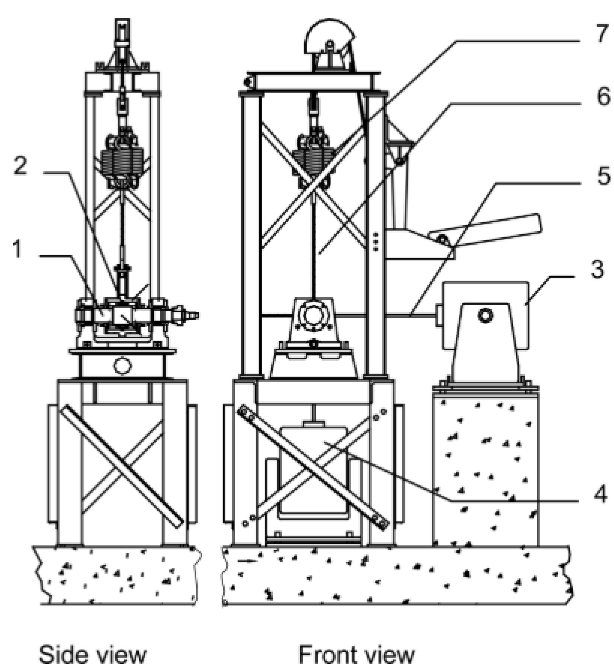

Figure 2.18: Diagram of test rig reproduced from Dmochowski and Blair [62]

The uncertainty for these two experiments are computed using "Type B" analysis specified by an edition of the GUM [72]. The elemental uncertainties shown in Figure 2.19 for Dmochowski & Blair [62] and Dmochowski [64] states the elemental uncertainties in the text: 2.5 micrometers (0.0001 in) for displacement and 0.01 g for acceleration. Though the studies were performed on the same test rig, the displacement uncertainty specified is different. The reason is not explicitly stated. It could be because the sensors used in the studies are different or different information from the sensor specification were used to compute the sensor uncertainty. An additional elemental uncertainty derived from the frequency domain identification method used in these experiments (power spectral density (PSD) method) is described in an appendix to Dmochowski & Blair [62]. Sensitivity coefficients estimating the partial fraction influence of each individual uncertainty on the identification are determined numerically by perturbing a small increment of the cross-spectral density and observing the resulting change in the frequency response function. One of the assumptions in calculating the uncertainty of the PSD method is that "the measurement of the dynamic excitation is error free." Furthermore, this assumption is "consistent with the assumption made for the PSD method." In other words, both the identification and the calculation of elemental uncertainty assume there is no measurement error for the dynamic excitation.

While the "Type B" analysis as described in the GUM does not

TABLE 3—MEASUREMENT UNCERTAINTIES

Measurement	Type of sensor	Limit of error of sensor
Temperature	Type T thermocouple	1°C or 0.75% (whichever is greater)
Shaft speed	Optical switch	±5 rpm
Bearing load	Load cell	±25 N at full scale
Excitation force	Load cell	±20 N
Oil flow	Turbine flow meter	±0.5%
Displacement	Eddy current probe	±0.003 mm
Acceleration	Piezoelectric accelerometer	0.01 g

Figure 2.19: Table of factors used to compute uncertainty reproduced from [62]

inherently capture the effects of systematic errors comprehensively, the analysis performed in these experiments can arguably determine the impact of some forms of systematic error. The main drawback is that unlike the method by Kostrzewsky and Flack [71], a true value is not available. Dmochowski and Blair's uncertainty analysis method [62] can thus estimate the effect of uncertainty on the identified transfer function but not offer insight into the uncertainty relative to the true value. The techniques developed can be used to complement the uncertainty analysis proposed in this dissertation but do not provide a comprehensive look at the impact of errors on identification uncertainty.

Simmons et al. [65]

Simmons et al. [65] included measurement uncertainty in temperature, static load, dynamic load, and displacement as sources of uncertainty in dynamic coefficients of various tilting-pad journal bearings with polymer-faced pads. As part of the data analysis, coherence between the dynamic force and pad displacement are plotted.

The test rig used for this experimental study is shown in Figure 2.20. The force application mechanism is different from most other rigs for dynamic coefficient identification.

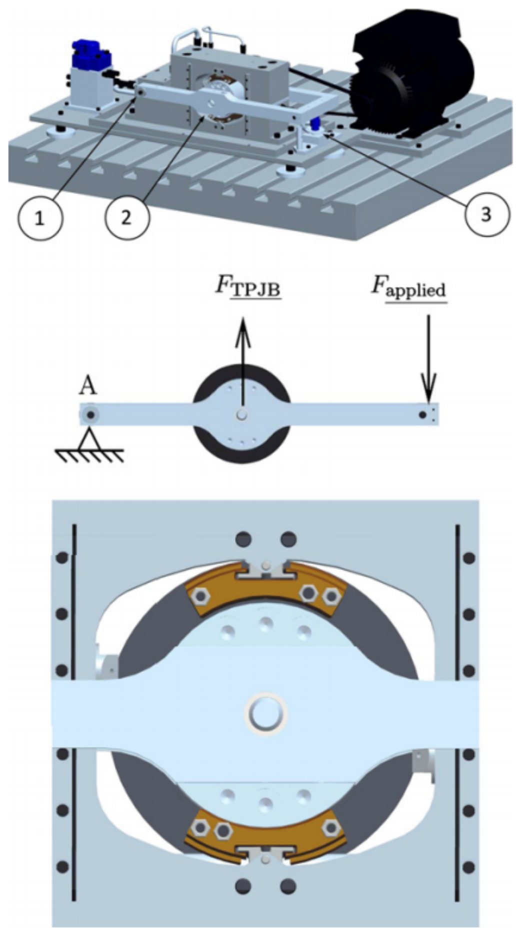

Figure 2.20: Image of test rig reproduced from Varela et al. [73]

While sources of uncertainty from systematic errors are stated and discussed, they are not addressed further in an estimate of uncertainty for dynamic coefficients. Some of the results have a band for the coefficients identified (see Figure 2.21) but this band is just a representation of the effect of repeatability on the system computed after 3 trials.

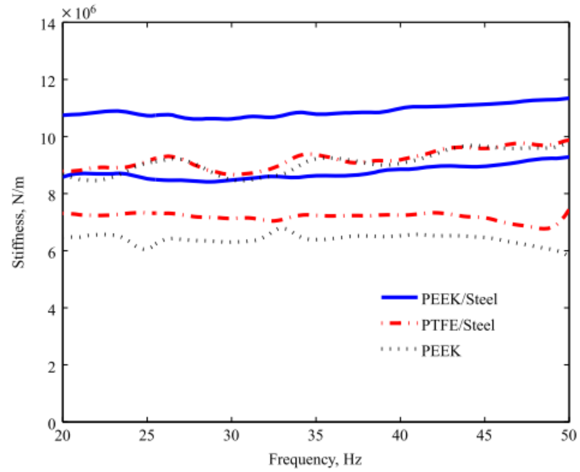

Figure 2.21: Results from Simmons et al. [65] showing an uncertainty band

The inclusion of uncertainty as a function of frequency is something that this dissertation will show to be important in properly presenting the uncertainty of dynamic coefficients. However, beyond that, the uncertainty analysis in this publication does not address uncertainty from systematic sources in any way.

Ciulli et al. [66]

Ciulli et al. [66] referenced a calculation of uncertainty that is further described in Forte et al. [74]. The test rig for this experiment is shown in Figure 2.22.

The test rig is designed for TPJBs of diameters between 150 to 300 mm, journal surface speeds of 150 m/s, static loads up to 270 kN, dynamic loads up to 30 kN, and test frequencies up to 350 kHz. The test rig can be classified as an excited housing test rig with the shaft held with roller bearings. The housing has three anti-pitch rods to constrain the rotor to

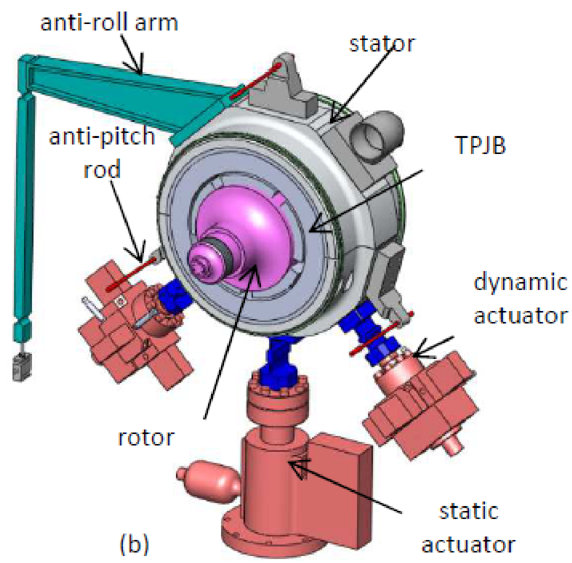

Figure 2.22: Image of test rig reproduced from Forte et al. [74]

only the plane perpendicular to the rotor axis. The static load is applied by a hydraulic actuator deemed compliant enough to not interfere with the dynamic actuators. The dynamic load is also applied by hydraulic actuators which were selected for higher load capacity. The dynamic coefficients are identified by measuring the applied force through the dynamic actuators, acceleration of the bearing housing to use for inertial compensation, and proximity measurements measuring the relative displacements of the shaft and the bearing.

The uncertainty analysis in Ciulli et al. with the details traced back to Forte et al. account for dynamics of the system. Models of each of the components of the system - rotor, bearings, load cells, stator, actuators - were developed and a dynamic simulation was created. The linked dynamic systems represented a truth model and coefficients are identified with a mathematical model that assumes an ideal rigid stator and ideal rolling element bearings. Three levels of fidelity are analyzed leading to the results presented in Figure 2.23.

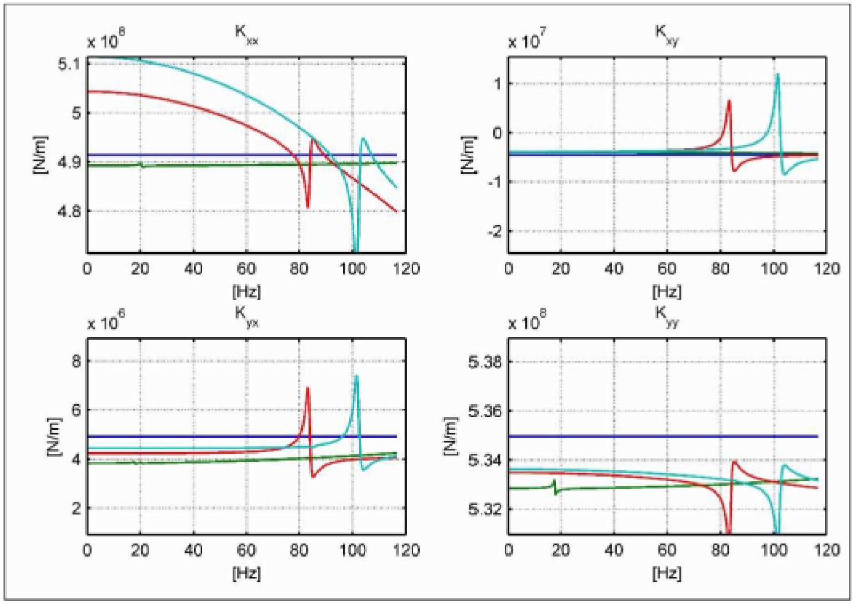

Figure 2.23: Uncertainty from systematic errors reproduced from Forte et al. [74]

The methodology used to develop these results were also used to analyze the effects of noise as seen in Figure 2.24.

It should be pointed out that the uncertainty from random errors noted here is just for one trial and that multiple trials will reduce the uncertainty by “an order of magnitude.”

The techniques used to perform this uncertainty analysis are along the lines of the framework presented in this dissertation. However, there are significant elements not analyzed. For example, there are no models of measurement error. It is possible that in Ciulli et al. [66] they are considered but no details are provided. Part of the goal of this dissertation in presenting an

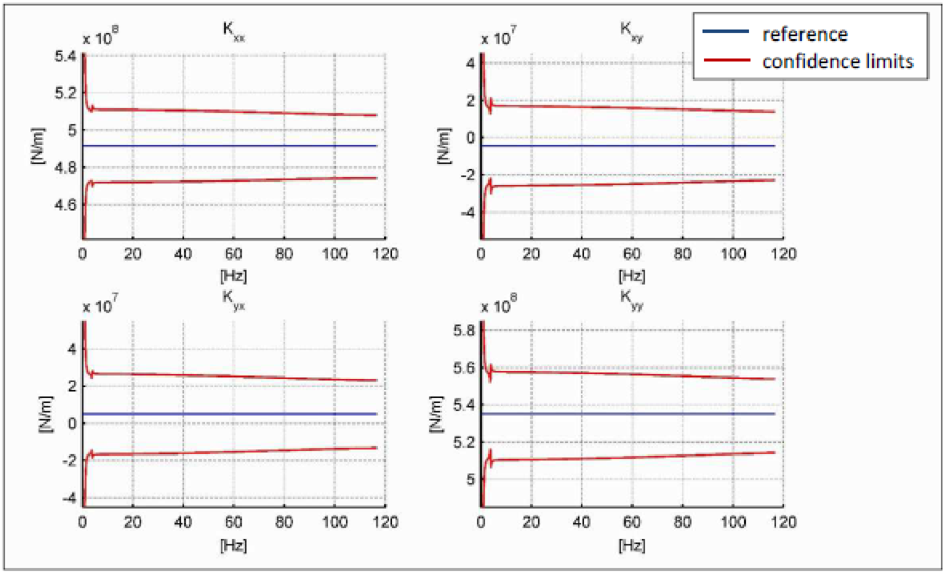

Figure 2.24: Uncertainty from random errors reproduced from Forte et al. [74]

uncertainty analysis framework will include guidance on a minimum level of detail and a standardized method of presenting the results.

Summary of Publications That Consider Systematic Errors

While a few sources of systematic errors are presented in the publications of this section, the uncertainty analysis typically fails to properly translate the sources of systematic errors to uncertainty in identified dynamic coefficients. Wygant et al. [60] [61], Flack et al. [63] used a simulation method of estimating uncertainty that is suitable for comprehensive uncertainty analysis but the method used to combine uncertainty contributions is problematic. Ciulli et al. [66] and Forte et al. [74] also use a simulation method and consider model differences between truth and identification. Ultimately, their analysis proved to be incomplete without including factors such as measurement uncertainty. While their analysis helped determine which material to use for a housing, it did not further serve as an uncertainty analysis for the coefficient identification. The remaining publications in this section do not analyze uncertainty using methods compatible with a comprehensive uncertainty analysis.

Though the publications using a simulation method for uncertainty analysis are on the right track, the methods are still different enough that a direct comparison is not immediately possible. A single framework that researchers can reference would iron out details such as how to combine uncertainties as well as define the sources of uncertainty that must be included and how the choices should be presented. This will provide greater awareness of how experimental results can compare with each other. Meaningful comparisons will help advance the state-of-the-art of model validation for TPJB dynamic coefficients.

2.3.4 Conclusions from the Literature Review

The major conclusions and observations of this literature review are summarized here.

- Uncertainty analysis is not common when identifying TPJB dynamic coefficients. The Tiwari et al. review [21] suggests that uncertainty analysis is more generally not common as well. The lack of uncertainty analysis leads to two challenges: 1) the accuracy of a dynamic coefficient identification experiment is not estimated and 2) the capabilities of different dynamic coefficient identification experiments cannot be easily compared. Even on the same test rig, identifying the dynamic coefficients of a different TPJB can yield different uncertainties and this can't be considered without uncertainty analysis.

- When uncertainty analysis is performed, many analyses only look at uncertainty resulting from random error sources. This provides insight into repeatability but cannot be considered comprehensive because uncertainty from systematic error sources are not considered.

- Even when sources of uncertainty from systematic errors are considered, the uncertainty analysis method may not be broadly capable of handling all sources of uncertainty. For example, in the publications analyzed in this dissertation, when systematic errors are considered the analysis is often able to handle measurement error but cannot handle the systematic error resulting from modeling error relative to truth.

- Regardless of the sources of uncertainty considered, the uncertainty analysis methods were not consistent. Direct comparisons of uncertainty between experiments are therefore difficult because the uncertainty estimate can be different based on differences in uncertainty sources considered. During the literature review, there were some difficulties in determining what factors were used in the uncertainty analysis. Both of these issues go hand-in-hand and a unified framework that guides the selection of factors to consider as well as how to present the analysis will help researchers understand and compare the uncertainty of TPJB dynamic coefficient identification experiments.

- Though analytical methods may be available, the most comprehensive uncertainty analyses of the publications in this review used simulation-based uncertainty analysis. Further investigation suggested that simulation-based methods can include more complex models that may include non-linearities and other effects in an attempt to increase model fidelity. This guided the development of the framework to being a simulation-based method.

The framework developed in this dissertation will provide a common ground for researchers and engineers when thinking about TPJB dynamic coefficient identification (and dynamic coefficient identification for components in general).

Chapter 3

Defining the Uncertainty Analysis Framework with Single-Axis Models

A simulation-based uncertainty analysis framework is proposed for TPJB dynamic coefficient identification experiments. The framework compares a representation of an experiment's physics to a model used for identifying dynamic coefficients using measurements from the experiment. To begin with, a truth model must be established. The truth model seeks to capture as much of a system's dynamics as possible. Second, an identification model (or measurement model) is selected. The identification model is how the data measured from the experiment will be used to identify dynamic coefficients. If 1) the truth and the identification models are the same and 2) the input and output signals are the same for both models (i.e. - the true signals are measured without error for use in the identification model), then there is no uncertainty. Figure 3.1 provides a diagram of the truth model, identification model, and how they are related in the uncertainty analysis framework for

TPJB coefficient identification.

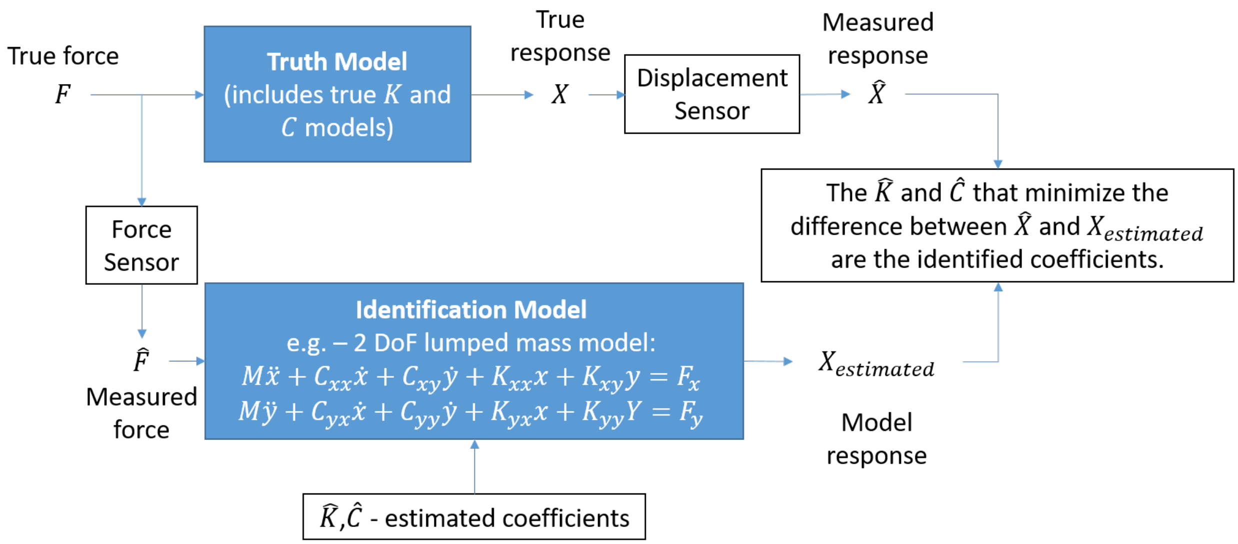

Figure 3.1: Schematic of Relationship Between Truth Model and Identification Model

In practice, the identification model will not match the real physics of the experiment. Since the truth model is designed to be as close as possible to the real physics, the identification model will typically also be different from the truth model. In cases where the identification model and the truth model contain the same elements (such as a substructure model or a rotor model), modeling uncertainty between the truth model and identification model should be included in the final uncertainty analysis. This will lead to differences in identified coefficients versus the true coefficients. Even if the identification and the truth model are the identical, models of measurement uncertainty will lead to differences between the true coefficients and the identified coefficients.

To perform a comprehensive uncertainty analysis of an experiment, the truth model should capture all significant dynamics affecting the experiment. Uncertainty analysis should be used to determine which dynamics are significant since the goal is to capture as much of the contributions to uncertainty as possible. As an example, consider a test rig where the rotor might be assumed rigid. This assumption is typically used when the rotor is expected to be much stiffer than any bearing tested. To determine the sensitivity of uncertainty to this modeling assumption, the uncertainty analysis can be performed with the truth model including rotor flexibility. The identification model will not consider the rotor's flexibility. Other sources of uncertainty such as measurement uncertainty are not included to isolate the estimate of uncertainty to just the effect of modeling the rotor flexibility in the truth model. If the modeling assumption of a rigid rotor is reasonable, then the uncertainty will be small. However, if there is a significant effect from including the rotor flexibility in the truth model, that suggests two things: 1) the truth model should include a flexible rotor model because it has a significant impact on the dynamic coefficient identification and 2) the engineer or researcher should strongly consider not using the rigid rotor assumption in the identification model. The final truth model and a suitable identification model can be determined through multiple sensitivity studies using carefully selected dynamics in the system modeled with the most appropriate methods. Once the final truth model and identification model are established, an estimate of the identification uncertainty can be made.

Determining the significant dynamics to include in the truth model is challenging because there may be unmodeled dynamics (either from a modeling assumption or by unintentional omission) that affect the dynamic coefficient identification process. When available, experimental measurements on a test rig can be used to calibrate a truth model. However, when designing a new test rig, this type of data may not be available. Another aspect of the uncertainty analysis framework is evaluating the experimental configuration for sensitivity to the effects of unmodeled dynamics. To use the rotor flexibility example again, there may be experimental configurations that are not sensitive to the dynamics of the rotor because of the signals selected for measurement to use in identifying coefficients. Section 3.1.5 provides an illustrative example.

In this chapter of the dissertation, the process for analyzing uncertainty comprehensively is developed carefully through single-axis models. First, a single degree-of-freedom (SDoF) mass-spring-damper model is used to investigate the impact of measurement errors. In the beginning it is possible to derive useful insights using analytical models but the complexity rapidly increases, requiring some other way of assessing the impact.

A Monte Carlo simulation is proposed for this purpose. Using simulations with the SDoF model, the impact of selecting measurements to use for identification are evaluated by going through several possible methods of instrumenting a test rig. Second, the model is extended by introducing a second degree of freedom (still with one axis). This model can be used to investigate the effect of simplified substructure dynamics on the identification of dynamic coefficients. Finally, an example of a higher-fidelity single-axis model is presented that combines a dynamic model developed from the finite element method with some lumped mass models. This gives an example of how models from a variety of different sources can be combined together.

3.1 Single Axis Models

One of the primary characteristics of TPJBs when compared with other oil-lubricated hydrodynamic bearings is the relative insignificance of cross-coupled forces relative to the forces from the principle stiffness and damping coefficients. For many systems this reduces the interaction between horizontal and vertical motion enough to allow the two axes to be treated independently. Single-axis models can then be used to understand the dynamics of the system. Researchers have used single-axis models to investigate tilting-pad journal bearing dynamics before. For example, Waldemar Dmochowski [75] developed a single-axis model for pad dynamics including pivot stiffness. Dmochowski's model provides useful information on how the pad dynamics are affected by the ratio of film stiffness and damping to pivot stiffness and damping. While a higher-fidelity model may be used to develop predictive models for TPJBs, single axis models offer useful insight into important properties and trends for bearing coefficient identification.

3.1.1 SDoF Analytical Analysis

Force and Displacement Measurement Error in SDoF Model

At the most basic level, a test rig for dynamic coefficient identification can be modeled as a mass-spring-damper system. The excited component of the test rig is approximated as a lumped mass. The fluid-film's dynamics are represented by the spring and damper. Figure 3.2 uses the test rig described by Flack et al. [63] to visually represent the simplification. At this level of analysis, the rigidly held component and its supports are assumed to be ideal (i.e. - not flexible). This assumption simplifies dynamics for a first analysis.

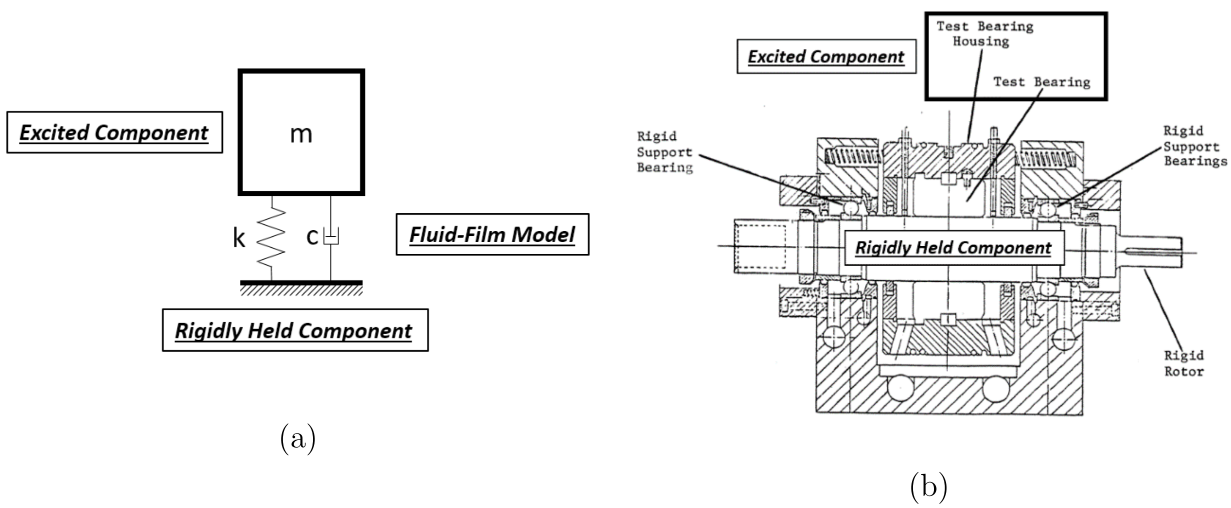

Figure 3.2: (a) Single-Axis, SDoF Model (b) Cross Section of Test Rig from Flack et al. [63]

One advantage of a simplified model is the ability to develop analytical equations. While model complexity grows rapidly, at the single-axis, SDoF level a set of equations may be derived for the effect of systematic errors on dynamic coefficient identification.

Starting with the equation of motion for the SDoF system,

$$m\ddot{x} = -kx - c\dot{x} + f \tag{3.1}$$

the dynamics can be expressed in the frequency domain as

$$\frac{F}{X} = ms^2 + cs + k \tag{3.2}$$

where $s = j\omega$ for the experimental methods modeled in this dissertation. F and X are complex values representing the magnitude and phase of the true signals. This method of modeling is useful for SDoF modeling and some other very basic analyses. For a more broadly generalizable formulation, linear algebra and matrix mathematics are required to describe the system and the dynamic coefficient identification. The simple, specific models are used to gain insight on important trends. Later, the uncertainty analysis is generalized to be more broadly applicable

Equation 3.2 represents the truth model. Because this is an illustrative example, the truth model is identical to the "real" system which has been defined to be a SDoF system. F and X must be measured in an experiment to identify dynamic coefficients. The measured force, $\hat{F}$, and measured displacement, $\hat{X}$, are different from the true values due to errors resulting from unknown variations in the sensor system. There will always be some level of variation that we cannot quantify exactly though typically this variation is relatively small through careful calibration of sensors. One of the basic models of measurement error is a multiplicative error:

$$\hat{F} = (1 + \delta_f)F \ , \ \hat{X} = (1 + \delta_x)X \tag{3.3}$$

The deltas (δ_f and δ_x) are complex numbers representing errors in magnitude and phase that arise from imperfect measurement. There are two assumptions in this model. The first assumption of this model is that the error does not change as a function of test frequency. This assumption is not a requirement of the framework but rather an assumption to simplify the analysis and extract trends from the model. Second, random errors are explicitly not considered. In a practical experiment this would mean taking many samples at a test frequency to reduce the effect of the random error on the total uncertainty. Since the literature review revealed that random errors are more commonly treated, this dissertation will focus on systematic errors. The uncertainty analysis framework developed in this dissertation is suitable for analyzing uncertainty from random errors as well as systematic errors.

With the two assumptions and using the measured values from Equation 3.3, the model of estimated coefficients (with $s = j\omega$) is:

$$\frac{\hat{F}}{\hat{X}} = \hat{k} - m\omega^2 + j\hat{c}\omega \tag{3.4}$$

The estimated transfer function (Eq. 3.4) and the true transfer function (Eq. 3.2) can be related:

$$\frac{\hat{F}}{\hat{X}} = \frac{F}{X}(\frac{1+\delta_f}{1+\delta_x}) = \hat{k} - m\omega^2 + j\hat{c}\omega \tag{3.5}$$

To derive an easily understandable analytical solution, we can assume the errors δ_f and δ_x are small in magnitude which allows for the following simplification:

$$\frac{1+\delta_f}{1+\delta_x} \approx 1 + \delta_f + \delta_x \approx 1 + \delta_{total} \tag{3.6}$$

This simplification is useful for deriving analytical equations. Simulations using linearized models of system components are developed in Section 3.1.2 and beyond to avoid using simplifications such as this one. The utility of these analytical results - where feasible - is the ability to understand where the trends seen in the simulation results come from.

The truth model can be substituted for $\frac{F}{X}$ in equation 3.5:

$$\left[k - m\omega^2 + jc\omega\right](1 + \delta_{total}) = \hat{k} - m\omega^2 + j\hat{c}\omega \tag{3.7}$$

Equation 3.7 can be separated into real and imaginary parts. The real components lead to:

$$k - m\omega^2 + \Re(\delta_{total})(k - m\omega^2) + \Im(\delta_{total})(jc\omega) = \hat{k} - m\omega^2 \tag{3.8}$$

Equation 3.8 can be rearranged to find the percent error of $\hat{k}$:

$$\frac{\hat{k} - k}{k} = \Re(\delta_{tot})(1 - \frac{m\omega^2}{k}) - \Im(\delta_{tot})\left(\frac{c\omega}{k}\right) \tag{3.9}$$

The imaginary parts from Equation 3.7 have the following relationship:

$$\hat{c}\omega = \Im(\delta_{tot})(k - m\omega^2) + (1 + \Re(\delta_{tot}))(c\omega) \tag{3.10}$$

Similar to the real components, a rearrangement of Equation 3.10 shows the percent error of $\hat{c}$:

$$\frac{\hat{c} - c}{c} = \Re(\delta_{tot}) + \Im(\delta_{tot})\left(\frac{k}{c\omega} - \frac{m\omega}{c}\right) \tag{3.11}$$

Equations 3.9 and 3.11 are directly related to the magnitude of uncertainty because δ_{total} is obtained from the full range of measurement errors (i.e. - the measurement uncertainty).

There are several important features of these analytically derived equations (Equations 3.9 and 3.11):

- As the magnitude of the true stiffness and true damping decrease, the percent errors (and thus uncertainty) increases. This can be understood by considering an example where a "softer" bearing (lower stiffness) is tested on the same test rig as a stiffer bearing. In both cases the instrumentation is identical so the magnitude of errors would be the same (e.g. - for sensors where the typical uncertainty is defined as a function of the full scale of the sensor measurement capability). This means that the magnitude of possible error in identified coefficient is the same while the true value is smaller, leading to increased uncertainty.

- On a similar note this suggests that the uncertainties in identifying cross-coupling in TPJBs will be large compared with the principal values. Of course the impact of this uncertainty may be small - a large uncertainty around a small value may have little noticeable impact on system level properties such as stability. On the other hand, validating predictions from TPJB codes might need cross-coupling with low uncertainty to use as additional evidence of proper modeling of TPJB physics.

- For a given operating condition, the stiffness uncertainty becomes dominated by a quadratic term, $\frac{m\omega^2}{k}$, as test frequency increases. This leads to a challenge in TPJB coefficient identification. TPJBs can exhibit varying dynamic coefficients as the frequency of excitation changes (while operating conditions such as rotation speed are constant) due to the impact of the pad dynamics on the system. The equations derived in this section suggest that coefficient identification at higher test frequencies result in larger uncertainties. Model validation for higher test frequencies becomes difficult.

- It should be noted that even at this level of analysis, a single uncertainty value cannot describe uncertainty for TPJB identification. First, the uncertainty is a function of test frequencies used in the experiment. Second, even if the test rig is the same, identifying coefficients of a different bearing would yield different uncertainties. The practical implication of this result is that for every bearing to be tested, an uncertainty analysis must be performed and the results presented as a function of the test article and the test frequencies of interest.

- The relationship between damping uncertainty and test frequency in Equation 3.11 suggests that damping is more difficult to identify at frequencies approaching zero. This is reasonable because as the excitation frequency decreases, the velocity of the excited component decreases. Damping forces are typically modeled as directly proportional to the velocity. With small velocities, the forces are small and the errors in damping forces become large relative to the true damping forces.

Many of these ideas are supported with simulations in Section 3.1.2 and beyond.

Force, Displacement, and Acceleration Measurement Error in the SDoF Model

One of the trends identified in Equation 3.9 is the quadratic relationship to the excitation frequency. For TPJBs, where the dynamic coefficients may be frequency-dependent depending on the TPJB configuration and the operating conditions, this trend can lead to large uncertainty for high test frequencies. Rather than rely on numerical integration of the displacement to get acceleration (as the ms^2 leading to the $m\omega^2$ term in the frequency domain implies), some test rigs measure the acceleration of the excited component. Modeling this measurement scenario similar to the mathematical representation in Equation 3.2 gives:

$$\frac{F - mA}{X} = k - jc\omega \tag{3.12}$$

On the surface, comparing Equation 3.12 with Equation 3.2 might suggest that the inertial component leading to the quadratic dependency on test frequency has been eliminated. To evaluate this, a measurement error for acceleration can be defined like the force and displacement errors in Equation 3.3:

$$\hat{A} = (1 + \delta_a)A \tag{3.13}$$

Through a similar process as before, we can determine the identified coefficients as:

$$\frac{\hat{F} - m\hat{A}}{\hat{X}} = \frac{F(1 + \delta_f) - mA(1 + \delta_a)}{X(1 + \delta_x)} = \hat{k} + j\hat{c}\omega \tag{3.14}$$

In the previous analysis with the single-axis, single degree-of-freedom model with only force and displacement measurement errors analyzed, a single simplification with the ratio of measurement errors lead to straightforward analytical conclusions. For this case, more intricate simplifications and manipulations would be required. Rather than rely on simplifications, the simulation method will be developed to avoid these types of simplifications altogether. Once the simulation has been developed, the SDoF cases are revisited.

3.1.2 Developing the Simulation Based Uncertainty Analysis

Modern tools such as MATLAB make it straightforward to model linear systems. To begin with, the single-axis, SDoF model with errors can be implemented with transfer function models according to Figure 3.3. One of the advantages of modeling the system in a simulation instead of working with analytical equations is that fewer simplifications are required.

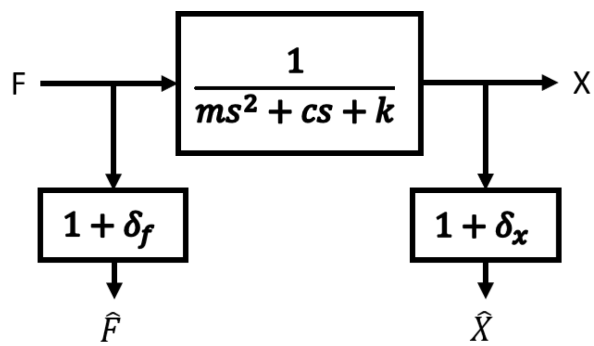

Figure 3.3: Modeling SDoF Model as Transfer Functions

The application of errors to the true signals to get $\hat{F}$ and $\hat{X}$ from F and X is done with complex numbers. The complex numbers δ_f and δ_x represent an error in magnitude and phase of a signal used in the identification model relative to the corresponding signal in the truth model. If a different model of measurement uncertainty is desired, the model can be adjusted here as needed. For example, measurement noise can also be included to incorporate random errors into the analysis.

For this dissertation the amplitude of the magnitude error and amplitude of the phase error are determined independently. Figure 3.4 shows a visual representation of the measurement error model in this dissertation.

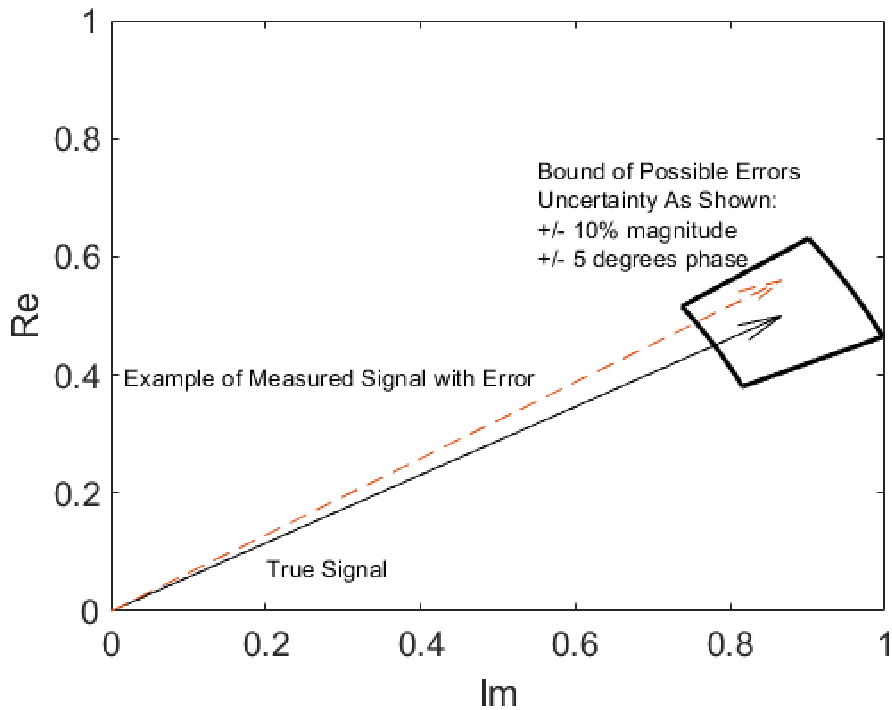

Figure 3.4: Errors Affecting Truth Signal

To account for the uncertainty in error, a Monte Carlo method will be used. Multiple trials of the simulated identification experiment will be run and each trial will have a value for error sampled from the defined measurement uncertainty. In this dissertation, the measurement error is defined to be uniformly distributed within the uncertainty bounds but any appropriate distribution may be used.

Once the errors are selected, the simulation can generate data for the identification model to use. For this dissertation, the identification of dynamic coefficients will use a single-frequency identification swept across the desired test frequencies. The scope of this dissertation is not to evaluate identification techniques such as multi-frequency identification or time domain identification methods. The motivation is to select a single identification method and hold it consistent across the various analyses such that differences in identification uncertainty arise from differences between the truth model and identification model without additional contributions from identification technique variation.

3.1.3 The Identification Process Used in This Dissertation

For a more detailed investigation of identification methods, the literature review by Dimond et al. [22] includes a discussion of identification methods.

In this dissertation, the bearing identification experiment is summarized as:

$$\mathbf{F} = \mathbf{H}\mathbf{U} \tag{3.15}$$

F is a matrix of force applied to the system. Each column would represent a different experiment and each row would represent a different force input to the system. **U** is a matrix of the responses of the system with a column for each trial. **H** is the frequency response matrix. The frequency response matrix will contain the bearing coefficients as well as the dynamics of any other modeled component such as the rotor or the substructure. Therefore, if

H can be identified, then the bearing coefficients are identified. The frequency response matrix is generally frequency-dependent.

The frequency response matrix (with frequency dependency represented) can be identified by solving for **H**:

$$\mathbf{H}(\omega) = \mathbf{F}(\omega)\mathbf{U}^{-1}(\omega) \tag{3.16}$$

The solution for $\mathbf{H}(\omega)$ typically relies on numerical methods for efficient computation. Directly inverting $\mathbf{U}(\omega)$ is often not the most efficient method. In effect, the typical solution process may be described as optimizing $\mathbf{H}(\omega)$ to minimize the difference between $\mathbf{H}(\omega)\mathbf{U}(\omega)$ and $\mathbf{F}(\omega)$. MATLAB documentation has an illustrative diagram (reproduced in Figure 3.5) for a function, mldivide(), that solves this type of equation with the options available to numerically solve this problem.

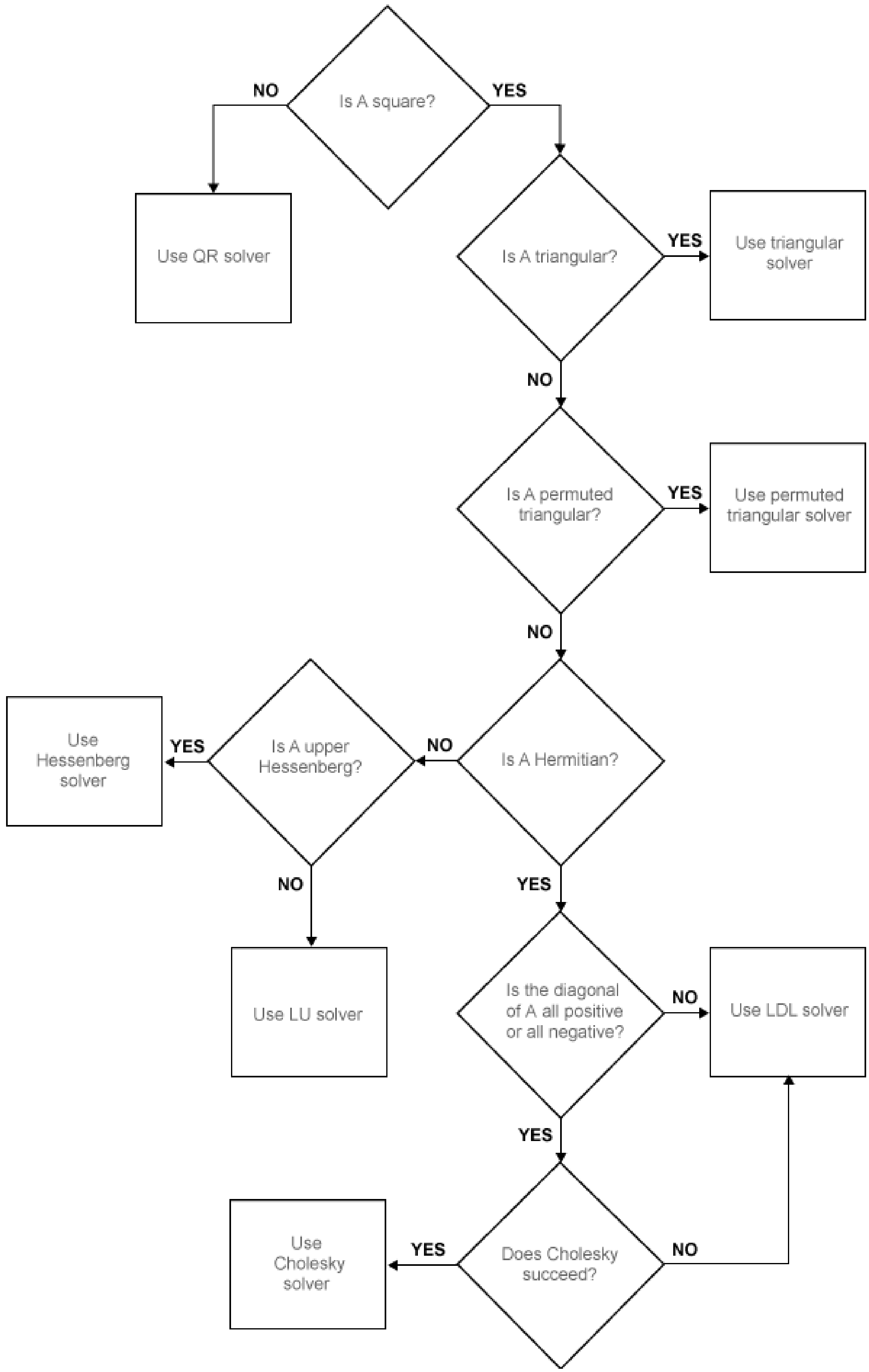

Figure 3.5: MATLAB Decision Tree for Solving for $\mathbf{H}(\omega)$ reproduced from [76]

3.1.4 First Results from the Simulation

The SDoF model described by Figure 3.3 is implemented with measurement uncertainties listed in Table 3.1.1. The mass is assumed to be known exactly. For a range of test frequencies from 1 Hz to 1000 Hz, the identification experiment is simulated by 1) finding $\mathbf{H}(\omega)$, 2) applying a true force $\mathbf{F}(\omega)$ to the system truth model, 3) obtaining the true response $\mathbf{U}(\omega)$, 4) applying a selected case of measurement errors to get $\hat{\mathbf{F}}(\omega)$ & $\hat{\mathbf{U}}(\omega)$, and 5) finally computing $\hat{\mathbf{H}}(\omega)$.

Table 3.1.1: Uncertainty Parameters for SDoF Model Simulation

Displacement Magnitude Uncertainty	$\pm 5\%$
Displacement Phase Uncertainty	± 5 degrees
Force Magnitude Uncertainty	$\pm 5\%$
Force Phase Uncertainty	± 5 degrees

Once $\hat{\mathbf{H}}(\omega)$ is found, stiffness and damping values are extracted by separating the real and imaginary components: $\hat{k} = \Re(\hat{\mathbf{H}}(\omega)) + m\omega^2$ and $\hat{c} = \Im(\hat{\mathbf{H}}(\omega))/\omega$. For each test frequency this process is repeated 3,000 times with a new combination of measurement errors sampled each time. The identified coefficients from the simulations are summarized in Figure 3.6 by indicating the largest and smallest identified values for each test frequency. The true value is included for reference.

The results can be further post-processed to present the results in a more typical plus-or-minus uncertainty value. The uncertainty magnitude

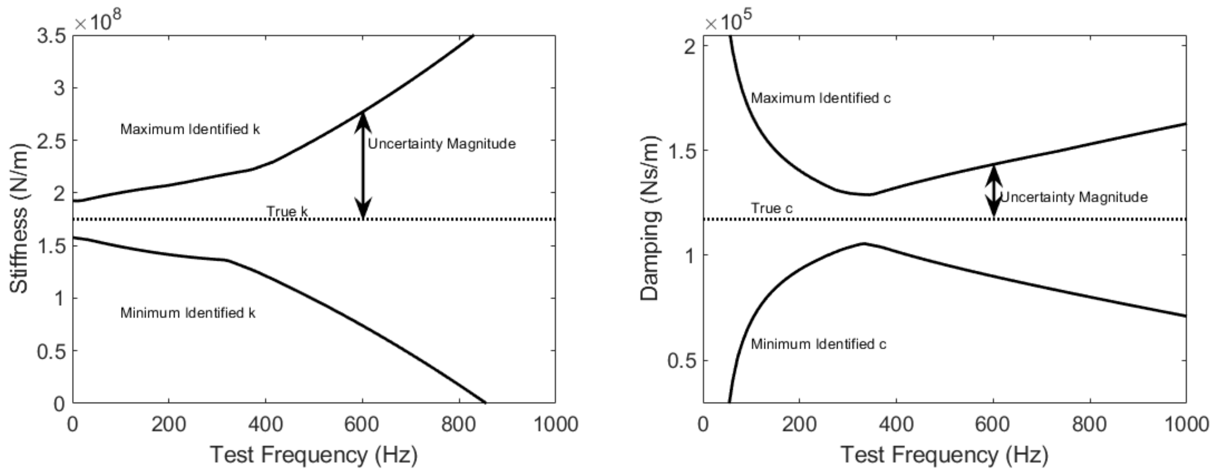

(a) Identified Stiffness Coefficients (b) Identified Damping Coefficients

Figure 3.6: Maximum and Minimum of Identified Coefficients for SDoF Model

(indicated in Fig. 3.6) can be normalized by the true value to get a plus-or-minus percent uncertainty. This is shown in Figure 3.7.

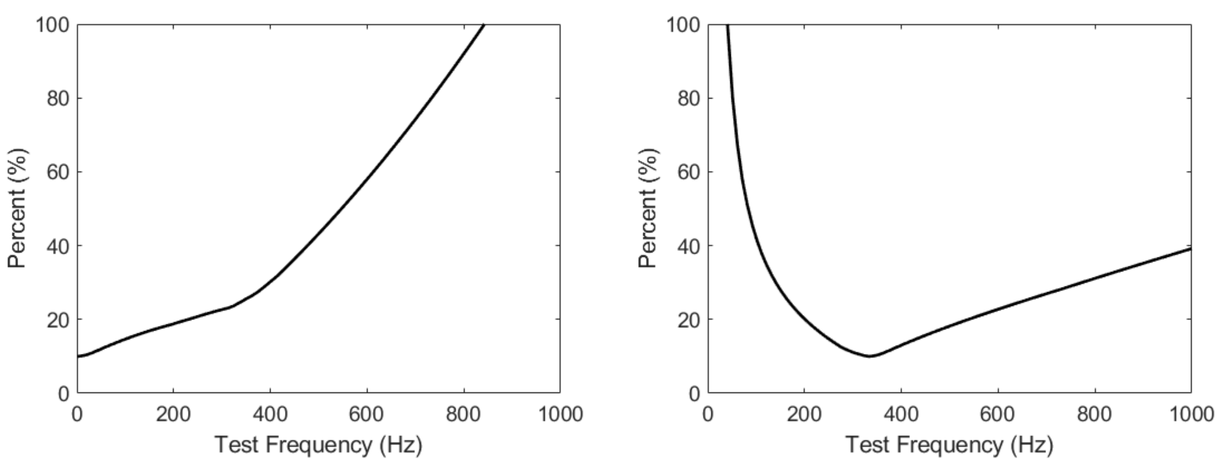

(a) Stiffness (b) Damping

Figure 3.7: SDoF Identification Uncertainty

A quick evaluation of the distribution of the identified coefficients can be presented by including a 95% confidence interval to the uncertainty. Figure 3.8 presents the uncertainty results with the confidence intervals included.

It is recommended that uncertainty analysis results present both pieces of information - the maximum uncertainty and a 95% confidence interval value - to offer insight in how the identified values are distributed. Furthermore, being able to see the maximum uncertainty in the results encourages conservatism.

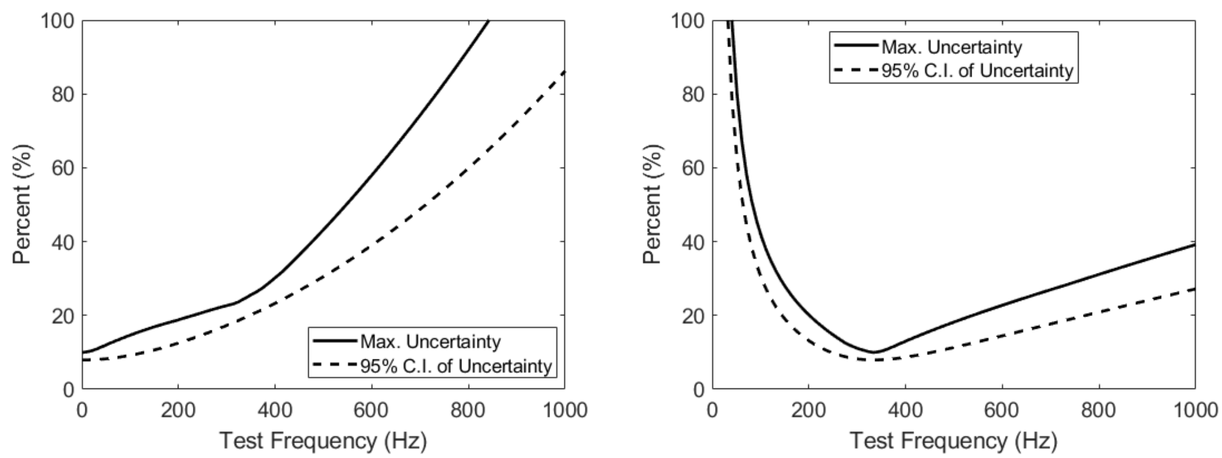

(a) Stiffness

(b) Damping

Figure 3.8: SDoF Identification Uncertainty with Confidence Interval

It is important to remember that the results shown in Figures 3.6, 3.7, and 3.8 are the worst-case results. “Worst-case” refers to the values farthest away from the truth in the simulations. Practically these results are actually the lower limit of achievable uncertainty for the measurement uncertainties given in Table 3.1.1. In other words, since we are considering minimal error sources, the uncertainty is the best (i.e. lowest) uncertainty possible for the modeled case and any real experiment will be worse than the analysis. This makes it all the more important that a systematic framework exists to ensure enough significant factors are considered to get as close as possible to the real-world uncertainty.

Comparing to Analytical Modeling

The overall trend in uncertainty for stiffness looks quadratic. This is in line with the expectation that Equation 3.9 indicated. Damping uncertainty increases asymptotically as test frequency approaches zero. The behavior as test frequency increases to infinity is linear. There's also a minimum point at approximately the natural frequency of the system. All three of these behaviors can be ascertained from the analytical results for damping in Equation 3.11. The matching trends between the analytical results and the simulation suggests that the simulations are accurate and suitable for modeling the uncertainty of identifying dynamic coefficients for more complicated systems, which will be evaluated in this dissertation.

Parameter Variation Effects on Uncertainty for SDoF Case

While simple, the SDoF simulation allows for the investigation of how physical parameter (stiffness, damping, mass) variations affect uncertainty. The analytical equations from Section 3.1.1 are used as a point of comparison for the effects to show how the simulation is behaving as expected in response to varying parameters of the model.

The first parameter variation is of the true stiffness of the model while damping and mass are constant. The results are shown in Figure 3.9 with only the maximum uncertainty shown to minimize clutter in the plots. The uncertainty results for stiffness show the same trend expected from Section 3.1.1 where the uncertainty increases as the true stiffness decreases. There is an effect on damping uncertainty as well when the stiffness is changed even with the damping held constant. The minimum point in damping uncertainty shifts as the stiffness changes and the undamped natural frequency of the system also changes. It's evident that the critical frequencies of the system are important to uncertainty, though the models suggest that it is not as simple as trying to increase the frequencies as much as possible. In the case of damping uncertainty, a larger critical frequency leads to increased uncertainty at lower frequencies even as the uncertainty at higher frequencies decreases. The effect of the system's dynamics on uncertainty is shown to be relatively complex even for a simple case such as the SDoF model.

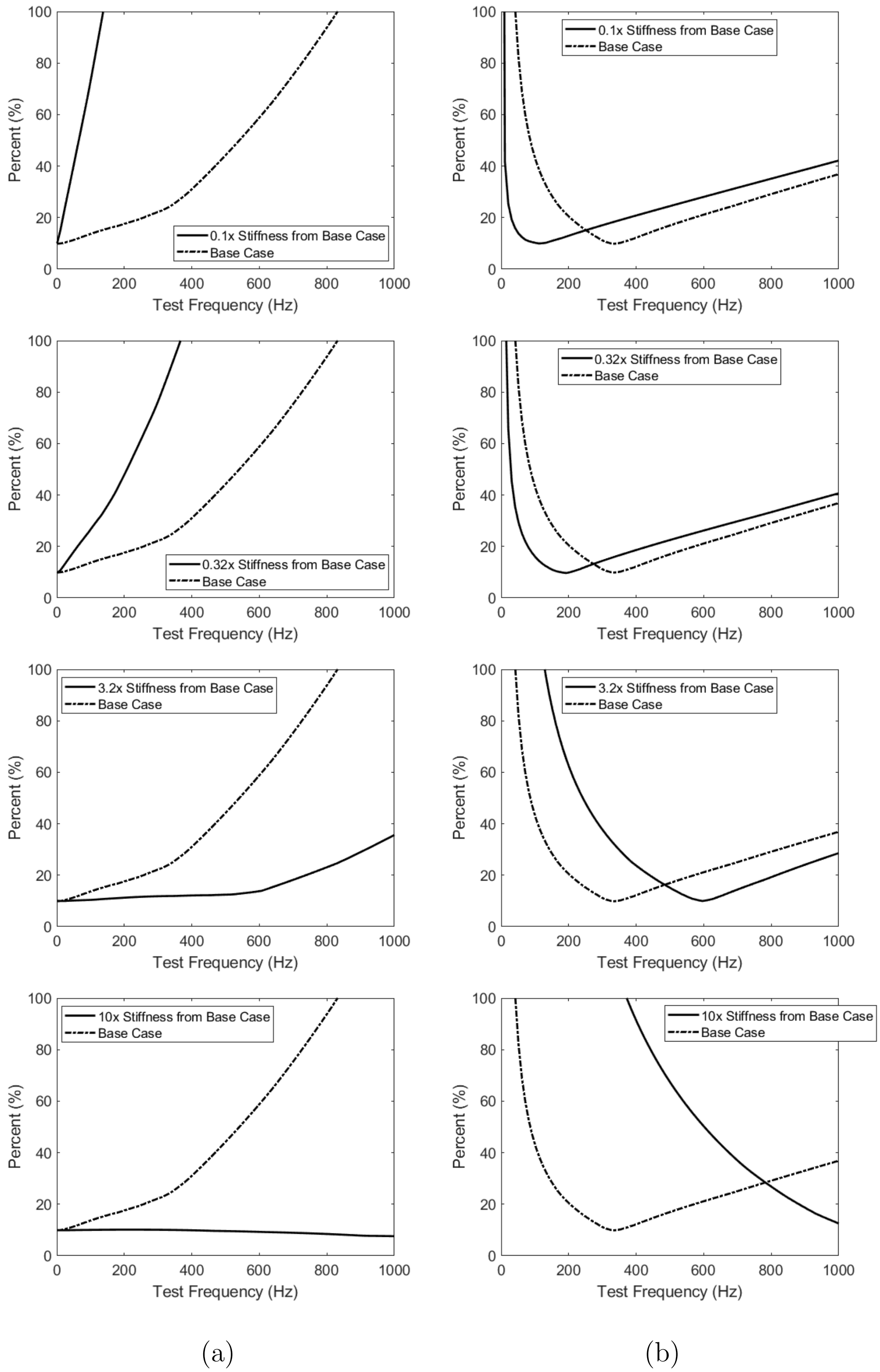

Figure 3.9: Effect of Varying True Stiffness (with damping and mass constant) in SDoF Model for (a) identified stiffness and (b) identified damping

The second parameter variation is of the true damping of the model while stiffness and mass are constant. Figure 3.10 shows the maximum uncertainty similar to the results for varying the true stiffness in the model in Figure 3.9.

As true damping decreases, the uncertainty increases. This matches the expected trend from the derived analytical equations. The stiffness uncertainty increases as damping increases. This also matches the equations. Physically, the explanation would be that with higher damping, damping forces are larger and the errors - being a multiplicative error - would be larger as a function of damping forces. The contribution to the measured force from stiffness would likely decrease as increased damping reduces displacements. In sum, the force error will be larger if damping is higher leading to larger uncertainty.

In the damping identification uncertainty, the point of minimum uncertainty for damping shifted noticeably in the case where true stiffness is varied without changing the other parameters. In this case with damping changing, the point of minimum uncertainty does not change noticeably. This means that the uncertainty increases or decreases consistently as a function of frequency.

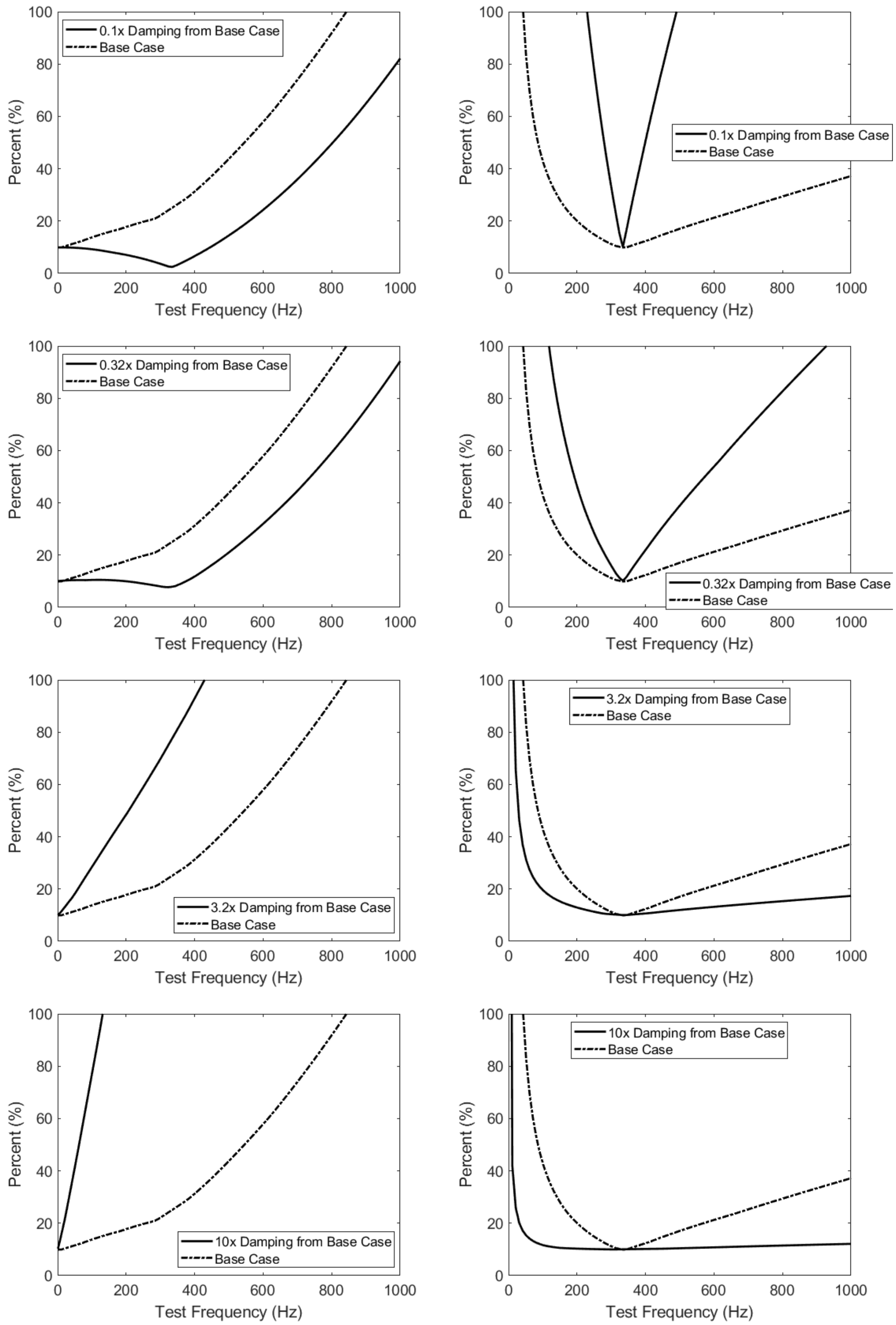

(a) (b)

Figure 3.10: Effect of Varying True Damping (with stiffness and mass constant) in SDoF Model for (a) identified stiffness and (b) identified damping

The third parameter variation analyzed is changing the mass of the model while holding stiffness and damping constant. Figure 3.11 shows the uncertainty results for identified stiffness and damping.

Varying stiffness and damping had opposite effects on identification uncertainty for stiffness and damping. When mass is varied, the effect on uncertainty is similar for stiffness and damping. As mass increases, the uncertainty increase at higher frequencies. Below a certain frequency the uncertainty decreases. The effect of the critical frequencies of the system are noticeable.

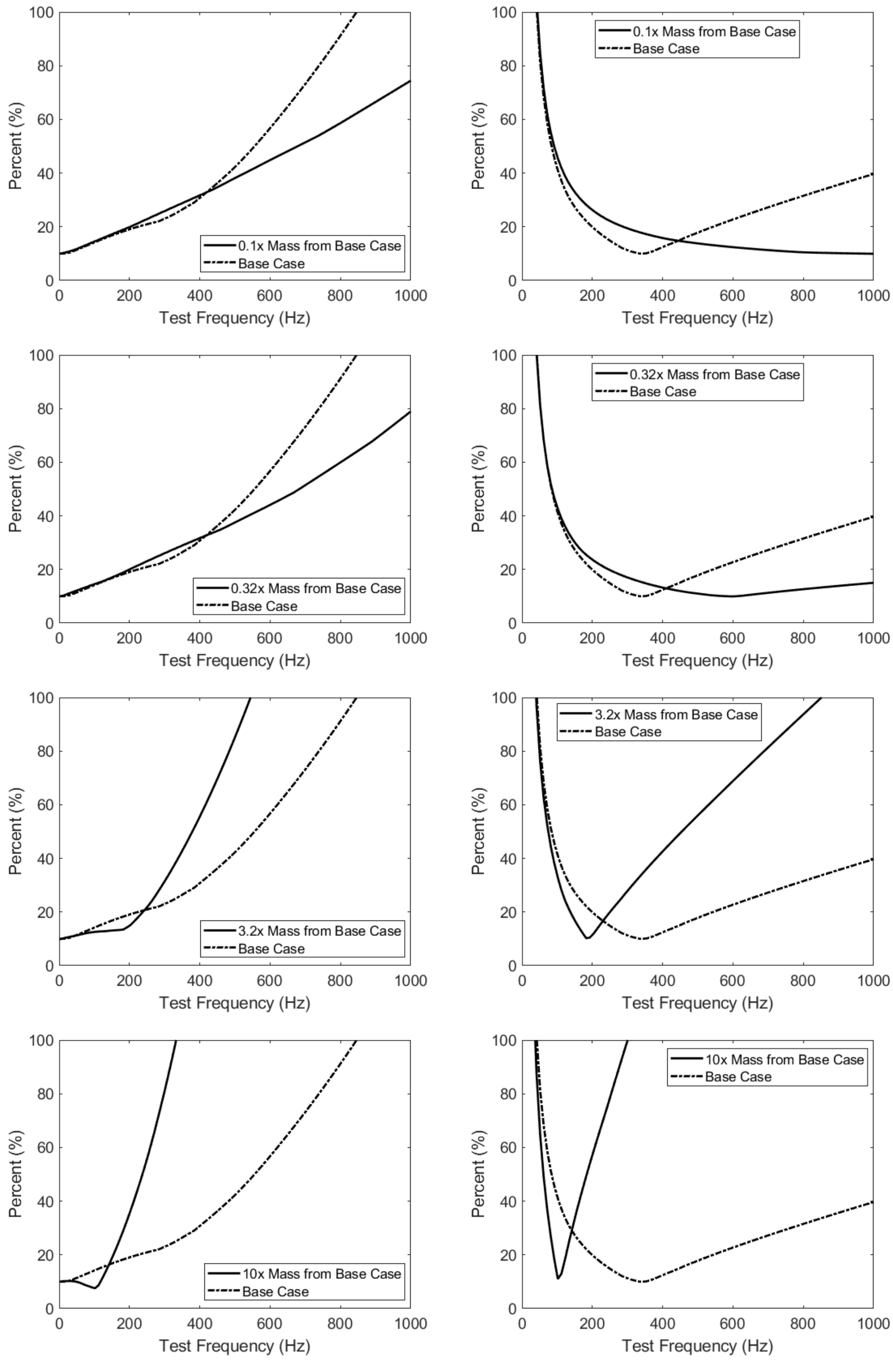

(a) (b)

Figure 3.11: Effect of Varying True Mass (with stiffness and damping constant) in SDoF Model for (a) identified stiffness and (b) identified damping

The results in Figures 3.9, 3.10, and 3.11 obtained from simulating an experiment to identify stiffness and damping of a SDoF system show the same trends expected from the equations derived in Section 3.1.1. Because the simulation trends match the analytical results, there is confidence that the simulation is a suitable tool for modeling coefficient identification uncertainty.

While the SDoF models are a substantial simplification of the dynamics a real system may have, the conclusions derived from these results hold value in identifying trends that will be applicable both in the SDoF model as well as a real system. Some of the most significant conclusions are summarized here:

- Increasing the mass of the system increases identification uncertainty for both stiffness and damping. This suggests that for a bearing test rig, the mass of the excited component should be kept to a minimum. Similarly, inertia for any dynamics affecting the system (such as bending modes of the rotor, flexural modes of the system) should be kept to a minimum.

- Larger magnitudes of true stiffness decreases stiffness identification uncertainty and (at higher frequencies) decreases the damping identification uncertainty as well. This suggests that model validation will be more accurate for higher stiffness bearings. And if a bearing model cannot be accurately validated in the best case validation scenario, then it certainly cannot be validated under actual testing that would yield higher uncertainties. Larger magnitudes of true damping increases stiffness identification uncertainty and decreases damping uncertainty. However, the cross-over point between decreasing-uncertainty for damping and increasing uncertainty for damping yields a minimum uncertainty point. This suggests that a high-stiffness, low-damping bearing has a small frequency range in which uncertainties are minimized. This region would be useful as a first bench-marking region for a bearing model before other frequency ranges and stiffness/damping combinations are tested. It should be kept in mind that the exact significance of this "sweet spot" will depend greatly on the dynamics of the system and the instrumentation being evaluated for uncertainty.

- The results from the simulation support the conclusions that the analytically derived equations would suggest. This provides evidence bolstering the idea that the method proposed in this dissertation can lead to valid conclusions about the uncertainty of coefficient identification.

Measuring Acceleration In Addition to Force and Displacement

A typical variation of test rig instrumentation includes an acceleration measurement on the excited component (usually the housing or another stationary component because measuring the acceleration of a spinning rotor is more challenging). In the SDoF model, this concept can be modeled by expanding the dynamics to allow for the extraction of the lumped mass's acceleration signal and then applying an acceleration measurement error. Figure 3.12 shows this.

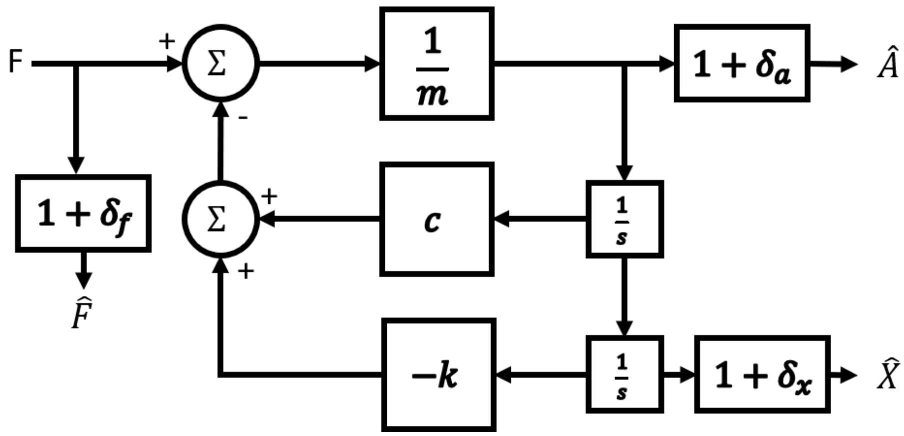

Figure 3.12: SDoF Model Diagram Including Measurement Errors for Displacement, Acceleration, and Force

From this model, a Monte Carlo analysis over the space of force sensor and displacement sensor uncertainties yields the results shown in Figure 3.13. The acceleration measurement is assumed to be error free to show an important property. The mass of the lumped mass is again required and assumed to be known perfectly to match with the case of measuring only applied force and resulting displacement.

The results (shown without the 95% confidence interval lines to avoid confusion) show that in this case when the acceleration of the lumped mass is measured, the uncertainty actually increases. These results may seem counter-intuitive at first. After all, if we are identifying the inertia and canceling it out of the measured applied force, we should be closer to the bearing's force and thus yield better results with the identification.

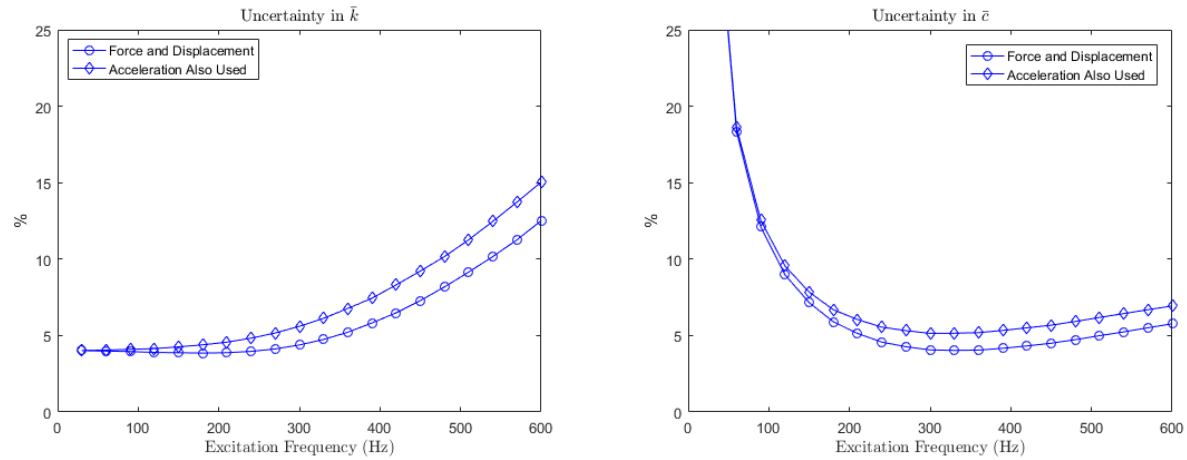

(a) Identified Stiffness

(b) Identified Damping

Figure 3.13: Uncertainty for SDoF Identification With and Without Acceleration Measurement

However, errors add even when quantities are subtracted (i.e. - applied force minus inertial force estimated with the accelerometer) and so the uncertainty in the force increases while the magnitude of the force (bearing force relative to the applied force) gets smaller. This makes the effective force error larger. While this is a simplified case, the results suggest that the selection of signals to measure is important and that more signals measured do not necessarily improve our ability to identify dynamic coefficients. Equation 3.17 shows this a different way, highlighting that even if the acceleration measurement is perfect ($\hat{A} = A$), the displacement measurement errors will affect the inertial compensation.

$$\frac{\hat{F}}{\hat{X}} = m\hat{A} + \hat{c}s + \hat{k} \rightarrow \frac{\hat{F}}{\hat{X}} - \frac{m\hat{A}}{X(1+\delta_x)} = \hat{c}s + \hat{k} \tag{3.17}$$

Conclusions must be drawn carefully from this set of simulations. It is not directly indicating that measuring the acceleration of the excited component is worse than not using the acceleration information. Since this is a simplified case, the elements involved must be accounted for more generally. For example, a model of inertia is required whether acceleration is measured or not. For the SDoF case, this is simply the mass of the excited component. When acceleration information is not used in the identification, the inertial uncertainty is driven by the mass uncertainty and the square of the test frequency. When the acceleration is measured, the sensor itself may yield better accuracy at higher frequencies because the acceleration is greater. So the inertial uncertainty as a combination of the mass uncertainty and acceleration measurement uncertainty may actually be lower at higher frequencies. This makes the relationship more complicated and could lead to improved uncertainty when acceleration measurement is used at higher frequencies. Though not analyzed in this dissertation, such uncertainty properties can be modeled and analyzed with the uncertainty analysis framework presented in this work.

The results demonstrate the power of the uncertainty analysis framework to provide comparisons. It is up to the engineer/researcher to perform all the comparisons necessary to determine the best identification method.

3.1.5 SDoF Uncertainty Analysis when Measuring Bearing Force Directly

The inertial force proved to be contributing significantly to uncertainty when applied force and the resulting response are measured. The uncertainty of coefficient identification when using an acceleration measurement also showed the inertial force's effect on uncertainty. Identifying bearing dynamic coefficients becomes more uncertain as a function of the square of test frequency.

Another option available for identifying bearing dynamic coefficients is measuring the hydrodynamic force generated by the fluid film more directly. Examples of measuring the component force more directly include constructing the force by numerically integrating pressure measurements within the component [77], load cells external to bearing housings (with applied excitation on the rotor) [39], and a null-balance type of force measurement [78].

The SDoF model offers useful insight for the case of measuring bearing force. The system model when measuring bearing force can be represented similar to Equation 3.2 as

$$\frac{F_b}{X} = cs + k \tag{3.18}$$

A system diagram with the signal to be measured is presented in Figure 3.14.

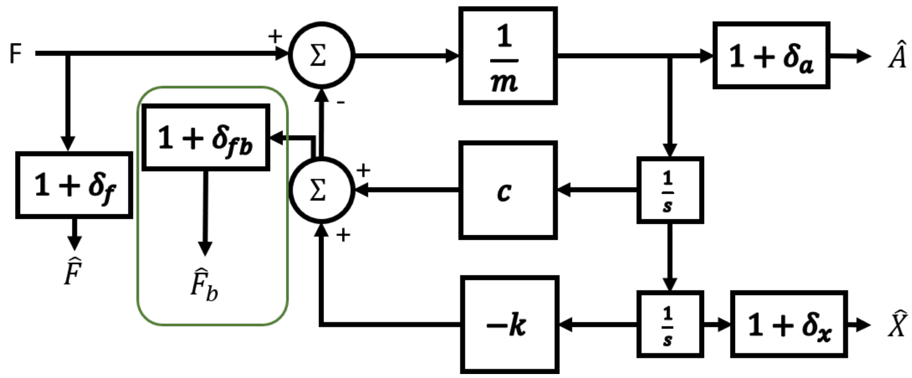

Figure 3.14: SDoF Model Diagram Highlighting Bearing Force Signal to be Measured

By performing the same analysis from Section 3.1.1, it can be shown that analytical equations modeling identification error when measuring bearing force are:

$$\frac{\hat{k}-k}{k} = \Re(\delta_{tot}) - \Im(\delta_{tot})\left(\frac{c\omega}{k}\right) \tag{3.19}$$

$$\frac{\hat{c}-c}{c} = \Re(\delta_{tot}) + \Im(\delta_{tot})\left(\frac{k}{c\omega}\right) \tag{3.20}$$

Equations 3.19 and 3.20 are analogous to Equations 3.9 and 3.11. The most notable difference is the absence of mass when bearing force is measured. For stiffness uncertainty, the effect on uncertainty is a shift in trend from quadratic to linear as a function of test frequency. For damping uncertainty, the uncertainty actually decreases as the test frequency increases.

An uncertainty analysis performed on the SDoF model when bearing force is measured supports the analytically derived trends, much like the applied force measurement case. In the analysis, the measurement uncertainties had the same definitions as the applied force case. The uncertainty magnitudes for measuring bearing force are compared with measuring the applied force in Figure 3.15.

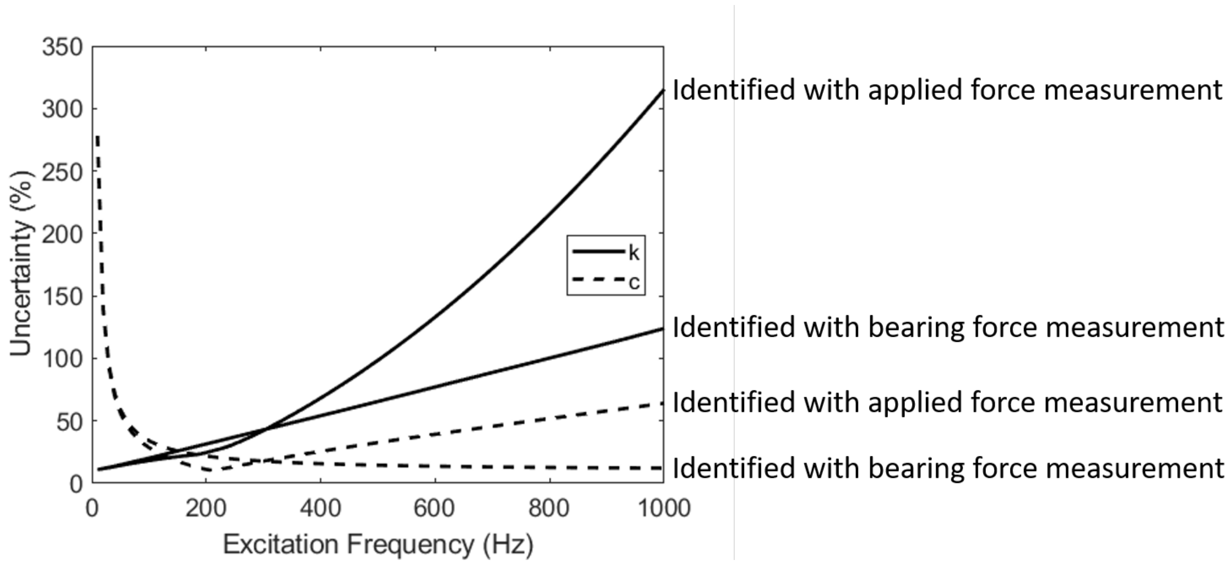

Figure 3.15: Comparing Uncertainty Magnitudes for Stiffness and Damping Identification When Measuring Applied Force vs. Bearing Force

There are some notable conclusions that these results point to:

- The uncertainty trends are improved when the bearing force is measured instead of the force applied to excite the system. The stiffness uncertainty is dominated by a linear trend instead of a quadratic trend and the damping uncertainty will actually decrease until it reaches an asymptote at a small, non-zero value directly related to the uncertainties in the measurement.

- While the analysis presented here uses the same measurement uncertainty to present a direct comparison between the measurement of applied force and the measurement of bearing force, the selection criteria for a test rig should be based on the actual expected uncertainty for measurements related to each method.

In Sections 3.1.1 to 3.1.5, the analyses presented reveal useful trends about the uncertainty of experimentally identifying TPJB dynamic coefficients. For further analysis, the truth model used in the uncertainty analysis framework can be changed to have higher fidelity relative to reality. By doing so, further properties of the uncertainty of TPJB coefficient identification can be observed.

3.2 Single-Axis, Two Degree-of-Freedom (2DoF) Models

Adding a second degree-of-freedom is a simple but powerful change to the truth model that can model many effects in a TPJB dynamic coefficient identification test rig. The previously referenced study by Waldemar Dmochowski [75] investigated the effect of pivot stiffness with a 2DoF model. Along the same lines the 2DoF model may be used to understand the effect of the substructure on the identified coefficients. Figure 3.16 shows the latter example in a diagram.

First, a model of a dynamic coefficient identification experiment that measures force applied to the excited component will be simulated. The displacement measurement modeled will be the relative displacement between the excited component and the substructure. This represents the

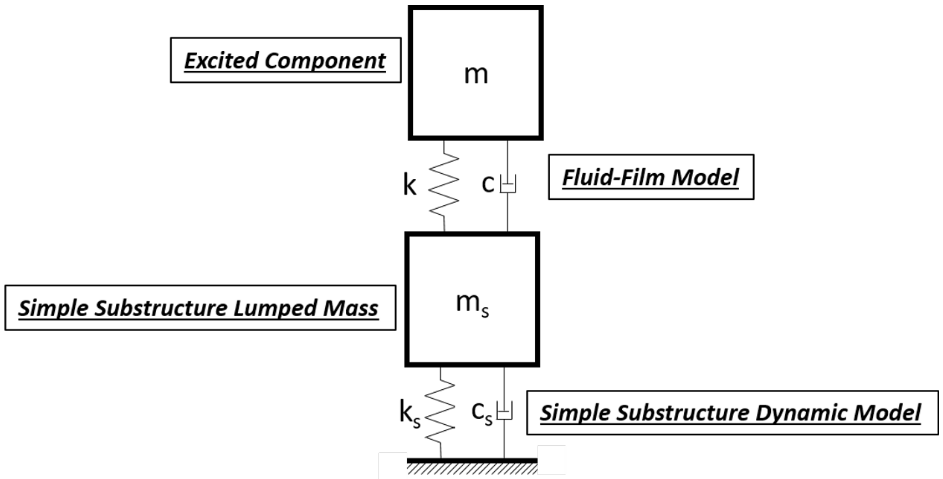

Figure 3.16: Diagram of Modeling Simplification to Two Degrees of Freedom

placement of the displacement sensor probe on the bearing housing to sense the displacement of the rotor. Regardless of if the rotor is excited or if the bearing housing is excited, the resulting displacement measurement will be the relative displacement between the rotor and the bearing housing. A diagram of the truth model used to model this case is shown in Figure 3.17. The identification model to be used in this analysis is shown in Figure 3.18. The identification model assumes that the substructure dynamics are negligible. In test rigs where the excitation force is applied on the housing, the rotor is designed to be as stiff as possible to make this assumption. The parameters for analysis are presented in Table 3.2.1.

An important detail regarding the simulation setup is the pedestal/substructure stiffness. It is larger than the bearing stiffness by a factor of 20. To put this into context, the API specification states that if the support stiffness is predicted to be greater than the bearing stiffness by a factor of 3.5, it does not need to be considered for analysis. The modeled

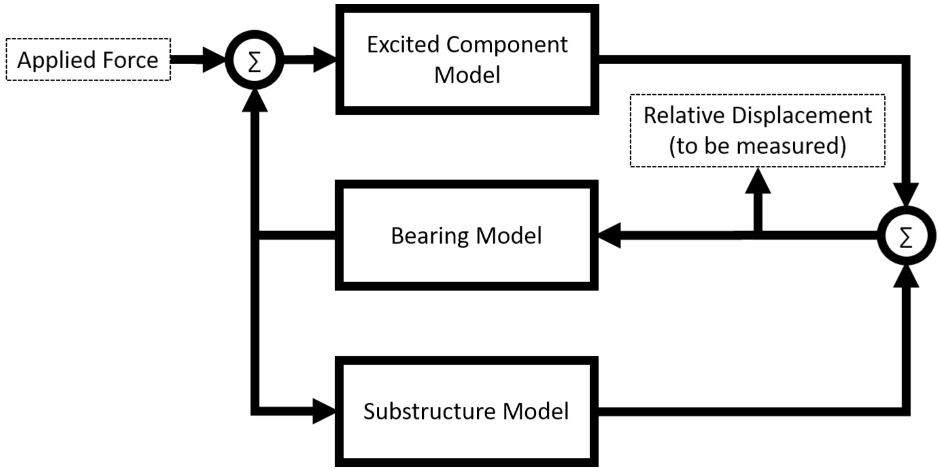

Figure 3.17: 2DoF Truth Model

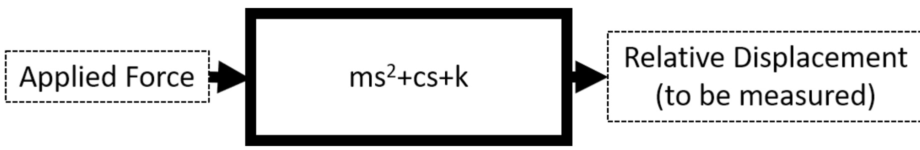

Figure 3.18: 2DoF Identification Model Not Compensating for Substructure Model

Displacement Magnitude Uncertainty	±5%
Displacement Phase Uncertainty	±5 degrees
Force Magnitude Uncertainty	±5%
Force Phase Uncertainty	±5 degrees
m (kg)	40
k (N/m)	175,127,000
c (N*s/m)	117,170
m_s (kg)	40
k_s (N/m)	3,502,500,000
c_s (N*s/m)	74,860

Table 3.2.1: 2DoF Simulation Parameters

stiffness ratio between bearing and substructure would be considered rigid as far as typical industrial analysis is concerned.

The uncertainty results of the 2DoF case are presented in comparison with the SDoF case results for reference. Figure 3.19 presents the stiffness results while Figure 3.20 presents the damping results.

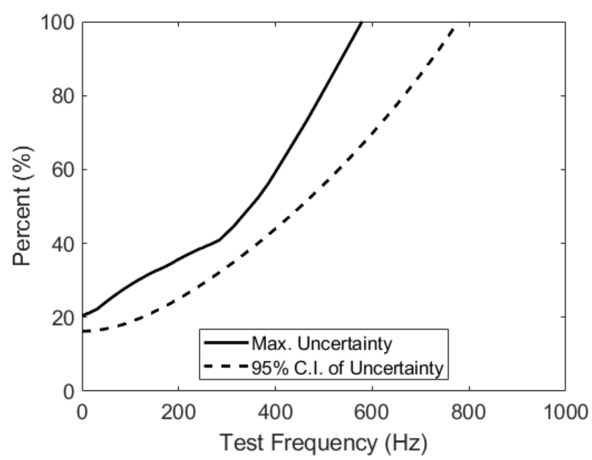

(a) 2DoF

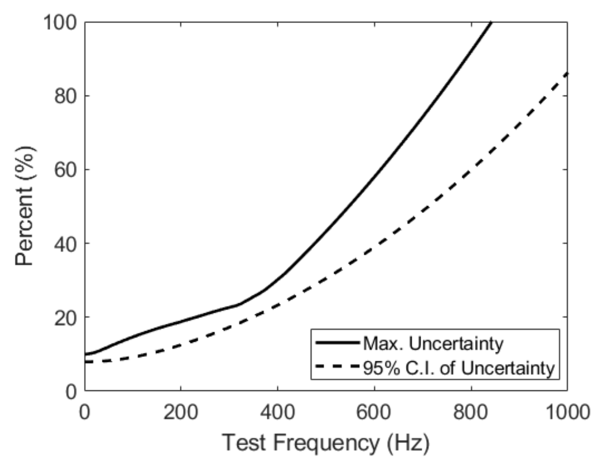

(b) SDoF

Figure 3.19: Comparing Identified Stiffness Uncertainty Between SDoF and 2DoF Uncertainty Analyses

The results show that the overall trend does not seem different between the SDoF case and the 2DoF case. The uncertainty for the 2DoF case is higher, however. This is evident even when the substructure is stiffer than the simulated test bearing by a factor of 20. This implies that fundamentally, the substructure is affecting the identification even when much stiffer than the test bearing. Rules of thumb that may suggest contributions from a substructure/pedestal are negligible must be reevaluated with this information.

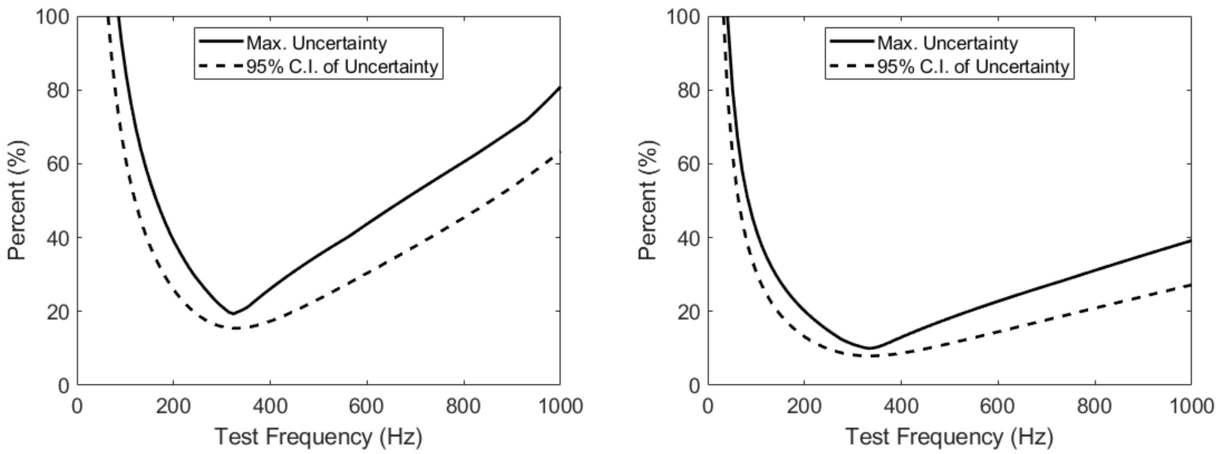

(a) (b)

Figure 3.20: Comparing Identified Damping Uncertainty Magnitude Between SDoF and 2DoF Uncertainty Analyses: (a) 2DoF (b) SDoF

At this point the results must be analyzed in terms of absolute identified stiffness and damping rather than percent uncertainty. A significant trend is shown when viewed this way. Figure 3.21 shows these results.

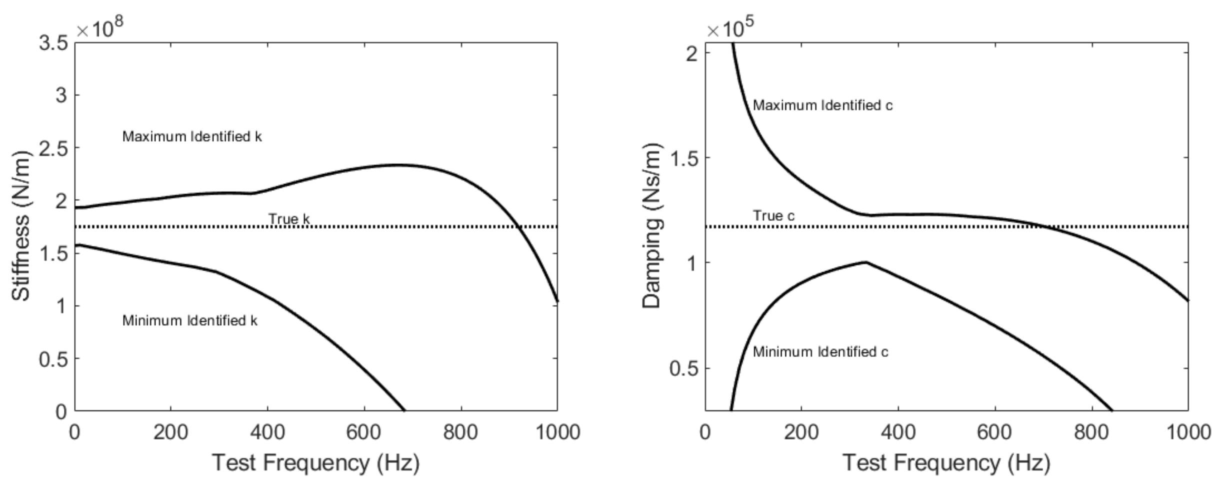

(a) Stiffness (b) Damping

Figure 3.21: 2DoF: Minimum and Maximum Identified Coefficients

The results in Figure 3.21 clearly show a trend of the identified coefficients deviating away from the true value. This means that if the bearing stiffness k and c were identified on a test rig that was well-represented by the 2DoF truth model, the identified coefficients at higher frequencies will not reflect the true value well (or perhaps a better phrasing is "less well than the uncertainty would indicate"). Both stiffness and damping will be under-predicted. From a model validation perspective the implication is that bearing codes cannot be validated with the experimental data from this hypothetical test rig above a certain test frequency (above approximately 350 Hz in the analyzed 2DoF example). If researchers adjusted the bearing code to better fit the data, predictions using that code would be deviating away from reality. Yet if typical industry guidance was applied to model validation through dynamic coefficient identification (i.e. - substructure is considered rigid enough to ignore), this bias may not be understood.

It is also clear from these results that the uncertainty by itself is not a complete picture of the uncertainty of dynamic coefficient identification. It is important to know if the identified coefficients are expected to deviate away from the truth due to system dynamics. This is important to know because if there is an expected bias, then even if the researchers tested 1,000 identical bearings or even 1,000,000 identical bearings on the same test rig, they would not be able to identify the bearing's true properties when conditions leading to biases are present. Statistical measures such as averaging would not be able to get to the truth.

Therefore, a bias or offset prediction for uncertainty is proposed for use alongside uncertainty. In this dissertation, it will be referred to as a bias. The bias will be predicted by using the mean of the identified coefficients in the uncertainty analysis. In the cases analyzed here and in most cases, the mean is assumed to be a reasonable measure of central tendency. The bias can also be normalized by the truth to obtain a percent bias relative to the true value.

Generally, it is advisable for an engineer or researcher developing a test rig for dynamic coefficient identification to reduce the bias as much as possible. However, it will be shown that reducing the bias by including additional models in the identification model may also increase uncertainty. The uncertainty analysis framework proposed in this dissertation is well-suited to analyze trade-offs between bias and uncertainty. The parameters in a cost-benefit analysis would include instrumentation of the test rig (such as if the applied force or bearing force is measured) in addition to models used in the identification model.

To present a more complete representation of the uncertainty of identifying dynamic coefficients, it is proposed that both the uncertainty and the bias be analyzed and presented together. Figure 3.22 shows an example of presenting the information together. Two plots are coupled together similar to frequency response plots that include magnitude and phase data. The graphs in Figure 3.22 are the uncertainty and bias results of the same case shown in Figure 3.21.

If the uncertainty analysis results show a bias, the researcher or engineer

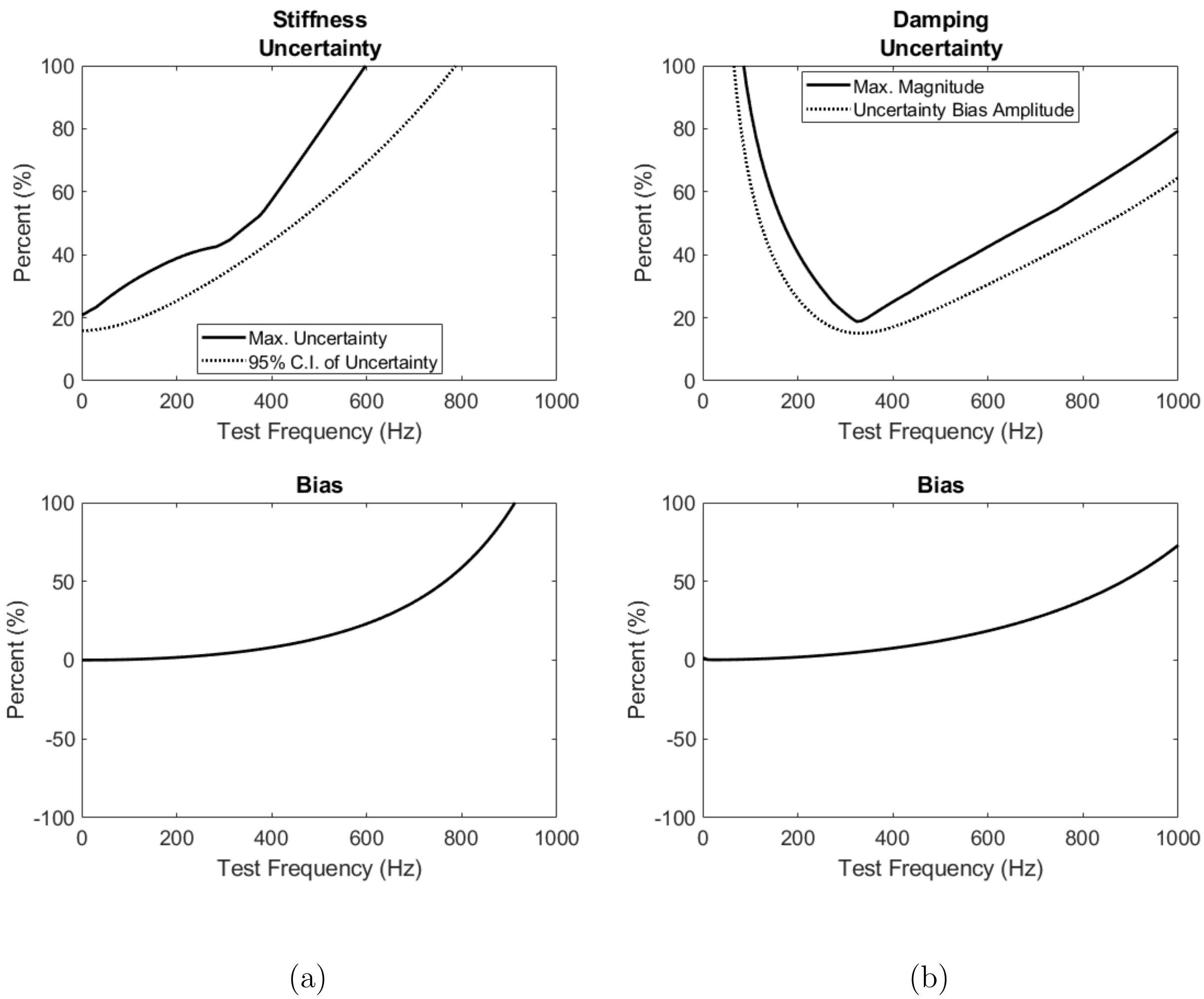

Figure 3.22: Uncertainty and Bias Results from 2DoF for (a) stiffness and (b) damping

must determine if the bias is significant or not. A thorough treatment of what makes bias significant for identified dynamic coefficients is not in the scope of this dissertation. However, on a simple level, there will be a threshold above which identified coefficients cannot be used to validate models and there will be a threshold below which the bias would be negligible. For example, if the bias is greater than the uncertainty, then the uncertainty analysis is suggesting that the true coefficients are not likely to be found. On the other hand, if the bias is predicted to be less than five percent, the net effect on identifying dynamic coefficients may be small (especially compared to other factors that may be contributing more to uncertainty).

Depending on the context of the uncertainty analysis, researchers and engineers will have different options for addressing various problems that may be highlighted by the uncertainty analysis. If the analysis is performed on a test rig that is already built, there are limited options for changing the expected uncertainty. The most direct path would be to minimize any uncertainty present in any sensors and/or improve the identification model used. When working on a new test rig design, bias (and uncertainty) can be affected in more ways. The instrumentation can be changed, or the fundamental layout of the test rig may be altered. The uncertainty analysis can guide the changes in design.

As a simple example of changes that can be considered when in the design phase, the mass of the added degree of freedom (relative to the SDoF model) in the 2DoF model is varied and uncertainty analysis is carried out on identifying dynamic coefficients. The results are shown in terms of uncertainty magnitude and uncertainty bias in Figures 3.23 to 3.26.

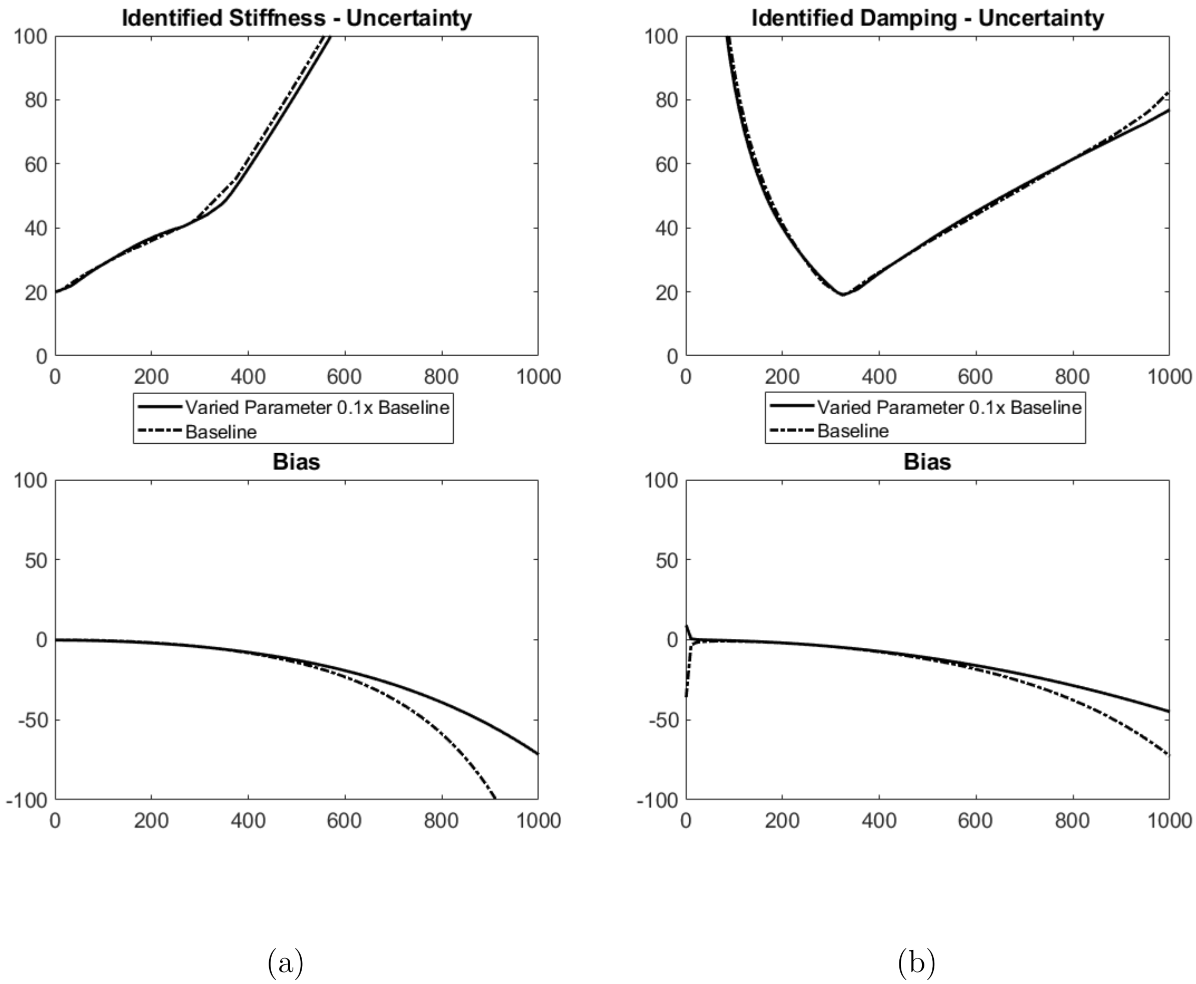

Figure 3.23: Comparing uncertainty when pedestal mass is 0.1x baseline for (a) stiffness and (b) damping. Only max. uncertainty shown to avoid clutter.

The most noticeable trend when the dynamics of the second DoF are changed is that the bias decreases when the second mass is decreased. The uncertainty does not change significantly until one of the system's critical speeds enters the frequency range of interest (such as in Figure 3.25). Interestingly, as seen in the damping uncertainty in Figure 3.26, the

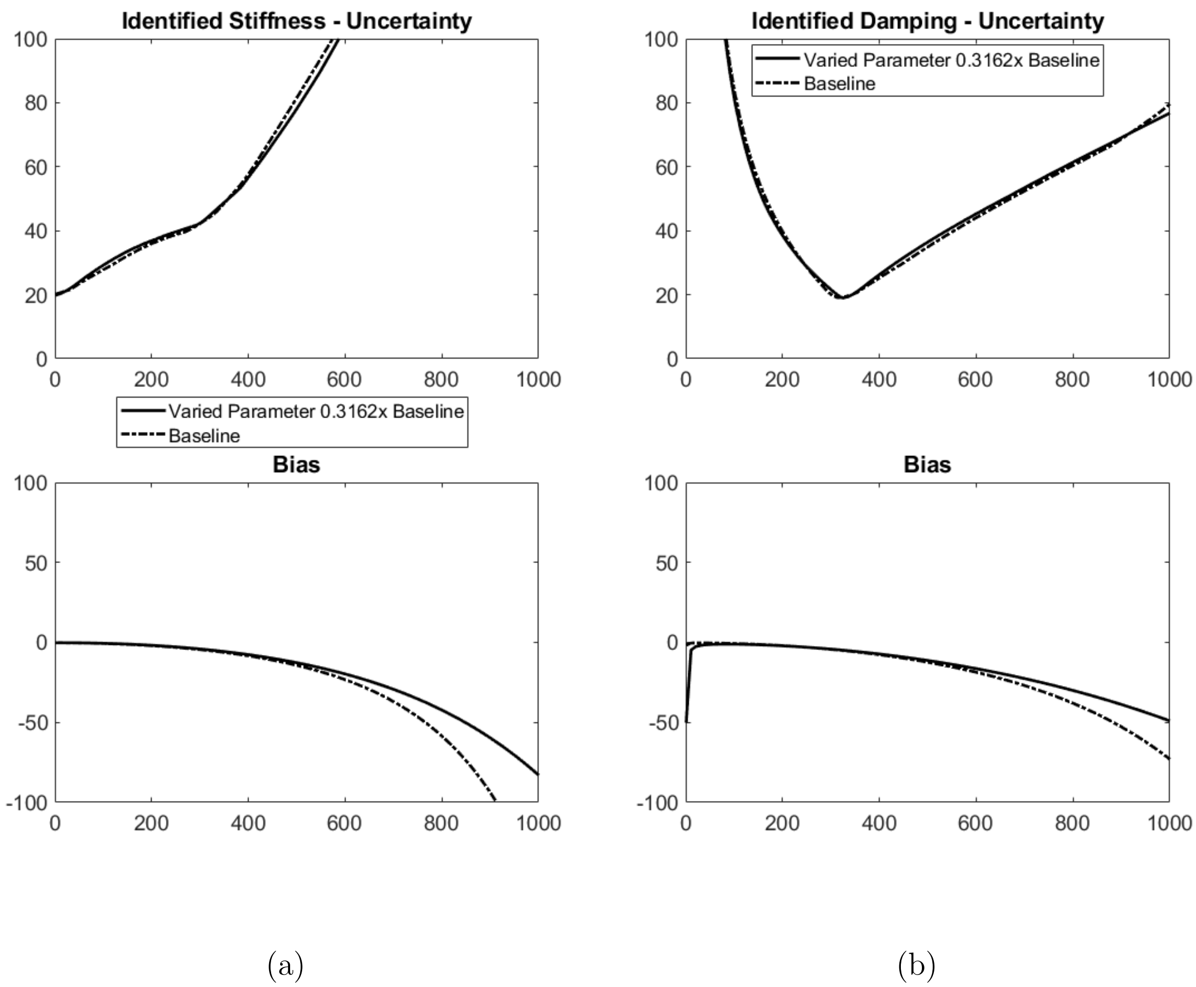

Figure 3.24: Comparing uncertainty when pedestal mass is 0.3162x baseline for (a) stiffness and (b) damping. Only max. uncertainty shown to avoid clutter.

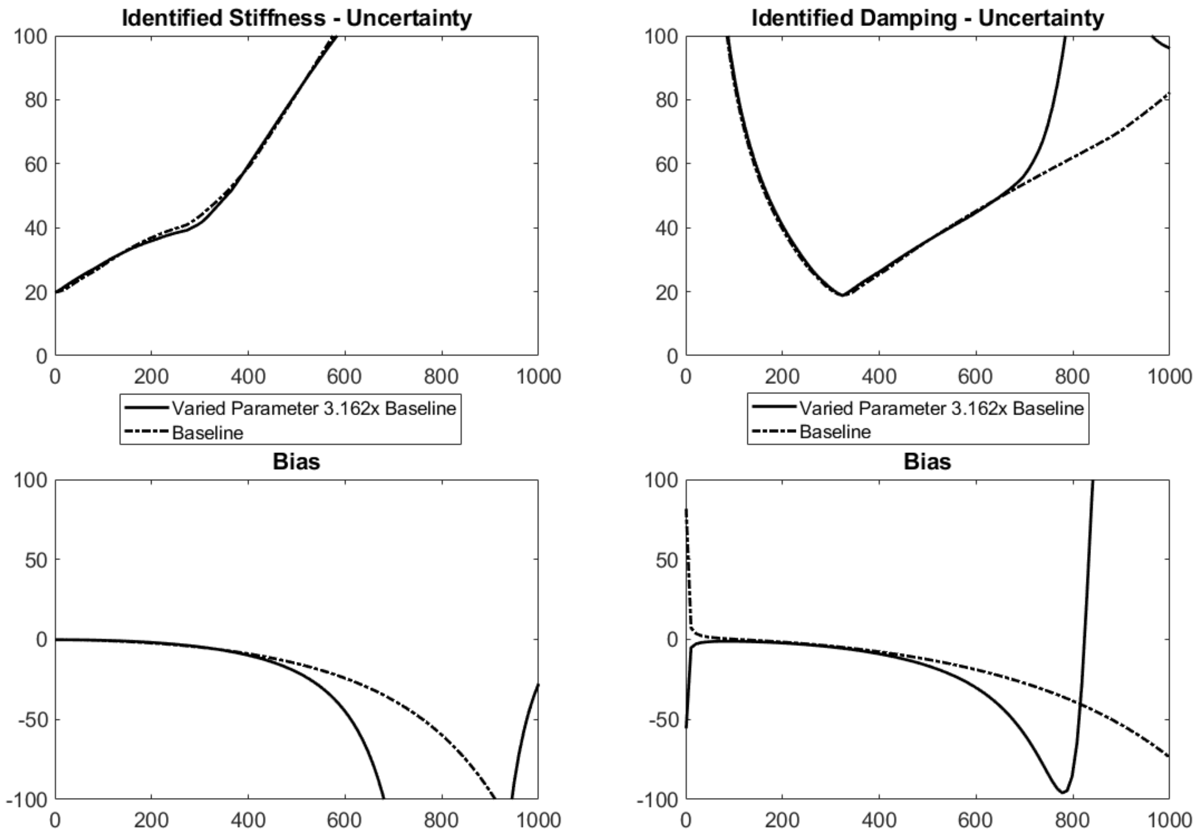

(a) (b)

Figure 3.25: Comparing uncertainty when pedestal mass is 3.162x baseline for (a) stiffness and (b) damping. Only max. uncertainty shown to avoid clutter.

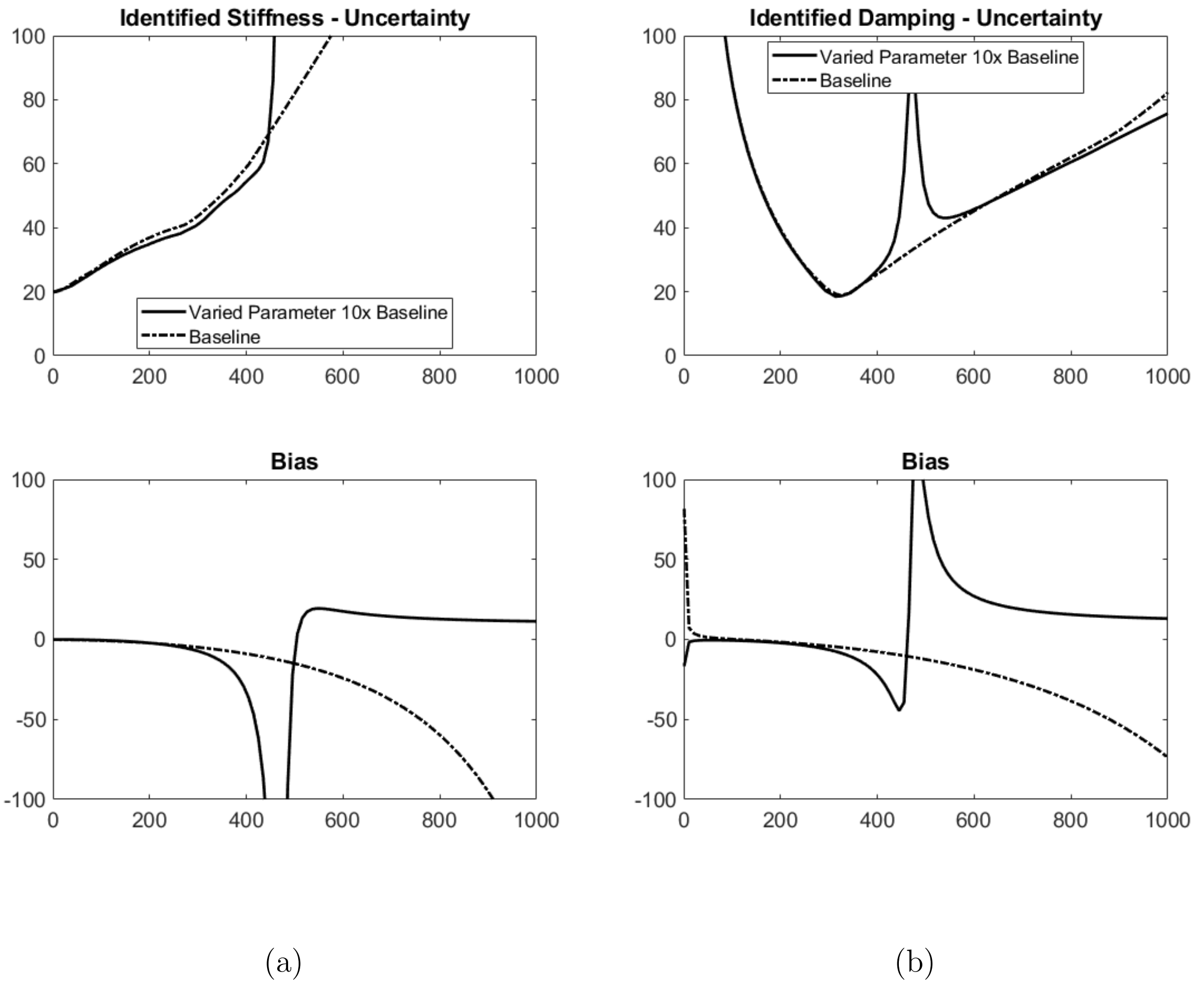

Figure 3.26: Comparing uncertainty when pedestal mass is 10x baseline for (a) stiffness and (b) damping. Only max. uncertainty shown to avoid clutter.

uncertainty peaks at the critical frequency but then returns to approximately the same as baseline afterward. It even seems like the growth of uncertainty is improved past the natural frequency. Furthermore, Figure 3.26 clearly shows a benefit to operating above a critical speed: the bias, instead of growing, levels off and seems to approach an asymptote. Figure 3.27 shows the same results when the frequency range is extended to be 1 Hz to 10,000 Hz for understanding this effect. The uncertainty, whether operating above a critical frequency or below, becomes greater than one hundred percent fairly quickly. The bias of the stiffness identification is smaller when operating above the critical frequency up to about 3,000 Hz. At this point, the baseline bias is smaller in absolute value. After about 6,000 Hz though the baseline once again has greater bias. For the damping bias, identifying when the system is operating above a critical frequency yields a potentially acceptable bias (about ten percent) for a majority of the frequency range while the base line model's bias is off the charts. These results generally reinforce the complexity of uncertainty when identifying dynamic coefficients. On a more specific note with respect to damping bias, the results support the idea that operating above critical frequencies may be of benefit rather than designing a test rig substructure to operate well below critical frequencies. The simulations here are only 2DoF systems while a real system is more complicated so the uncertainty analysis must be performed with a higher fidelity model to get stronger conclusions

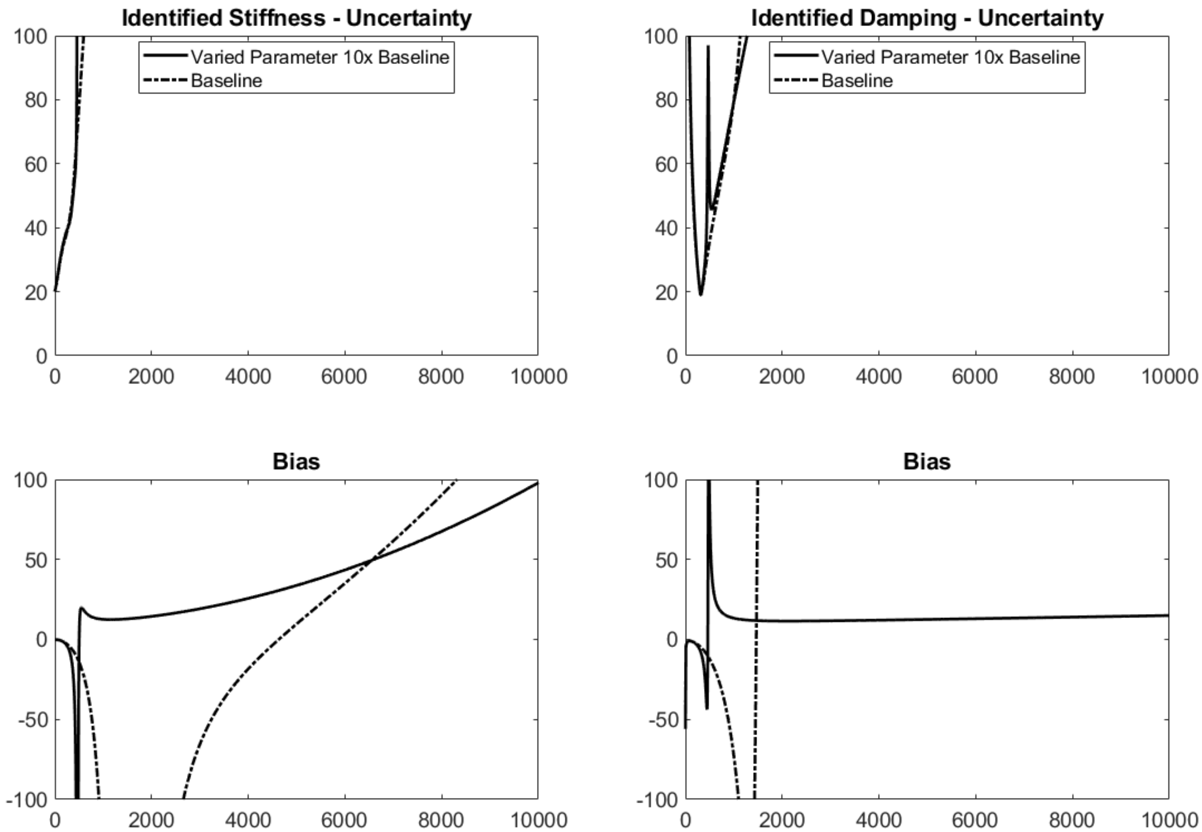

(a) (b)

Figure 3.27: Comparing uncertainty when pedestal mass is 10x baseline for (a) stiffness and (b) damping. Only max. uncertainty shown to avoid clutter.

3.2.1 Including More Fidelity in the Identification Model

When identifying with an identification model that does not include the second degree of freedom, the uncertainty increases and a bias is introduced relative to the SDoF model. The bias in the 2DoF case comes from the dynamics introduced by the second degree of freedom (the substructure model in Figure 3.17) that is not accounted for in the identification model. Though it is possible that the dynamics may be altered by changing the design of the test rig (especially design changes that impact the critical frequencies), the simulations indicate that this may not be a comprehensive solution. The case tested in this dissertation had some favorable bias results, but the uncertainty was not significantly improved. There is also the case of analyzing uncertainty of an already-completed test rig - design changes may not be feasible.

Since the identification model's lack of accounting for the second DoF is the root of the issue, it follows then that if we had knowledge of the substructure properties, it would compensate for the new dynamics. This can be evaluated by adjusting the identification model for the 2DoF model to include the pedestal dynamics. In other words, both the truth model and identification model are now the same (represented by Figure 3.17). In this case, with the same parameters originally analyzed, the uncertainty and bias results of the identified coefficients are presented in Figure 3.28. It can be seen that with perfect knowledge of the substructure, the bias can be completely compensated. However, the uncertainty is actually greater. Of course in a real experiment we would not know the substructure perfectly. Either our modeling will have some errors relative to truth or identifying the subsystem dynamics would have uncertainties associated with it. This is analyzed by implementing an uncertainty on the pedestal model used in the identification model. To compare the three cases, the stiffness uncertainty and the stiffness biases are compared in Figure 3.29. The damping results showed the same behavior.

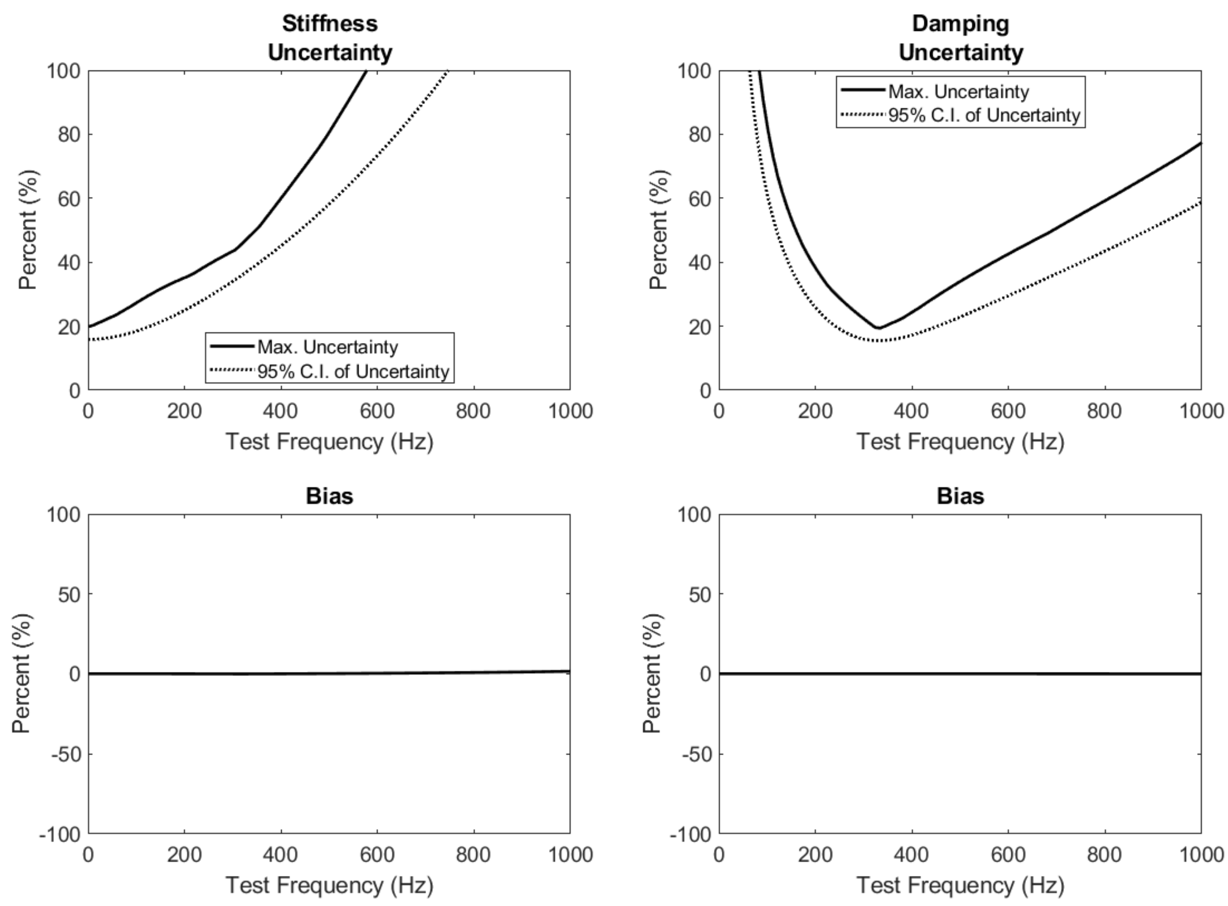

(a) (b)

Figure 3.28: Identification uncertainty when identification model includes error-free substructure model.

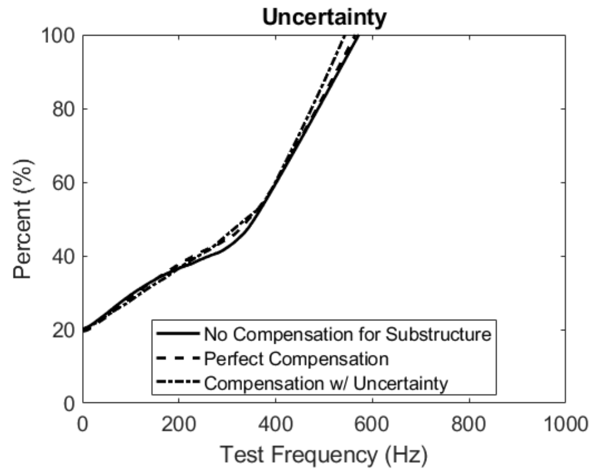

(a)

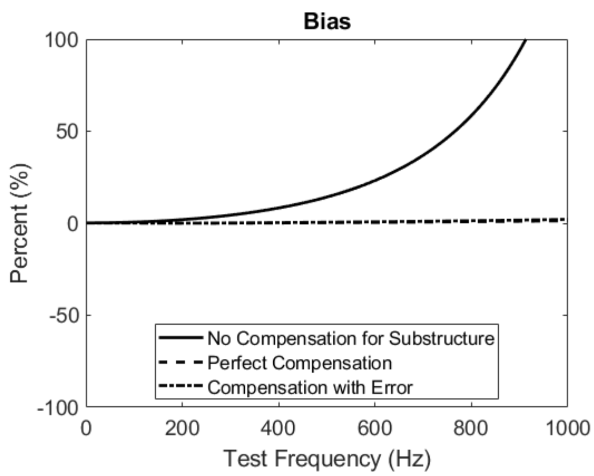

(b)

Figure 3.29: Comparing stiffness (a) uncertainty and (b) bias with different compensation models for the substructure

3.2.2 2DoF Identification Using Measured Bearing Force

So far the dynamic coefficients have been identified with applied force measurement and displacement measurements between the excited component and the substructure mass. In the SDoF model, it was observed that measuring the bearing force for identification instead of the applied force lead to improvements for uncertainty. If we repeat the same analysis for the 2DoF model, we get some interesting results shown in Figure 3.30. Even without any knowledge of the substructure model, measuring the bearing force improved the uncertainty and eliminated bias. Furthermore, much like in the SDoF model, the trend ends up being dominated by a linear term for the stiffness (versus a quadratic term when measuring applied force).

The results in this section suggest the following:

- Figure 3.29 supports the idea that requiring more knowledge increases uncertainty. Even when the substructure model is known perfectly, the uncertainty still increases.

- Measuring the bearing force again shows an improvement in uncertainty trends. In addition to reducing uncertainty, bias is reduced as well. The reduction of bias is an important feature when trying to validate bearing models on a test rig.

- Uncertainty has an interesting relationship with critical frequencies. At the critical frequencies there is a spike in uncertainty (as expected),

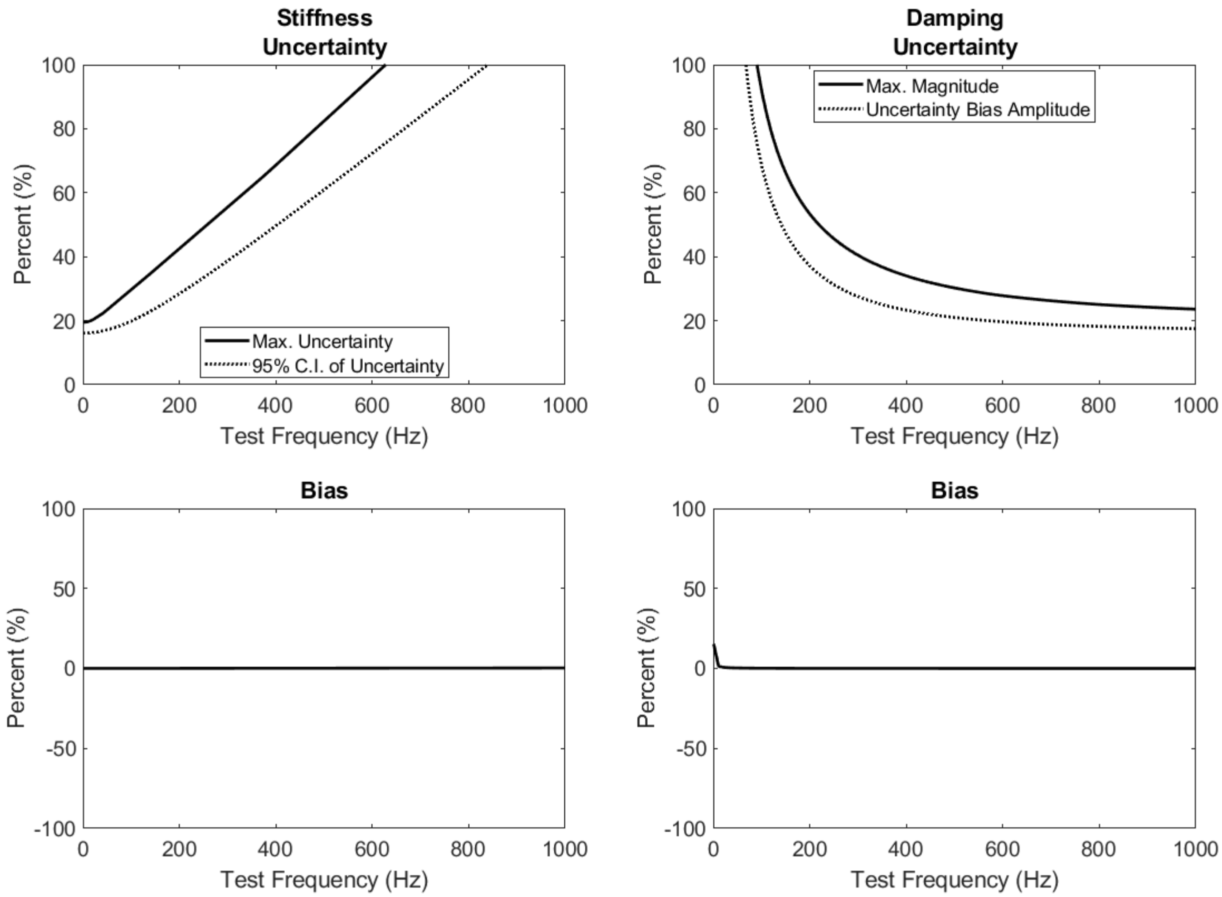

(a) Stiffness (b) Damping

Figure 3.30: Identifying with bearing force measurement, no substructure compensation

but afterwards the uncertainty trends return to the original trajectory. Caution must be used however as in more complex systems the way the mode interacts with the system will also be important.

3.3 Single-Axis Models Including Models based on Finite-Element Analysis (FEA)

It is possible to continue adding degrees of freedom to the systems analyzed for uncertainty in this chapter so far. In an attempt to achieve higher uncertainty accuracy, it is advantageous to break down solid bodies into elements to better model the flexibility of components such as bearing housings, rotor, foundations, etc. Since this basic idea is the principle behind FEA, tools using FEA to develop dynamic models can be implemented within the uncertainty analysis framework. The ability to pull in models based on FEA is a powerful feature of the uncertainty analysis proposed in this dissertation. It would eventually allow for the inclusion of non-linearities and other complex dynamics. Furthermore, some aspects of the system may still be approximated with lumped mass models.

A model will be developed for a coefficient identification test rig with higher fidelity than the SDoF or 2DoF model. The system modeled will be the same test rig described by Flack et al. [63] seen in Figure 3.2. A force will be applied to the housing through a load cell. The load cell will be modeled as a simple mass-spring-damper and the force measurement will be a function of the deformation of the load cell in one-axis (to represent the real physics in which a signal in a load cell is generated when the load cell experiences strain from an applied load). The load cell model will be connected to a housing model which will also be a lumped mass. The housing model will be connected to the bearing model. Also connected to the bearing model, a FEA-based rotor model will be used. This will be connected to a fixed ground through a flexible connection with extremely high stiffness (representing the rolling element bearings holding the rotor in place). Finally, two displacement sensors will be placed on either side of the bearing housing (not at the center of the bearing). A simple depiction of the model setup is shown in Figure 3.31.

The truth model for this system is shown in Figure 3.32. The identification model for a first analysis will be the same as in Figure 3.18. In other words, the force and displacement data will be collected and will be used to identify coefficients with the assumption that all the components are behaving ideally. The rotor is assumed to be rigid, the bearings and foundation holding the rotor are rigid, and the bearing housing is rigid.

As an example of the dynamic properties of the system, the dynamic model from force input on the rotor at the bearing location to the averaged output displacement at the sensor locations without the bearing active is shown in Figure 3.33.

Figure 3.34 shows the results when the complete system is analyzed with identification based on an applied force measurement and averaged

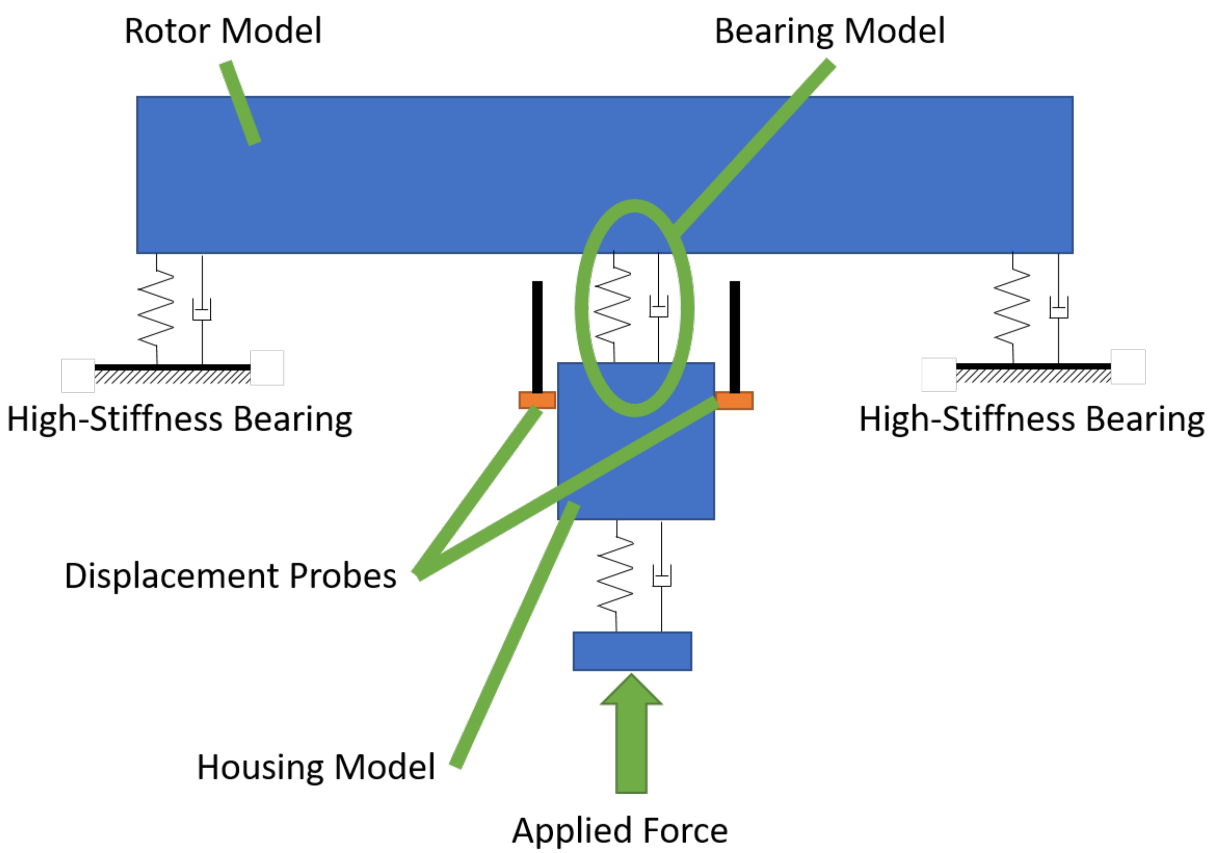

Figure 3.31: Higher Fidelity Single-Axis Model to be Analyzed with the Uncertainty Analysis Framework

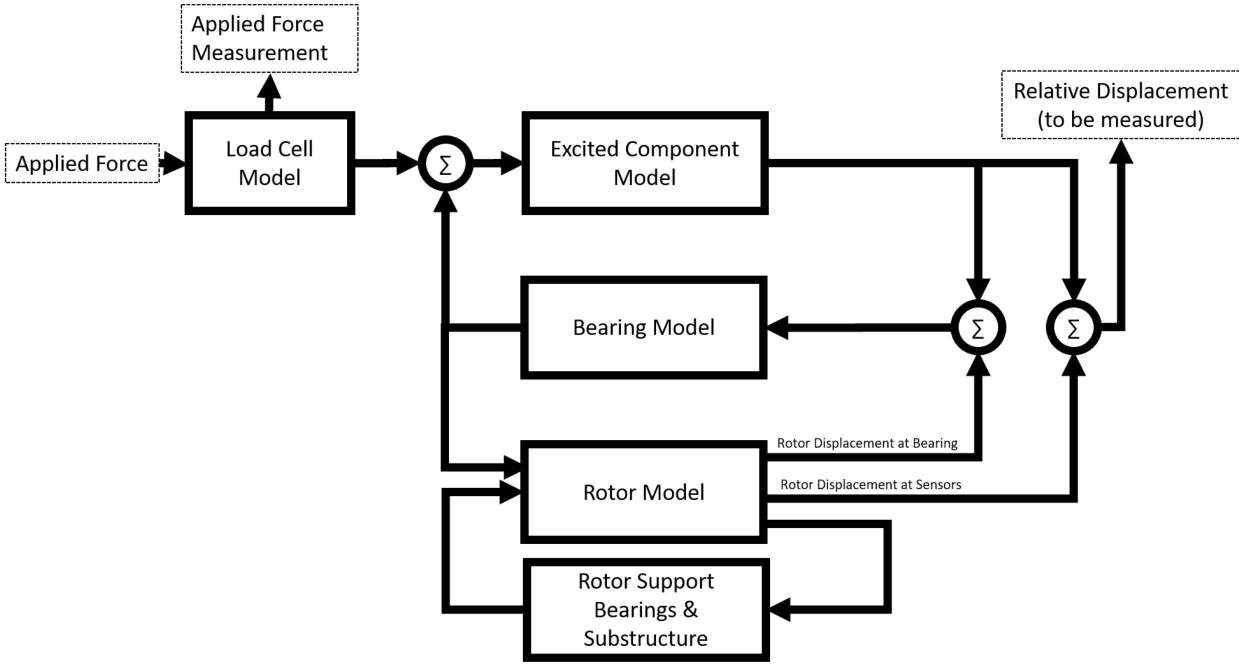

Figure 3.32: Higher Fidelity Single-Axis Truth Model

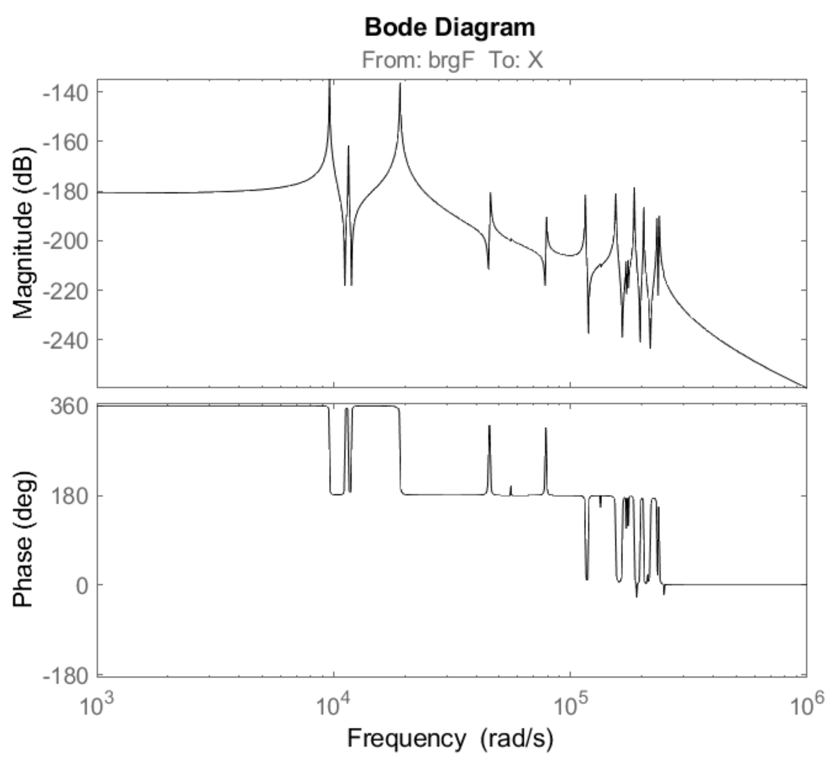

Figure 3.33: Rotor Model w/ Support Bearings

displacement probe measurements. The results show a strong bias - as large in magnitude as the uncertainty itself! Further inspection reveals that this is indicative of the stiffness and damping of the bearing being under-predicted by a significant margin.

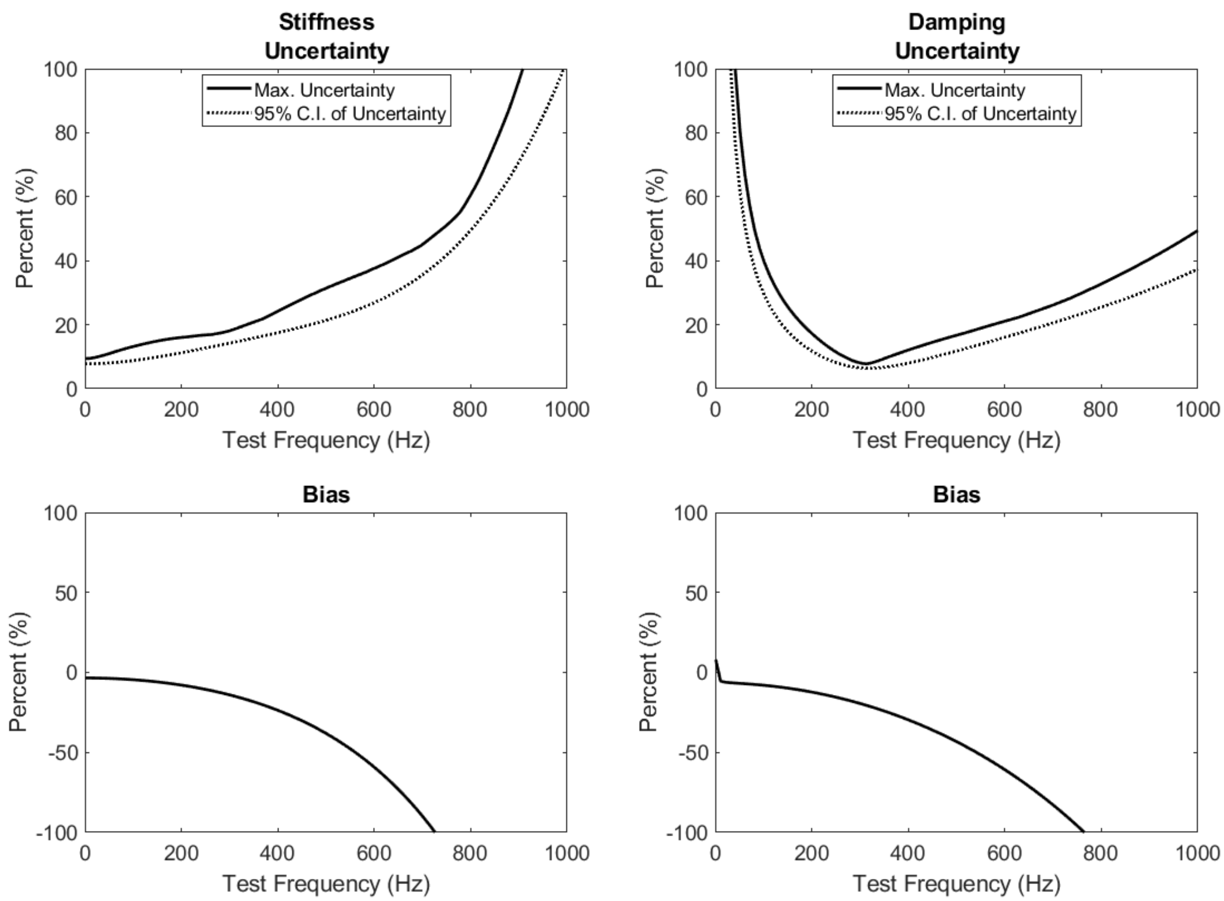

(a) (b)

Figure 3.34: Identifying 2DoF using applied force measurement (and not compensating for substructure): (a) Stiffness Uncertainty (b) Damping Uncertainty.

Figure 3.35 shows the results when bearing force is used instead of applied force. The results clearly demonstrate that even with the more complicated dynamics modeled, measuring the bearing force has improved trends. The uncertainty grows linearly as opposed to quadratically and the bias is smaller in magnitude and grows at a slower rate. One of the benefits of using these simpler models is identifying these types of trends. If a more realistic bearing was modeled instead of a constant stiffness and constant damping model, the variation in dynamic coefficients as a function of test frequency would have also affected the growth rate of uncertainty. This would make it harder to identify the underlying trends.

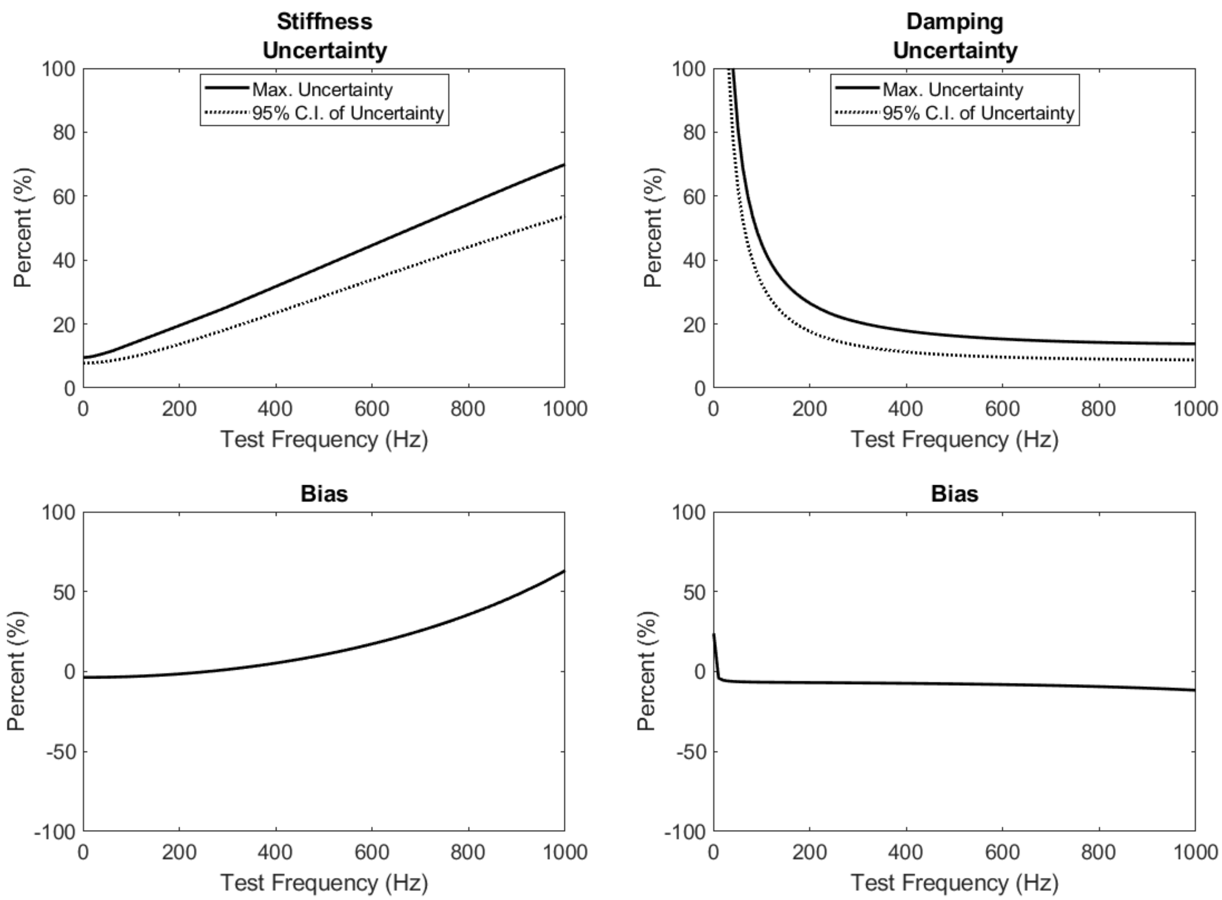

(a) (b)

Figure 3.35: Identifying 2DoF using bearing force measurement (and not compensating for substructure): (a) Stiffness Uncertainty (b) Damping Uncertainty

Perhaps the most significant observation from these two sets of results is that even on a system that has many attributes that would typically be considered rigid enough to assume rigid, the dynamics are affecting the identification uncertainty significantly. The rolling element bearings supporting the rotor are twenty times stiffer than the bearing as is the load cell stiffness. The rotor was originally considered short enough and large enough in diameter (i.e. - the L/D ratio of the rotor was small enough) to be considered rigid.[1] Nevertheless with these dynamics, the system results in significantly increased dynamic coefficient identification uncertainty.

In some experimental studies such as the testing in Childs et al. [50], a "dry shake" is used to try and account for some system dynamics. In the "dry shake", the system is excited without the fluid-film bearing being active. Without oil being supplied to the bearing, the connection between rotor and stator is broken. There is a load path through the foundation but it's effect is typically minimal. So for the "dry shake" the only dynamics identified are the dynamics directly connected to the excited component (the housing). One of the biggest contributors to the uncertainty bias in the higher-fidelity single-axis model is the rotor's flexibility. Without accounting for the rotor's dynamics in some form the bias will still be present. The study referenced, Childs et al. [50], does not make it clear if there was any attempt to reconcile the data with a model of the rotor or experimentally

[1] Another reason for assuming the rotor was rigid is that the first bending mode was calculated to be much higher than the original testing speeds. A further analysis in Chapter 4 reveals that the assumption is troublesome even at those lower frequencies.

identified rotor properties between where the bearing is located and where the displacement probes are located.

There is a clear advantage when measuring bearing force. Theoretically, the identification is only affected by the dynamics affecting the displacement measurement. Another alternative this suggests is that instrumentation that can measure the film thickness directly could lead to improved dynamic coefficient identification. The compensation using modeled or identified dynamics when measuring the applied force is possible still. However, even in the case where everything is compensated perfectly, the resulting uncertainty from measurement errors would still yield a quadratic increase in uncertainty as a function of frequency versus a linear increase of uncertainty magnitude when bearing force is measured. This should of course be weighed against the measurement uncertainty associated with each setup. Depending on the frequency range of interest (particularly at lower frequencies), applied force measurement may still result in better uncertainty because the quadratic term has not become dominant.

3.4 Summary and Conclusions of Single-Axis Models to Understand Uncertainty Analysis

In this chapter, the proposed uncertainty analysis framework is developed with simple examples. These examples, although relatively simple, offer valuable insight into factors that significantly affect the uncertainty of dynamic coefficient identification. The factors explored in this chapter are not meant to be exhaustive but serve as a starting point for engineers and researchers to build upon.

The major conclusions developed in this chapter are summarized below:

- The results of an uncertainty analysis cannot be captured adequately in a single value. The recommendation presented in this dissertation is to present results with test frequency on the horizontal axis and uncertainty magnitude as a percent on the vertical axis. The driving motivation for using uncertainty magnitude as a percent is for the purpose of validating bearing codes that predict dynamic coefficients. In addition to the uncertainty magnitude, an uncertainty bias value as a percent of the truth used in the simulation should also be presented as an indication of how well the identification model matches the actual system.

- Identifying dynamic coefficients with the bearing force measured (as opposed to the applied force) through some method leads to a linear growth in uncertainty magnitude rather than a quadratic growth when applied force measurements are used. Compensation through acceleration measurements or otherwise cannot eliminate this trend. Therefore, especially as systems are moving towards requiring validated models for higher excitation frequencies, measuring the bearing force is strongly recommended. In the literature reviewed for this dissertation, the large majority of test rigs measured applied force.

Chapter 4

Applications of the Uncertainty Analysis Framework

Chapter 2 of this dissertation reviewed the state-of-the-art of uncertainty analysis for TPJB dynamic coefficient identification experiments and found it lacking. Chapter 3 developed a framework for uncertainty analysis using single-axis models that addresses the shortcomings of uncertainty analysis currently. The single-axis models identify some important factors for analyzing uncertainty, offering insight into practical test rig considerations to minimize the uncertainty of TPJB dynamic coefficient identification. With the uncertainty analysis framework established, this chapter applies the framework to a test rig that was previously used to identify TPJB coefficients. The test rig described in Flack et al. [79] is used as a reference to build models for analysis.

4.1 Higher-Fidelity Uncertainty Analysis Based on the Test Rig Described in Flack et al. [79]

4.1.1 Description of the Test Rig

The test rig described by Flack et al. [79] was used to measure static and dynamic properties of a variety of bearings including TPJBs. Figures of the test rig's cross section (Figure 4.1) and layout (Figure 4.2) are reproduced for convenience.

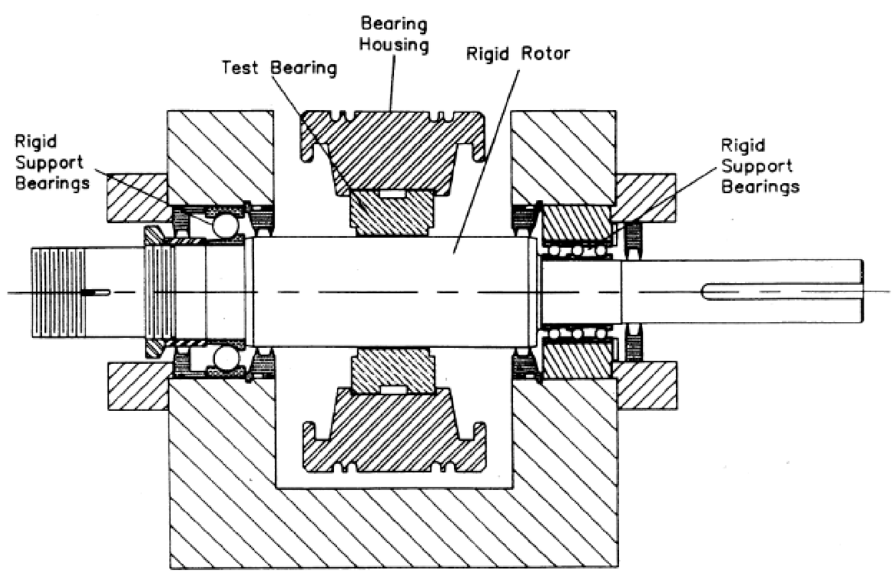

Figure 4.1: Test Rig Cross Section Reproduced From Flack et al. [79]

This test rig has a floating bearing housing which is excited with electrodynamic shakers. The rotor is supported by rolling element bearings modeled as a rigid connection to ground. This configuration was chosen for the convenience of applying and measuring forces on the excited component. The rotor was designed to be "rigid" by ensuring the system's

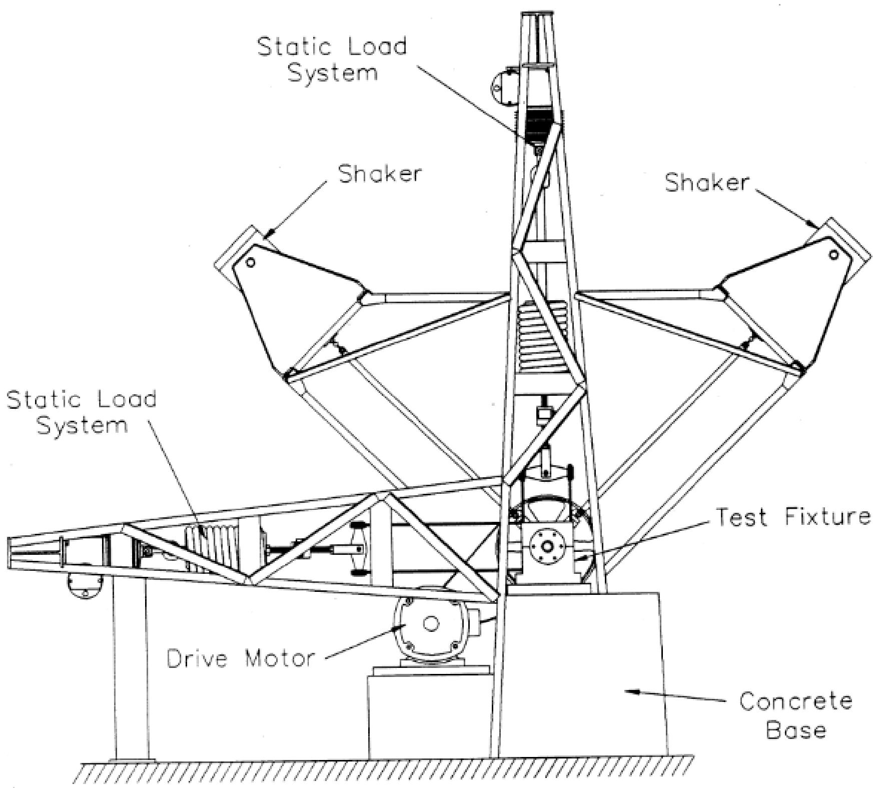

Figure 4.2: Test Rig Layout Reproduced From Flack et al. [79]

first critical speed was much higher than the running speed of the rotor. The first critical speed is quoted to be 16,000 RPM compared with the original maximum running speed of 1,800 RPM. Some later studies ran the system at slightly higher speeds.

Dynamic loads were applied to the floating housing using electrodynamic shakers connected with rigid stingers long enough such that the motion of the housing would not significantly affect the loading. Some additional details of the dynamic load system are seen in Figure 4.3 including a preload spring. The stinger joints could not support compression loads so the preload springs ensured the joints always experienced tensile loads. The applied dynamic force was measured with strain gage load cells at the point of application. Structural modes in the operating range were removed to minimize undesired dynamics. The static loading is applied through electric linear actuators connected via a "soft" spring of 175 kN/m. The low-stiffness spring was selected to minimize static load variation due to the motion of the actuator and the bearing. The rotational alignment of the bearing housing is maintained with a constraint system shown in Figure 4.4.

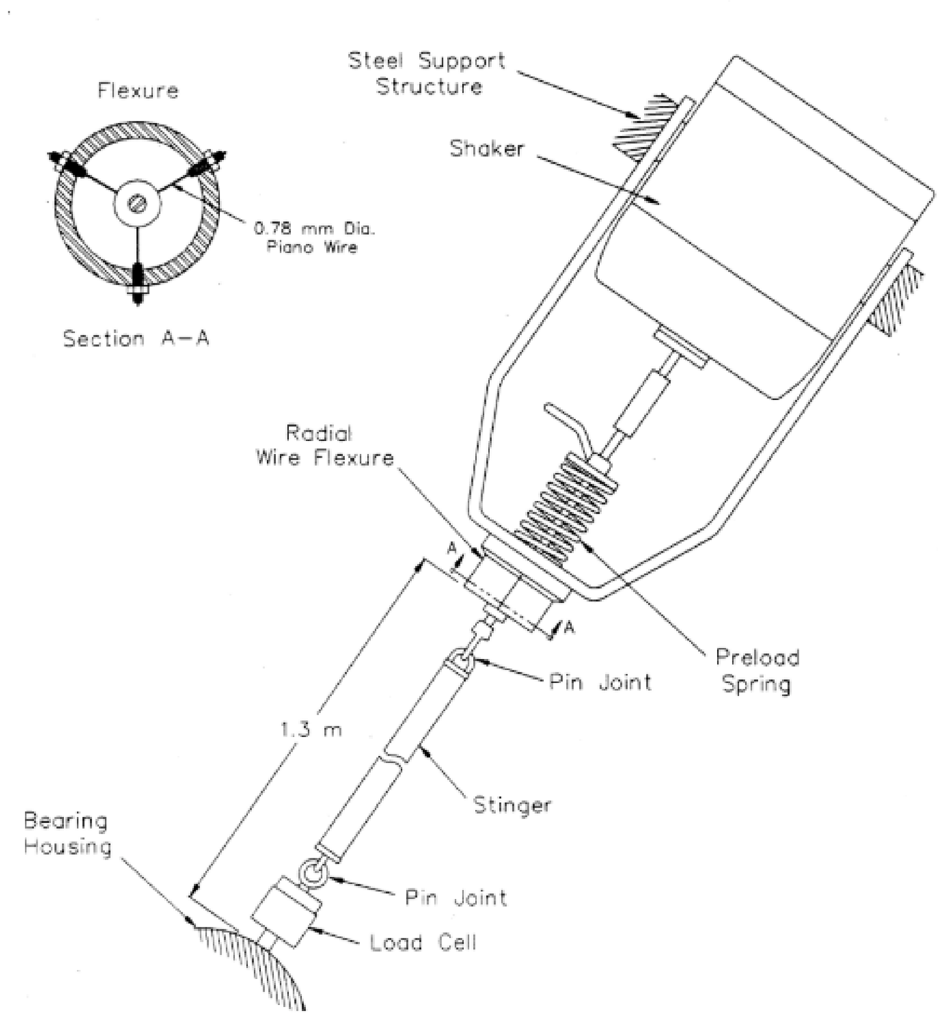

Figure 4.3: Test Rig Dynamic Loading System Reproduced from Flack et al. [79]

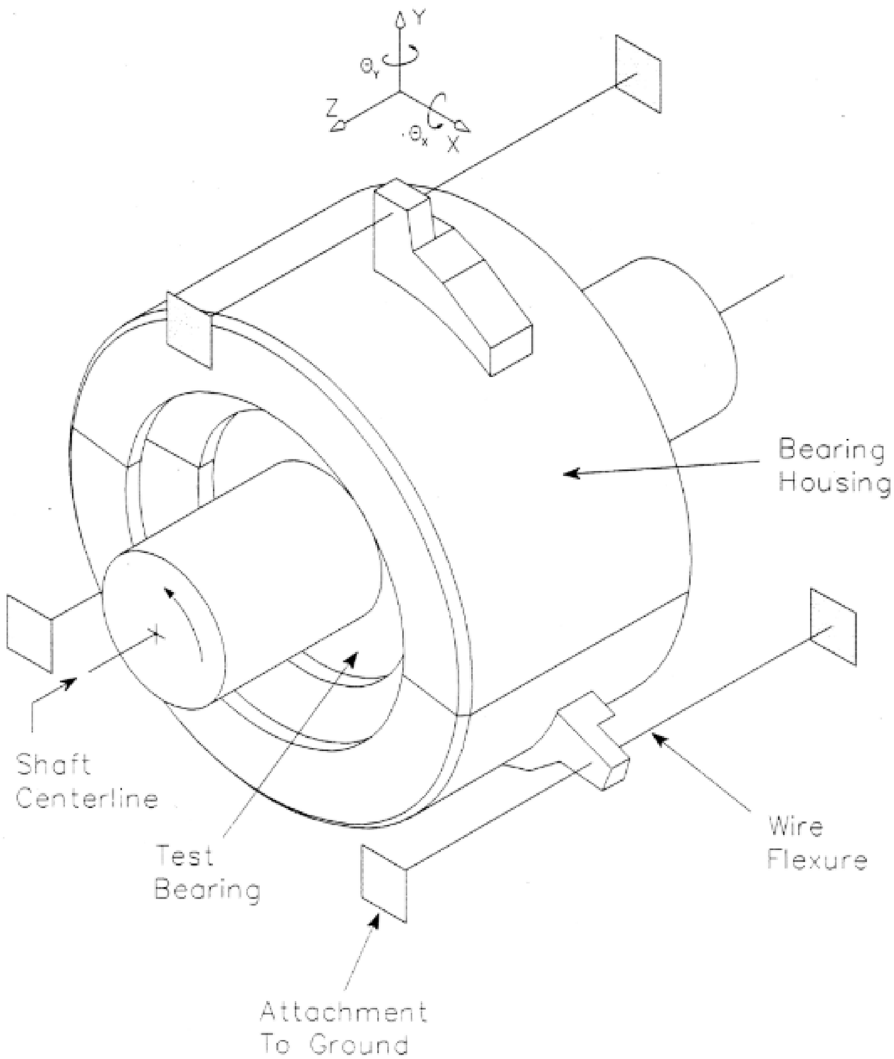

Figure 4.4: Housing Constraint System of Test Rig Reproduced From Flack et al. [79]

4.1.2 Developing Models of the Test Rig Components/Subsystems for Analysis

The uncertainty analysis framework is applied to a study of pad pivot friction by Wygant et al. [60] which was performed on the Flack test rig. This study compared the dynamic properties of two TPJBs with different pivot types - spherical seated ball-and-socket pivots and line contact rocker-back pivots. Experiments were conducted with synchronous excitations at 15 Hz (900 RPM), 27.5 Hz (1,650 RPM), and 37.5 Hz (2,250 RPM).

Models were developed representing the TPJBs identified in the experiment, the rotor, and measurement instrumentation (force and displacement measurement).

TPJB Model

The modeling parameters and operating conditions used for the uncertainty analysis are presented in Table 4.1.1.

Table 4.1.1: TILTING PAD JOURNAL BEARING PARAMETERS

Parameter	Value
Number of Pads	5
c_b, μm	81.3
c_p, μm	91.4
Preload	0.125
Pivot Offset Ratio	0.500
Length/Diameter	0.750
Pad Arc Length (degs)	52
Oil Inlet Configuration	flooded
Pad Material	steel

A fluid-film bearing modeling algorithm developed by Branagan [80] is used to perform TEHD analysis with these parameters to generate a truth model. The resulting true coefficients are presented in Figure 4.5. It was discovered that the bearing coefficients differed only slightly as a function of operating speed so a single operating speed was selected. Furthermore, though some variation is expected with varying loading, a single loading case is selected. The goal is not to match the experimental results exactly but rather to compare the uncertainty published in the paper with the uncertainty computed using the uncertainty analysis framework developed in this dissertation.

The dynamic coefficients from the model are presented in Figure 4.5. The vertical principal coefficients (K_{yy}, C_{yy}) are larger in magnitude than the horizontal principal coefficients (K_{xx}, C_{xx}). The cross-coupled stiffnesses are negligible relative to the principal stiffnesses up to about 60 Hz. The cross-coupled damping remain negligible in the entire range of test frequencies plotted.

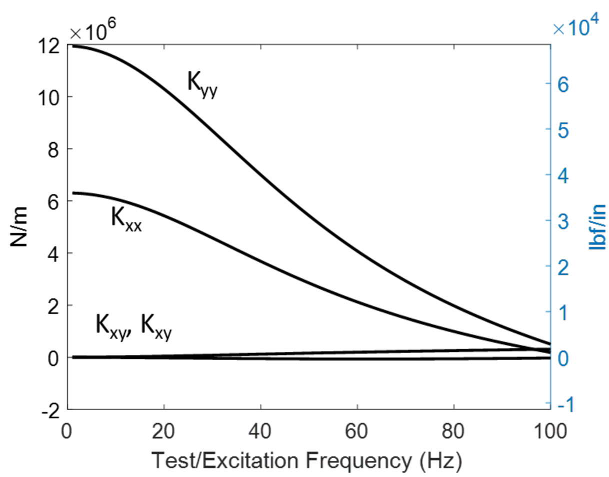

(a) Stiffness Coefficients

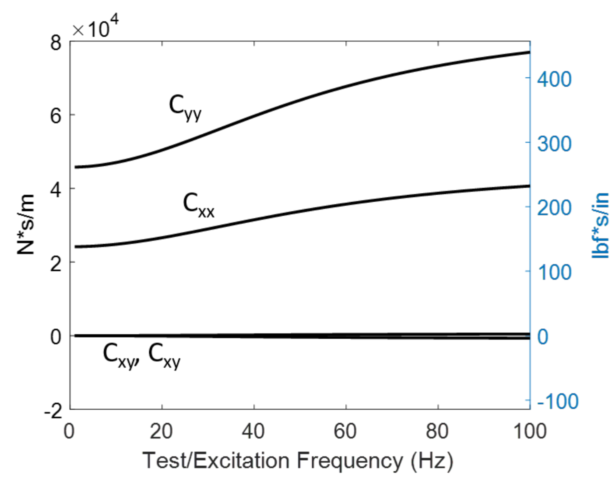

(b) Damping Coefficients

Figure 4.5: Bearing Truth Model Based on Wygant et al. [60]

Rotor Model

Based on a scale drawing of the rotor and some critical measurements, a finite element model was developed for the rotor. The model was imported into the uncertainty analysis as a state-space model which could be combined with the other models. The state-space model included inputs for the TPJB model and a model of the rolling element bearings. The substructure was not directly modeled because there was not enough information to recreate a high fidelity model. The dynamic properties of the supports (i.e. - rolling element bearings) are shown in Table 4.1.2.

Table 4.1.2: Additional Parameters - Relative to Test Bearing Max. Stiffness and Damping

Support Bearing Stiffness	20x
Support Bearing Damping	0.01x
Load Cell Stiffness	20x
Load Cell Damping	0.01x
Load Cell Mass	1 kg

Measurement Instrumentation Model

The measurement model for displacement assumed the bandwidth of the sensor system was high enough that the only significant effect was the measurement error model. Additionally, the rotor model allowed the displacement measurement to be non-collocated with the bearing location. Two sets of sensors are used on either side of the bearing housing. The measurements are averaged to obtain the displacement measurement.

The force measurement was modeled with a simple mass-spring-damper model for each axis representing the two load cells for two orthogonal axes. Model parameters are shown in Table 4.1.2. The load cells output a signal that corresponds with force when they experience a strain and this is captured in the measurement model.

4.1.3 Uncertainty From Force and Displacement Error Alone

A first analysis is performed using only the higher-fidelity TPJB model for the test bearing. The rotor is assumed to be rigid, and thus treated as a lumped mass. The support bearings and substructure are also assumed rigid.

This analysis serves two purposes. First, the higher fidelity model - now including a TPJB model in two axes - can be compared with the results obtained with the single-axis models. Second, the original publication states that "the combined uncertainty analysis included, but was not limited to, uncertainty in the magnitude and phase of the sinusoidal applied force and the resulting sinusoidal response." The description implies that while the uncertainty analysis in the publication allows for other factors, only measurement errors were analyzed and presented. Therefore, the uncertainty analysis framework in this dissertation can be compared with the uncertainty analysis performed by Wygant et al.

The uncertainty parameters are listed in Table 4.1.3. These values have been selected to be representative of typical uncertainties for load cells and displacement probes. For each trial in the Monte Carlo method an

Displacement Magnitude Uncertainty	±2%
Displacement Phase Uncertainty	±2 degrees
Force Magnitude Uncertainty	±7%
Force Phase Uncertainty	±4 degrees

Table 4.1.3: Uncertainty Parameters for Higher Fidelity Uncertainty Analysis

independent error case is generated for the principle lateral directions as well as for cross-coupling in the system based on the values in Table 4.1.3.

The results of this first analysis for the stiffness terms are shown in Figure 4.6. Note that the vertical axis scale has been relaxed for the K_{xy} and K_{yx} results to show the magnitude of uncertainty for the cross-coupled terms. The reason the cross-coupled term uncertainties are so large is because the magnitude of the cross-coupled stiffness terms are so much smaller than the direct terms.

Vertical lines at the rotating frequencies of the experiments are included as a reference to Wygant et al. Since the TEHD algorithm used to develop the truth model did not vary significantly based on the operating speeds, the dynamic coefficients should be representative at all three speeds. Some variation is expected due to loading changes in the Wygant et al. experiments.

Depending on the pivot being tested, uncertainties computed by Wygant et al. for the principal coefficients varied from as low as 5% for the K_{yy} with the rocker-back pivot to 82% for the ball-and-socket pivot TPJB. To provide a more direct comparison, the K_{xx} results in the present uncertainty analysis have representative points from the Wygant et al.

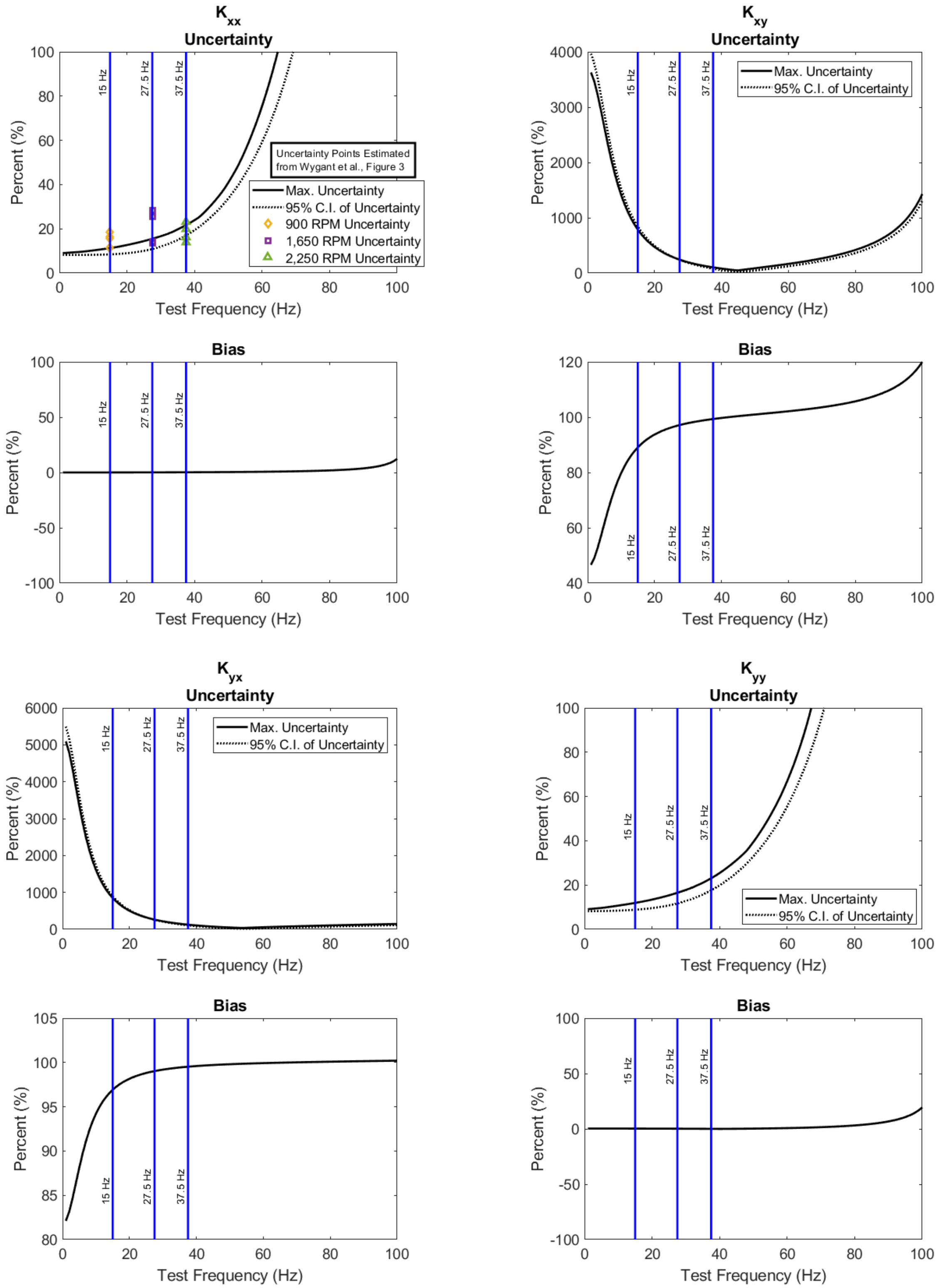

Figure 4.6: Stiffness Uncertainty with Only Measurement Errors

uncertainty analysis plotted. These points have been estimated from the computed experimental uncertainty for K_{xx} for the TPJB with rocker-back pivots. The uncertainties computed by Wygant et al. are comparable to the uncertainties computed with the proposed uncertainty analysis framework. Differences can be attributed to differences in static load, sensor uncertainty definition (absolute vs. relative), and dynamics implications of experimental methods. For example, it is stated that "the uncertainties varied due to decreasing orbit peak-peak response as stiffness increased." To achieve a closer comparison to the published uncertainty values, more detail than given in the publication is required of how the peak-peak response varied relative to the sensor capability to measure the response. Regardless of the differences, the uncertainties are reasonably close to each other and provide support that the uncertainty analysis framework in this dissertation estimates uncertainty accurately.

The cross-coupled term uncertainties in Wygant et al. were much larger typically though not quite as large as predicted by the uncertainty analysis in this dissertation. Still, because the cross-coupled terms are much less significant to system dynamics for TPJBs, they will not be presented beyond Figure 4.6. The uncertainty results for damping are shown in Figure 4.7. The values predicted by the uncertainty analysis in this dissertation are reasonable relative to the values of uncertainty computed in Wygant et al. [60].

In addition to the comparison to the published results, an important observation is that the uncertainty behaves in a similar fashion to the

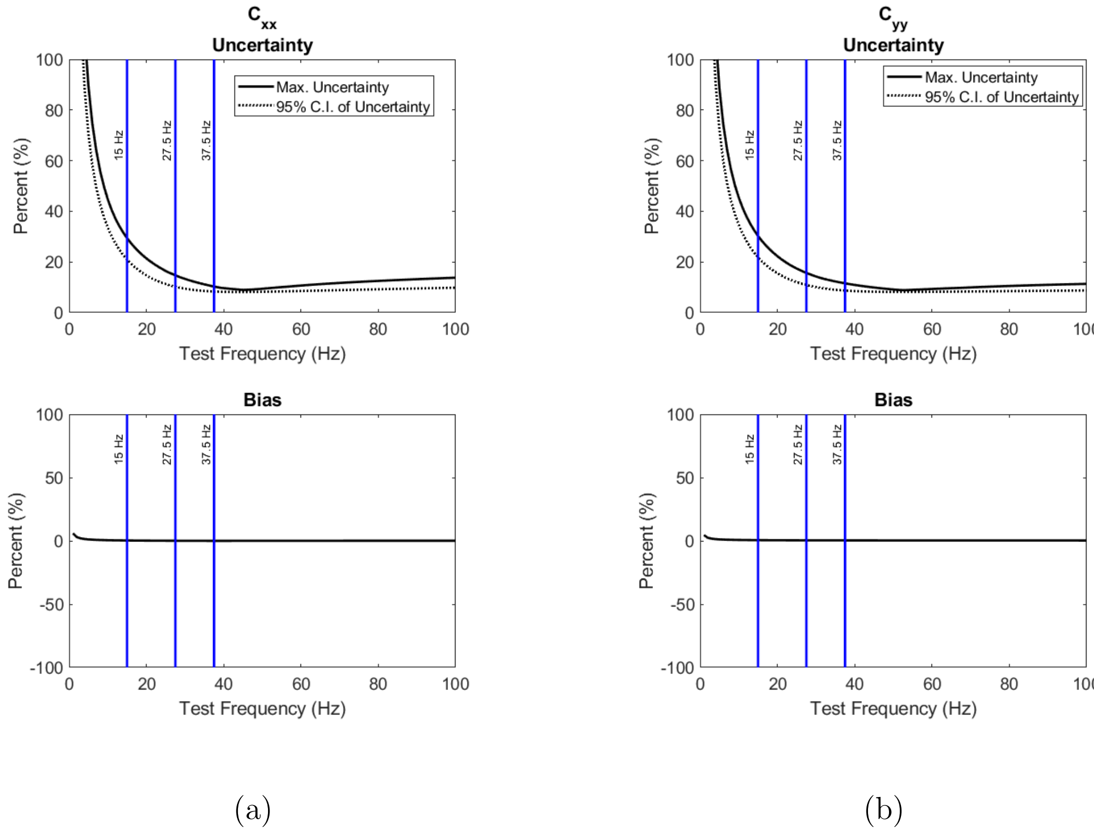

Figure 4.7: Damping Uncertainty with Only Measurement Errors

uncertainty results from the single-axis models including the SDoF models. The principal stiffness uncertainty follows a roughly quadratic curve which is expected. The behavior is exaggerated because instead of a constant true stiffness, the higher fidelity TPJB model has decreasing true stiffness - which is expected to increase the uncertainty further on top of just the frequency effects. The cross-coupled stiffnesses were expected to be much more uncertain than the direct terms because they were much smaller in magnitude and the results show this. It is interesting to note that there is a little bit of bias introduced at about 100 Hz, most noticeable in K_{xx}. This bias, even though there are no additional dynamics, results from the direct stiffness becoming about the same magnitude as the cross-coupling, so the cross-coupling is introducing a bias. This result reinforces the importance of a complete uncertainty analysis. Even if the system dynamics have been designed to be as close to ideal as possible, it is possible that the cross-coupling can introduce biases. While the bias is broken out here to show the described effect, it is small enough in the test frequency range that the researchers could say, “Bias is estimated to be within ±5% in the test frequency range of interest.” This way only the uncertainty results need to be shown. The damping uncertainty results also demonstrate the same trends identified in the single-axis models.

4.1.4 Adding More Dynamics to the Two-Axis Analysis of Uncertainty

The first uncertainty analysis of the higher fidelity, two-axis model based on the Flack et al. test rig analyzed the effects of measurement errors alone. The analysis is extended to include additional dynamics similar to Section 3.3. The following dynamics are considered:

- A two-axes finite-element model for the rotor that will include the effect of the rotor flexibility as well as displacement sensor non-collocation relative to the bearing center-line. Gyroscopics from the rotation of the rotor will also be modeled.
- A simple model of the connection to ground through the rotor support

bearings and substructure.

- A simple load cell model.

These additional dynamics are mostly the same as the dynamics in Section 3.3 and the common factors included will provide a comparison between the uncertainty analysis with only one axis to the higher-fidelity, two-axes analyses. The parameters such as load cell stiffness and rotor support bearing stiffness are kept the same to make the most effective comparison.

The results are shown in Figures 4.8 and 4.9. Cross-coupling coefficient uncertainties are omitted due to the large uncertainties for values orders of magnitude smaller than the principal coefficients.

The frequency range analyzed is 1 Hz to 100 Hz which is different from the frequency range in the single-axis analyses which ranged from 1 Hz to 1000 Hz. In this frequency range, the most notable bias was in K_{xx}. Otherwise, the bias is within 10%. As noted in the uncertainty analysis with just measurement error, the basic trends match the expected trends from the single-axis models.

An interesting relationship is observed when comparing stiffness uncertainty to damping uncertainty. For the lower test frequencies, the stiffness uncertainty is lower but the damping uncertainty is higher.

If any sort of model compensation is performed for the bias in the K_{xx}, the uncertainty would increase. For Wygant et al., given the range of

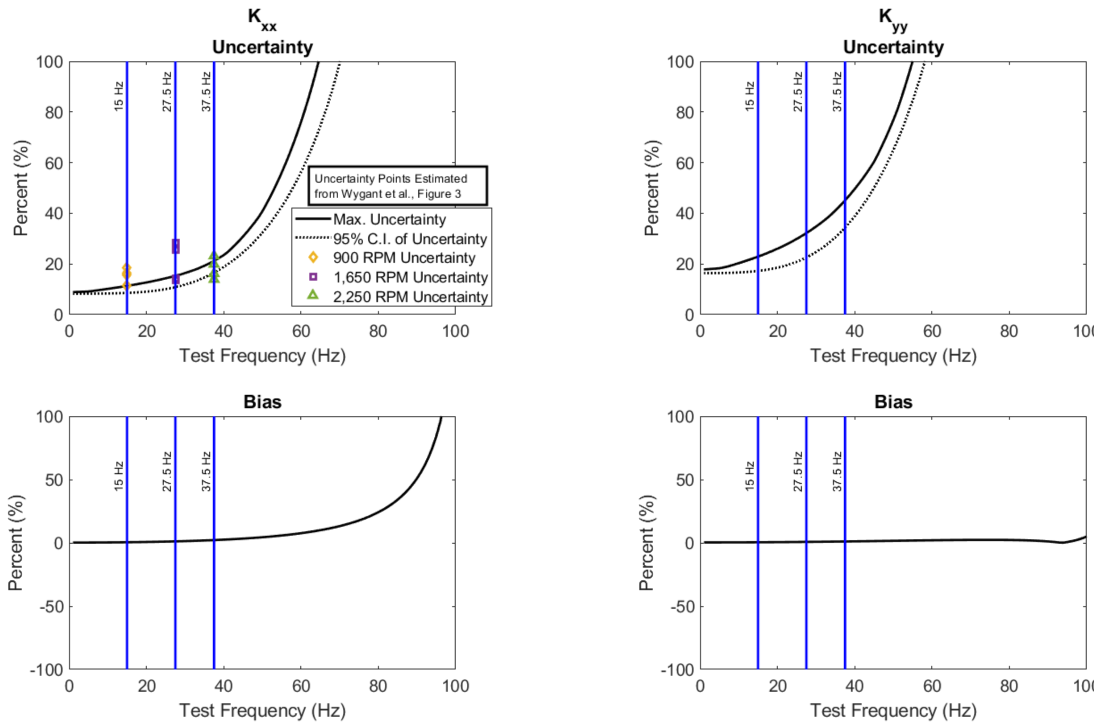

Figure 4.8: Stiffness Uncertainty With More Dynamics

frequencies tested, this may not be an issue. However, modern systems operate at much higher speeds and experience excitations at much higher frequencies. There are many test rigs with a very similar design still in use to identify TPJB dynamics and it is very likely that they have acceptable uncertainty at very low frequencies, but at test frequencies more applicable to modern machinery, the uncertainty for stiffness would definitely be unacceptable. However, it appears that at higher frequencies damping uncertainty may in fact improve. The primary take-away from this is that uncertainty analysis is more important than ever to truly understand these trade-offs in the identification process.

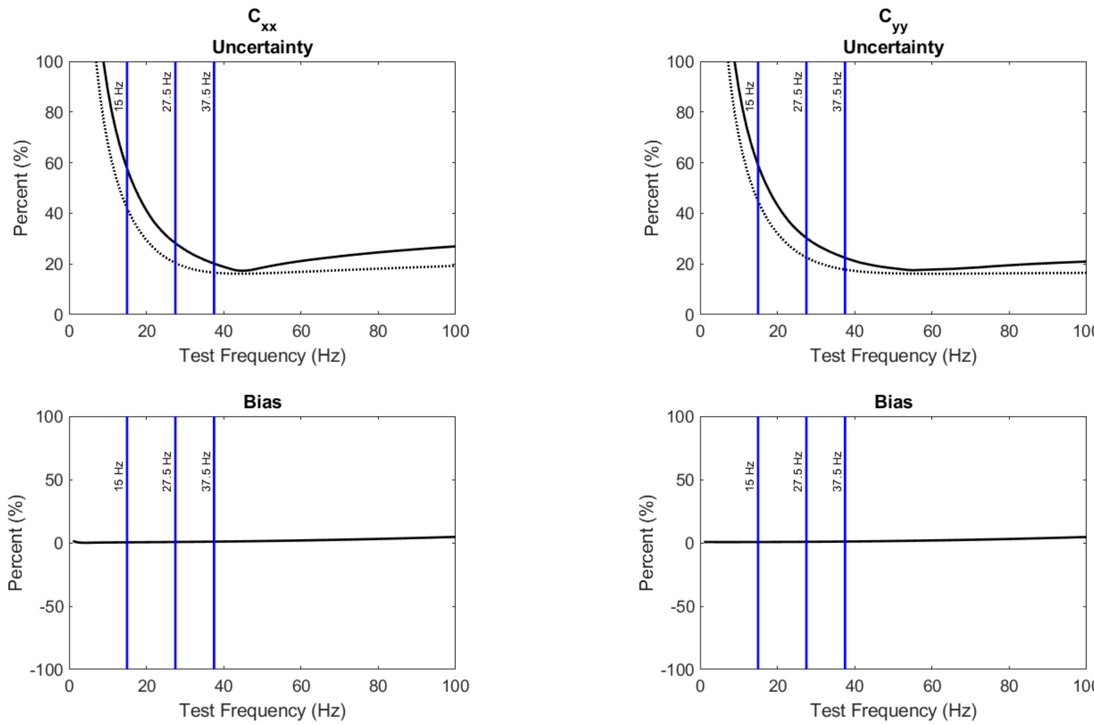

Figure 4.9: Damping Uncertainty With More Dynamics

4.1.5 Evaluation of Measuring Bearing Force and Bearing Film Thickness More Directly

One of the interesting features of the test rig described by Flack et al. [79] is the presence of transducers on the shaft. These transducers rotate with the shaft and provide measurements from within the bearing that stationary transducers connected to the housing or elsewhere typically cannot. There are three pressure probes and two displacement probes along the axial direction of the bearing. Details of the placement are shown in Figure 4.10.

The typical use of applied force measurements and external displacement measurements takes the full dynamics of the bearing and reduces it to a spring-damper equivalent operating at a single point. This is convenient

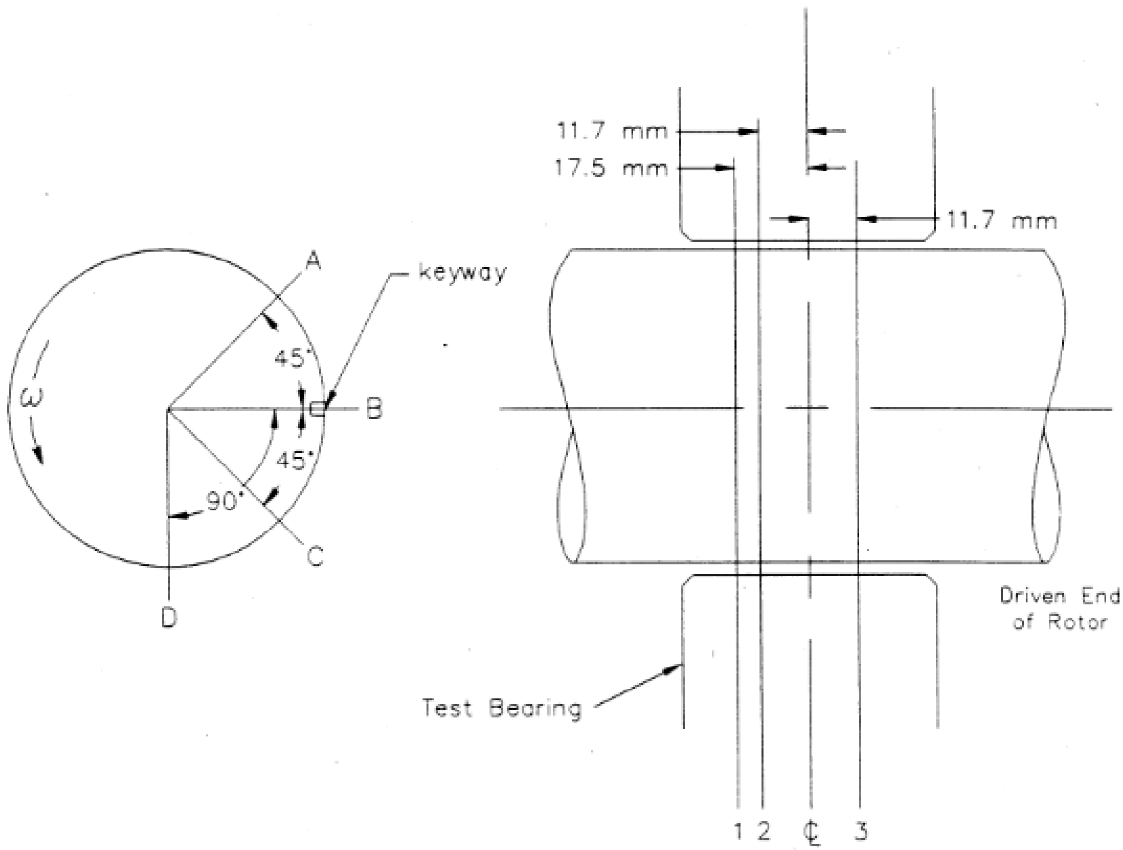

Transducer Type	Transducer Designation	Axial Position	Angular Orientation
Pressure	Telemetery	1	B
	Center	℄	D
	Drive	3	B
Displacement	Telemetery	2	C
	Drive	3	C
Temperature	Telemetery	1	A
	Center	℄	A

Figure 4.10: Shaft Probe Locations from Flack et al. reproduced from [79]

relative to using data from within the bearing for several reasons. First, the practical realities of trying to extract dynamic force and displacement information from a sensor that is also rotating requires extremely high performance sensors which can be costly for high-speed applications or possibly non-existent. Second, uncertainties such as the uncertainties in integrating a pressure profile for force may prove to be large enough to be problematic even if the dynamics of the identification are favorable.

The first point may be mitigated by using pressure and displacement sensors in the pad of a TPJB. The challenge with this setup is that with limited real estate it may be more difficult to get a full pressure profile or displacement profile whereas a rotating sensor can, in theory, see the entire circumferential profile. This may perhaps be mitigated by using both transducers in the pad and rotating transducers in the shaft together to create a complete picture. The second point may be mitigated by using new advancements in computational fluid dynamics (CFD) to develop a better understanding of where probes would need to be located to get the most relevant information.

Though these considerations are coming from the perspective of dynamic coefficient identification, the same probes for looking within the bearing also have benefits for bearing code validation as a whole by providing valuable steady-state data within the bearing.

The uncertainty analysis framework developed in this dissertation is used to determine if it might be worthwhile to develop the hardware and techniques to measure quantities within the bearing such as pressure (to determine force) and displacement (to determine film thickness). The truth model in this uncertainty analysis will include all of the dynamics described in Section 4.1.4. The identification model will not include any details of the dynamics. Some assumptions are implicit to this analysis including 1) transducer locations are carefully planned to allow for the tracking of the dynamic pressure profile and dynamic film thickness and 2) the transducers have the bandwidth to track the real-time signals while rotating. As a simple model of some of the increased challenges associated with this instrumentation, the uncertainties for each measurement have been increased by a factor of 1.5 as shown in Table 4.1.4.

Displacement Magnitude Uncertainty	$\pm 3\%$
Displacement Phase Uncertainty	± 3 degrees
Force Magnitude Uncertainty	$\pm 10.5\%$
Force Phase Uncertainty	± 6 degrees

Table 4.1.4: Uncertainties Used for Within-Bearing Transducer Analysis

The results of this uncertainty analysis are presented in Figures 4.11 and 4.12. For the stiffness uncertainty, at first glance it may seem like this method is worse in terms of uncertainty. Compared with measurements of applied force and displacements at probes on the sides of the housing, the stiffness uncertainty is slightly higher. However, the bias is significantly improved as the test frequency approaches 100 Hz. It must be considered that to eliminate the bias in Figures 4.8 and 4.9, the engineer must identify or model (1) the rotor, (2) the connection of the rotor to ground, and (3) the load cell model. Needing to identify or model these dynamics may eliminate the bias but will increase the uncertainty which can quickly become equal to or greater than when measuring bearing force and film thickness directly. Furthermore, there may be other dynamics that are not modeled or the reality may not have been fully captured in the truth model. Because measuring the bearing force and film thickness seems less sensitive to these additional dynamics, there can be more confidence that hidden dynamics in the test rig will not impact the dynamic coefficient identification uncertainty as much.

The damping uncertainty results are in favor of measuring bearing force and film thickness. There was not a significant bias to begin with. The uncertainty, however, is decreased noticeably compared with Figure 4.12.

4.1.6 Improving Identification Uncertainty by Improving Sensor Accuracy

The uncertainty analysis in Section 4.1.5 using the sensor uncertainties in Table 4.1.4 was conservative, assuming that sensor uncertainties for rotating sensors would be worse than for stationary sensors. This provides an opportunity for improving the identification experiment by improving the accuracy of the sensors.

The same analysis with sensors on the shaft is re-run with the uncertainties in Table 4.1.3. The results are shown in Figure 4.13 and Figure 4.14. In all cases the uncertainty analysis results are better than the case of measuring

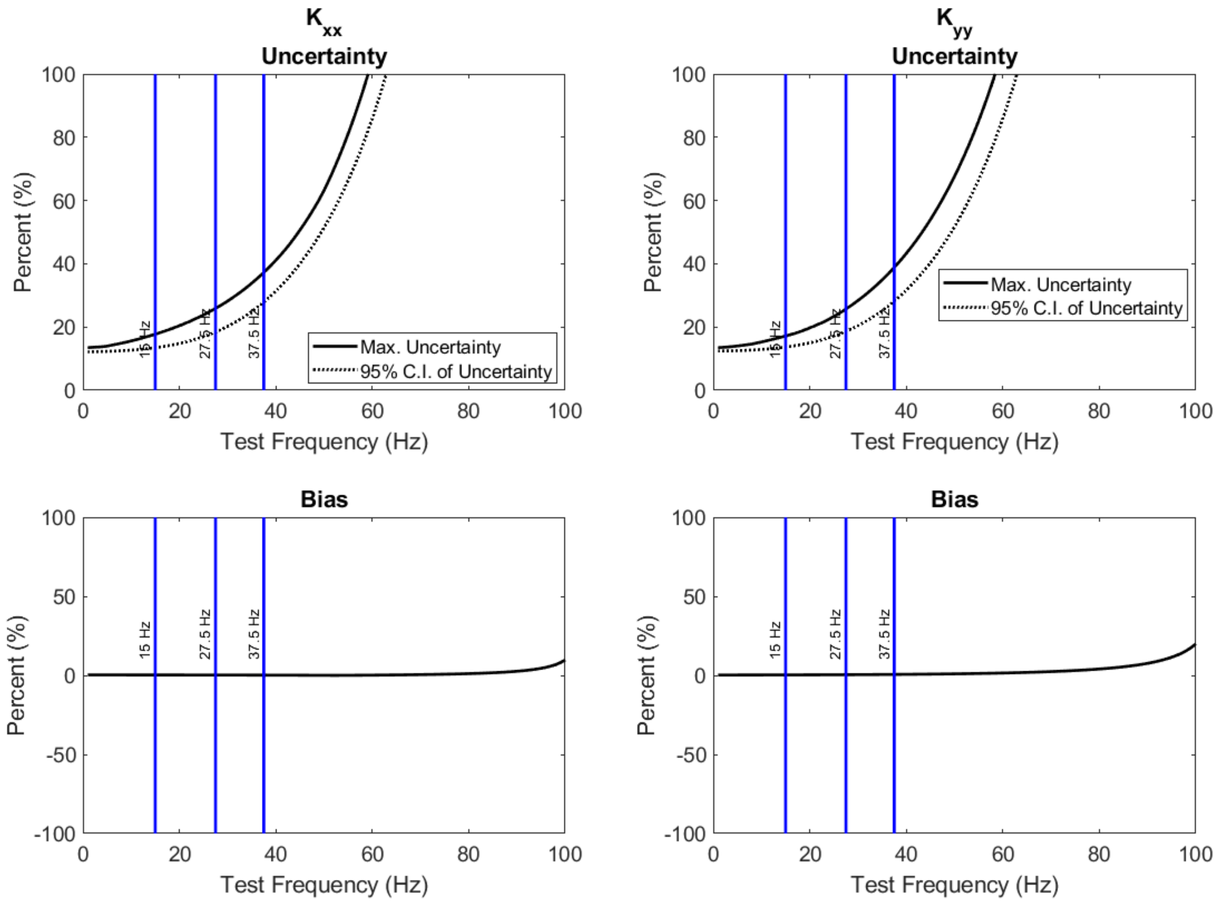

Figure 4.11: Stiffness Uncertainty With Direct Force and Film Thickness Measurement

applied force and displacement from sensors besides the bearing.

The results demonstrate that improving the uncertainty of TPJB dynamic coefficient identification is a multi-pronged effort. First, the system configuration (especially measurement systems) can reduce the sensitivity of the test rig to physics that can lead to biases in the identified dynamic coefficients. Second, the uncertainty analysis framework can be used to evaluate and minimize the modeling requirements for identification which will reduce the uncertainty. Third, sensor accuracy can be improved. Typically this would mean higher-cost sensors with better performance.

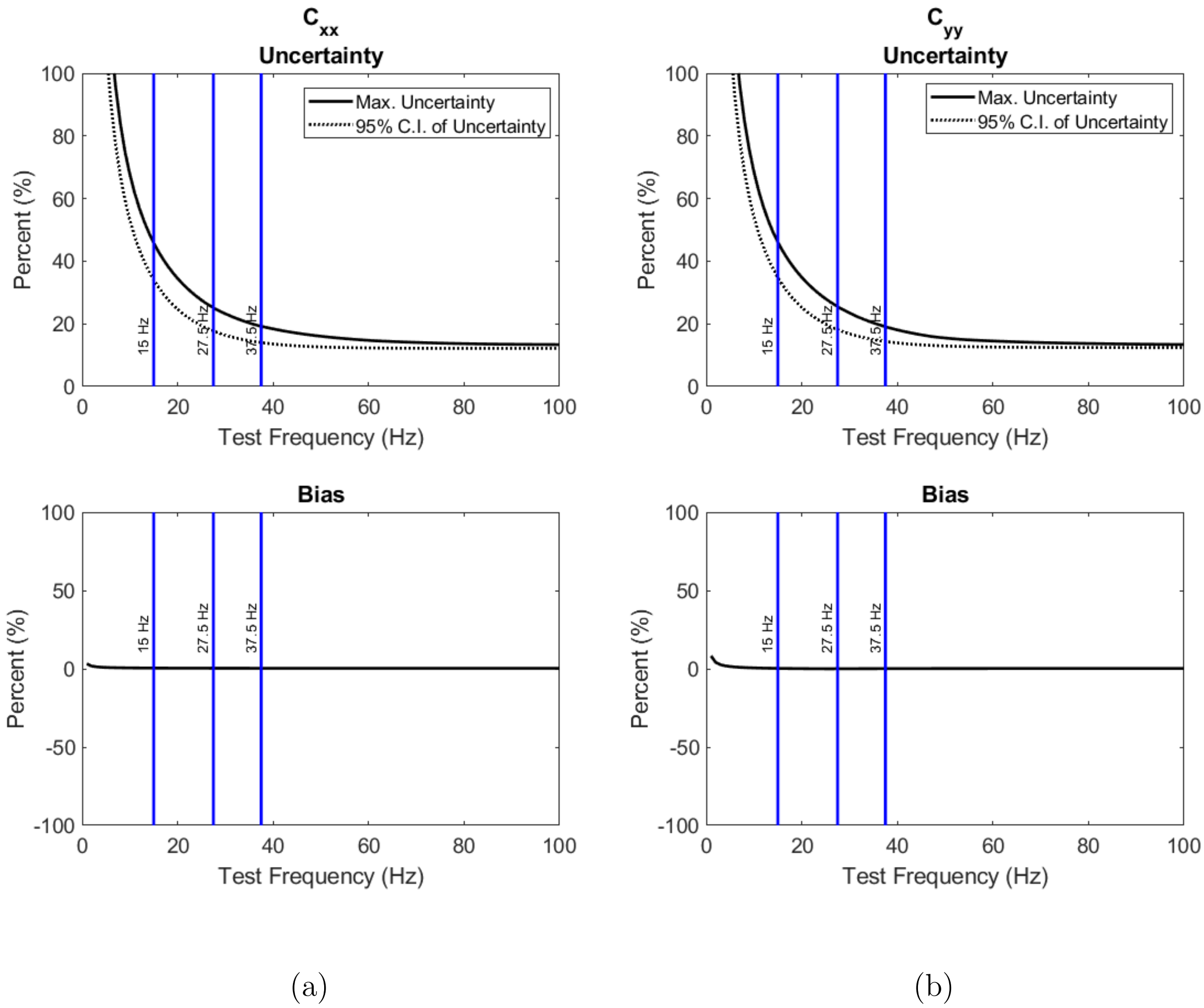

Figure 4.12: Damping Uncertainty With Direct Force and Film Thickness Measurement

To further demonstrate the significance of improving sensor accuracy, Figure 4.15 shows the K_{xx} results for three different cases for comparison. The first and second cases are the K_{xx} uncertainty results from Figure 4.11 and Figure 4.13. The third case models uncertainty when sensor performance (displacement and force) achieves 1% magnitude uncertainty and 1 degree phase uncertainty. Gancitano [78] demonstrates how this may be achieved for force measurement. There is a trade-off for the accuracy.

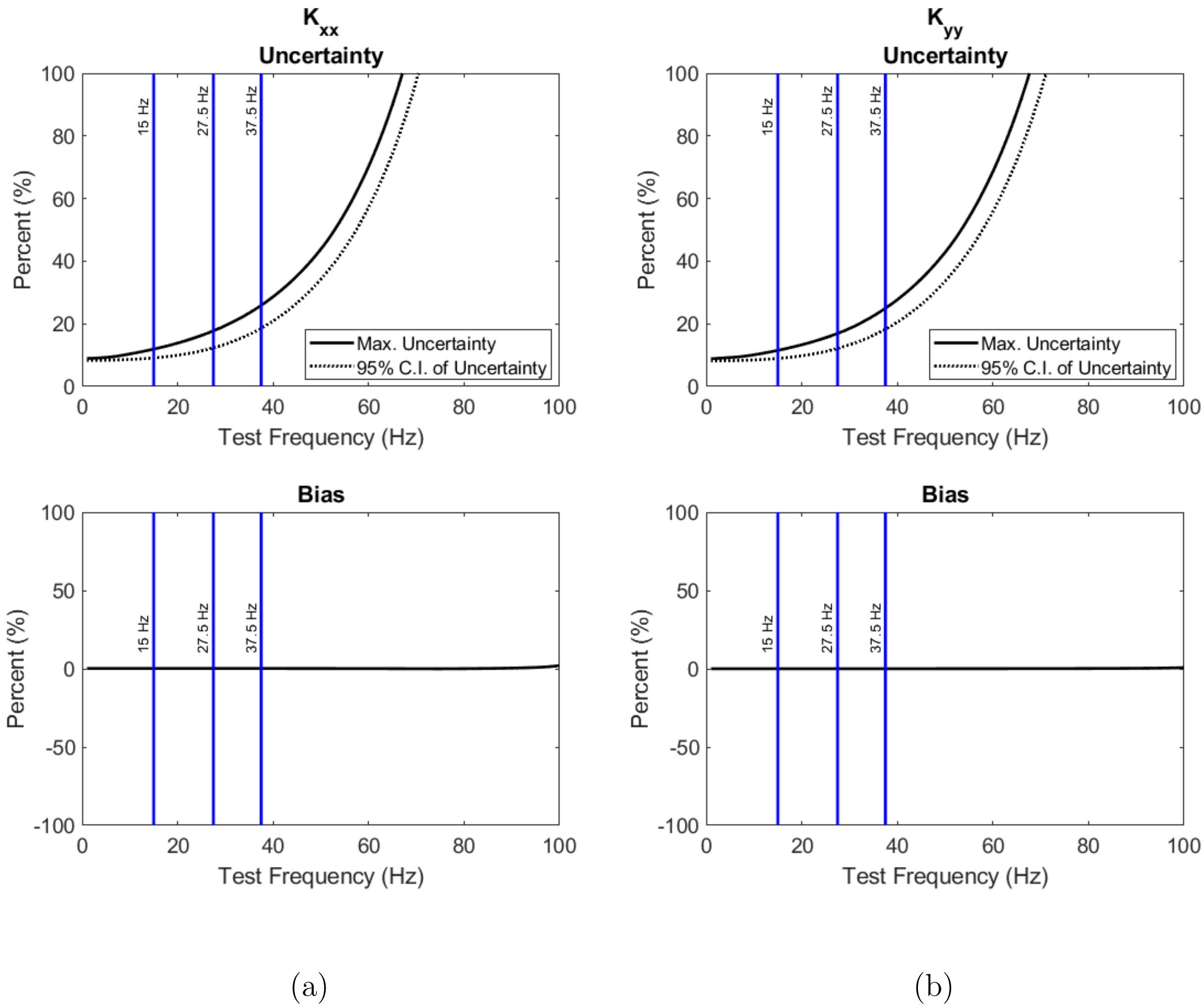

Figure 4.13: Uncertainty Analysis Results Measuring Bearing Force and Film Thickness Directly With Improved Sensor Uncertainty (a) Kxx (b) Kyy

Since the method described by Gancitano uses systems external to the bearing, the pressure within the bearing can no longer be measured without additional instrumentation separate from the force measurement system. Ultimately this means more cost if both capabilities are to be retained. The trade-off may be worthwhile as the uncertainty and bias are significantly improved when the measurement uncertainty is accurate to within 1% in magnitude and 1 degree in phase.

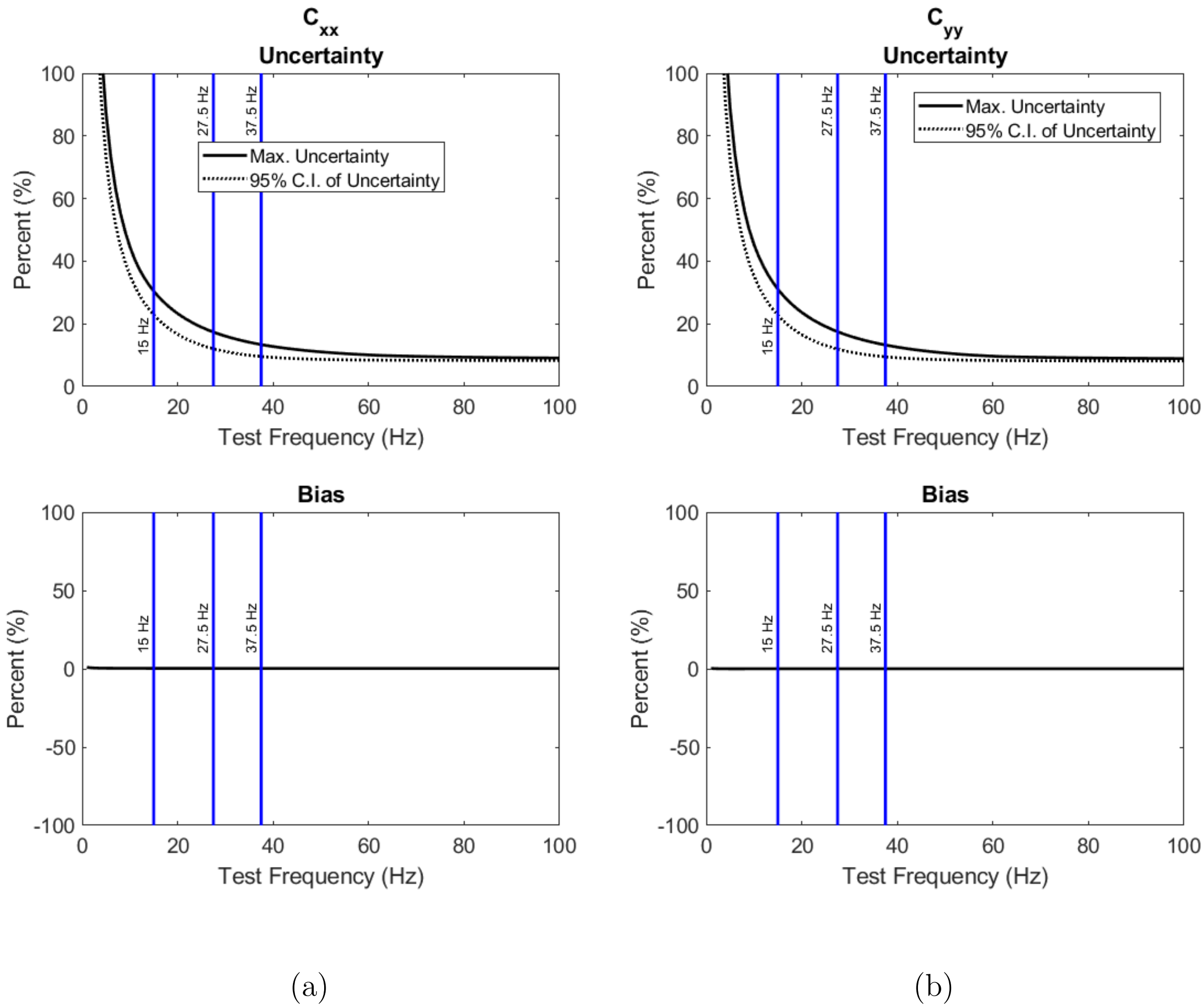

Figure 4.14: Uncertainty Analysis Results Measuring Bearing Force and Film Thickness Directly With Improved Sensor Uncertainty (a) Cxx (b) Cyy

4.2 Uncertainty Analysis Applications - Summary

The models of the application discussed in this chapter show results that demonstrate several important points:

- The uncertainty analysis results in this chapter reflect the trends and observations seen in Chapter 3. The value in the single-axis models is demonstrated when the same trends emerge in the higher-fidelity,

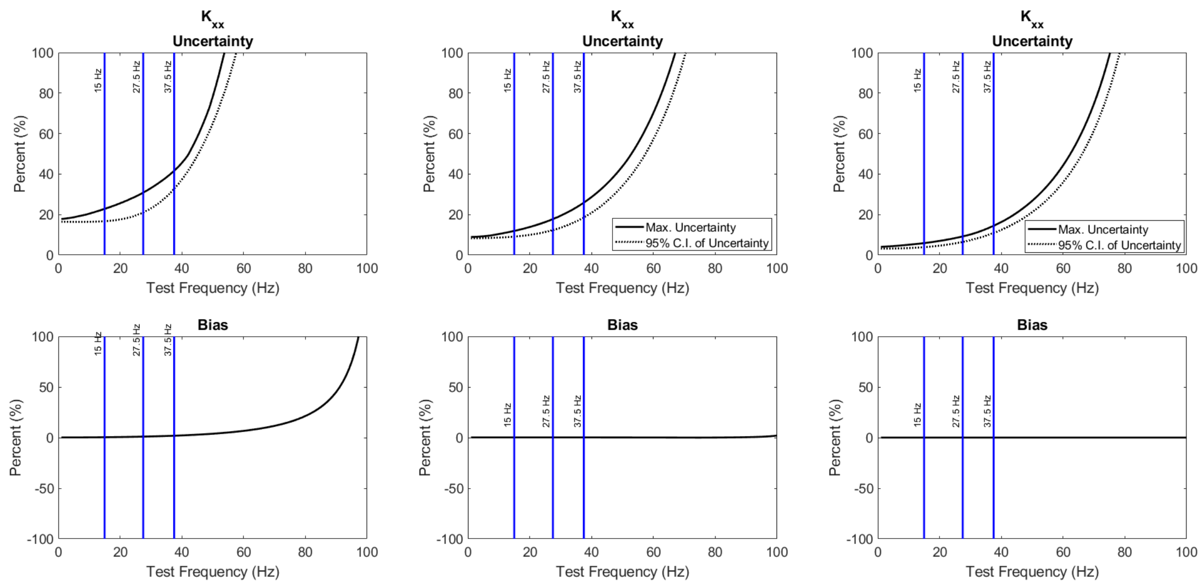

(a) (b) (b)

Figure 4.15: Comparing K_{xx} Uncertainty and Bias Results (a) Measuring Applied Force and Rotor Displacement (b) Measuring Bearing Force and Film Thickness (c) Improved Measurement of Bearing Force and Film Thickness

two-axes models. A bearing model that includes dynamic coefficients that change with test frequency shows how the basic trends may express themselves with a real bearing even without additional dynamics modeled. Further study with measuring bearing force and measuring film thickness more directly mirrored the measurement of bearing force in the single-axis models. By measuring the hydrodynamic film more directly, the identification is shown to become less sensitive to dynamics such as rotor flexibility. The more direct measurement of force and displacement also completely avoids some issues such as sensor non-collocation.

- The additional fidelity of having a second axis in the models reveals that - even when additional dynamics are not included - the inherent dynamic characteristics of the TPJB could add biases at high frequencies. At higher frequencies, the principal stiffnesses for the bearing design modeled decreases while the cross coupling increases. Thus, even with perfect measurement, bias is introduced. Careful modeling will allow researchers to evaluate the impact of this phenomenon on dynamic coefficient identification.

- Analyses with increasing measurement accuracy demonstrate how important it is that the instrumentation be as accurate as possible. In Figure 4.15, modifying the measurement signals showed noticeable benefits. The improvement of measurement accuracy also showed significant improvement. Engineers/researchers should therefore ensure that sensor selection and measurement scheme are made as accurate as possible and evaluated to ensure suitability.

Chapter 5

Novel Test Rig Design Using The Uncertainty Analysis Framework

The uncertainty analysis framework developed in this dissertation features the capability to guide the design of dynamic coefficient identification test rigs. Chapter 3 showed that single-axis models of test rigs can demonstrate significant trends in the uncertainty of identified dynamic coefficients. Chapter 4 showed that higher-fidelity models provide further insight on significant factors affecting the uncertainty of identified dynamic coefficients. In this chapter, the uncertainty analysis predictions identify problematic features of a test rig design and act as a design parameter to evaluate design changes. A test rig is designed that considers the uncertainty of identified coefficients as part of its development.

5.1 Original Concept For the Bearing Test Rig

A test rig design presented in a dissertation by Tim Dimond [81] is evaluated with the uncertainty analysis framework developed in this dissertation. Figure 5.1 shows the test rig layout.

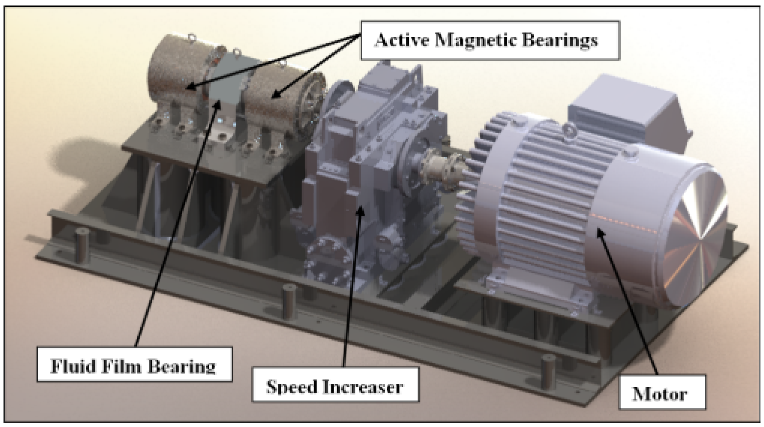

Figure 5.1: Test rig layout reproduced from Dimond [81]

A 350 HP (261 kW) motor drives the system through a speed-increasing gearbox with a 1:5.0625 ratio. A quill shaft connects the gearbox to the hollow test rotor. The quill shaft is designed to minimize the transmission of vibration to the test rotor from the gearbox and motor. A hollow test rotor design allows coupling with the quill shaft at the center of the test rotor. This design minimizes asymmetric dynamics and moments that might occur as the test rotor is displaced during testing.

The test bearing will be located at the center of the shaft with a five inch diameter for the journal section. There are two active magnetic bearings (AMBs), one on either side of the test bearing. The active magnetic bearings apply static and dynamic loading in addition to levitating the rotor. Figure 5.2 shows a cross section of the original design.

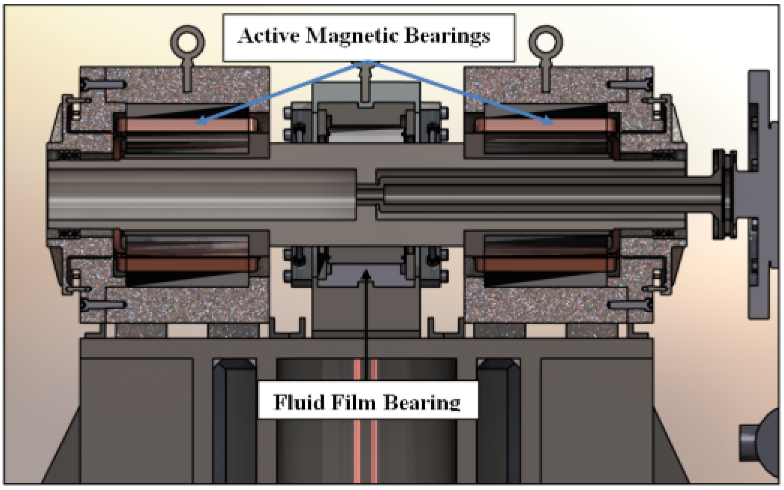

Figure 5.2: Test rig cross section reproduced from Dimond [81]

5.2 Bearing Test Rig Specifications

Table 5.2.1 lists key target specifications for the original test rig design. The speed and diameter were selected to achieve surface speeds relevant to industrial applications that may include turbulent flows of the lubricant. The maximum load rating was selected to work with the surface speed to simulate a wide range of industrial applications. Sizing was performed assuming fully-flooded bearings using ISO VG46 as the lubricant. Active magnetic bearings were selected for applying forces to the system due to their asynchronous non-contact excitation capabilities

The original specifications did not consider uncertainty. Based on

Table 5.2.1: Fluid Film Bearing Test Rig Specifications

Test Bearing Diameter	5 in (127 mm)
L/D Ratios	0.50 - 0.75
Pad Pivot Offsets	0.5
Orientations	LBP, LOP
Rotational Speed Range	9,000 - 22,400 RPM
Surface Speed Range	196 ft/s (60 m/s) - 480 ft/s (149 m/s)
Lubricants	ISO VG 32, ISO VG 46, Water
Maximum Bearing Unit Load	480 psi (3.3 MPa)
Dynamic perturbation displacement (p-p)	0.001 in (24 μm)
Excitation Frequency Range	10 Hz - 515 Hz

feedback from members of the Rotating Machinery and Controls (ROMAC) lab's industrial consortium, a target of twenty percent uncertainty or better was set. Since a comprehensive uncertainty analysis includes a plus-minus uncertainty as well as a bias, the goal will be to reduce the sum of the uncertainty and bias below 20%.

5.3 Motivations for Design Changes

A design audit of the test rig revealed some challenges for achieving the specifications in Table 5.2.1. The AMB design was insufficient for the maximum bearing unit load specification. Along with the AMB actuator design, an uncertainty analysis was performed. The uncertainty analysis began simply and eventually exercised many of the capabilities of the uncertainty analysis framework developed in this dissertation. The results of the uncertainty analysis were used to guide the design changes presented in this chapter to achieve acceptable predicted uncertainty for TPJB dynamic coefficient identification experiments.

Prior studies in this dissertation included single-axis models to understand important uncertainty trends and higher-fidelity models on previously built test rigs. In this chapter, the uncertainty analysis framework is applied to a test rig in the design phase. The exercise is a demonstration of how uncertainty analysis can become a part of the design phase. Examples of design modifications for improving TPJB identified coefficient uncertainty are explored. The test rig design will be modified to reduce the uncertainty of identified coefficients using the results of the uncertainty analysis while also working within the practical constraints of the test rig design.

5.4 Modifying the Active Magnetic Bearing Design

The original AMB design was a continuous-backiron, E-core design with coils on each salient stator pole. The journal diameter was six inches for the rotor laminations. Based on the original specifications, the maximum unit load (480 psi) for the test bearing could only be achieved for an L/D ratio of 0.5 and then only by fully saturating the AMB which would leave little to no capacity for dynamic loading. While this would allow for steady-state properties to be measured, dynamic testing would be difficult. The AMBs were redesigned to broaden the range of bearing L/D ratios that can be tested at the specified maximum 480 psi while still retaining dynamic force capacity.

The main goal of the redesign was to maximize pole-face area available for the magnetic flux path across the air-gap between the stator and rotor. To accomplish this, a single-coil E-core stator lamination design was adopted. Additionally, rather than a continuous backiron design a segmented stator design was adopted. Figure 5.3 shows the original AMB cross-section compared with the new AMB cross-section. While this adds some complexity in the mechanical design, each sector would become magnetically isolated from each other which has some benefits for the flux density across the air gap, further increasing the maximum force capability of the AMBs. There are drawbacks for this type of design including challenges with redundancy if an amplifier fails and an increased diametral space requirement. While an industrial machine might struggle with those trade-offs, for this test rig it was determined that these trade-offs were acceptable.

The original AMB design was analyzed using 2-D FEA to estimate force capacity. Figure 5.4 shows the results for the maximum load condition assuming linear operation. A perturbation current of 27 A about a bias of 27 A was applied to the top two quadrants and the bottom quadrants were not energized. The FEA predicted a force of 11.1 kN resulting in a bearing specific load of 2.7 MPa (391 psi) for a test article with an L/D ratio of 0.5.

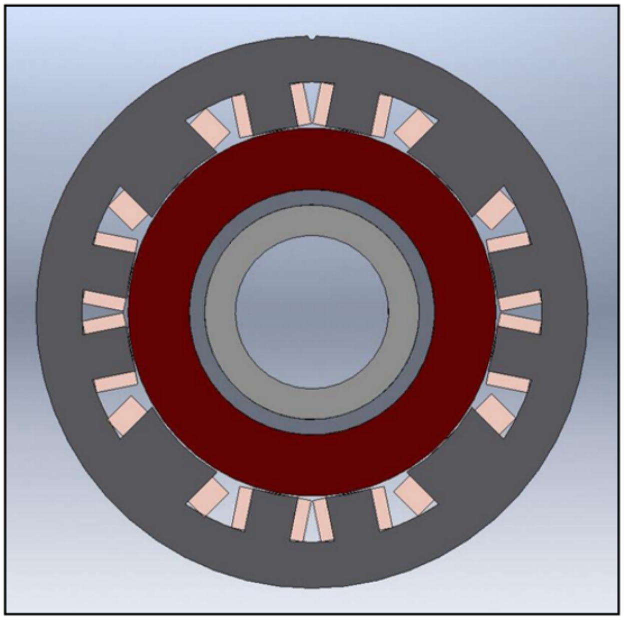

(a)

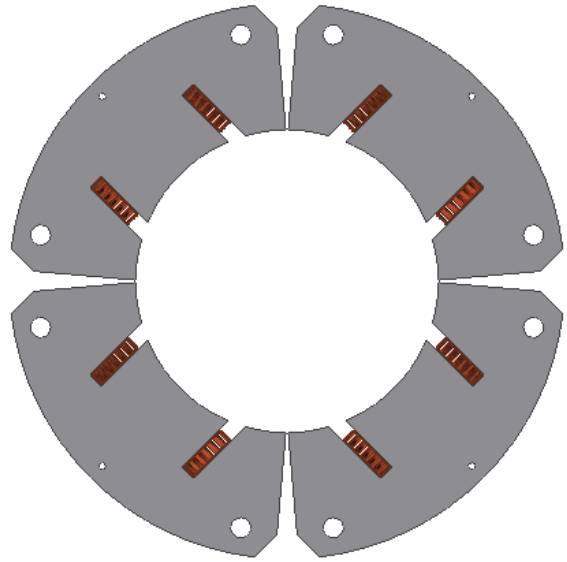

(b)

Figure 5.3: Comparing the AMB cross section of (a) the original design reproduced from Dimond [81] and (b)

Flux density across the air gap is approximately 1.3 T and in the backiron, the peak flux density was between 1.5-1.7 T. The flux density in the backiron can be considered saturated and therefore additional current in the coils will yield diminishing results. The only feasible way to achieve the 480 psi target was to go well into this saturated zone at which point the dynamic load capacity is significantly diminished.

With the new design, the bias current is only 7.5A with a perturbation current of 7.5A to reach peak current. For a similar flux density across the air gap and in the backiron, the new AMB design achieves a FEA predicted force of 22,500 N for a unit load of 770psi for with a test bearing L/D ratio of 0.5. The unit load for the maximum L/D ratio of 0.75 would be approximately

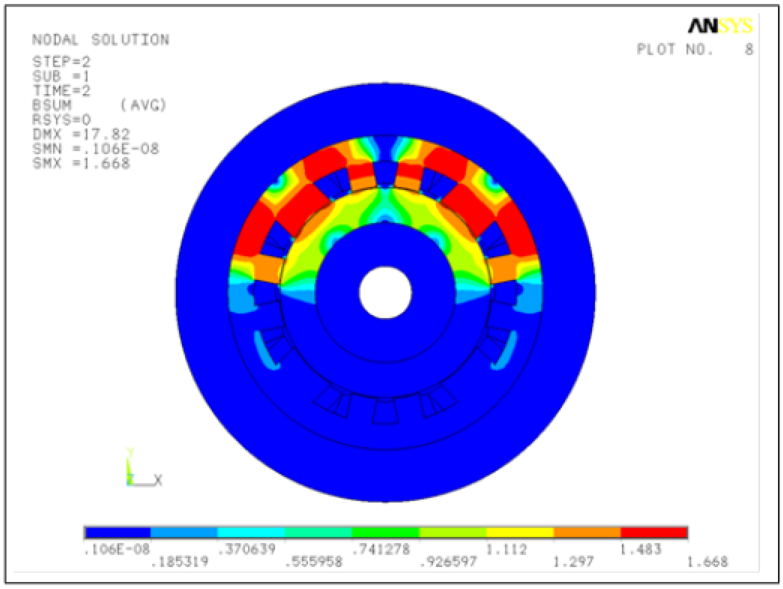

Figure 5.4: Original AMB FEA

Original AMB FEA reproduced from Dimond [81]

510 psi. The results shown in Figure 5.5 are generated using the FEMM finite element package for electromagnetics created by David Meeker [82]. These results correspond to the backiron being saturated again but with the additional headroom afforded by the increased force capacity, the target of 480 psi can be achieved for a much broader range of bearings while preserving some dynamic load capacity.

5.4.1 First Analysis of Uncertainty with AMBs

As the basic AMB design was reconsidered, a simple analysis of uncertainty was performed that began a process of adjusting the configuration of the test rig to improve uncertainty. The AMBs were originally intended to act as calibrated load cells for the test rig as well as actuators. Hall sensors would

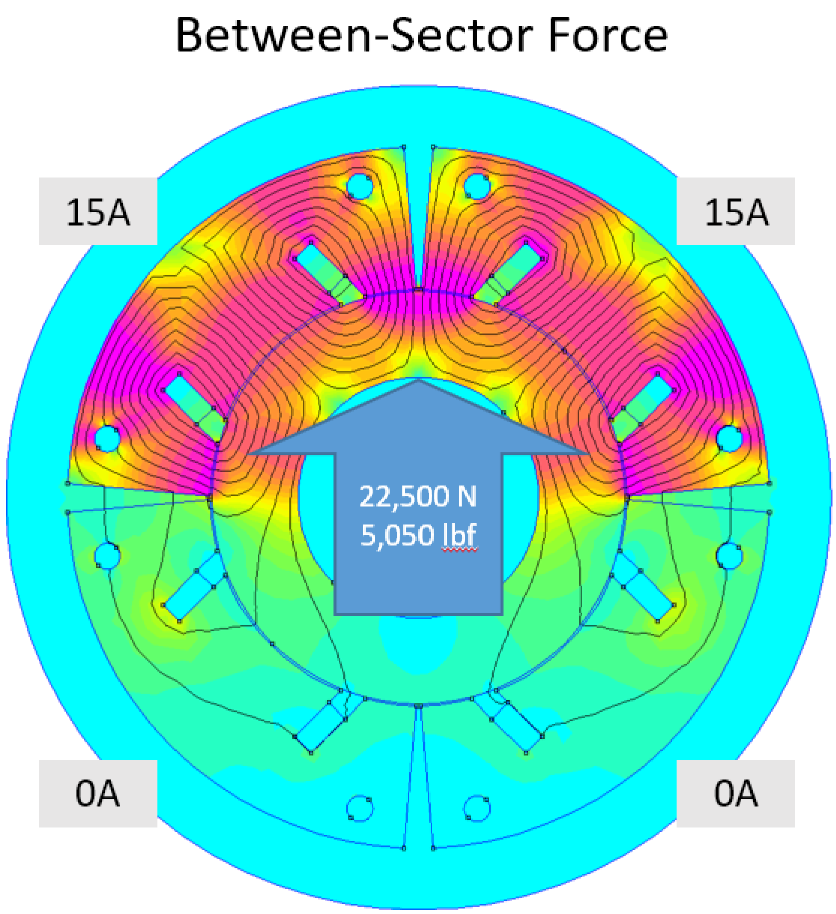

Figure 5.5: Updated FEA Result

be included in the AMB to measure the magnetic flux. Combined with the position of the rotor in the AMB measured with displacement sensors, the force applied through the AMB can be calculated. Fiber optic strain gages were planned as secondary sensors to estimate the force applied by the AMB through a measurement of the AMB stators' strain. In either method the force measured would be the total applied force: static loading plus dynamic excitation.

Measurement error in this case would be applied to the total applied force measurement. The error then will be larger relative to the dynamic force applied for the experiment which is typically a smaller portion of the total force applied. Table 5.4.1 presents a numerical case study. The analyses in Chapters 2, 3, and 4 clearly demonstrate that the increased uncertainty relative to the dynamic force magnitude will be problematic for dynamic coefficient identification.

Table 5.4.1: Numerical Example of Dynamic Force Error from Total Force

Static Force	2,500 lbf
Dynamic Force Magnitude	500 lbf
Total Peak Force	3,000 lbf
Force Measurement Uncertainty (% Full Scale)	3%
Force Uncertainty at Peak Force	90 lbf
Force Uncertainty Relative to Dynamic Force Magnitude	18%

The first design change to address this issue was to separate the static loading and dynamic excitation by having a set of AMBs to apply the static force and a set of AMBs applying the dynamic forces. The basic design for the bearings will be the same. The two main differences will be the axial length of the two AMB types (the static loading bearings will be longer axially for larger force capability) and the controller for the two applications. Figure 5.6 shows a schematic of the updated configuration. In addition to reducing the measurement uncertainty for dynamic excitation, the separation of the AMB actuators into a pair of static loading AMBs and a pair of dynamic excitation AMBs allows tuning each AMB pair for their application. This would further help reduce uncertainty by minimizing any additional dynamics introduced by a controller not optimized for either application if the AMBs are combined.

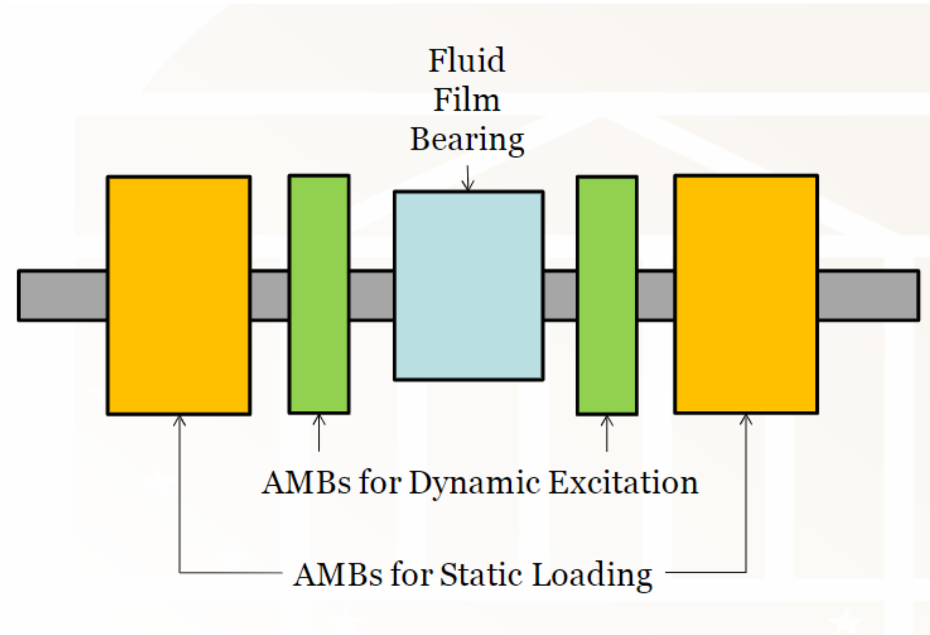

Figure 5.6: Splitting the Dynamic Loading and Static Loading Sources

Further investigation with a lumped-mass, single-axis approximation of the system (see Section 3.1.2 for the basic principles) indicated that further reduction of force uncertainty was required if possible. The simple computation performed first showed that the application of static loading and dynamic excitation needed to be split. Figure 5.7 shows the uncertainty results from three different speed cases analyzed for a bearing design in a simulation of the test rig. The bias is negligible for these analyses. The results are shown both for the case where the AMB actuator is combined for static and dynamic loading as well as the case where the AMB actuator is split to perform the functions separately. The uncertainty is significantly improved when the actuator is split, but the combination of the quadratic inertial term and the decreasing stiffness as test frequency increases becomes problematic at higher test frequencies. The impact on identification uncertainty at higher frequencies made it important to reduce the dynamic force uncertainty even further to achieve the uncertainty target in the specified test frequency range.

5.4.2 Improving Force Measurement Uncertainty - The “Active Load Cell” Concept

As the importance of reducing force measurement uncertainty became evident, a new concept was developed to improve AMB actuator force measurement beyond the capability of hall sensors and/or strain gages. The idea proposed measuring the force of the AMBs through an externally attached electrodynamic shaker that was inertially canceling the motion of the AMB stator. A detailed investigation of the “Active Load Cell” concept’s ability to measure component force is presented in a MS Thesis by Paul Gancitano [78]. A simple representation of the operation is shown in Figure 5.8. As with typical test rig operation, an excitation force is applied to the excited component (the rotor in this case). For the proposed test rig this would be through AMBs. The applied force, $F_{excitation}$, will generate a reaction force on the AMB housing, $F_{reaction}$, resulting in an acceleration of the stator measured by an accelerometer (shown in yellow). The electrodynamic shaker (shown in blue) will apply a force to counteract

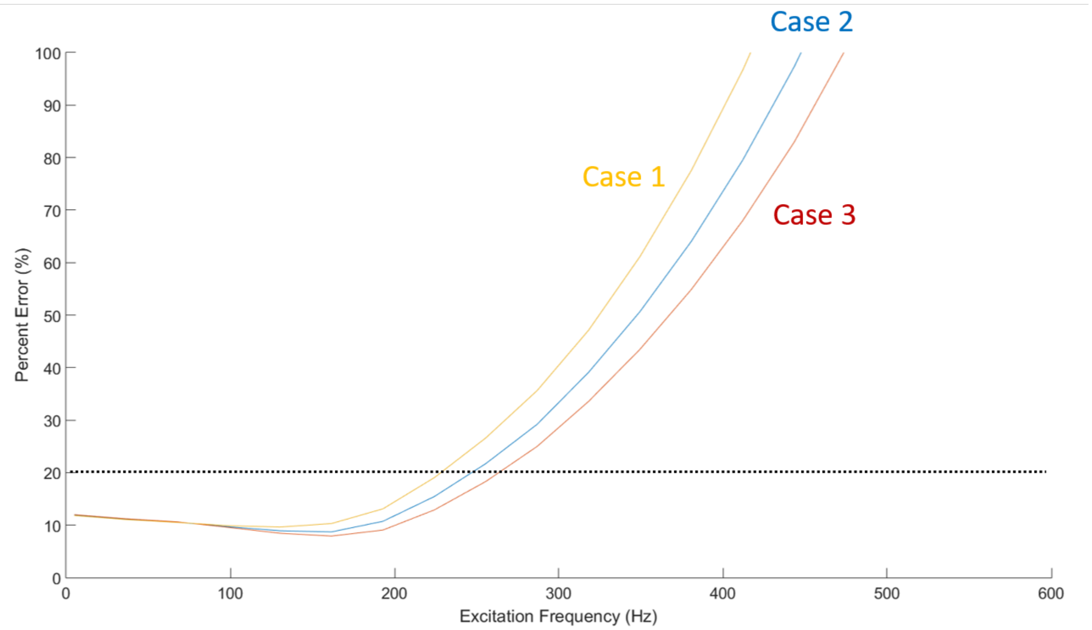

(a)

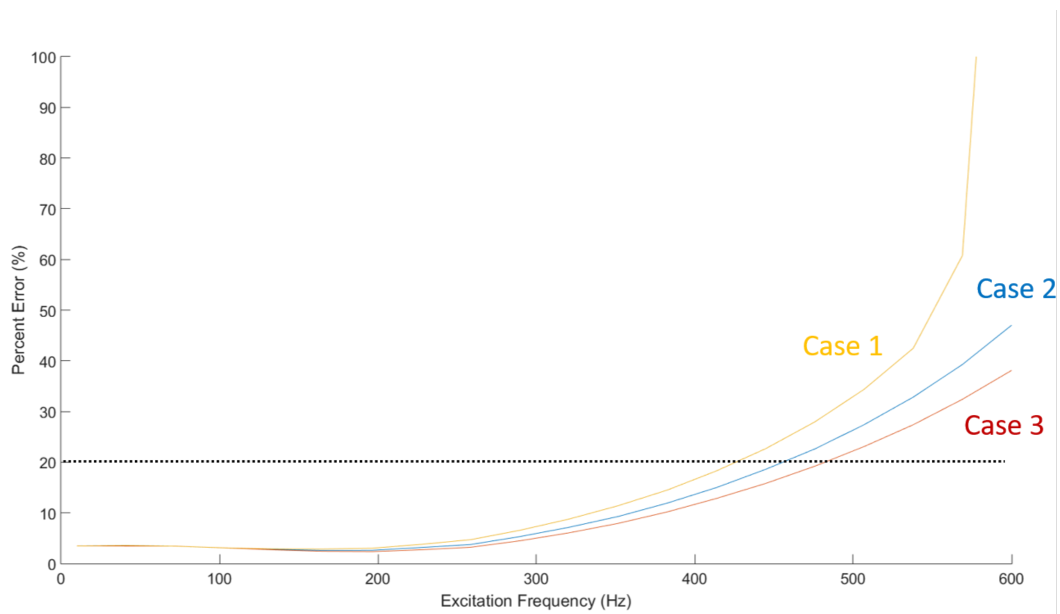

(b)

Figure 5.7: Comparing K_{xx} Uncertainty for Combined AMB vs. Split-AMB Configuration for 3 Speeds - (a) AMB combined (b) AMB split into separate static loading and dynamic excitation actuators

$F_{reaction}$. The force from the shaker, F_{cancel}, will be adjusted until the accelerometer reading is zero. This indicates that $F_{cancel} = -F_{reaction}$.

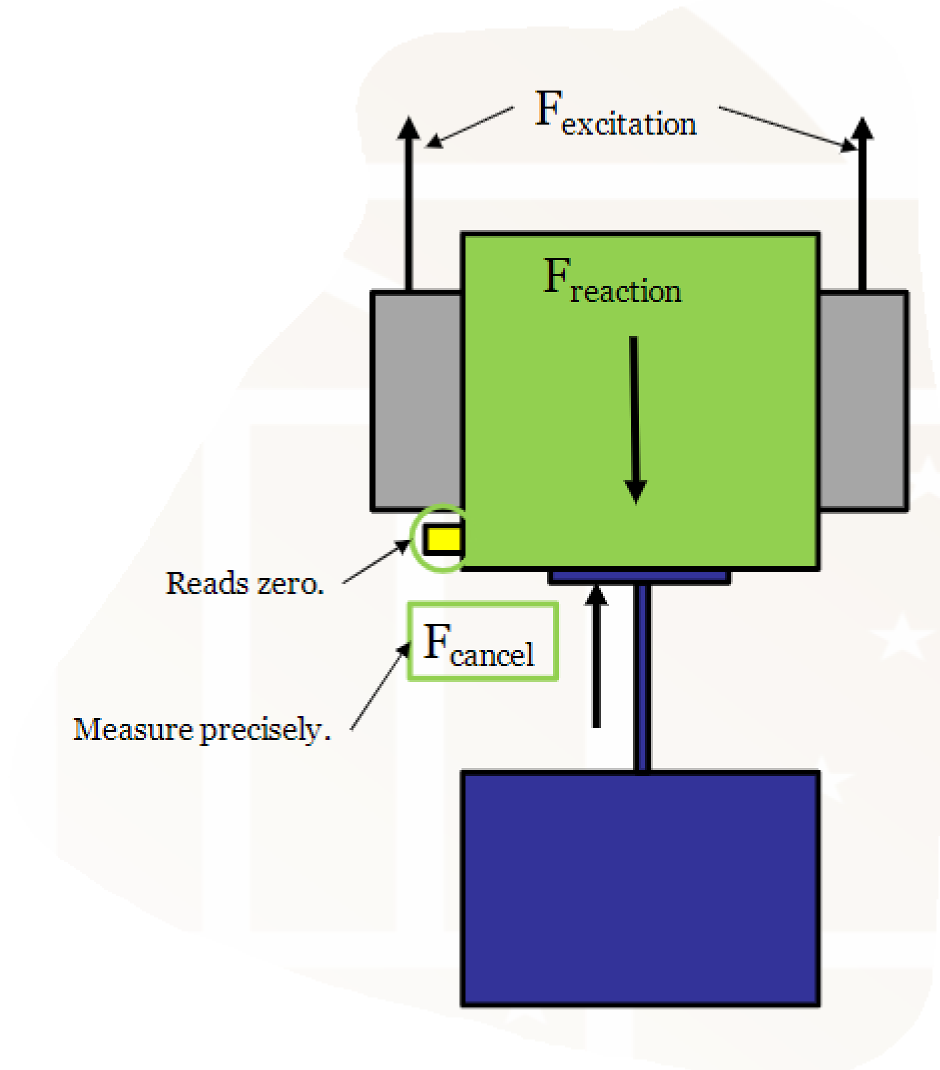

Figure 5.8: Operating Schematic of “Active Load Cell” concept

In the original conception, the electrodynamic shaker force is a proxy for the force applied through the AMB. (As discussed in Section 5.5, the concept can also be applied to measure the force generated within the TPJB.) Estimation of the shaker's electrodynamic force can be more accurate (better than 1% uncertainty) than measuring the AMB forces with hall sensors (about 3% at best) or strain gages. The trade-off is added complexity in the support structure required to achieve the force measurement.

There are some other benefits of using a proxy for force measurement. For example, one of the most accurate ways of measuring the force of an AMB is to measure the flux density across the air gap with hall sensors. However, from a practical design perspective this requires space for the sensor between the rotor and stator, increasing the effective air gap. This affects the force capability of the AMB. A proxy force measurement allows for designing the AMB without worrying about an effective increase in air gap with a hall sensor. Additionally, hall sensors only measure flux at a single location. This may not capture the full distribution of the flux in the air gap. This adds another error in force measurement using hall sensors relative to using the "active load cell" concept.

Similar to the analyses with results shown in Figure 5.7, the capability of the active load cell was modeled and the same analysis was re-run. The AMB actuators were still split and the active load cell concept was modeled as measuring the dynamic force applied on the rotor. The results are shown in Figure 5.9.

Though the results are promising, only measurement uncertainties have been modeled thus far. For a truly comprehensive uncertainty analysis, additional dynamics such as rotor flexibility must be included. Adding fidelity to the uncertainty analysis shows that even though the uncertainty

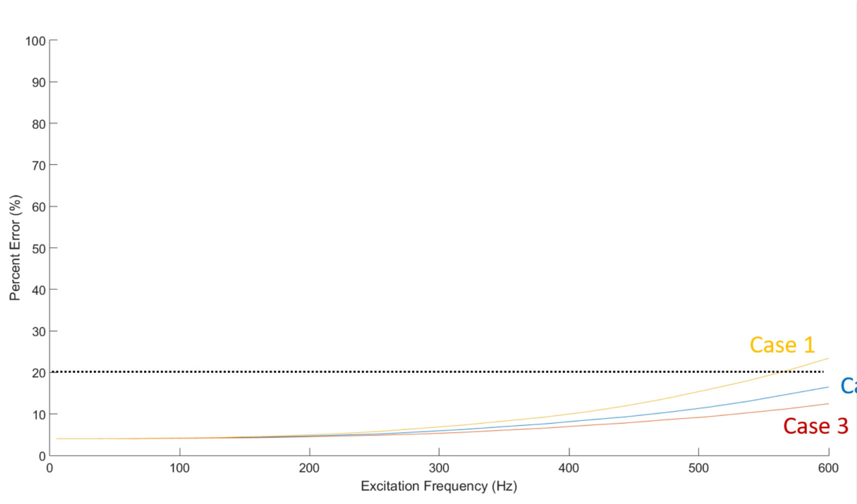

Figure 5.9: Uncertainty Results for 3 Speed Cases with “Active Load Cell” Measurement of Dynamic Excitation Force Modeled

of applied force measurement has been significantly improved, the dynamics of the test rig may still be problematic. Following these new findings, the test rig design was modified to look at measuring the hydrodynamic bearing force instead of the dynamic excitation force applied on the rotor.

5.5 Measuring Bearing Force Instead of Applied Force

To investigate the impact of additional dynamics, a rotor model was developed allowing a comparison between an ideal transfer function and a transfer function that includes the effects of rotor flexibility and noncollocation of forces and displacements. Figure 5.10 shows a representation of the model that was developed. The ideal or desired transfer function represents the response between the forces at the bearing location and the resulting displacement at the bearing location. As this test rig was originally designed, the input force would not be applied at the bearing location but away from the center where the AMBs would be acting. The displacements would not be measured at the bearing location but with probes on either side of the bearing housing.

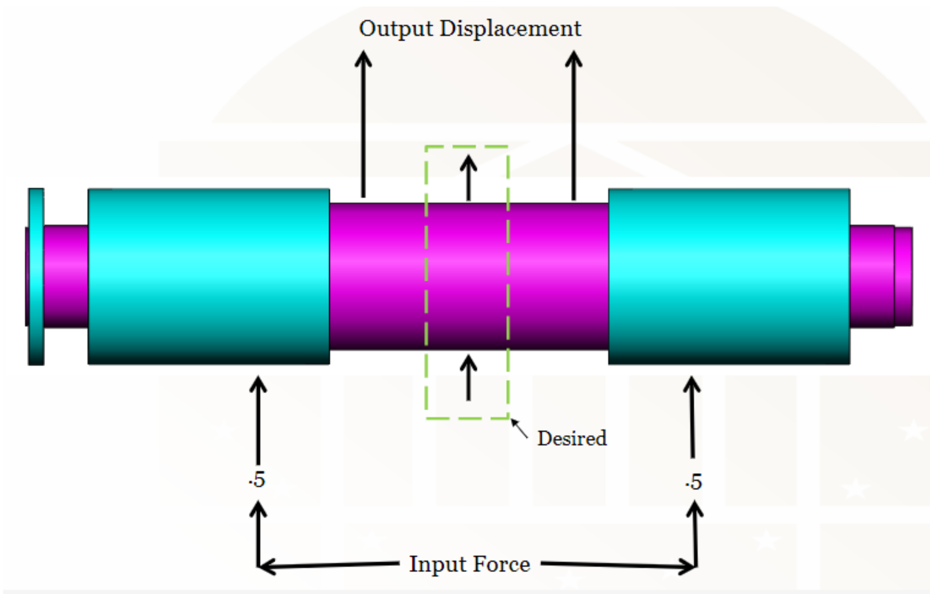

Figure 5.10: Diagram Showing Example of Non-collocation Modeled in Analysis With Flexible Rotor Truth

Even without performing an uncertainty analysis, a simple comparison of the ideal and more practical transfer function showed a significant effect of the dynamics modeled in this analysis. Figure 5.11 shows the difference in the magnitudes of the transfer functions relative to the ideal transfer function.

The conclusion from this analysis is that the experimental setup is sensitive to the dynamics of the rotor. A critical frequency is observed in the target test frequency range. While modeling the rotor would reduce this sensitivity, a different course of action was chosen based on the work presented in this

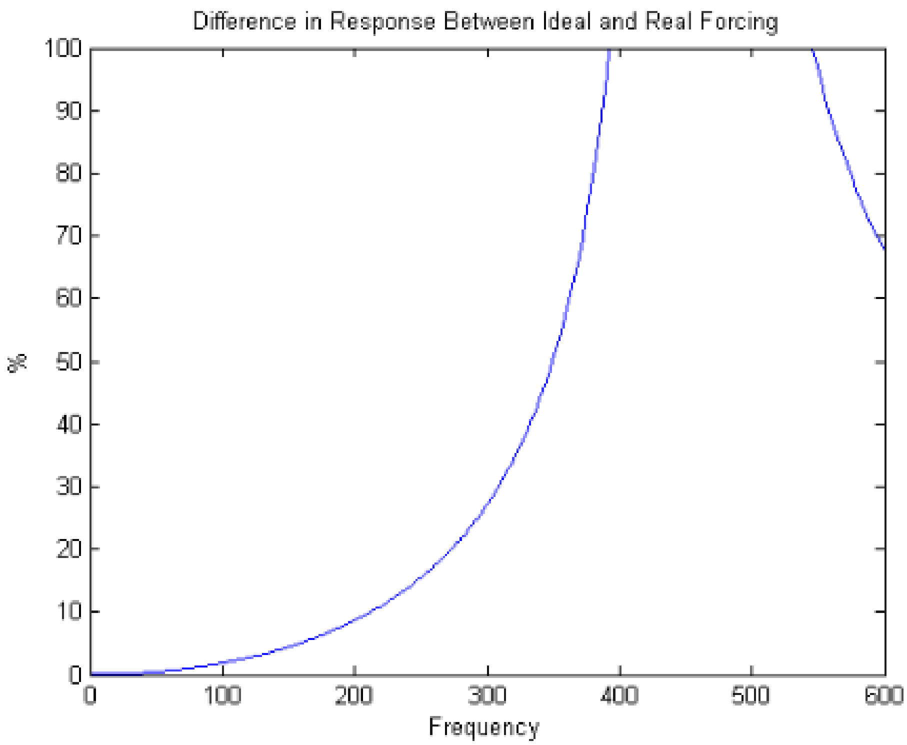

Figure 5.11: Impact of Rotor Flexibility - Difference Between Truth and Identification

dissertation. With the current analysis, the sources of this sensitivity are 1) the noncollocation of force measurement location and the dynamic force in the test article and 2) the noncollocation of the displacement measurement and the actual film thickness of the TPJB. This reflects analysis shown in Section 3.3 and Section 4.1. The first point - the force non-collocation - was addressed by using the "Active Load Cell" concept to measure the forces exerted by the fluid-film in the TPJB rather than the applied force at the AMBs.

Figure 5.12 shows the first results from evaluating this configuration. Uncertainty analysis was performed on an identical case with sensor uncertainties defined for the original configuration with combined static loading and dynamic excitation, the case where the dynamic excitation is split from the static loading, and the case where the active load cell concept is used to measure TPJB force. It is clear that measuring the bearing force behaves better from the perspective of uncertainty. Furthermore, it has been shown in this dissertation that measuring bearing force is less sensitive to additional dynamics such as the force noncollocation issue. The displacement noncollocation between film thickness and prox probes will still affect the identification. While not modeled in this example, the displacement noncollocation will affect all three cases.

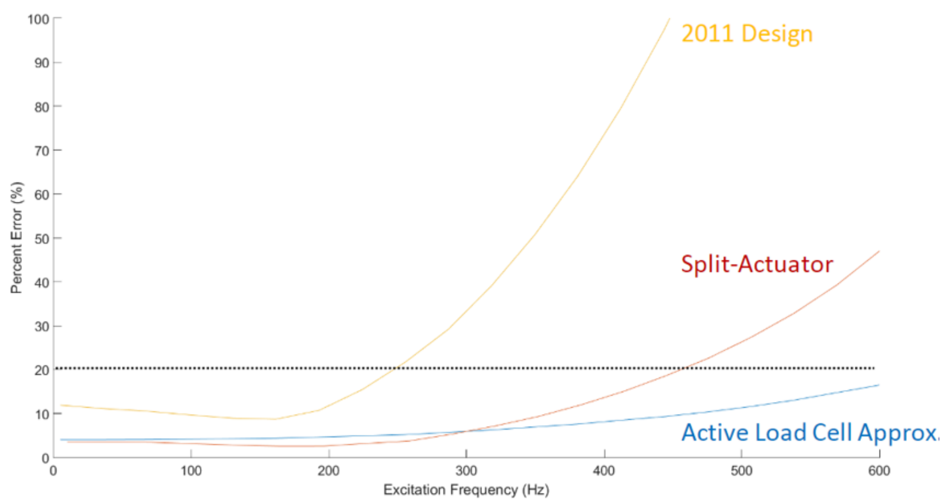

Figure 5.12: Uncertainty Analysis Results for Kxx Comparing Original Test Rig Design, Splitting the Actuators, and Active Load Cell for Measuring TPJB Force

Some design work was undertaken to evaluate the measurement of TPJB forces with the active load cell concept further. The anticipated experimental method required two electrodynamic shakers installed orthogonally to perform the cancellation. The bearing housing would also have to be supported at frequencies other than the test frequency, particularly at zero frequency for the static loading. Due to the size of the electrodynamic shakers for forces required to support the total force, the electrodynamic shakers were limited to dynamic cancellation forces while a series of electromagnetic actuators were designed to levitate the housing and keep it in place. Another issue with sizing the electrodynamic shakers is that the already installed foundation would require extensive changes to a third of the substructure. Figure 5.13 shows the required layout for this model of force measurement. The section with the AMBs and electrodynamic shakers must be completely modified including dropping the floor to accommodate the shakers. This would also entail splitting a large metal foundation that had been previously designed, built, and installed.

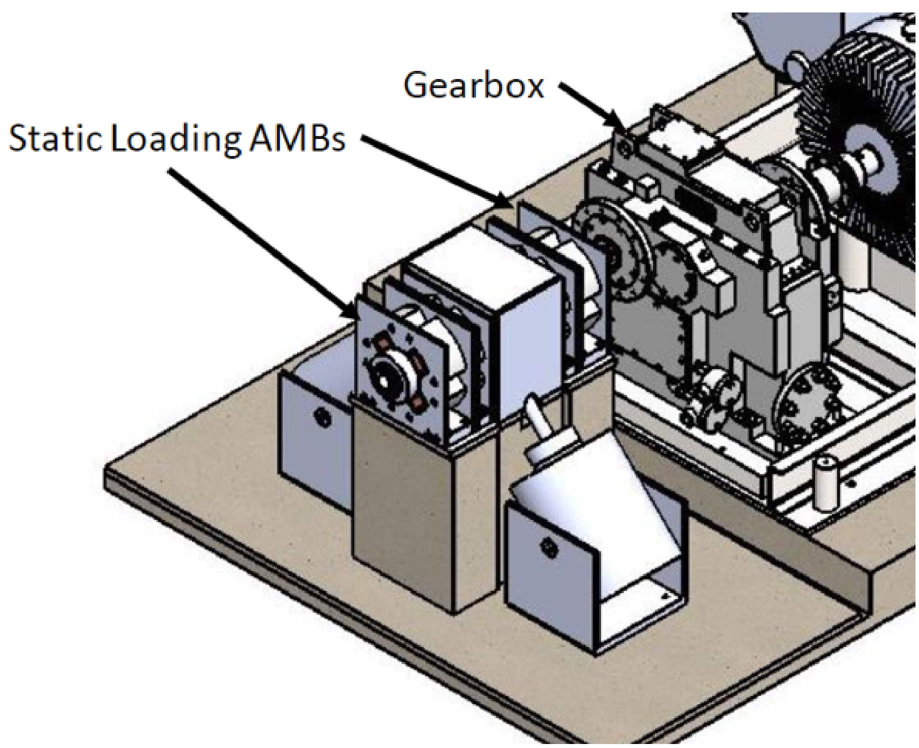

Figure 5.13: Isometric View of Foundation Changes Required for Active Load Cell Concept

Some ideas to circumvent this issue were discussed such as hanging the electrodynamic shakers from the ceiling and using them similar to shakers used for modal testing. This may also require some infrastructure changes to allow for this. Ultimately, it was determined that an alternative method would be required.

5.6 Estimating Bearing Force Using Piezoelectric Load Cells

The typical instrumentation on dynamic coefficient identification test rigs of measuring applied force leads to high uncertainty as test frequency increases. The most common configuration for force measurement uses load cells at the point of application (usually at the connection between a shaker and the excited component). In this test rig where the actuator applying forces is a magnetic bearing, the applied force needed to be measured in a different way. Originally designed to be hall probes and/or strain gages to construct the force measurement, the active load cell concept was proposed to further reduce uncertainty. Based on the development of the uncertainty analysis framework in this dissertation, the measurement of force was redesigned to be taken from the bearing housing, leading to a measurement that approximates the bearing force. While this showed the most promise for reducing uncertainty, the practical challenges of implementing the concept forced a redesign.

All the analysis so far supports measuring bearing force to minimize uncertainty and sensitivity to dynamics. To approximate this measurement, piezoelectric load cells between the test article housing and the foundation are proposed. In the active load cell concept, active cancellation would have zeroed the housing acceleration, resulting in a force measurement that in principle does not include an inertial component. With piezoelectric load cells, the housing will still experience vibration and thus there will be some inertial component in addition to the bearing force captured by the load cells. However, the uncertainty analysis framework is used to evaluate if the additional error is small enough to make the overall configuration still viable.

Piezoelectric load cells were selected from the available types of load cells for two main characteristics: 1) high stiffness and 2) high sensitivity to dynamic forces. Piezoelectric load cells take advantage of the piezoelectric effect which generates an electric charge in response to an applied stress. It is important to note that the piezoelectric effect responds to *changes in force* so if the applied force is a static force, the reading from the piezoelectric load cell will eventually return to zero. This effect on the test rig might mean some loss of accuracy in reading the static applied load, but the trade-off is that dynamic force measurements for forces acting on the load cell are more accurate. The importance of the high stiffness of the load cell is to minimize the dynamics of the housing within the desired test frequency range.

The piezoelectric load cell model selected for this test rig application is the PCB M260A03. Figure 5.14 shows an image of the load cell with some important specifications. This model is a tri-axial load cell because each load cell is expected to experience some part of horizontal and vertical forces from the bearing. Due to the piezoelectric physics, the force resolution of this load cell is well-suited for this application. The stiffness values are much larger than the expected stiffnesses of bearings tested on the rig. A model of the piezoelectric load cell was developed using 3D FEA and calibrated to the manufacturer specifications. The load cell model was incorporated in a comprehensive dynamic model to perform an uncertainty analysis for coefficient identification on the proposed test rig design. The model used in the uncertainty analysis incorporates some features such as the cross-talk between the axes of measurement in the load cell to properly account for its impact on identification uncertainty.

The proposed configuration on the test rig with the piezoelectric load cells is shown in Figure 5.15 with an isometric view of the test rig as well as an exploded view of the test bearing section. The placement of the piezoelectric load cells was developed using dynamic FEA of the test section. Originally, the piezoelectric load cells were placed between the lower bearing housing and the foundation. This led to problems with moment loading on the bearing housing from horizontal bearing loads. The dynamic models shows that the housing would respond dynamically with a tilting motion. The magnitude of the motion caused problems with the measurement by introducing more

(a)

PERFORMANCE		
Sensitivity (±20 %) (Z Axis)	0.25 mV/lb	0.06 mV/N
Sensitivity (±20 %) (X or Y Axis)	1.25 mV/lb	0.28 mV/N
Measurement Range (Z Axis)	10000 lb	44.48 kN
Measurement Range (X or Y Axis)	4000 lb	17.79 kN
Maximum Force (z axis)	11000 lb	48.93 kN
Maximum Force (x or y axis)	4400 lb	19.57 kN
Maximum Moment (z axis)	240 ft-lb	325.4 Nm
Maximum Moment (x or y axis)	325 ft-lb	440.7 Nm
Broadband Resolution (z axis)	0.05 lb-rms	0.222 N-rms
Broadband Resolution (x or y axis)	0.01 lb-rms	0.04 N-rms
Upper Frequency Limit	39000 Hz	39000 Hz
Low Frequency Response (-5 %) (z-axis)	0.01 Hz	0.01 Hz
Low Frequency Response (-5 %) (x or y axis)	0.001 Hz	0.001 Hz
Non-Linearity	≤1 % FS	≤1 % FS
Cross Talk (between x and y axis)	±3 %	±3 %
Cross Talk (between (x or y axis) and z axis)	±5 %	±5 %

(b)

Figure 5.14: Details of M260A03 Piezoelectric Load Cell: (a) Image (b) Some Specifications

inertial forces into the force measurement. After some iterations, the present configuration was selected. The piezoelectric load cells are attached to the sides of the lower housing and then attached to side supports that are tied to the foundation. This solution reduced the bearing housing motion and minimized additional complications. The entire substructure including the foundation and the components shown in the exploded view of Figure 5.15 were modeled with 3D FEA for the uncertainty analysis.

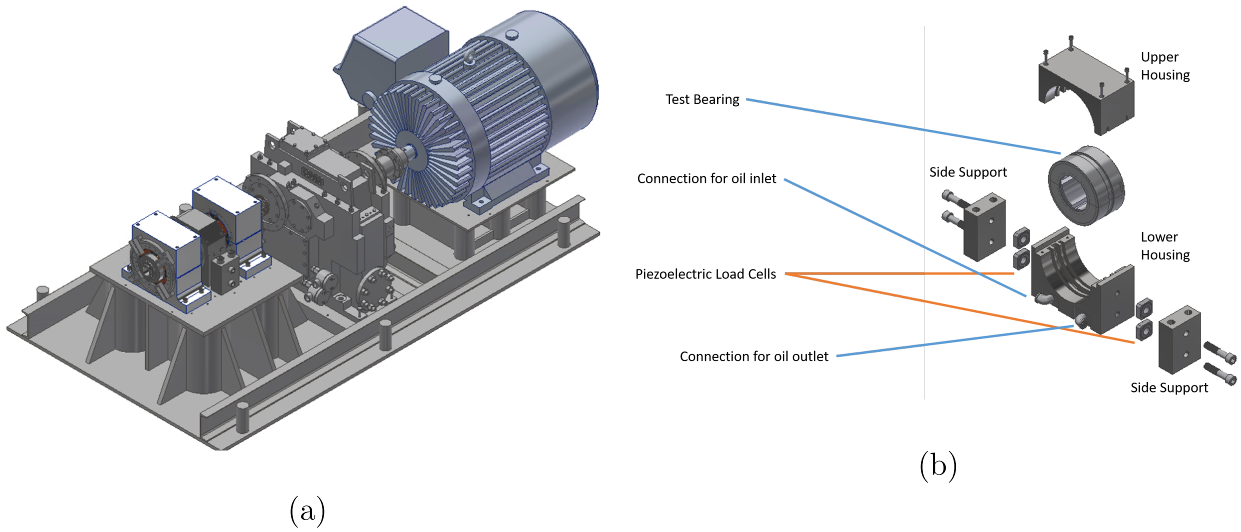

Figure 5.15: Design Configuration Layout with Piezoelectric Load Cells

5.7 High Fidelity Uncertainty Analysis of Proposed Test Rig Redesign

A high-fidelity uncertainty analysis was carried out for the proposed design with models developed using various finite element analysis tools. First, a bearing truth model was developed using a fluid-film bearing modeling algorithm developed by Branagan [80]. The truth model's dynamic coefficients are presented in Figure 5.16.

A schematic representation of the interaction between the models in the uncertainty analysis is shown in Figure 5.17. The truth model includes a rotor model, bearing model, and substructure model that includes all the components in the force measurement such as the load cells and side supports. The measured signals are sent to the truth model which includes a rotor model but does not include any model of the substructure.

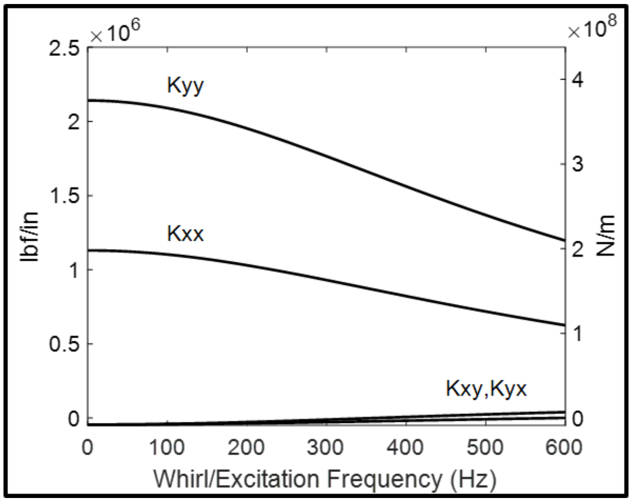

(a)

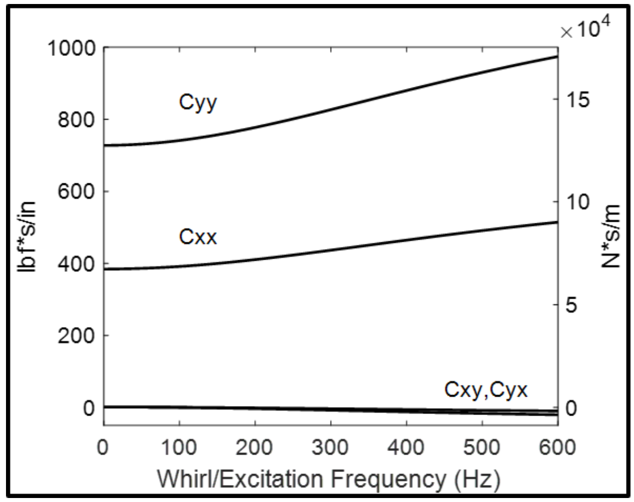

(b)

Figure 5.16: Truth Model for Bearing Test Rig TPJB

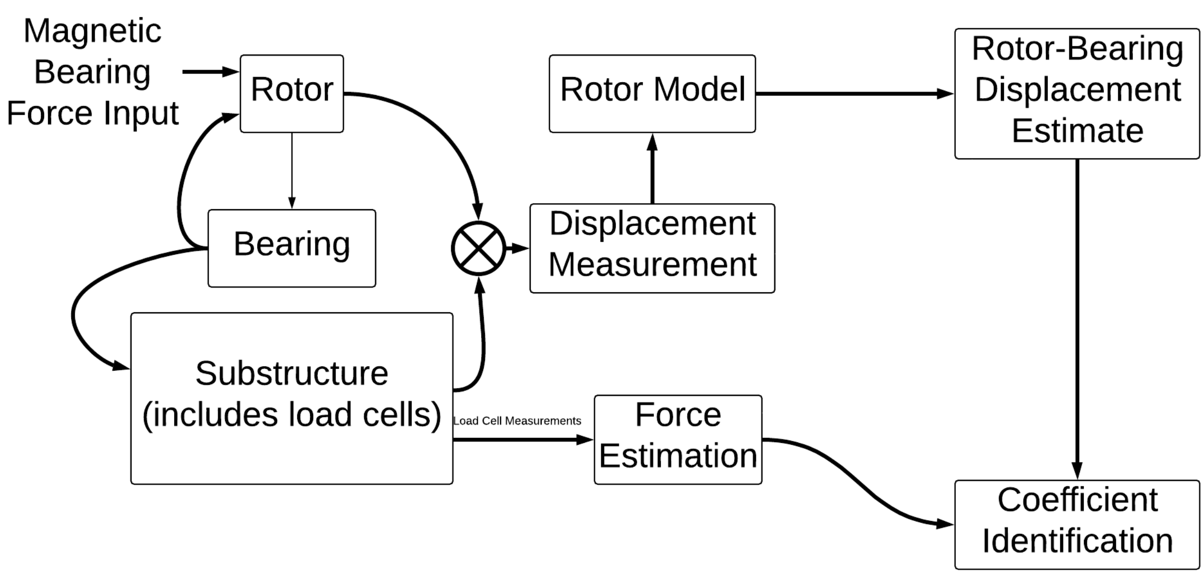

Figure 5.17: Truth and Identification Model for Test Rig Uncertainty Analysis

To build a complete understanding of the total uncertainty in identified coefficients, analyses including only one source of error were performed. By using the uncertainty analysis framework with single sources of error, the relative significance of each source of error on uncertainty and bias can be determined.

5.7.1 Rotor Modeling Effects on Uncertainty and Bias

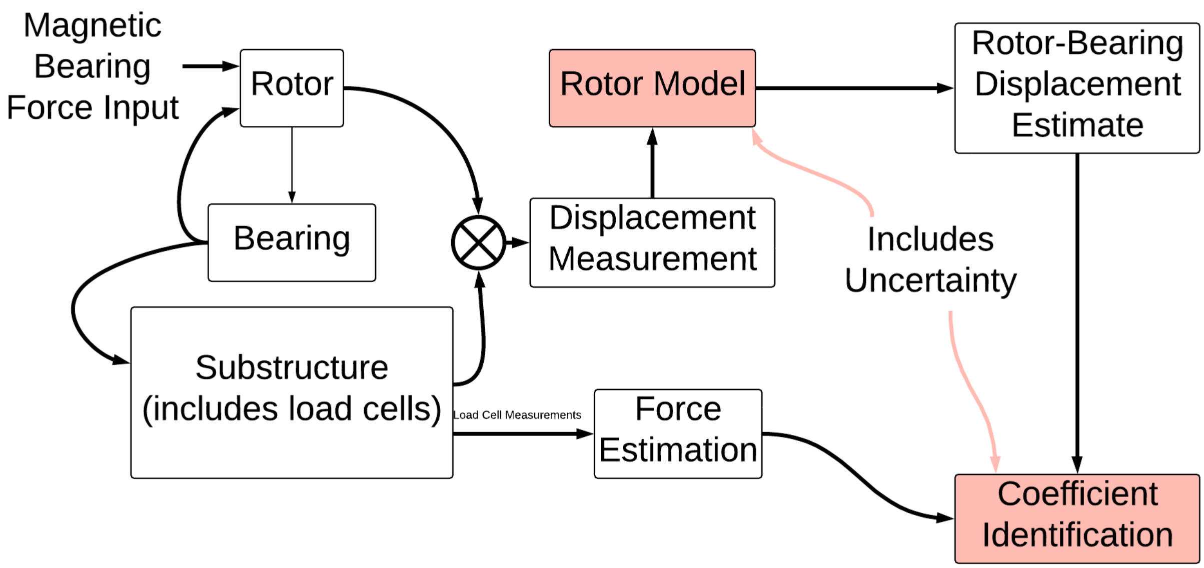

Figure 5.18: System Diagram for Uncertainty Analysis Investigating Rotor Modeling Effects

A finite element model of the rotor is developed for the identification model because of early analysis that showed a rotor critical frequency in the specified test frequency range (see Figure 5.11). The exact frequency is expected to vary based on the test article's design and also the controller design of the AMBs. In the present analysis, it is assumed that the static loading AMBs are able to levitate the system (i.e. - apply zero frequency forces) while impacting the system negligibly at test frequencies. An open-loop algorithm using the dynamic excitation AMBs will apply the test forces to the system. The open-loop algorithm will not affect the system dynamics by design. As a result of these two features of a system only possible with AMBs, the rotor is basically operating in a free-free conditions with only the test bearing's dynamic coefficients influencing the system.

The rotor model is also used to compensate for the non-collocation of the displacement measurement and the location of the actual bearing. This is expected to increase uncertainty but reduce bias. The uncertainty analysis will reveal how much of an effect this will have. In practice, the modeling error between the truth and the identification model may be improved by identifying the rotor experimentally and using the identified rotor model as the identification model. Some uncertainty must still be included but this can be developed using the uncertainty analysis framework in this dissertation as well.

A model of error is introduced to the identification model for the rotor by using the same finite element model used for the truth model. Figure 5.18 shows where these errors are applied. In this way, the identification model is perturbed about the truth. The perturbations included $\pm 5\%$ difference in structural damping, $\pm 5\%$ difference in Young's modulus for each element, and $\pm 5\%$ for material density per each element. The variations resulting from these error sources within the rotor model are designed to try and bound the variation in rotor behavior due to various effects such as the dynamic effects of friction between sleeves and the rotor and dynamic effects of the AMB lamination stack.

First, Figure 5.19 shows identified dynamic coefficients with the only difference between truth and identification model being the identification model does not include the rotor model. Another set of data is plotted where the identification model includes a rotor model identical to the one in the truth model. No additional errors are included. This demonstrates that in principle, biases in identification can be addressed with the appropriate models. Figure 5.20 then shows the results of an uncertainty analysis when errors in the identification rotor model relative to the truth is introduced. Results for the cross-coupled coefficient results are omitted because these coefficients are small relative to the principal coefficients and have little impact on the overall system dynamics. Any impact on the principal coefficients will be captured because the cross-coupling is included in the simulations for uncertainty analysis.

The uncertainty analysis results including only rotor modeling errors between the truth and identification shows a flat uncertainty curve as test frequency varies until just above 500 Hz. A slight bias exists at lower frequencies and at higher frequencies. The bias plot is shown for reference, but this is a case where it may be possible to summarize the bias as "below 10%" without needing to show the plot. The uncertainty at higher frequencies is the result of a rotor critical frequency just outside the range plotted. Though it has a reasonable separation from the operating speed of the bearing, it still has an effect on identified coefficient uncertainty.

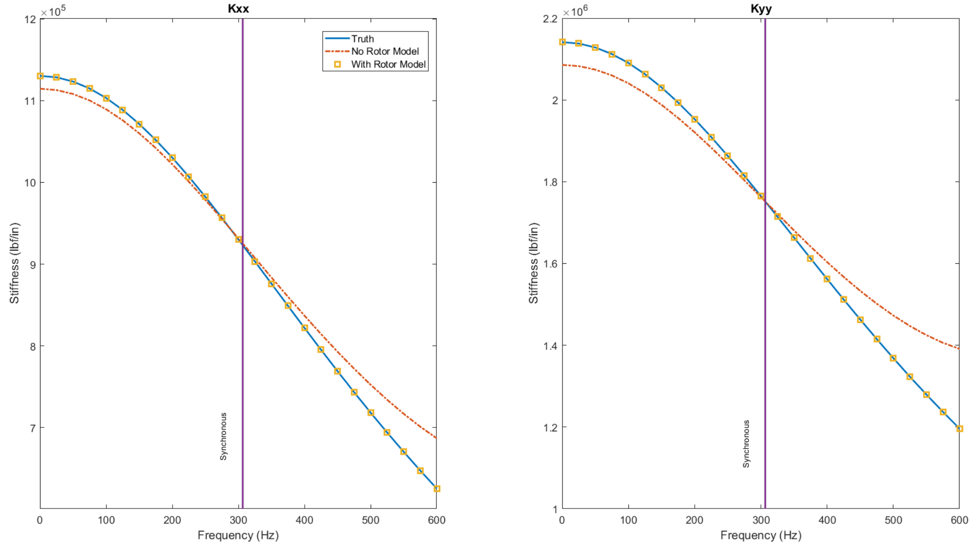

(a)

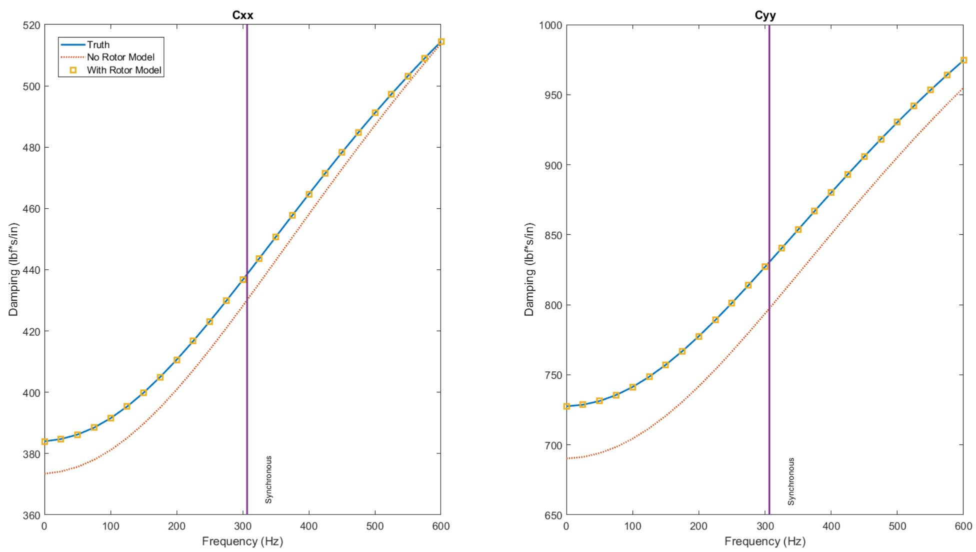

(b)

Figure 5.19: The Effect of Including a Perfect Rotor Model in the Identification Model for (a) Kxx/Kyy and (b) Cxx/Cyy

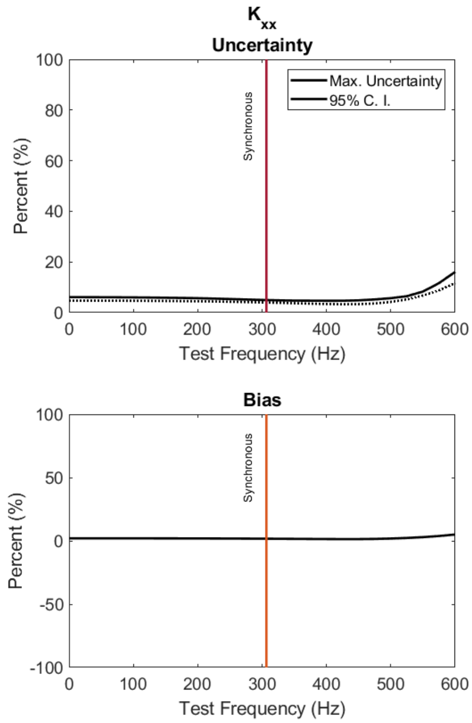

(a) K_{xx}

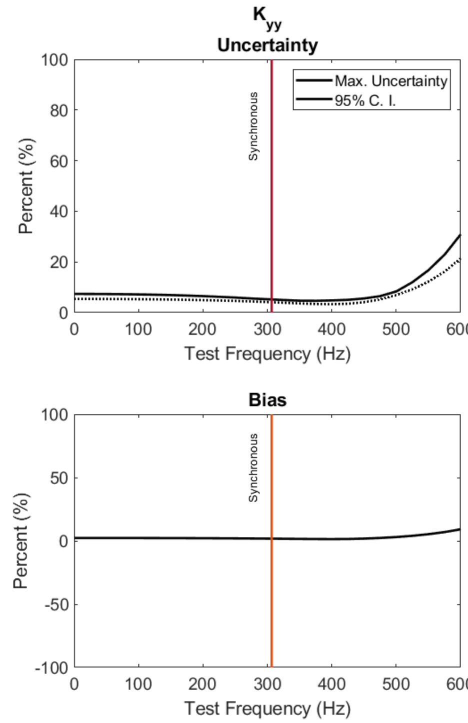

(b) K_{yy}

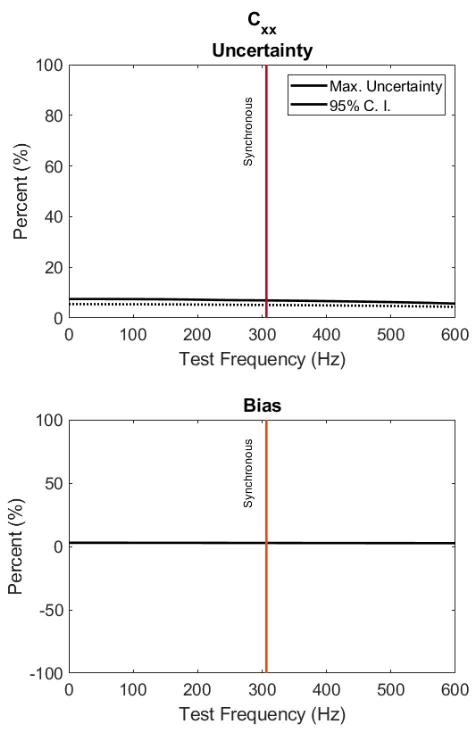

(c) C_{xx}

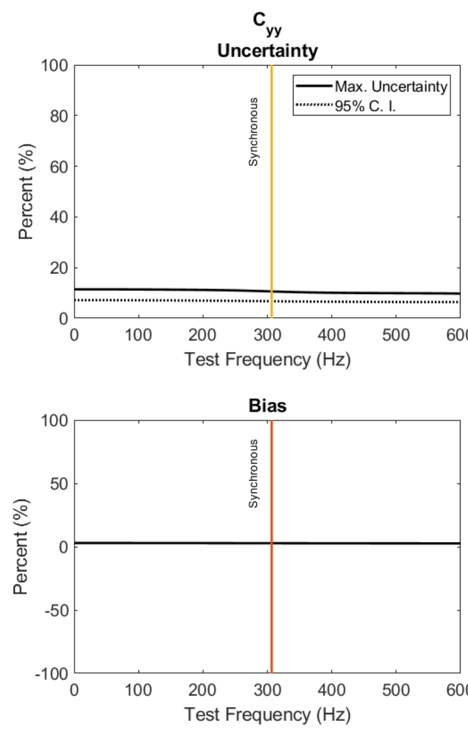

(d) C_{yy}

Figure 5.20: Uncertainty Results from Rotor Model Variation

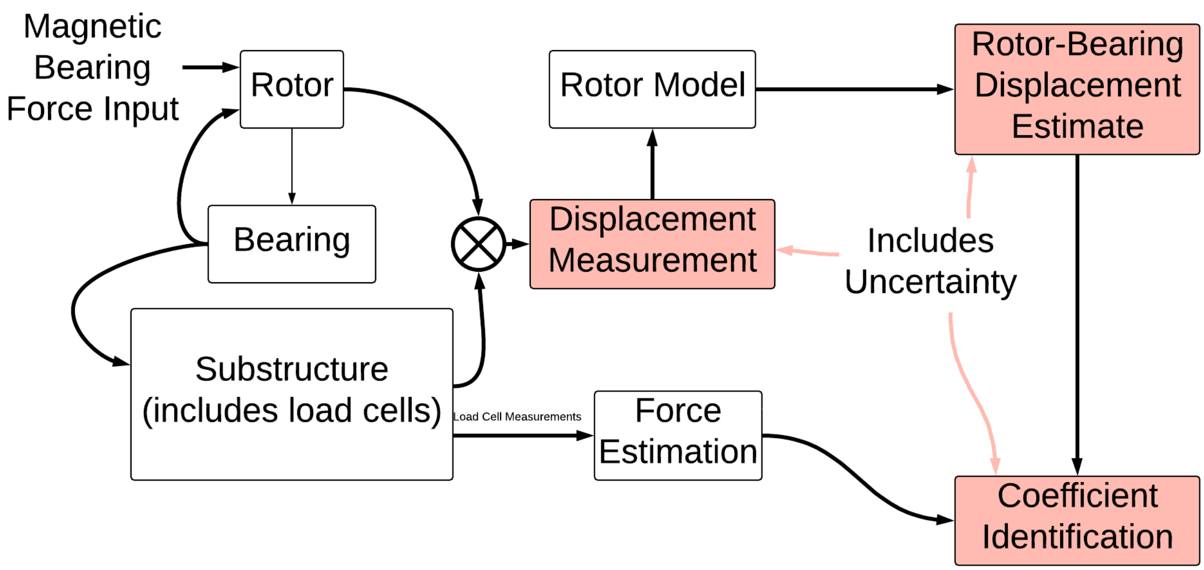

Figure 5.21: System Diagram for Uncertainty Analysis With Displacement Errors Only

5.7.2 Displacement Measurement Error Effects on Uncertainty and Bias

To determine the sensitivity of uncertainty to displacement measurement error, an analysis similar to Section 5.7 was performed with displacement measurement errors being the only difference between truth and the identification model as shown in Figure 5.21. The results of this analysis are shown in Figure 5.22. It should be noted that with these results, the force is assumed to be known perfectly and the rotor model is assumed to be known perfectly. Since the force model is tied to the substructure model through the load cells, knowing the bearing force perfectly implicitly assumes all the substructure dynamics are accounted for.

While the bias results are shown for completeness, in this case it would be sufficient to say that the stiffness bias results are all less than 5%. With damping uncertainty and bias, there is a growth towards infinity as the test frequency approaches 0 (as expected from the model development in this dissertation). For stiffness, the uncertainty increases as test frequency increases, approaching 20% at 600 Hz (which is above the target maximum frequency of 510 Hz for the test rig).

5.7.3 Force Measurement Error & Substructure Effects on Uncertainty and Bias

The last sensitivity study for uncertainty of identified coefficients is for force measurement and the substructure. These components are analyzed together because the load cells measuring force are effectively a part of the substructure. Because the housing will experience some vibration, this analysis was performed with models of accelerometer on the housing to measure the inertial forces of the housing. This is expected to increase uncertainty but reduce bias. Figure 5.24 shows a diagram of the force measurement model and the details going into simulating the force measurement.

The inclusion of the substructure model introduces several contributors to uncertainty. First, AMB forces (from both static loading bearings and dynamic excitation bearings) will be transmitted to the load cells through the substructure. The substructure's dynamics will also respond to the forces in an experiment and add to the test bearing's dynamics. In addition to the force measurement error, the impact of the substructure will be

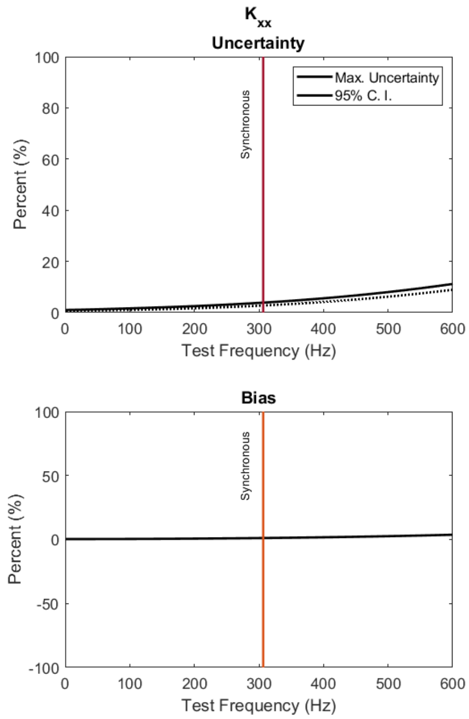

(a) K_{xx}

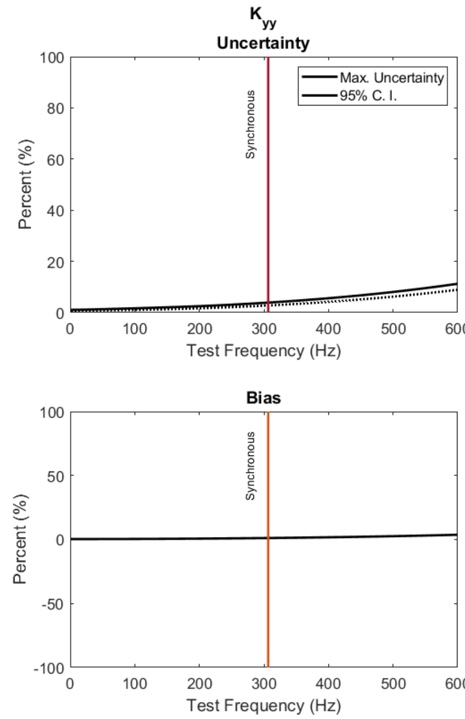

(b) K_{yy}

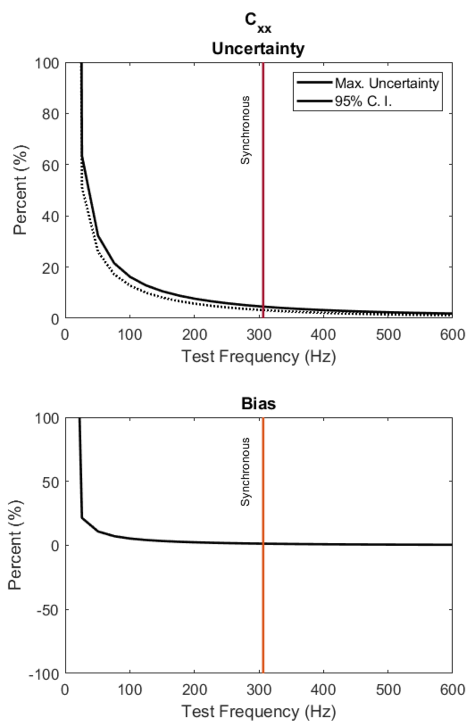

(c) C_{xx}

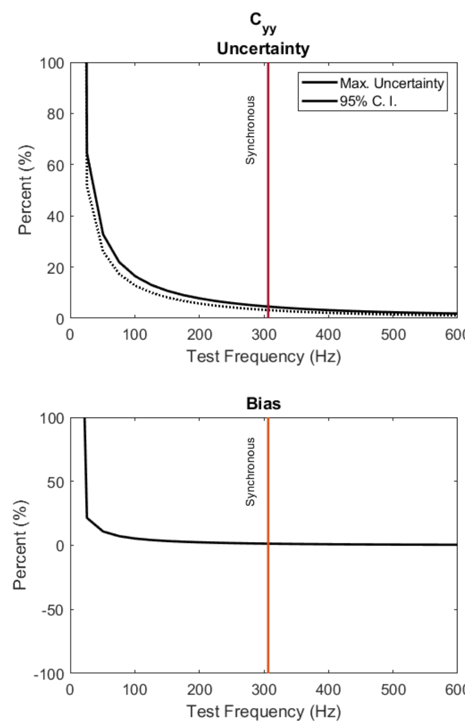

(d) C_{yy}

Figure 5.22: Uncertainty Results from Displacement Errors

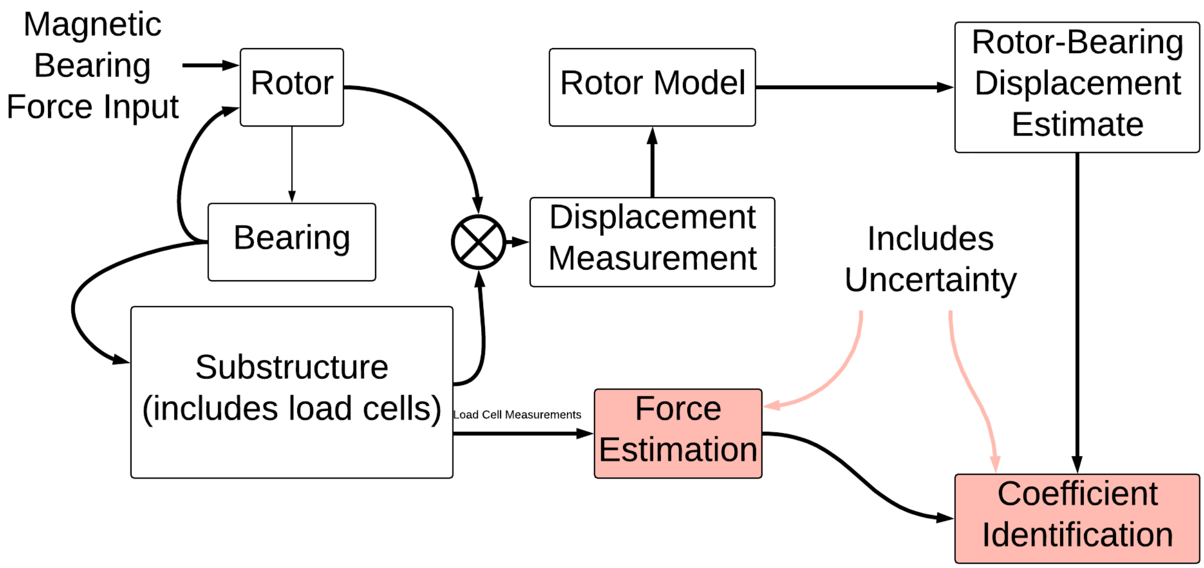

Figure 5.23: System Diagram for Uncertainty Analysis With Only Force Measurement Errors

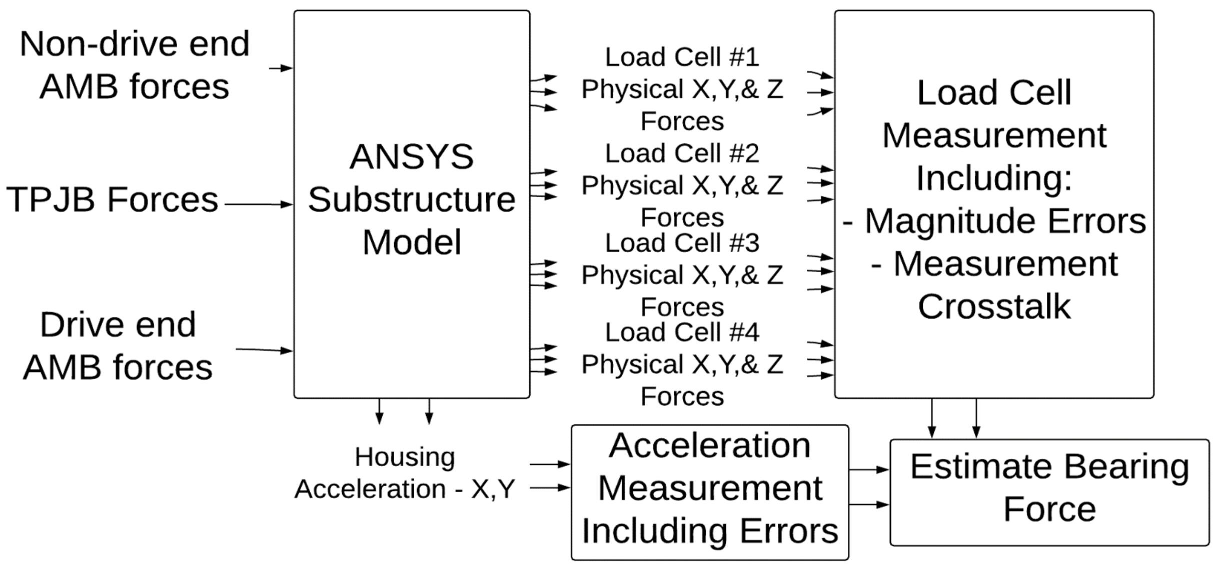

Figure 5.24: Measurement Model for Force

evaluated by including it in the truth model and not in the identification model. In practice it may be possible to model or identify the substructure's dynamics, but this would be more challenging than modeling and/or identifying the rotor. Therefore, if it is possible to identify TPJB dynamic coefficients accurately enough without needing to model and/or identify the substructure, the experiment will be significantly simpler.

Figure 5.25 shows the uncertainty analysis results only considering force measurement error and the inclusion of the substructure model in the truth. The difference between the horizontal axis and the vertical axis is clearly demonstrated in this analysis. The difference can be traced back to a mode of the substructure that affects the horizontal axis dynamics of the system. In effect, this shows that any experiment on this test rig will be wrestling with the effect of this mode on the identification. At this stage, the foundation has already been built and installed so design changes would be prohibitive in time and cost. Therefore, in Section 5.7.4 when the uncertainty factors are combined, the substructure effects will still be present.

5.7.4 Total Uncertainty of Coefficient Identification on the Test Rig

Figure 5.27 shows the results of the uncertainty analysis including displacement measurement errors, force measurement errors, rotor model errors in the identification model relative to the truth, and substructure dynamics (which are included in the truth model but not in the identification model).

Overall, the total uncertainty and bias results have trends that are combinations of the individual trends observed in the sensitivity studies. At

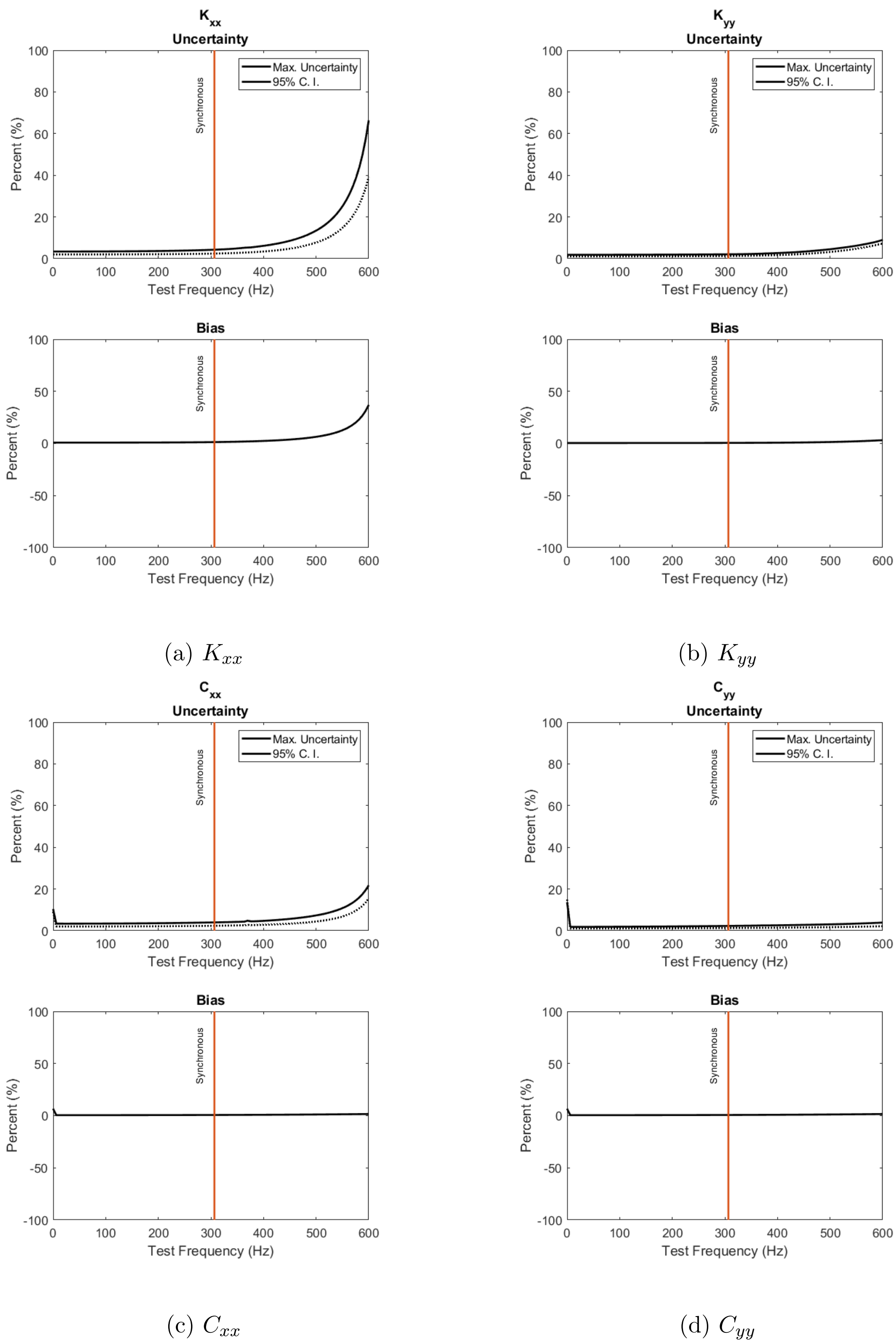

(a) K_{xx} (b) K_{yy}

(c) C_{xx} (d) C_{yy}

Figure 5.25: Uncertainty Results from Force Errors and Truth Substructure Model

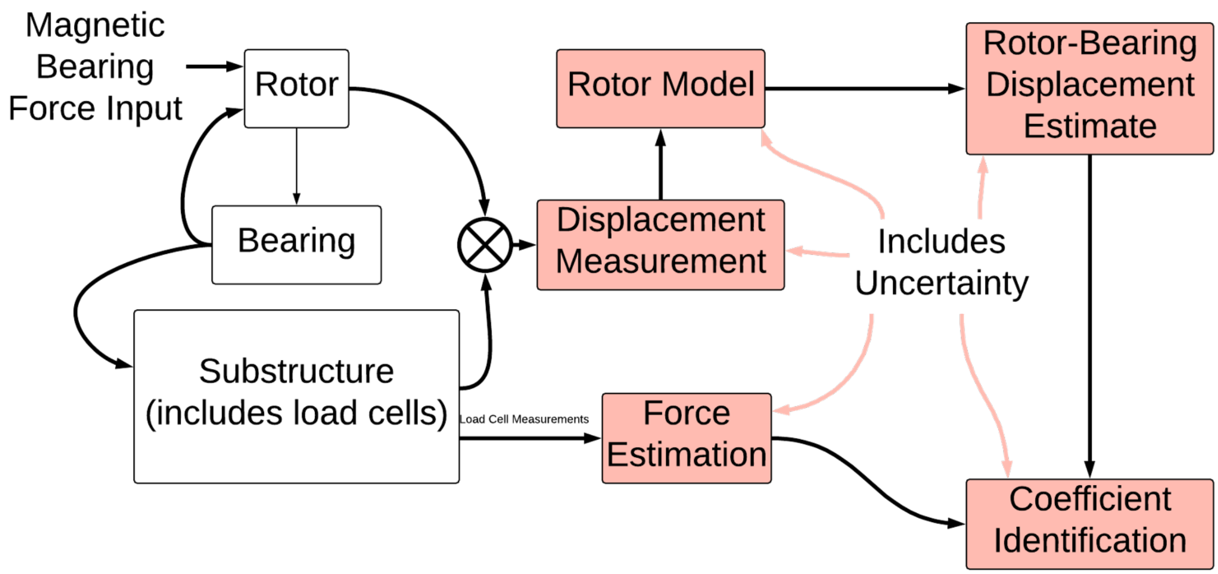

Figure 5.26: System Diagram for Total Uncertainty Analysis

low frequencies for stiffness, the uncertainty is dominated by the rotor model errors' contribution. At higher frequencies, the substructure dynamics' effects become dominant.

5.7.5 Evaluating Uncertainty for Different Bearings

Thus far a single TPJB model was used to perform the uncertainty analysis. While it is impossible to analyze every possible bearing that may be analyzed on this test rig, some studies can be performed to determine if changing the true properties will still allow accurate TPJB identification. Since the uncertainty analysis indicates that higher stiffness and damping would result in lower uncertainty, a second case was explored that had lower stiffness and lower damping. Figure 5.28 shows the dynamic coefficients for this bearing model. For a real system there would be challenges with this

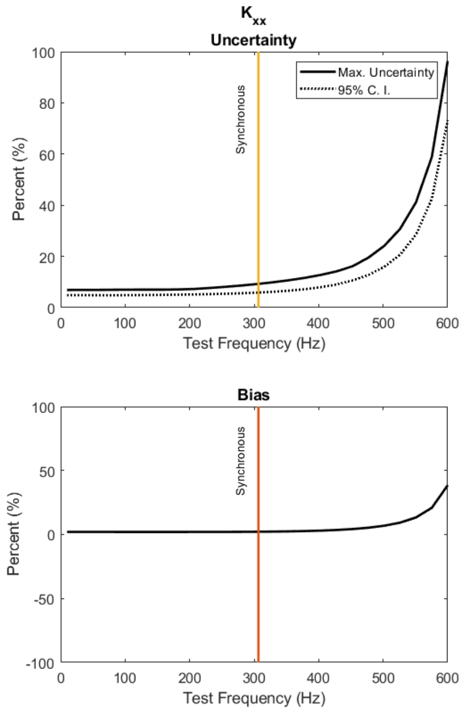

(a) K_{xx}

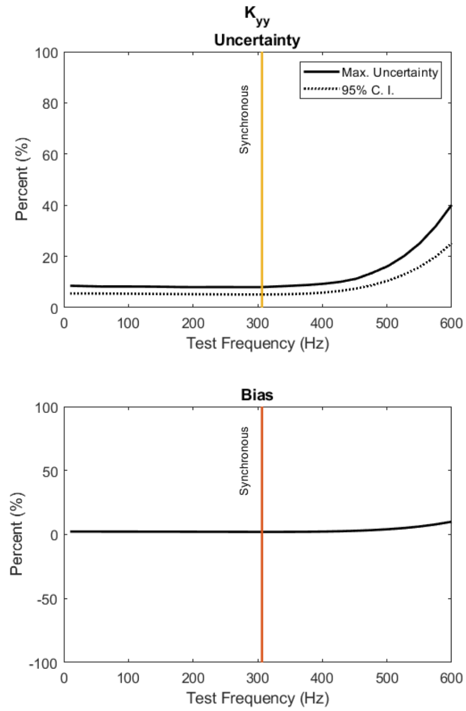

(b) K_{yy}

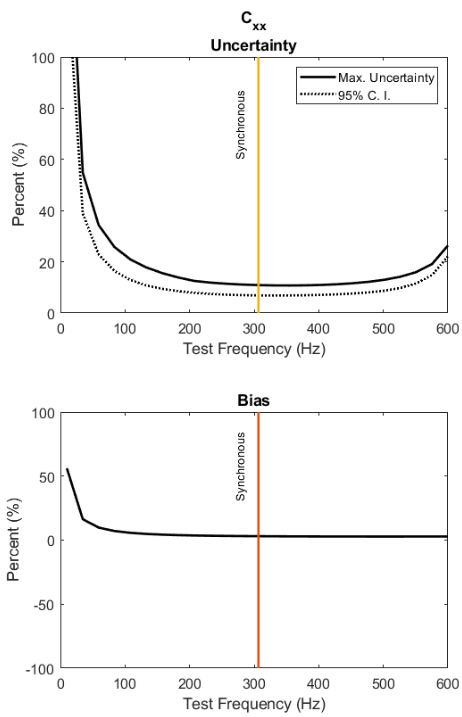

(c) C_{xx}

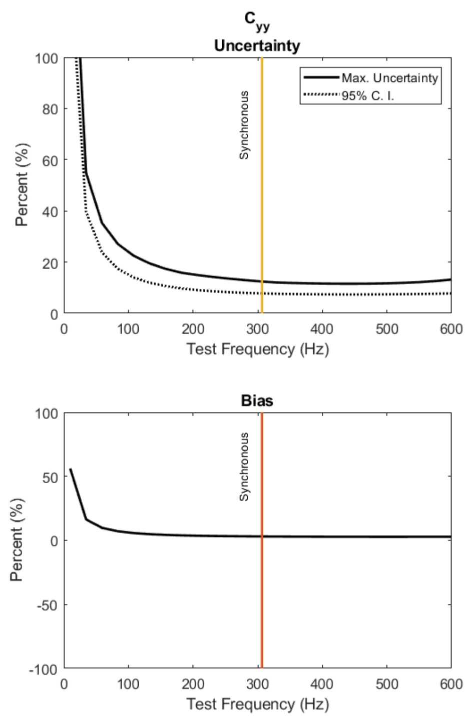

(d) C_{yy}

Figure 5.27: Total Uncertainty

bearing design (the damping is negative at very low frequencies, for example) but for understanding the impacts on uncertainty analysis, this case is useful. In addition to having stiffness approximately an order of magnitude lower than the first case analyzed, the principal horizontal and vertical stiffness and damping coefficients are identical. The cross-coupling is also similar in magnitude for some part of the frequency range (low frequency for damping, high frequency for stiffness).

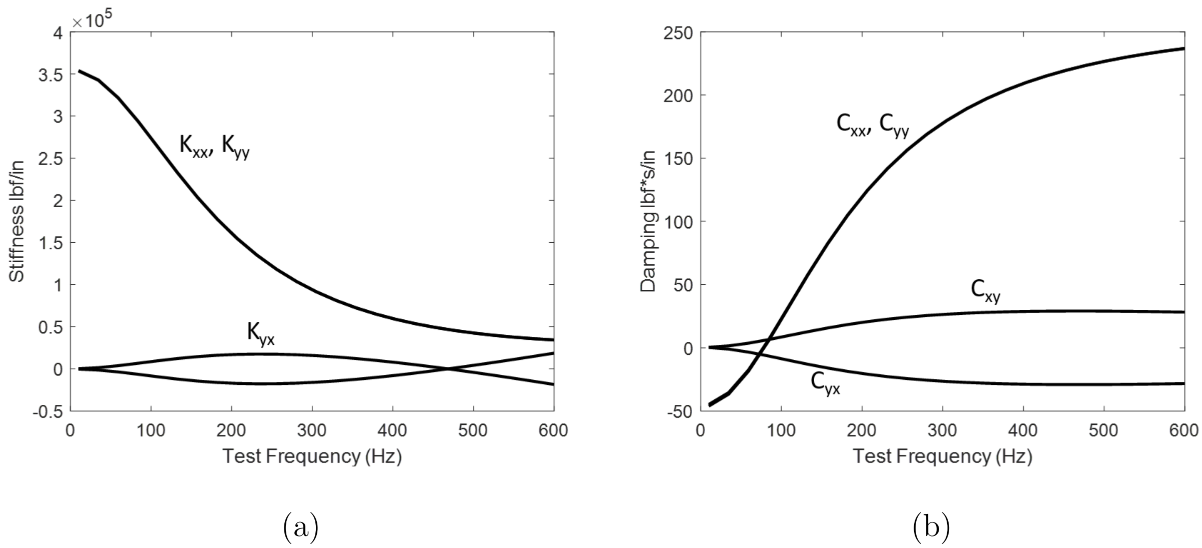

Figure 5.28: Truth Model for Bearing With Lower Stiffness and Damping

The transfer function from applied forces (horizontal and vertical) to measured forces (horizontal and vertical) are plotted in Figure 5.29. This shows how the difference in bearing properties affects the overall system dynamics.

The results after performing uncertainty analysis with the same uncertainty features and parameters as the higher stiffness bearing are shown in Figure 5.30. Stiffness uncertainty and bias increase rapidly at a

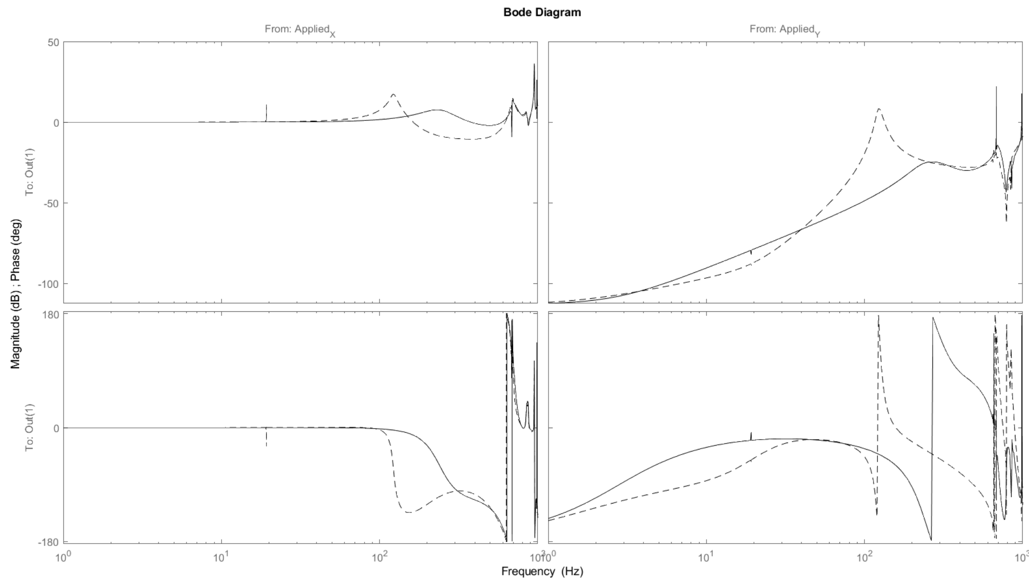

(a)

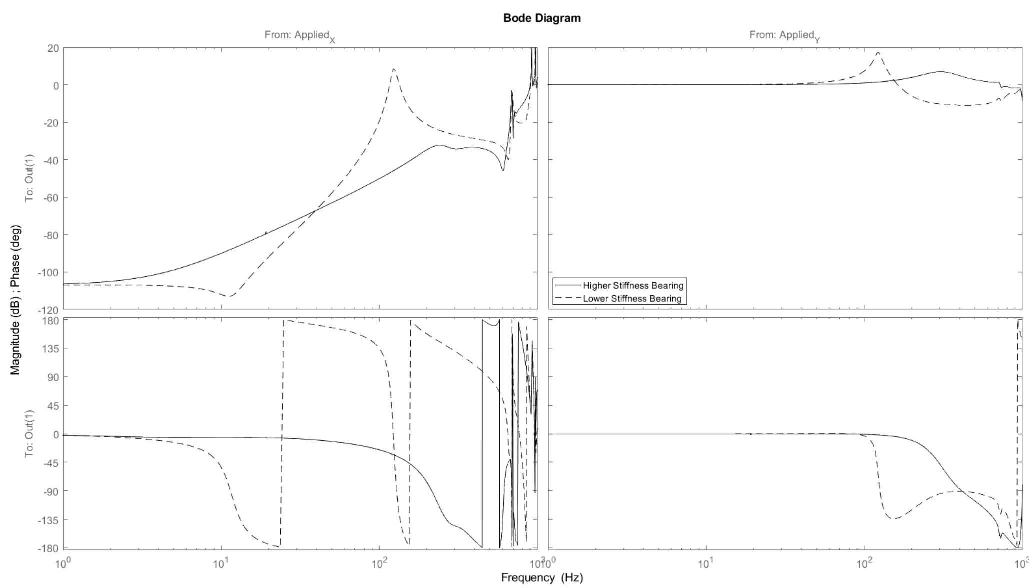

(b)

Figure 5.29: Dynamics from Applied Forces to Sum of Load Cell Forces in (a) x and (b) y

lower test frequency than with the higher stiffness bearing. Therefore, the uncertainty target cannot be achieved for the entire specified test frequency range. However, the stiffness uncertainty and bias are within the target below the nominal design synchronous frequency of this hypothetical bearing design. Damping uncertainty and bias meet the uncertainty targets across most of the test frequency range specification. The damping identification struggles at lower frequencies over a greater range than the higher stiffness bearing (which also had higher damping). Nevertheless, above 200 Hz the uncertainty is low and the bias is also close to zero. Ultimately, though there are challenges over the entire frequency range, this bearing model if tested on the system would accurately identify damping between approximately 150 Hz to 510 Hz. Stiffness would also be identified accurately between 0 Hz and 300 Hz. The model can be validated between 150 Hz and 300 Hz for both stiffness and damping which would build confidence for dynamic coefficient predictions at test frequencies outside this range.

Comparing the two examples highlights how differently the system behaves when the test article is different. This adds emphasis to the idea that a single uncertainty value would not make sense for dynamic coefficient identification over a range of test frequencies and between test articles. Careful consideration is required to understand the conditions which lead to the most accurately identified coefficients. Bearing model predictions can be validated only with the most accurate identified coefficients.

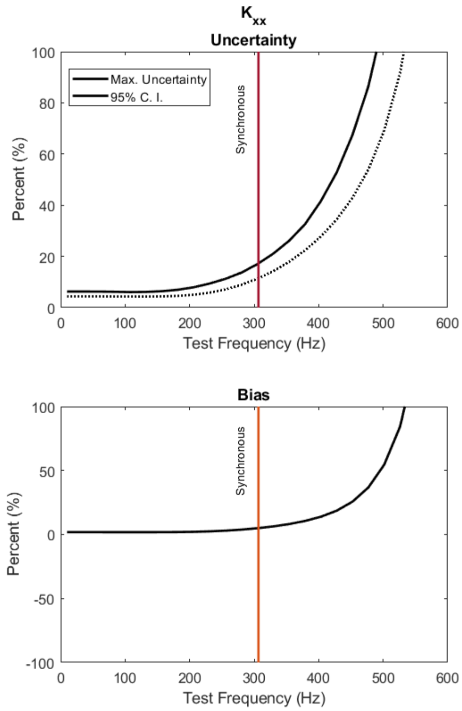

(a) K_{xx}

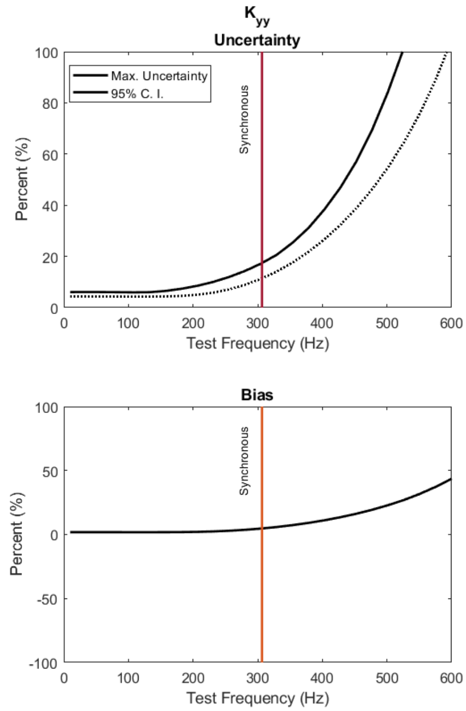

(b) K_{yy}

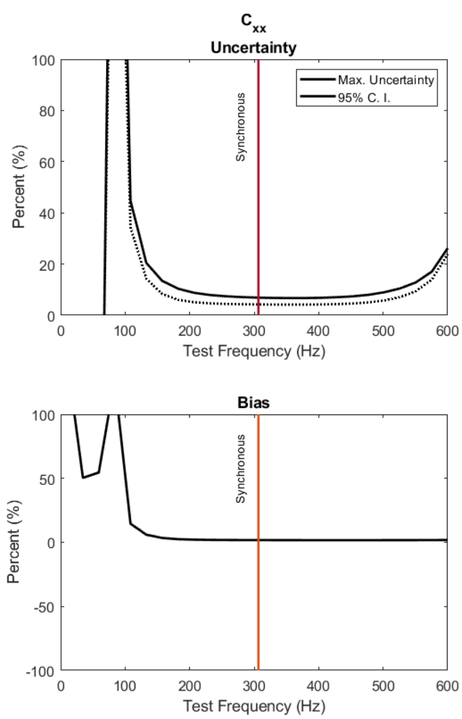

(c) C_{xx}

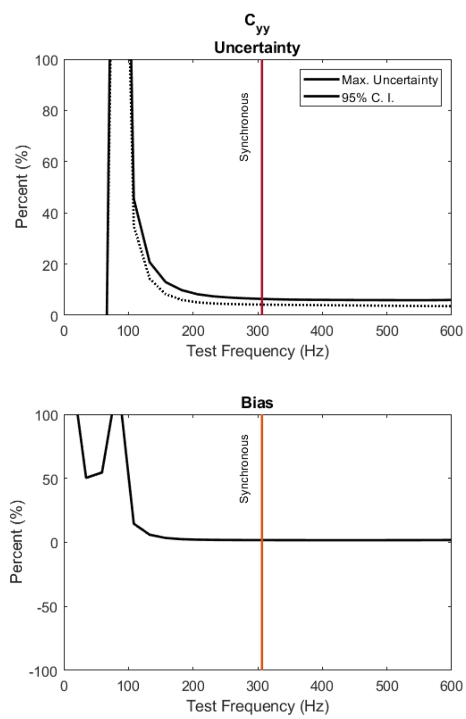

(d)

Figure 5.30: Total Uncertainty, Case 2

5.8 Summary

The analyses in this chapter guided the redesign of a test rig to reduce uncertainty. Approximating the bearing force using piezoelectric load cells connected to the test bearing housing was shown to be capable of meeting accuracy requirements. The redesign process demonstrated how the uncertainty analysis framework can work with practical considerations for the design and construction of a bearing test rig. Ultimately, the third objective of this dissertation has been achieved with the work presented in this chapter. Some further conclusions are listed here:

- The original design for the test rig would have been capable of identifying coefficients. However, as the uncertainty analysis results in Figure 5.7 show, the uncertainty of identified coefficients grows large very quickly. Without any changes, the cases analyzed exceed the 20% threshold accepted by the ROMAC industrial members by about 250 Hz. This does not include bias from various dynamics in the system which would decrease the usefulness of the identified coefficients. The framework for comprehensive uncertainty analysis was required to identify this challenge and overcome it with design changes.

- The bearing model with higher stiffness and higher damping can be identified confidently within the accuracy limits specified for this test rig.

- The bearing model with lower stiffness and lower damping has some challenges related to uncertainty in the target test frequency range. For the stiffness coefficients, uncertainty below 20% with minimal bias is achievable up to approximately 300 Hz. For the damping coefficients, the uncertainty target is achievable above approximately 150 Hz. The horizontal damping (C_{xx}) uncertainty shows some effects of the substructure dynamics as the test frequency approaches 600 Hz but the uncertainty is still below the target of 20%.

- The models used in the high-fidelity uncertainty analyses in Section 5.7 provide engineers with flexibility as far as how the models are developed. Analysis-based methods were used in this dissertation including FEA for the rotor and for the substructure. The models can be experimentally identified as well and the experimentally identified model can be incorporated into the uncertainty analysis. For due diligence, the same uncertainty analysis can be used with the experimental identification of the subsystem to estimate the identification uncertainty which can be used in the uncertainty analysis of the complete system.

Chapter 6

Conclusions and Recommendations

This dissertation developed a framework for estimating the uncertainty of experimentally identified TPJB dynamic coefficients. The single-axis development in Chapter 3 established the fundamentals of the uncertainty analysis framework including important concepts such as the truth model, identification model, and implementations of uncertainty. Single-axis, higher-fidelity models demonstrated the combining of models such as finite-element models and lumped-mass simplifications of dynamics. Chapters 4 and 5 implement the framework with two-axes models. Regardless of the component that is being experimentally identified (TPJB, fixed-geometry bearing, foil bearing, seal, etc.), the framework can be used to analyze uncertainty with a consistent method. Having a common framework allows more significant comparisons between identification experiments, paving the way for determining the appropriate test rig to identify the dynamic coefficients of various components.

As the framework was developed, studies were performed looking at the impact of varying parameters and experimental methods. These studies highlighted the impact of factors such as measurement method (especially for force measurement), the properties of the bearing tested, and differences between the identification model and truth model. The trends and effects identified in this dissertation can guide future test rig designs.

Finally, a test rig design was updated using the uncertainty analysis framework as a tool to guide the design. From the original configuration, the uncertainty of identified coefficients was reduced to acceptable levels for a broader range of bearings. The reduction of uncertainty was balanced with the cost and schedule impact of required design changes. For example, while the active load cell concept would have provided the best accuracy (lowest uncertainty), the cost to implement this would have been prohibitive. The uncertainty analysis framework provided the means to evaluate alternatives and identify a test rig configuration that was still able to meet the uncertainty targets.

6.1 Conclusions

The conclusions from this research are summarized in groups according to which objective of this dissertation the points satisfy.

6.1.1 Establishing the Uncertainty Analysis Framework

- The framework proposes analyzing the uncertainty of identifying dynamic coefficients with a simulation-based method. A Monte Carlo method is recommended to iterate over combinations of errors affecting the identification. The errors are selected from the uncertainty of subsystems such as measurement systems or models of subcomponents such as the foundation. The two main parts of the uncertainty analysis are the truth model and the identification model. The truth model is a representation of the real physics of the system. The identification model represents how the measurements taken from an experiment are translated into dynamic coefficients.

- The truth model should include as much of the dynamics affecting the experiment as possible. The inputs to the truth model will be the inputs to the experiment. For a simple model this may simply be forces applied on the excited component. For a higher fidelity model, the input may be commands given to the system (such as from a computer system) with models for how this translates into actual force on the excited component. The outputs of the truth model are measured signals that act as inputs to the identification model. Measurement models should include uncertainty. Analytical tools such as finite-element analysis can be used to develop models for the analysis. Experimental techniques can also be used to identify relevant dynamics if a physical system is available. If a test rig is in the design phase this may not be possible. The uncertainty analysis framework can be used for a sensitivity study of components in the truth model to determine what parts of the test rig have the greatest effect on the dynamic coefficient identification.

- The identification model represents how the experimental measurements will be used to compute dynamic coefficients. The inputs to the identification model are the simulated measurements from the truth model. If models of any parts of the system (such as the rotor) are used in the identification model to process the signals in any way, uncertainty may be included with the models to understand the effects of errors in modeling the physical system. The uncertainty analysis can be iterated with different models for components in the truth model to determine which models are significant for uncertainty and which models are not significant. For example, when measuring applied force, the rotor model played a significant role as evidenced by large bias when the identification model did not include a rotor model. This would mean the rotor model is significant in that uncertainty analysis and should be included. On the other hand, when bearing force is measured the effect of the rotor model is less significant. If the uncertainty and bias from not including the rotor model is small enough, it does not need to be included in the identification model for the analysis.

- Identification uncertainty should be presented with both uncertainty and bias as demonstrated in this dissertation. If the bias is small (such as less than five percent), then plots are not required but a statement of maximum bias in the caption of a figure or in the text of the publication should still be included. (e.g. - "The bias in the target test frequency range is less than 5%") The uncertainty is presented with the maximum uncertainty as well as a 95% confidence interval to provide a description of how the uncertainty is distributed.

- All dynamic coefficient identification experiments should be accompanied by uncertainty analysis using the framework described in this dissertation. The analysis results should be presented with accompanying information describing the models used in the truth model and models used in the identification model. Where feasible, results of intermediate sensitivity studies can be presented to support the selection of models in the final uncertainty analysis. With a common framework used in uncertainty analysis, different experiments (both on the same test rig and on different test rigs) can be compared more directly.

6.1.2 Factors Affecting Identified Coefficient Uncertainty

- Uncertainty analysis results with higher fidelity models exhibit the same trends identified in single-axis models and in analytically derived models.

TPJBs are particularly suited for this type of comparison due to the lack of cross-coupling but even when the cross-coupling is more significant, the trends corroborate well over all the analyses. This is strong evidence for the applicability of lessons learned from simple models to complex systems when analyzing uncertainty.

- The uncertainty of identified coefficients is frequency-dependent. Components such as TPJBs may have frequency-dependent dynamic coefficients depending on the design. For a given operating point (speed, load, etc.), dynamics at different frequencies will experience different bearing properties. This makes understanding the frequency-dependence important. Furthermore, the frequency-dependence changes depending on the measurement scheme. If the applied force on the excited component is measured, for high test frequencies the dominant behavior is quadratic growth for stiffness and linear growth for damping. If the bearing force is measured, then for high test frequencies the dominant behavior is linear growth for stiffness and constant for damping. In both force measurement schemes, damping also has another trend for very low frequencies. As test frequency approaches zero, the damping uncertainty increases to infinity.

- The uncertainty of identified coefficients is dependent on the magnitude of the true property. Lower stiffness and lower damping values lead to increased uncertainty. For TPJBs, stiffness typically decreases as test frequency increases so there is an added component to the increasing uncertainty from the decreasing true stiffness. Combined with the quadratic dependence on test frequency, identifying stiffness coefficients at high frequencies can be challenging. In the big picture, this also highlights challenges of identifying gas bearing or foil bearing dynamic coefficients as they are typically less stiff and have less damping than TPJBs. Another area where this property is evident is in the identified coefficient uncertainty for cross-coupling coefficients.

- Bias is introduced into the dynamic coefficient identification if the identification model does not include the effects of dynamics that are affecting the experiment. Bias can be reduced by including models of the dynamics in the identification model. This comes at the expense of uncertainty, however, so the pros and cons must be carefully evaluated to determine if including additional models is worthwhile for an experiment.

- If the measurement uncertainties are equal, the uncertainty of identifying dynamic coefficients is minimized when the bearing force and film thickness are measured directly. This insight along with the uncertainty analysis framework described in this dissertation will allow for more focused design of test rigs for dynamic coefficient identification. Practical consideration may make it difficult to measure the signals from within the bearing but if at all possible the bearing force should be considered for measurement. (The "Active Load Cell" concept referenced here can measure bearing force without requiring instrumentation inside the bearing, for example) The measurement of bearing force has been shown to significantly improve the trends in uncertainty when identifying coefficients so this is critical for advancing the state-of-the-art.

- Based on the SDoF analysis, decreasing the true stiffness while the other properties remain constant increases the uncertainty of identified stiffness. The effect on damping is a little bit more complex. At lower frequencies the uncertainty is decreased but at higher frequencies the uncertainty is higher. This can be observed as the point at which the damping uncertainty changes from decreasing to increasing shifts to lower frequencies when the true stiffness decreases.

- Based on the SDoF analysis, decreasing the true damping while the other properties remain constant increases the uncertainty of identified damping and decreases the uncertainty of identified stiffness. The transition point from decreasing uncertainty to increasing uncertainty for damping does not change. This supports the idea that the critical frequencies of a system play a significant role in uncertainty. When stiffness and mass change and the critical frequencies change significantly, behaviors such as the transition point change while when the damping is changed, the behaviors such as the transition point do not change significantly.

- Based on the SDoF analysis, decreasing the true mass of the excited component decreased identification uncertainty for both stiffness and damping. Since the critical frequency is changing, behaviors such as the transition point of decreasing uncertainty to increasing uncertainty for damping shift in frequency. In general, these results suggest that the lowest mass possible for the excited component is preferable. For real systems that will have additional dynamics for the excited component (such as rotor modes), the takeaway is that the modal mass of various modes in the system should be as small as possible to minimize uncertainty.

- The fewest number of measurements and models should be used for the identification. Every measurement or model required for the identification of dynamic coefficients increases uncertainty. In some cases this may be a required trade-off for reducing bias. The uncertainty analysis framework should be used to identify which models are critical and which models may be omitted for an experiment.

- In addition to more favorable trends for stiffness and damping uncertainty as test frequency increases, measuring bearing force is also shown to be less sensitive to dynamics in the system.

- When additional degrees of freedom are introduced, the uncertainty behavior becomes more complex. For example, in the 2DoF models, when the pedestal mass is increased by a factor of ten, there are ranges of frequency where the system with the higher pedestal mass offers better uncertainty and bias. Right around the critical frequency, however, the uncertainty and bias spike extremely high.

6.1.3 Novel Test Rig Design

- The final design for the test rig is capable of identifying dynamic coefficients with less than 20% uncertainty for a large fraction of the specified frequency range. The exact uncertainty will depend on the bearing to be tested. Bearings with higher stiffness and damping will have lower uncertainty and bias than the cases presented in this dissertation. Bearings with lower stiffness and damping than the cases analyzed in this dissertation will have higher uncertainty and bias. The dynamics of the substructure may also affect different bearings differently. Therefore, every bearing to be analyzed on the test rig will need to have a comprehensive uncertainty analysis performed.

- The first changes to the test rig design involved the AMBs. Modifying the design from the continuous back-iron stator design to the segmented e-core design improved the load capacity of the bearings and ensured adequate dynamic force capacity to hit the performance targets for unit load and test frequencies in the specifications. Furthermore, with the uncertainty analysis framework as a guide, the AMBs were split into two pairs: One pair dedicated to providing static loading for the system and the other pair applying dynamic excitation on the rotor. The separation of functions would also reduce the uncertainty of dynamic force measurement with the AMBs, though ultimately a different force measurement scheme was developed to meet the desired uncertainty requirements.

- While analysis showed that the active load cell concept would have the best accuracy, the cost and schedule impact for changes to the test rig design and existing hardware would have been prohibitive. Piezoelectric load cells were selected to estimate the bearing force and the uncertainty analysis showed that the resulting accuracy would meet the targets set for this test rig.

6.2 Recommendations for Uncertainty Analysis for Identified TPJB Dynamic Coefficients

- First and foremost the analyses presented in this dissertation should make it clear that when focusing on the problem of identifying dynamic coefficients, uncertainty analysis must be performed both as forethought and as part of hindsight. Uncertainty analysis is a valuable tool during the design phase of test rigs and once the experimental phase is reached, uncertainty must be analyzed for each bearing tested because the true bearing coefficients affect the uncertainty of the identified coefficients.

- Results of the uncertainty analysis must be presented as a function of frequency.
- Uncertainty analysis results should include the maximum uncertainty of the simulations, a 95% confidence interval, and bias results.
- Modeling decisions for the truth model and identification model should be justified using the uncertainty analysis framework.

6.3 Future Research Opportunities

- This dissertation focused on using a consistent, single-frequency identification method for isolating differences in uncertainty estimates to differences in modeled dynamics (the identification model) versus a more realistic model of true physics (the truth model). The scope of the analysis can be expanded to evaluate methods of identification in conjunction with modeling and instrumentation choices.
- The uncertainty analysis framework has a lot of untapped potential that is not covered in this dissertation. Non-linear models can be incorporated into the uncertainty analysis, for example, if this is valuable to the experiment being analyzed. The cases analyzed in this dissertation are suitable for linear analysis because the perturbations

will be kept small. If an experiment is investigating large-orbit dynamics for TPJBs, then non-linear models may be required. The significance for any experiment can be determined using the uncertainty analysis framework to investigate the sensitivity of identified coefficient uncertainty to linear versus nonlinear models.

- Methods for measuring bearing force more directly should be explored. The "Active Load Cell" concept briefly mentioned in this dissertation offers one possible alternative. High-performance pressure transducers are another example.

- This dissertation focused on experimental identification of TPJBs on dedicated test rigs. It is possible to use the uncertainty analysis framework for identifying the dynamics of a system in the field. Though such an experiment may not be useful for accurate component-level model validation, system models may be validated.

- The measurement error models used in this dissertation are multiplicative models. This can be extended with additive components that can incorporate other forms of error including noise. This can be explored further to more comprehensively document the effects of measurement error on the uncertainty of identified dynamic coefficients.

- It may be possible to develop a TPJB that exhibits dynamic coefficient properties that end up being favorable for minimizing identification uncertainty. This TPJB design may have no value for industrial applications but could be used to evaluate if the physics models in a bearing code are working as intended. By decreasing the experimental identification uncertainty, models can be validated with more confidence.

- In a similar vein, methods of validating test rig capability may be developed. For example, it may be valuable to validate that a test rig can identify bearing coefficients accurately even if it is not the component intended for testing on that system. This would require additional design consideration. A rolling element bearing without lubrication may be useful in this application as they have high stiffness and very little damping. The modeling of a rolling element bearing without lubrication may also be more straightforward than fluid-film bearings, for example, that require fluid mechanics to be modeled. In fact, if rotation is not required, the test article used to validate test rig capability may not even be a bearing! It could simply be a rigid link at the test bearing location.

- A notable challenge not addressed in this dissertation is the measurement of cross-coupling coefficients for TPJBs. While the effect in the field may be insignificant, model validation for dynamic coefficients is challenging if half the dynamic coefficients cannot be accurately identified. With the uncertainty analysis framework now established, further research can develop methods of validating TPJB models' capability to predict cross-coupling coefficients as well as principal coefficients.

Bibliography

[1] Seong-Wook Hong and Van-Canh Tong. Rolling-element bearing modeling: A review. *International Journal of Precision Engineering and Manufacturing*, 17(12):1729–1749, 2016.

[2] Minhui He, C Hunter Cloud, James M Byrne, José A Vázquez, et al. Fundamentals of fluid film journal bearing operation and modeling. In *Asia Turbomachinery & Pump Symposium. 2016 Proceedings.* Texas A&M University. Turbomachinery Laboratory, 2016.

[3] Gerhard Schweitzer, Eric H Maslen, et al. *Magnetic bearings: theory, design, and application to rotating machinery*, volume 9. Springer Berlin, 2009.

[4] CR Knospe, RW Hope, SM Tamer, and SJ Fedigan. Robustness of adaptive unbalance control of rotors with magnetic bearings. *Modal Analysis*, 2(1):33–52, 1996.

[5] Beauchamp Tower. First report on friction experiments. *Proceedings of the institution of mechanical engineers*, 34(1):632–659, 1883.

[6] Osborne Reynolds. On the theory of lubrication and its application to mr. beauchamp tower's experiments, including an experimental determination of the viscosity of olive oil. *Proceedings of the Royal Society of London*, 40(242-245):191–203, 1886.

[7] BL Newkirk. Shaft whipping. *Gen. Elect. Rev.*, 27:169, 1924.

[8] JW Lund. A theoretical analysis of whirl instability and pneumatic hammer for a rigid rotor in pressurized gas journal bearings. *ASME J. Lubr. Technol*, 89(2):154–166, 1967.

[9] Stephen H Crandall. Heuristic explanation of journal bearing instability. Technical report, DTIC Document, 1982.

[10] R Leonard and WB Rowe. Dynamic force coefficients and the mechanism of instability in hydrostatic journal bearings. *Wear*, 23(3):277–282, 1973.

[11] JC Wachel. Rotordynamic instability field problems. 1982.

[12] John C Nicholas. Tilting pad bearing design. In *Proceedings of the Twenty Third Turbomachinery Symposium, The Turbomachinery Laboratory, Texas A&M University, College Station, Texas*, 1994.

[13] Paul E Allaire, Ronald D Flack, et al. Design of journal bearings for rotating machinery. In *Proceedings of the 10th Turbomachinery Symposium*. Texas A&M University. Turbomachinery Laboratories, 1981.

[14] John C Nicholas and R Gordon Kirk. Selection and design of tilting pad and fixed lobe journal bearings for optimum turborotor dynamics. In *Proceedings of the Eight Turbomachinery Symposium, Texas A&M University, College Station, TX*, pages 43–57, 1979.

[15] Luis San Andrés. Static and dynamic forced performance of tilting pad bearings : Analysis including pivot stiffness. 2010.

[16] Wikipedia contributors. Southwest airlines flight 1380 — Wikipedia, the free encyclopedia, 2019. [Online; accessed 18-November-2019].

[17] Neville F Rieger. The high cost of failure of rotating equipment. *co DTIC*, page 3, 1990.

[18] Edgar J Gunter and Brian K Weaver. Kaybob revisited: What we have learned about compressor stability from self-excited whirling. *Advances in Acoustics and Vibration*, 2016, 2016.

[19] DW Childs. The space shuttle main engine high-pressure fuel turbopump rotordynamic instability problem. *Journal of Engineering for Power*, 100(1):48–57, 1978.

[20] John A Kocur, John C Nicholas, Chester C Lee, et al. Surveying tilting pad journal bearing and gas-labyrinth seal coefficients and their effect on rotor stability. In *Proceedings of the 36th turbomachinery symposium*. Texas A&M University. Turbomachinery Laboratories, 2007.

[21] R Tiwari, AW Lees, and MI Friswell. Identification of dynamic bearing parameters: a review. *Shock and Vibration Digest*, 36(2):99–124, 2004.

[22] TW Dimond, PN Sheth, PE Allaire, and M He. Identification methods and test results for tilting pad and fixed geometry journal bearing dynamic coefficients–a review. *Shock and vibration*, 16(1):13–43, 2009.

[23] Jason C Wilkes and Dara W Childs. Improving tilting pad journal bearing predictions—part i: Model development and impact of rotor excited versus bearing excited impedance coefficients. *Journal of Engineering for Gas Turbines and Power*, 135(1):012502, 2013.

[24] J Schoukens, R Pintelon, and Y Rolain. Time domain identification, frequency domain identification. equivalencies! differences? In *Proceedings of the 2004 American Control Conference*, volume 1, pages 661–666. IEEE, 2004.

[25] Lennart Ljung. Frequency domain versus time domain methods in system identification–revisited. In *Control of Uncertain Systems: Modelling, Approximation, and Design*, pages 277–291. Springer.

[26] Lion Precision. Capacitive sensor operation and optimization (how capacitive sensors work and how to use them effectively).

[27] Lion Precision. Lion precision cpl190/cpl290 brochure.

[28] JCGM JCGM et al. Evaluation of measurement data—guide to the expression of uncertainty in measurement. *Int. Organ. Stand. Geneva ISBN*, 50:134, 2008.

[29] ISO ISO. 5725-1: 1994, accuracy (trueness and precision) of measurement methods and results-part 1: General principles and definitions. *International Organization for Standardization, Geneva*, 1994.

[30] Laura Deldossi and Diego Zappa. Iso 5725 and gum: comparison and comments. *Accreditation and quality assurance*, 14(3):159–166, 2009.

[31] JCGM JCGM et al. Evaluation of measurement data—supplement 1 to the 'guide to the expression of uncertainty in measurement'—propagation of distributions using a monte carlo method. *Int. Organ. Stand. Geneva ISBN*, 2008.

[32] Kemin Zhou and John Comstock Doyle. *Essentials of robust control*, volume 104. Prentice hall Upper Saddle River, NJ, 1998.

[33] AC Hagg and GO Sankey. Some dynamic properties of oil-film journal bearings with reference to the unbalance vibration of rotors. *Journal of Applied Mechanics*, 78:302–306, 1956.

[34] JDCM Glienicke, D-C Han, and M Leonhard. Practical determination and use of bearing dynamic coefficients. *Tribology international*, 13(6):297–309, 1980.

[35] S Hisa, T Matsuura, and T Someya. Experiments on the dynamic characteristics of large scale journal bearings. In *Proc. of IMechE International Conference Vibrations in Rotating Machinery C*, volume 284, pages 223–230, 1980.

[36] D Sudheer Kumar Reddy, S Swarnamani, and BS Prabhu. Experimental investigation on the performance characteristics of tilting pad journal bearings for small ld ratios. *Wear*, 212(1):33–40, 1997.

[37] Hyun Cheon Ha and Seong Heon Yang. Excitation frequency effects on the stiffness and damping coefficients of a five-pad tilting pad journal bearing. *Journal of tribology*, 121(3):517–522, 1999.

[38] Sebastian Kukla, Thomas Hagemann, and Hubert Schwarze. Measurement and prediction of the dynamic characteristics of a large turbine tilting-pad bearing under high circumferential speeds. In *ASME Turbo Expo 2013: Turbine Technical Conference and Exposition*, pages V07BT30A020–V07BT30A020. American Society of Mechanical Engineers, 2013.

[39] Steven Chatterton, Paolo Pennacchi, Phuoc Vinh Dang, and Andrea Vania. Identification dynamic force coefficients of a five-pad tilting-pad journal bearing. In *Proceedings of the 9th IFToMM International Conference on Rotor Dynamics*, pages 931–941. Springer, 2015.

[40] Phuoc Vinh Dang, Steven Chatterton, Paolo Pennacchi, Andrea Vania, and Filippo Cangioli. Behavior of a tilting–pad journal bearing with different load directions. In *ASME 2015 International Design Engineering Technical Conferences and Computers and Information in Engineering Conference*, pages V008T13A067–V008T13A067. American Society of Mechanical Engineers, 2015.

[41] Phuoc Vinh Dang, Steven Chatterton, Paolo Pennacchi, and Andrea Vania. Effect of the load direction on non-nominal five-pad tilting-pad journal bearings. *Tribology International*, 98:197–211, 2016.

[42] P Arumugam, S Swarnamani, and BS Prabhu. Experimental identification of linearized oil film coefficients of cylindrical and tilting pad bearings. In *ASME 1994 International Gas Turbine and Aeroengine Congress and Exposition*, pages V005T14A012–V005T14A012. American Society of Mechanical Engineers, 1994.

[43] Luis E Rodriguez and Dara W Childs. Frequency dependency of measured and predicted rotordynamic coefficients for a load-on-pad flexible-pivot tilting-pad bearing. *Journal of tribology*, 128(2):388–395, 2006.

[44] Adnan M Al-Ghasem and Dara W Childs. Rotordynamic coefficients measurements versus predictions for a high-speed flexure-pivot tilting-pad bearing (load-between-pad configuration). *Journal of engineering for gas turbines and power*, 128(4):896–906, 2006.

[45] John Eric Hensley. *Rotordynamic coefficients for a load-between-pad, flexible-pivot tilting pad bearing at high loads.* PhD thesis, Texas A&M University, 2006.

[46] Dara Childs and Joel Harris. Static performance characteristics and rotordynamic coefficients for a four-pad ball-in-socket tilting pad journal bearing. *Journal of Engineering for Gas Turbines and Power*, 131(6):062502, 2009.

[47] Joel Harris and Dara Childs. Erratum:"static performance characteristics and rotordynamic coefficients for a four-pad ball-in-socket tilting pad journal bearing"[asme j. eng. gas turbines power, 2009, 131 (6), p. 062502. *Journal of Engineering for Gas Turbines and Power*, 140(5):057001, 2018.

[48] Adolfo Delgado, Giuseppe Vannini, Bugra Ertas, Michael Drexel, and Lorenzo Naldi. Identification and prediction of force coefficients in a five-pad and four-pad tilting pad bearing for load-on-pad and load-between-pad configurations. *Journal of Engineering for Gas Turbines and Power*, 133(9):092503, 2011.

[49] Chris D Kulhanek and Dara W Childs. Measured static and rotordynamic coefficient results for a rocker-pivot, tilting-pad bearing with 50 and 60% offsets. *Journal of engineering for gas turbines and power*, 134(5):052505, 2012.

[50] Dara W Childs, Adolfo Delgado, and Giuseppe Vannini. Tilting-pad bearings: measured frequency characteristics of their rotordynamic coefficients. In *40th Turbomachinery Symposium, Houston, TX, Sept*, pages 12–15, 2011.

[51] Dara W Childs and Clint R Carter. Rotordynamic characteristics of a five pad, rocker-pivot, tilting pad bearing in a load-on-pad configuration; comparisons to predictions and load-between-pad results. *Journal of Engineering for Gas Turbines and Power*, 133(8):082503, 2011.

[52] Chris David Kulhanek. *Dynamic and Static Characteristics of a Rocker-Pivot, Tilting-Pad Bearing With 50% and 60% Offsets.* PhD thesis, Texas A & M University, 2012.

[53] Adolfo Delgado, Mirko Librashi, and Giuseppe Vannini. Dynamic characterization of tilting pad journal bearings from component and system level testing. In *ASME Turbo Expo 2012: Turbine Technical Conference and Exposition*, pages 1007–1016. American Society of Mechanical Engineers, 2012.

[54] Jason C Wilkes and Dara W Childs. Improving tilting-pad journal bearing predictions: Part ii—comparison of measured and predicted rotor-pad transfer functions for a rocker-pivot tilting-pad journal bearing. In *ASME Turbo Expo 2012: Turbine Technical Conference and Exposition*, pages 979–990. American Society of Mechanical Engineers, 2012.

[55] David Coghlan. *Static, Rotordynamic, and Thermal Characteristics of a Four Pad Spherical-Seat Tilting Pad Journal Bearing With Four Methods of Directed Lubrication*. PhD thesis, 2014.

[56] David P Tschoepe and Dara W Childs. Measurements versus predictions for the static and dynamic characteristics of a four-pad, rocker-pivot, tilting-pad journal bearing. *Journal of Engineering for Gas Turbines and Power*, 136(5):052501, 2014.

[57] Jennifer E Gaines and Dara W Childs. The impact of pad flexibility on the rotordynamic coefficients of tilting-pad journal bearings. *Journal of Engineering for Gas Turbines and Power*, 138(8):082501, 2016.

[58] David M Coghlan and Dara W Childs. Characteristics of a spherical seat tpjb with four methods of directed lubrication—part ii: Rotordynamic performance. *Journal of Engineering for Gas Turbines and Power*, 139(12):122503, 2017.

[59] Brian Pettinato and Pranabesh De Choudhury. Test results of key and spherical pivot five-shoe tilt pad journal bearings—part ii: dynamic measurements. *Tribology transactions*, 42(3):675–680, 1999.

[60] Karl D Wygant, Lloyd E Barrett, and Ronald D Flack. Influence of pad pivot friction on tilting-pad journal bearing measurements—part ii: Dynamic coefficients©. *Tribology transactions*, 42(1):250–256, 1999.

[61] Karl D Wygant, Ronald D Flack, and Lloyd E Barrett. Measured performance of tilting-pad journal bearings over a range of preloads—part ii: dynamic operating conditions. *Tribology transactions*, 47(4):585–593, 2004.

[62] WM Dmochowski and B Blair. Effect of oil evacuation on the static and dynamic properties of tilting pad journal bearings. *Tribology transactions*, 49(4):536–544, 2006.

[63] RD Flack, KD Wygant, and LE Barrett. Measured dynamic performance of a tilting pad journal bearing over a range of forcing frequencies. In *Proc. 7th International Conference on Rotor Dynamics*, volume 1, 2006.

[64] Waldemar Dmochowski. Dynamic properties of tilting-pad journal bearings: experimental and theoretical investigation of frequency effects due to pivot flexibility. *Journal of engineering for gas turbines and power*, 129(3):865–869, 2007.

[65] Gregory F Simmons, Alejandro Cerda Varela, Ilmar Ferreira Santos, and Sergei Glavatskih. Dynamic characteristics of polymer faced tilting pad journal bearings. *Tribology International*, 74:20–27, 2014.

[66] Enrico Ciulli, Paola Forte, Mirko Libraschi, Lorenzo Naldi, and Matteo Nuti. Characterization of high-power turbomachinery tilting pad journal bearings: first results obtained on a novel test bench. *Lubricants*, 6(1):4, 2018.

[67] Brian Pettinato and Pranabesh De Choudhury. Test results of key and spherical pivot five-shoe tilt pad journal bearings—part i: Performance measurements. *Tribology transactions*, 42(3):541–547, 1999.

[68] GJG Upton. Applied multivariate data analysis, volume 1: regression and experimental design, by jd jobson. pp 621. dm 118. 1991. isbn 3-540-97660-4 (springer). *The Mathematical Gazette*, 78(481):98–100, 1994.

[69] Ernest O Doebelin and Dhanesh N Manik. Measurement systems: application and design. 2007.

[70] Karl D Wygant, Ronald D Flack, and Lloyd E Barrett. Influence of pad pivot friction on tilting-pad journal bearing measurements—part i: Steady operating position©. *Tribology transactions*, 42(1):210–215, 1999.

[71] Gregory J Kostrzewsky and Ronald D Flack. Accuracy evaluation of experimentally derived dynamic coefficients of fluid film bearings part i: development of method. *Tribology Transactions*, 33(1):105–114, 1990.

[72] IEC ISO and BIPM OIML. Guide to the expression of uncertainty in measurement. *Geneva, Switzerland*, 1995.

[73] Alejandro Cerda Varela, Bo Bjerregaard Nielsen, and Ilmar Ferreira Santos. Steady state characteristics of a tilting pad journal bearing with controllable lubrication: Comparison between theoretical and experimental results. *Tribology International*, 58:85–97, 2013.

[74] Paola Forte, Enrico Ciulli, and Diego Saba. A novel test rig for the dynamic characterization of large size tilting pad journal bearings. In *Journal of Physics: Conference Series*, volume 744, page 012159. IOP Publishing, 2016.

[75] Waldemar Dmochowski. Industrial application of gas turbines committee.

[76] MATLAB. mldivide.

[77] EPNA Feder, PN Bansal, and A Blanco. Investigation of squeeze film damper forces produced by circular centered orbits. *Journal of Engineering for Power*, 100(1):15–21, 1978.

[78] P Gancitano, B. Schwartz, R. Fittro, and C. Knospe. Development of an active load cell force measurement test rig. *16th International Symposium on Magnetic Bearings*, 2018.

[79] Ronald D Flack, Gregory J Kostrzewsky, and David V Taylor. A hydrodynamic journal bearing test rig with dynamic measurement capabilities. *Tribology transactions*, 36(4):497–512, 1993.

[80] Lyle Arthur Branagan. Thermal analysis of fixed and tilting pad journal bearings including cross-film viscosity variations and deformations. 1990.

[81] Timothy William Dimond. *Modeling of Fluid Film Bearings and Design of a Fluid Film Gearing Rig.* PhD thesis, University of Virginia, 2011.

[82] David Meeker. Finite element method magnetics. *FEMM*, 4:32, 2010.